AFOSR-TR- 93 0197

Electrical Engineering Department
UNIVERSITY OF MARYLAND, COLLEGE PARK, MD 20742

FINAL TECHNICAL REPORT

Optically Controlled Solid State Opening Switches

Grant No. AFOSR 88-0246

submitted by

Dr. Chi H. Lee
Dr. M.J. Rhee

Electrical Engineering Department
University of Maryland

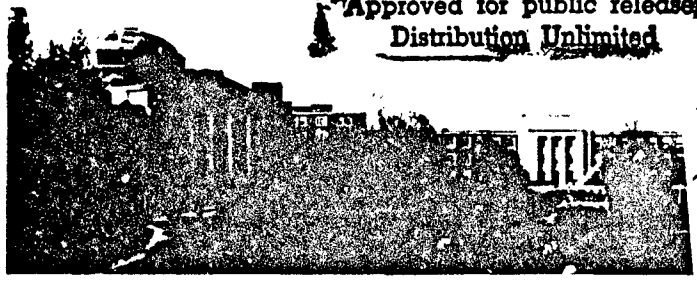

REPORT DOCUMENTATION PAGE

Form Approved
OMB No. 0704-0188

1. AGENCY USE ONLY (Leave blank)	2. REPORT DATE	3. REPORT TYPE AND DATES COVERED
		Final Report 01 Aug 88 - 31 May 92

4. TITLE AND SUBTITLE
OPTICALLY CONTROLLED SOLID STATE REPETITIVE OPENING SWITCHES: HIGH TC SUPERCONDUCTORS AND DIAMOND AND GRAPHITE

5. FUNDING NUMBERS
AFOSR-88-0246

6. AUTHOR(S)
Dr Chi Lee

7. PERFORMING ORGANIZATION NAME(S) AND ADDRESS(ES)
Univ of Maryland
Department of Electrical Engineering
College Park, MD 20742

8. PERFORMING ORGANIZATION REPORT NUMBER

9. SPONSORING/MONITORING AGENCY NAME(S) AND ADDRESS(ES)
AFOSR/NE
110 DUNCAN AVENUE, SUITE B115
BOLLING AFB, DC 20332-0001

10. SPONSORING/MONITORING AGENCY REPORT NUMBER
2301/A7

11. SUPPLEMENTARY NOTES

12a. DISTRIBUTION/AVAILABILITY STATEMENT
UNLIMITED

12b. DISTRIBUTION CODE

This is the final technical report for a research program to study optical controlled solid state opening switches. This program covers the period between August, 1988 and May, 1992 under the grant No. AFOSR-88-0246.
The goal of the research is to study fundamental issues in a novel scheme to generate high power electrical pulsed power using optical controlly solid state opening switches. An optically controlled pulsed power system has been developed which is capable of delivering high power pulsed energy.
This system employs a photoconductive semiconductor switch (PCSS) in an inductive energy storage pulsed power system (IESPPS). IESPPS offer advantage of small size with voltage and power step-up. However IESPPS imposes several stringent requirements on the switch. In fact, the switch must be nearly ideal with regard to fast opening time and low on-state resistance. Nevertheless, the PCSS performs quite well, yielding power gains of 50 with power output of nearly 100 KW. In this work, the pulse forming theories in the dual of the LC generator, the current charged transmission line (CCTL) and the dual of the Blumlein line (DBL) are studied for the first time.

14. SUBJECT TERMS

15. NUMBER OF PAGES

16. PRICE CODE

17. SECURITY CLASSIFICATION OF REPORT	18. SECURITY CLASSIFICATION OF THIS PAGE	19. SECURITY CLASSIFICATION OF ABSTRACT	20. LIMITATION OF ABSTRACT
UNCLASSIFIED	UNCLASSIFIED	UNCLASSIFIED	UL

FINAL TECHNICAL REPORT

Optically Controlled Solid State Opening Switches

Grant No. AFOSR 88-0246

submitted by

Dr. Chi H. Lee

Dr. M.J. Rhee

Electrical Engineering Department

University of Maryland

FINAL TECHNICAL REPORT

Optically Controlled Solid State Opening Switches: Semiconductors, High T_c Superconductors, Diamond and Graphite

Grant No. AFOSR 88-0246
For the period 08/01/88 to 05/31/92

Submitted to
Air Force Office of Scientific Research

Submitted by

Dr. Chi H. Lee
Dr. M.J. Rhee

Electrical Engineering Department
University of Maryland
College Park, MD 20742

TABLE OF CONTENTS

Abstract

This is the final technical report for a research program to study optically controlled solid state opening switches. This program covers the period between August, 1988 and May, 1992 under the grant No. AFOSR-88-0246.

The goal of the research is to study fundamental issues in a novel scheme to generate high power electrical pulsed power using optically controlled solid state opening switches. An optically controlled pulsed power system has been developed which is capable of delivering high power pulsed energy.

This system employs a photoconductive semiconductor switch (PCSS) in an inductive energy storage pulsed power system (IESPPS). IESPPS offers advantage of small size with voltage and power step-up. However IESPPS imposes several stringent requirements on the switch. In fact, the switch must be nearly ideal with regard to fast opening time and low on-state resistance. Nevertheless, the PCSS performs quite well, yielding power gains of 50 with power output of nearly 100 KW.

In this work, the pulse forming theories in the dual of the LC generator, the current charged transmission line (CCTL) and the dual of the Blumlein line (DBL) are studied for the first time.

I. Introduction

Over the past two decades the need for a switch for use in high-power pulsed applications has increased. Some of these applications include electrical discharge lasers, electron-beam pumped lasers, flash x-ray power supplies, and high power microwave generation. Switching voltage requirements can be up to a megavolt, and the timing must often be very accurate.

An optically controlled pulsed power system has been developed which is capable of delivering high-power pulsed energy for some of these applications. This system employs a photoconductive semiconductor switch (PCSS) in an inductive energy storage pulsed power system (IESPPS). Using an inductor rather than a capacitor as the energy storage element, an IESPPS offers the advantage of small size with voltage and power step-up. We shall see that the IESPPS scheme imposes several stringent requirements on the switch. In fact, the switch must be nearly ideal with regard to fast opening time and low on-state resistance. Nevertheless, the PCSS performs quite well, yielding power gains as high as 49 with output powers as high as 88 kW.

There are three fundamental areas of concern in the development of the system. First, there is an interest in the performance of GaAs as a photoconductive closing and opening switch. Characteristics of the switch such as on-resistance, and opening time dictate the choice of other component values which must be used to optimize power output.

Next, we are interested in the development of the inductive energy storage system which the PCSS will control in order to produce pulsed power. The use of a transmission line as the inductive elements is preferred to lower-Q lumped inductors. We will examine a system employing a transmission line inductor known as the current charged transmission line (CCTL). The CCTL in conjunction with the PCSS was first demonstrated at the University of Maryland. Since then, the CCTL scheme has been further refined to produce higher output voltages and higher power gains.

Finally, we are concerned with the source of the optical pulse which controls the PCSS. The type of optical control pulse which is required to "turn on" the PCSS is determined by the properties of both the energy storage scheme and the PCSS itself. We find that a rather unique optical pulse is required. Therefore, developing a laser with properties

tailored to the PCSS and CCTL scheme was part of our effort.

Developing the best inductive energy storage system with the highest output power and power gain lies in the skill of tailoring the laser pulse, and circuit components to meet the characteristics of the switch. In this endeavor, we first consider the theoretical operation of various inductive energy storage pulsed power systems. A in depth theoretical analysis of the pulse forming in the dual of the LC generator, the CCTL and the dual of the Blumlein line (DBL) are studied for the first time. The performances of the IESPPS using PCSS in CCTL and DBL are compared. A number of publications results in the course of this research. In addition one M.S. and one Ph.D. thesis are the results of this research. They are all included here as appendices.

II. Summary of Research

1. Power gain in an IESPPS

A breakthrough of the research has been achieved. It was reported in a paper entitled, "Observation of power gain in an inductive energy pulsed power system with an optically controlled semiconductor opening switch," published in the Applied Phys. Lett. **57**, 2330 (1990), and included in this report as Appendix A. Power gain has been observed, for the first time, in an IESPPS with an optically controlled PCSS. A specially tailored 1.054 μm pulse from a Nd:glass laser was utilized to activate the GaAs switch, producing an electrical output pulse with a power gain of 10.

2. Multi-KW pulsed power generation

The performance of the GaAs photoconductive opening switch has been optimized in the current charged transmission line configuration to produce a power gain of 45 with an output pulse of 80 KW. The switch was activated by a specially designed laser which generates a square optical pulse with fast rise- and fall-time and long pulse duration. The switch activated by such an optical pulse exhibited a low on-state resistance which substantially improved the power gain. These results were reported in a paper entitled, "80-KW Inductive Pulsed Power System with a Photoconductive Semiconductor Switch," IEEE Photonics Tech Lett., Vol. 3, 576 (1991). This paper is included here as Appendix B.

3. Kilovolt square pulse generation using the dual of the Blumlein line (DBL)

A new pulse forming network, the dual of the Blumlein line (DBL) is used as the IESPPS. In the DBL configuration, the load is placed away from the switch end and moved to the center of the transmission. Thus, it will reduce the electromagnetic interference effect on the output waveform. Furthermore, the peak power from the DBL can be twice of that from the current charge transmission line. Generations of kilovolt square electrical pulses by a DBL with a fast PCSS opening switch has been demonstrated.

The experimental results are in good agreement with the theoretical calculations. This result was published in a paper entitled, "Kilovolt square pulse generation by a dual of the Blumlein line with a photoconductive semiconductor opening switch," IEEE Photonic Tech. Lett. Vol. 4, 621 (1992). It is included in this report as Appendix C.

4. Theoretical analysis of inductive energy storage pulse forming network

In order to design an optimum energy storage system one needs to understand the pulse forming theory thoroughly. In this work, the pulse forming theories in the dual of the LC generator, the current charged transmission line (CCTL), and the dual of the Blumlein line (DBL) which are charged with a voltage source are discussed for the first time. Furthermore, we have demonstrated the feasibility of using a 5mm cube GaAs p-i-n diode PCSS to generate multi-kilovolt pulses from the CCTL and the DBL. These experimental results clearly illustrate that the PCSS can be treated as an ideal opening switch when it is activated by a nearly square laser pulse. Also, the potential of employing the PCSS in these two inductive systems to obtain voltage/power gain through electrical pulse compression has been realized for the first time. By combining the experimental waveforms with an appropriate circuit model, the switch dynamic resistance during the closing and opening period has been computed and analyzed. The calculated results strongly suggest that the switch on-resistance can be as low as few ohms and the abnormal conduction of the switch during the opening stage might be related to the "lock-on" effect observed in the closing switch experiments. The details related to this abnormal conduction still requires further investigation.

This is the Ph.D. research work of Jay C.C. Kung whose thesis entitled, "Inductive Energy Storage Systems and Photoconductive Semiconductor Opening Switch," is included

here as Appendix D. In addition a review article was written by one of the P.I. as an invited paper entitled, "Optical IEEE Trans. on Electron Devices, Vol. 3. ?426 (1990). This paper is included as Appendix E.

III. List of Publications and Conference Papers Resulting from this Grant

A. Journal Papers

1. E.A. Chauchard, C.C. Kung, M.J. Rhee, C.H. Lee, "Repetitive Semiconductor Opening Switch and Application to Short Pulse Generation," Laser and Particle Beams (1989), Vol. 7, Part 3, pp. 615-626.
2. M.J. Rhee, T.A. Find, and C.C. Kung, "Basic Circuits for Inductive-Energy Pulsed Power Systems," pp. 4333-4337, J. Appl. Phys. Vol. 67(9), May, 1990.
3. C.C. Kung, E.A. Chauchard, Chi H. Lee, M.J. Rhee, and L. Yan, "Observation of Power Gain in an Inductive Energy Pulsed Power System with an Optically Controlled Semiconductor Opening Switch," Appl. Phys. Lett. 57(22), pp. 2330-2332, Nov. 1990.
4. E.E. Funk, E.A. Chauchard, M.J. Rhee and Chi H. Lee, "80 KW Inductive Pulsed Power System with a Photoconductive Semiconductor Switch," IEEE Photonics Tech. Lett. Vol. 3, 576, June 1991.
5. C.C. Kung, E.A. Chauchard, Chi H. Lee, and M.J. Rhee, "Kilovolt Square Pulse Generation by a Dual of the Blumlein Line with a Photoconductive Semiconductor Opening Switch," IEEE Photonics Technology Letters, Vol. 4, No. 6, pp. 621-623, June 1992.
6. Chi H. Lee, "Optical Control of Semiconductor Closing and Opening Switches," IEEE Trans. Electron. Devices, Vol. 37, 2426-2438, December 1990.

B. Conference Papers

1. E.A. Chauchard, C.C. Kung, Chi H. Lee, and M.J. Rhee, "Performance of Laser Activated Semiconductor Opening Switches," Conference Record-Abstracts, 1989 IEEE International Conference on Plasma Science, pp. 125-126, Buffalo, New York, May 22-24, 1989.

2. E.A. Chauchard, C.C. Kung, M.J. Rhee, and Chi H. Lee, "Observation of Current Build-Up with a Semiconductor Switch and a Transmission Line," Digest of Technical Papers of the 7th IEEE Pulsed Power Conference (IEEE, New York, 1989), pp. 128-130.
3. C.C. Kung and M.J. Rhee, "Circuit Description of Inductive Energy Storage Pulsed Power Systems," Conference Record-Abstracts, 1989 IEEE International Conference on Plasma Science, pp. 125, Buffalo, New York, May 22-24, 1989.
4. C.C. Kung, E.A. Chauchard, Chi H. Lee, M.J. Rhee, and L. Yan, "Experimental Study of Power Gain in an Inductive Energy Pulsed Power System with an Optically Activated Semiconductor Opening Switch," Conference Record-Abstracts, 1990 IEEE International Conference on Plasma Science, May 21-23, 1990.
5. C.C. Kung, Eve A. Chauchard, M.J. Rhee, Chi H. Lee, and Li Yan, "Voltage Multiplication with an Optically Activated Semiconductor Opening Switch," Conference on Lasers and Electro-Optics, 1990 Technical Digest Series, Vol. 7, pp. 80-82, Optical Society of America, Washington, DC, 1990.
6. C.C. Kung, E.A. Chauchard, M.J. Rhee, L. Yan, and Chi H. Lee, "Peak Power Gain and Pulse Compression in an Inductive Energy Storage System by a Photoconductive Closing and Opening Switch," Workshop Proceedings of the 2nd Workshop on "Optical and Electron-Beam Controlled Semiconductor Switches," August 1990, Norfolk, VA.
7. C.C. Kung, E.E. Funk, E.A. Chauchard, M.J. Rhee, Chi H. Lee, L. Yan, "Observation of Power Gain in an Inductive Pulsed Power System with an Optically Activated Semiconductor Closing and Opening Switch," Proceedings of the SPIE Conference on Optically Activated Switching, Vol. 1378, pp. 250-258, Nov. 1990.
8. C.C. Kung, E.A. Chauchard, E.E. Funk, Chi H. Lee, M.J. Rhee, and L. Yan, "Generation of Kilovolt Square Pulse by a Current Charged Transmission Line Using an Optically Controlled Semiconductor Opening Switch," Bulletin of the American Physical Society, Division of Plasma Physics, Nov. 12-16, 1990.
9. C.C. Kung, E.A. Chauchard, M.J. Rhee, and Chi H. Lee, "Generation of Square Pulses by a Dual of the Blumlein Line with a Photoconductive Semiconductor

Opening Switch," Conference on Lasers and Electro-Optics, 1991 Technical Digest Series, Vol pp. 126-128, Optical Society of America, Washington, DC, 1991.

10. C.C. Kung, E.A. Chauchard, Chi H. Lee, and M.J. Rhee, "Observation of Square Pulse Generation in a Dual of the Blumlein Line with an Optoelectronic Opening Switch, Conference Record-Abstracts, 1991 IEEE International Conference on Plasma Science, p. 207, June 3-5, 1992.
11. C.C. Kung, E.A. Chauchard, M.J. Rhee, and Chi H. Lee, "Square Pulse Generation with a Photoconductive Semiconductor Opening Switch in the Dual of the Blumlein Line," Digest of Abstracts of the 8th IEEE Pulsed Power Conference (IEEE, New York, 1991), p. 3-43, June 17-19, 1991, San Diego, CA. It will also be appearing in the Digest of Technical Papers of the 8th IEEE Pulsed Power Conference.
12. E.E. Funk, P.S. Cho, C.C. Kung, E.A. Chauchard, M.J. Rhee, P.-T. Ho, J. Goldhar, and Chi H. Lee, "Recent Advances in Research on Photoconductive Power Switching at the University of Maryland," Proceedings of the SPIE Conference on Optically Activated Switching, Paper 1632-27, January 1992.

Appendix A

Observation of power gain in an inductive energy pulsed power system with an optically controlled semiconductor opening switch

C. C. Kung, E. A. Chauchard, Chi H. Lee, M. J. Rhee, and L. Yan
Department of Electrical Engineering, University of Maryland, College Park, Maryland 20742

(Received 19 February 1990; accepted for publication 30 August 1990)

Power gain has been observed, for the first time, in an inductive energy storage pulsed power system with an optically controlled semiconductor opening switch. A specially tailored 1.054 μm pulse from a Nd:glass laser was utilized to activate a GaAs switch of the *p-i-n* diode configuration, producing an output pulse with a power gain of more than 10.

During the last decade, the development of inductive energy storage pulsed power systems (IESPPSs) has been spurred by potential applications to diverse areas in which a compact pulsed power system is required. Accordingly, considerable research has been conducted on the opening switch,[1-4] which is the key element in an IESPPS. Our optically controlled semiconductor opening switch (OCSOS) is a normally insulating photoconductive semiconductor. A long optical pulse sets the switch into the conducting state, allowing inductive energy to be stored in the circuit. If the optical pulse is extinguished rapidly and the semiconductor has a short recombination time, the switch will open and convert the stored energy into an output pulse. We have demonstrated that OCSOS's are capable of opening inductive energy storage circuits on a nanosecond time scale,[5,6] making OCSOSs the fastest among existing opening switches. Some other advantages[5,6] of the OCSOSs include: repetitive operation, controllable conduction period, and jitter-free triggering. However, due to the available laser and the restricted switch fabrication technique, the output pulse power was limited to a very low level. In this letter, we report an experiment that demonstrates a substantial amount of power gain achieved in an IESPPS, which consists of a current charged transmission line (CCTL)[6,7] and an OCSOS. The experimental setup is schematically shown in Fig. 1. A transmission line (RG-213) of characteristic impedance $Z_0 = 50\ \Omega$, and length $l = 2.5$ m, with one end shorted [0.1 Ω current viewing resistor, (CVR)] is connected through a semiconductor switch to a capacitor $C = 0.1\ \mu$F, which is initially charged to V_0. The output wave form was measured at the switch side of CCTL through a 50 Ω transmission line as shown in Fig. 1. In order for the system to be useful as an IESPPS, the period of switch conduction time should be long enough so that the charging current is multiplied in the inductive energy storage circuit, giving rise to power multiplication. In the experiment, a specially tailored laser pulse was used to illuminate a semiconductor switch providing a long period of conduction time. The laser used was a Nd:glass pulsed laser of wavelength 1.054 μm and total energy of $\sim$2 mJ. The intensity of light increases slowly in time for 200 ns and then falls rapidly to near zero within 10 ns. The switch used in this experiment is a GaAs *p-i-n* diode,[8] for which the carrier recombination time is $\sim$2 ns. The *p-i-n* diode is a 0.5 mm thick, 5×5 mm^2 square wafer of GaAs doped with *p*-type impurity on one surface and *n* type on the other. A ring-shaped gold electrode is ev rated to the *p*-type surface so that the laser light can p agate into the switch material, and a flat electrode is e orated onto the opposite side.

To characterize the switch, on-resistance of the a mentioned switch and some other type switches were sured, using the circuit shown in Fig. 1 without the C connected. The circuit is then a simple resistive divide switch resistance and the load resistance of 50 Ω (a divides the charging voltage V_0 of the capacitor. Th resistance of the switch is easily determined from the put wave form obtained as the laser pulse activate switch. The lowest on-resistance was found to be 0.5 the GaAs *p-i-n* diode switch operated at a charging vo of 100 V. Tests of other switches fabricated from va materials and of different dimensions show that the mum operating voltage, in general, scales with the ness of the switch. However, the higher on-resistan measured for the thicker switches, indicating that the power level used is insufficient for these switches.

The pulse formation experiment was performed the CCTL and the GaAs *p-i-n* diode as shown in Fi Upon activation of the switch by the laser pulse, th pacitive energy initially stored in the 0.1 μF capa which is charged to voltage 100 V, is transferred t CCTL. The charging current, which is monitored by Ω current viewing resistor, increases in time up to 16 shown in Fig. 2(a). This is substantially less than the rent that is predicted by the same circuit with an switch, $I_{max} = (C/L)^{1/2} V_0 = (0.1\ \mu\text{F}/0.63\ \mu\text{H})^{1/}$ V = 40 A. This indicates that the switch has a highe resistance early in time when the laser light intensity is

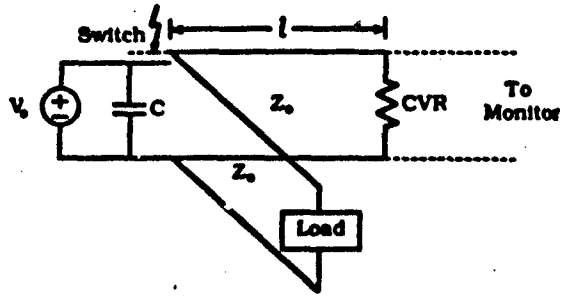

FIG. 1. Schematic representation of experimental setup. *S*: switch, current viewing resistor (0.1 Ω), *C*: capacitor (0.1 μF).

 0003-6951/90/482330-03$02.00

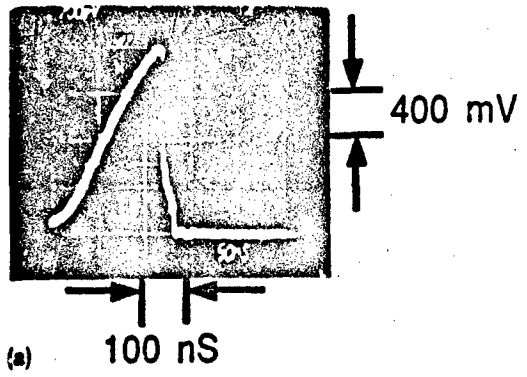

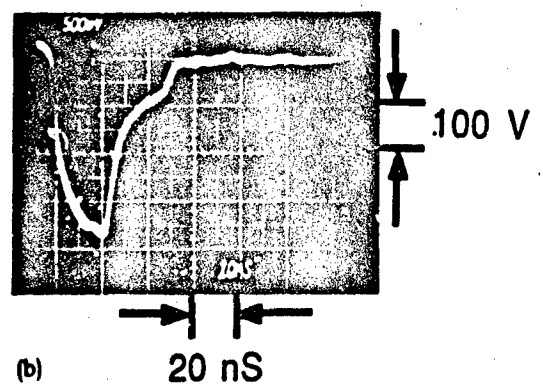

FIG. 2. Wave forms obtained with 0.5-mm-thick GaAs *p-i-n* diode switch operated at a charging voltage of 100 V. (a) The charging current monitored by 0.1 Ω current viewing resistor (400 mV corresponds to 4 A). (b) Output voltage wave form.

As the pulse of laser light ends, the switch opens and releases the inductive energy into the resistive load. The load, in this case, consists of parallel connection of a 50 Ω coaxial cable (connected to a 50 Ω oscilloscope) and the off-resistance of the switch. Therefore, the equivalent load resistance R_L is always less than or equal to 50 Ω. A typical output-pulse wave form with the main pulse amplitude of 360 V, obtained with a charging voltage of 100 V, is shown in Fig. 2(b). Higher output voltages are produced with higher charging voltages of up to 150 V. Switch breakdown occurs at 163 V charging voltage for the 0.5-mm-thick GaAs switch.

It is straightforward to show[9] that the CCTL produces a main pulse and a train of post-pulses into an arbitrary resistive load R_L with amplitudes given by

$$V_{\text{out}}^n = R_L Z_o I_o (Z_o - R_L)^n/(Z_o + R_L)^{n+1}, \qquad (1)$$

where n designates the nth post-pulse and $n = 0$ corresponds to the main pulse. In this experiment (see Fig. 1), only an infinitely high switch resistance (matched load, i.e., $R_L = Z_o = 50$ Ω), will produce just one main pulse $V_{\text{out}}^0 = Z_o I_o/2$. Otherwise, $R_L < Z_o$ because of finite switch resistance, and a gradually decreasing, staircase-shaped wave form is produced (see Fig. 3). A typical wave form shown in Fig. 2(b) demonstrates such a decreasing staircase. The ratio of the main pulse to the first post-pulse

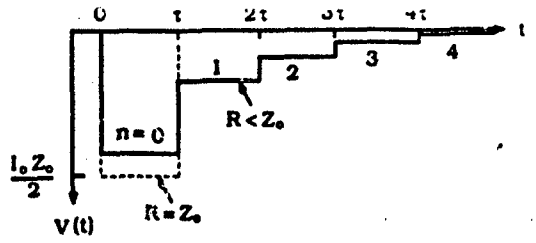

FIG. 3. Depiction of output voltage wave forms produced by the current charged transmission line with an ideal opening switch, showing matched and mismatched cases.

amplitudes is used to estimate the off-resistance of the switch by using Eq. (1), and found to be typically ~200 Ω.

In order for a pulsed power system to be useful, the power gain, which may be defined as the ratio of the output power of the system to the power that the source would produce directly into the same load, should be greater than unity. In this experiment, the output and the source powers are $P_{\text{out}} = (V_{\text{out}}^0)^2/Z_o$ and $P_s = V_o^2/Z_o$ respectively. The highest power gain obtained is 13. At charging voltages higher than 100 V, higher output power was observed, but lower power gain resulted. This suggests that the switch off-resistance becomes lower as the electric field induced across the switch by the output voltage increases. This phenomenon may be attributed to an effect similar to the "lock-on" effect[10] observed in the closing switch experiments.

In conclusion, it has been demonstrated for the first time, that a current charged transmission line with a GaAs *p-i-n* diode switch, controlled by a specially tailored Nd:glass laser pulse, produced an output pulse with a power gain up to 13. The system may be scaled up to a higher voltage system by employing a thicker switch, which may require higher laser power. The phenomenon of dropping power gain with increased operating voltage needs further investigation.

The authors are grateful to A. Rosen of the David Sarnoff Research Center for supplying the GaAs *p-i-n* diode switch. We also thank E. E. Funk for critical reading of the manuscript. This work was supported by the Air Force Office of Scientific Research.

[1] A. Guenther, M. Kristiansen, and T. Martin, eds. *Opening Switch* (Plenum, New York, 1987).
[2] K. H. Schoenbach, V. K. Lakdawala, R. Genuer, and S. T. Ko, J. Appl. Phys. 63, 2460 (1988).
[3] M. S. Mazzola, K. H. Schoenbach, V. K. Lakdawala, and S. T. Ko, Appl. Phys. Lett. 55, 2102 (1988).
[4] F. J. Zutavern, G. M. Loubriel, B. B. McKenzie, W. M. O'Malley, R. A. Hamil, L. P. Schanwald, and H. P. Hjalmarson, in *Digest of Technical Papers*, edited by R. White and B. H. Bernstein (IEEE, New York, 1989), p. 412.
[5] E. A. Chauchard, M. J. Rhee, and Chi H. Lee, Appl. Phys. Lett. 47, 1293 (1985).
[6] E. A. Chauchard, C. C. Kung, Chi H. Lee, and M. J. Rhee, Laser Particle Beams 7, 615 (1989).
[7] M. J. Rhee and R. F. Schneider, IEEE Trans. Nucl. Sci. NS-30, 3192 (1983).

[8]A. Rosen, P. J. Stabile, A. M. Gombar, W. M. Janton, A. Bahasadri, and P. Herezfeld, Photon. Tech. Lett. 1, 132 (1989).
[9]M. J. Rhee, T. A. Fine, and C. C. Kung, J. Appl. Phys. 67, 4333 (1990).
[10]G. M. Loubriel, M. W. O'Malley, F. J. Zutavern, B. B. McKenzie, R. Conley, and H. P. Hjalmarson, *Proceedings of the Record of the 1 Power Modulator Symposium* (IEEE, New York, 1988), p. 312.

80-kW Inductive Pulsed Power System with a Photoconductive Semiconductor Switch

E. E. Funk, E. A. Chauchard, M. J. Rhee, and Chi H. Lee

Abstract—**The performance of the GaAs photoconductive semiconductor switch has been optimized in the current-charged transmission-line configuration to produce a power gain of 45 with an output pulse of 80 kW. The switch was activated by a square optical pulse resulting in a low on-state switch resistance and substantially-improved power gain.**

A jitter-free-opening switch with a fast opening time is necessary in an inductive energy storage pulsed power system (IESPPS)—where energy is stored by current in an inductor or transmission line. The GaAs photoconductive semiconductor switch (PCSS) appears to be ideal for this application [1]–[4], and we have demonstrated its operation in an IESPPS delivering an 80-kW output pulse with a power gain of 45.

The IESPPS used in this work is a current-charged transmission line (CCTL) [2], [5] with PCSS coupled to a capacitor as shown in Fig. 1. This configuration is capable of delivering into the matched load a square voltage pulse of amplitude greater than the initial voltage across the capacitor. When the switch is closed, the capacitor, initially charged to V_o, is the source of a current traveling wave of amplitude $I = V_o/Z_o$, where Z_o is the characteristic impedance of the CCTL. As the traveling wave meets either end of the CCTL, it is reflected back in the opposite direction causing the current to increase by a step of $I = 2V_o/Z_o$ after each round trip in the CCTL. For the purpose of estimating the charging current, the IESPPS may be treated as a lumped circuit by replacing the CCTL with its equivalent inductance L. Taking R_s as the on-state switch resistance and R_l as the load resistance, the current $I(t)$ through the inductor L is given by

$$I(t) = I_o e^{-\alpha t} \sin \omega t \qquad (1)$$

where $I_o = (V_o R_l)/[L\omega(R_l + R_s)]$, $\omega = \sqrt{R_l/[LC(R_l + R_s)] - \alpha^2}$, and $\alpha = (R_l R_s C + L)/[2LC(R_l + R_s)]$.

The GaAs PCSS was tested in the IEPPS configuration of Fig. 1. The switch is activated by a custom-tailored 1.05-μm square laser pulse, generated by a free-running Nd:Glass laser flashlamp pumped just above the lasing threshold. The laser produces a 2-μs pulse. A Pockels cell between crossed polarizers chops the pulse into a 540-ns square pulse that is then sent through a two-stage double-pass amplifier. The final output energy is ~10 mJ.

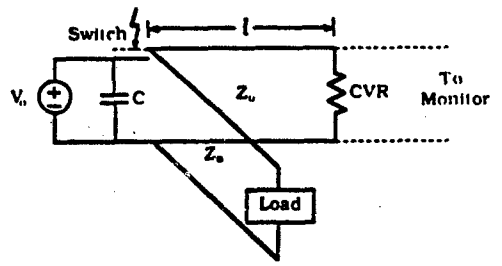

Fig. 1. Current charged transmission line scheme for this experiment, $l = 2.0$ m, $Z_o = 50\ \Omega$, $R_{load} = 50\ \Omega$, $C = 1.1\ \mu$F, $R_{CVR} = 0.1\ \Omega$ (current viewing resistor).

The switch under test was a 5-mm cube of GaAs of the p-i-n configuration [6] operated under reverse bias. The $C = 1.1\ \mu$F capacitor was initially charged to $V_o = 300$ V. When the PCSS was closed by the optical pulse, the current through the current viewing resistor, $I(t)$, and the voltage across the matched 50 Ω load, $V_{out}(t)$, were monitored simultaneously with oscilloscopes. The dynamic switch resistance $R_s(t)$ was then numerically computed according to the equation

$$R_s(t) = \left(V_o - \frac{1}{C}\int I(t)\,dt - V_{out}\right)/I(t). \qquad (2)$$

The 2.0 kV, the 80-kW output pulse produced by a 2.0-m CCTL is shown in Fig. 2. With $V_o = 300$ V, this output pulse corresponds to a voltage gain of 6.7. If the power gain is taken as the ratio of the peak power delivered through the CCTL configuration to the peak power that would be delivered directly into the load from the capacitor, the corresponding power gain is 45. This is the highest power gain achieved to date using this configuration.

The square optical pulse offers two advantages over the slowly rising pulse that was used in previous work [4]. First, the rate at which current builds up in the CCTL is increased since the on-state switch resistance drops, not gradually, but immediately to a low value. It can be seen in Fig. 3 that $R_s(t)$ quickly drops below 10 Ω and remains low until the switch opens. The low on-state switch resistance combined with a longer charging time produces a much higher current in the CCTL than in our previous work, accounting for the great improvement in power gain [4]. Second, the square pulse produces a nearly constant on-state switch resistance

Manuscript received March 18, 1991; revised April 5, 1991. This work was supported in part by the Air Force Office of Scientific Research and by the Strategic Defense Initiative Organization/Innovative Science and Technology, Office of Naval Research.

The authors are with the Department of Electrical Engineering, University of Maryland, College Park, MD 20742.

IEEE Log Number 9100751.

1041-1135/91/0600-0576$01.00

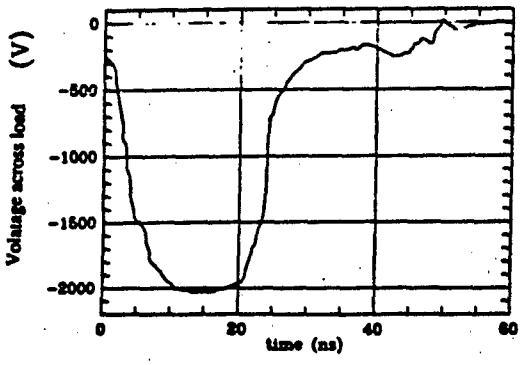

Fig. 2. 2.0-kV output pulse across R_{out} achieved when $V_o = 300$ V.

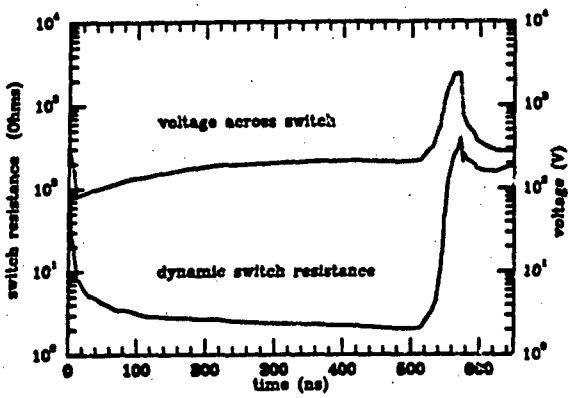

Fig. 3. Dynamic switch resistance $R_s(t)$ and voltage across the switch $V_s(t)$. Switch closes at $t = 0$ and opens at $t = 540$ ns, $V_o = 300$ V.

R_s, allowing direct comparison to the theoretical prediction of (1). Both the theoretical and experimental waveforms of current through the CVR are shown in Fig. 4 . The reasonable fit to the experimental curve suggests that the experimental R_s may be as low as 1.2 Ω.

A prominent feature of the dynamic switch resistance curve shown in Fig. 3 is the drop in switch resistance that occurs after the laser pulse has been extinguished. This occurs when the voltage drop across the switch V_s reaches a critical value of 2.2 kV corresponding to an electric field of 4.4 kV/cm across the switch. That may be compared to the critical lock-on field [7], [8] of ~3.6 kV/cm suggesting that this behavior may be related to the lock-on effect seen in many closing switch experiments. This effect limited the output voltage to ~2 kV even when higher charging voltages were used. In the future this effect will be countered by use of a longer switch that will in turn increase the voltage required to produce the critical field. The characteristics of this phenomenon in the opening switch will also be further investigated.

In conclusion, a power gain of 45 has been demonstrated

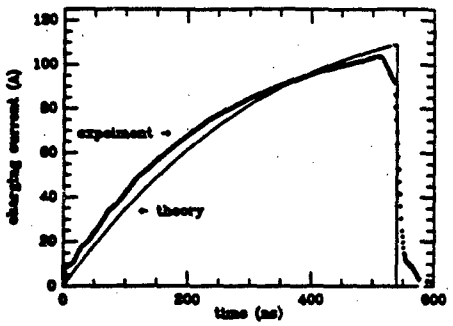

Fig. 4. Charging current waveform monitored by the current viewing resistor (CVR), experimental result (switch opens at $t = 540$ ns) and theory (switch resistance set to $R_s = 1.21$ Ω).

in a current-charged transmission line with a GaAs PCSS. The fast falltime of the switch resistance produced by the specially tailored optical pulse that activates the PCSS is mainly responsible for the high power gain achieved in this experiment. An effect similar to lock-on was found to limit the output voltage to ~2 kV.

Acknowledgment

The authors wish to thank A. Rosen of the David Sarnoff Research Center for providing the GaAs p-i-n diode switches.

References

[1] E. A. Chauchard, M. J. Rhee, and Chi H. Lee, "Optically activated semiconductors as repetitive opening switches," *Appl. Phys. Lett.*, vol. 47, pp. 1293–1295, 1985.

[2] E. A. Chauchard, C. C. Kung, C. H. Lee, M. J. Rhee, and V. Dmdiuk, "A new method to generate square pulses: optoelectronic switching in a current charged transmission line," *IEEE Trans. Plasma Sci.*, vol. PS-15, pp. 70–72, 1987.

[3] E. A. Chauchard, C. C. Kung, Chi H. Lee, and M. J. Rhee, "Repetitive semiconductor opening switch and application to short pulse generation," *Laser Particle Beams*, vol. 7, pp. 615–626, 1989.

[4] C. C. Kung, E. A. Chauchard, Chi H. Lee, M. J. Rhee, and L. Yan, "Observation of power gain in an optically controlled semiconductor opening switch," *Appl. Phys. Lett.*, vol. 57, no. 22, pp. 2330–2332, 1990.

[5] M. J. Rhee, T. A. Fine, and C. C. Kung, "Basic circuits for inductive energy pulsed power systems," *J. Appl. Phys.*, vol. 67, pp. 4333–4337, 1990.

[6] A. Rosen, P. J. Stabile, A. M. Gombar, W. M. Janton, A. Bahasadri, and P. Herzfeld, "100 kW DC-biased, all semiconductor switch using Si p-i-n diodes and AlGaAs 2-D laser arrays," *IEEE Photon. Tech. Lett.*, vol. 1, pp. 132–134, 1989.

[7] G. M. Loubriel, M. W. O'Malley, F. J. Zutavern, B. B. McKenzie, W. R. Conley, and H. P. Hjalmarson, "High current photoconductive semiconductive switches," in *Proc. 18th Power Modulator Symp.*, New York, 1988, pp. 312–317.

[8] F. J. Zutavern, G. M. Loubriel, B. B. McKenzie, W. M. O'Malley, R. A. Hamil, L. P. Schanwald, and H. P. Hjalmarson, "Photoconductive semiconductor switch (PCSS) recovery," in *Dig. Tech. Papers, 7th IEEE Pulsed Power Conf.*, R. White and B. H. Bernstein, Eds., New York, 1989, pp. 412–417.

Kilovolt Square Pulse Generation by a Dual of the Blumlein Line with a Photoconductive Semiconductor Opening Switch

C. C. Kung, E. A. Chauchard, Chi H. Lee, and M. J. Rhee

Abstract—**Generation of kilovolt square pulse by a dual of the Blumlein line with a fast photoconductive semiconductor opening switch is demonstrated. The experimental results are in good agreement with the theoretical expectations.**

INDUCTIVE-energy-storage pulsed-power system with an opening switch have been studied extensively [1], [2]. It was shown [3] that square pulses can be generated by inductive energy-pulse forming line systems, the current charged transmission line and the dual of the Blumlein Line (DBL). We have demonstrated 80 kW square pulse generation by using a current charged transmission line with a fast photoconductive semiconductor switch (PCSS) as an opening switch [4]. In this letter, for the first time, kilovolt square pulse generation by a DBL with a fast PCSS is reported.

The experimental realization of the DBL is schematically shown in Fig. 1. The matched load, $Z_o/2 = 25\ \Omega$ (see [3]), is placed at the junction of two identical RG-213 transmission lines of length $l = 1.5$ m and characteristic impedance $Z_o = 50\ \Omega$. This resistive load is a parallel connection of a 50-Ω resistor and a 50-Ω oscilloscope via a short RG-213 transmission line. The end of one line is shorted with a 0.1-Ω current viewing resistor (CVR), which is used to monitor the charging current in the experiment. The end of the other line is connected through the PCSS to a capacitor, $C = 1\ \mu$F, which is initially charged to voltage V_o and serves as an approximately constant voltage source.

A specially designed Nd:glass pulsed laser system is used to control the PCSS. This laser system produces a nearly square pulse of ~12 mJ pulse energy at 1.054 μm wavelength. The pulse duration is 540 ns and both the risetime and fall-time, which are determined by those of a Pockels cell used, are ~7 ns. The switch used is a 5-mm cube GaAs of p-i-n diode configuration for which the carrier recombination time is ~5 ns [5]. In order to achieve the best performance of the switch, this p-i-n diode is reverse biased; the positive terminal of the charged capacitor is connected to the n-type side of the switch. The switch is illuminated in the direction perpendicular to the electric field which appears across the switch.

Manuscript received December 26, 1991. This work was supported by the Air Force Office of Scientific Research and the Strategic Defense Initiative Organization through the Office of Naval Research.

The authors are with the Department of Electrical Engineering, University of Maryland, College Park, MD 20742.

IEEE Log Number 9200603.

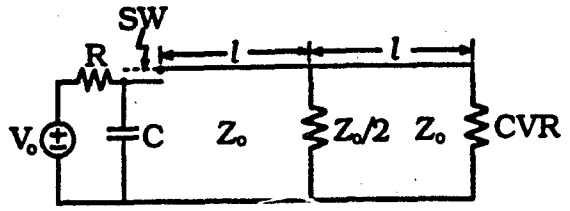

Fig. 1. Schematic representation of the dual of the Blumlein Line. CVR: current viewing resistor (0.1 Ω); *C*: capacitor (1 μF); *R*: charging resistor (2.7 kΩ); Z_o: characteristic impedance (50 Ω); SW: GaAs p-i-n diode switch.

In an ideal circuit of the DBL, one can show that the charging current waveform measured at the shorted end is staircase-like if a constant voltage source is used. This ideal current waveform is shown in Fig. 2(a). In this case, the height and duration of each current step is V_o/Z_o and $\tau = 2l/v$, respectively, where v is the traveling wave velocity in the transmission line. If the period of the current charging time is T_{ch}, the final charging current, I_o, in the DBL is multiplied as

$$I_o = (T_{ch}/\tau)(V_o/Z_o). \tag{1}$$

The prepulse, which is the voltage appearing across the load resistance in this charging period, is found to be $V_o/2$. The charging current may be decomposed into a positively traveling wave (PTW), I^+, and that of a negatively traveling wave (NTW), I^-, where $I^+ = I^- = I_o/2$ and their corresponding voltage waves are $V^+ = -V^- = I_oZ_o/2$. It can be readily shown (see [3]) that as soon as the switch is opened a square output pulse with $V_{out} = I_oZ_o/2$, $I_{out} = I_o$, and $\tau = 2l/v$ is produced. This ideal output voltage waveform with the prepulse is shown in Fig. 2(b). During this pulse forming period, τ, the voltage across the switch, V_{sw}, is the sum of the voltages of two traveling waves, V^+ and V^-, and the voltage across the capacitor

$$V_{sw} = V^+ + V^- + v_c(t) = I_oZ_o + v_c(t) \tag{2}$$

where $v_c(t)$ is the voltage of the capacitor, C, and $V^+ = V^-$

1041-1135/92$03.00

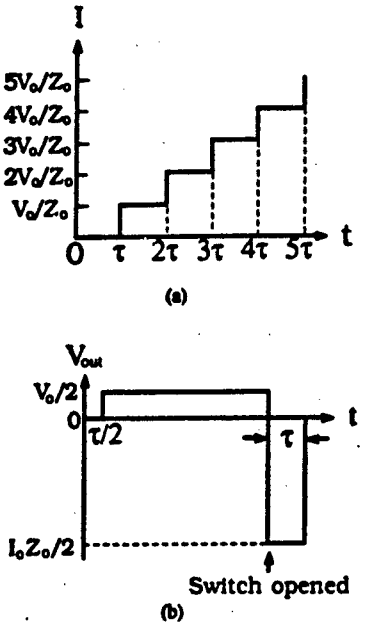

Fig. 2. Depiction of the theoretical waveforms in the dual of the Blumlein line (DBL). (a) The charging current waveform; (b) the output voltage waveform where $\tau = 2l/v$ is the round trip time of the electromagnetic wave.

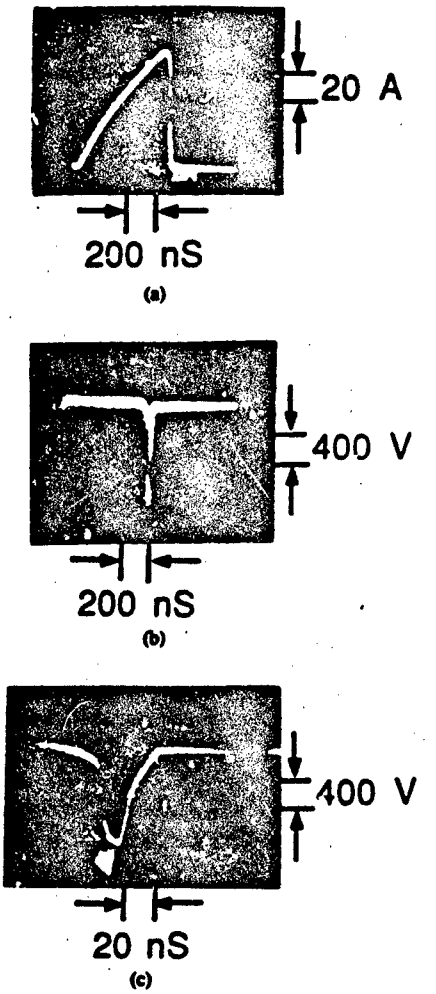

Fig. 3. Experimental results obtained with the GaAs p-i-n diode switch operated at 200 V. (a) The charging current waveform, (b) the output voltage waveform with the prepulse, (c) the main output pulse voltage waveform shown in a faster time scale.

$= I_0 Z_0/2$. As a result, the voltage across the switch during this period is approximately twice the output voltage.

In the experiment, the switch is initially opened and the capacitor C is charged. Upon activating the switch by the laser pulse, the capacitively stored energy is transferred to the inductive energy in the DBL. The charging current waveform at $V_0 = 200$ V is shown in Fig. 3(a). Although the staircase-like waveform is not clearly shown in Fig. 3(a), an oscillogram for the same current waveform with a faster time scale confirms such a waveform with the predicted height and duration. Equation (1) with $\tau = 15$ ns predicts the charging current in the ideal case at the end of $T_{ch} = 540$ ns to be $I_0 = (540/15\ \text{ns})(200\ \text{V}/50\ \Omega) = 144$ A. However, the charging current shown in Fig. 3(a) reaches only 75 A. This is because the actual switch on-resistance and the capacitance are finite. For the purpose of estimating the charging current, the circuit may be treated as an RLC circuit with $L = 0.75$ μH, the total inductance of the DBL, and R, the switch on-resistance. By solving the second order differential equation for the current waveform and using the best fit for the experimental data, the switch on-resistance is estimated to be less than 2 Ω.

The output voltage waveforms from the DBL at a charging voltage, $V_0 = 200$ V, are shown in Fig. 3(b) and (c). The peak voltage pulse reaches 1.3 kV, which is less than the expected value, $I_0 Z_0/2 = 75 \times 50/2 = 1875$ V, for the ideal case. This is attributed to a dynamic switch opening process. In this process, it is estimated that the resistance of the PCSS is evolved from less than 2 Ω to a few kΩ in tens of nanoseconds. The amplitude of the prepulse is measured to be 100 V [Fig. 3(b)] which agrees to the expected value $V_0/2$. The duration of the output voltage pulse is ~ 15 ns which corresponds to the round trip time of the wave in the 1.5-m-long transmission line [Fig. 3(c)]. The voltage gain may be defined as the ratio of the output pulsed voltage to the charging voltage. The resultant voltage gain for this experiment is 6.5.

It was found in the previous current charged transmission line experiments [4] that there exists a limiting electric field of ~ 4.8 kV/cm across the switch. If the field resulted from (2) exceeds this value, it will cause the switch failure. This field is equivalent to the "lock-on" field in the closing switch experiments [6]. If the same limiting field is assumed, the maximum voltage across this 5 mm cube switch would be ~ 2.4 kV, and thus the maximum achievable output voltage would be 1.2 kV, assuming $v_c = 0$ V in (2). The measured highest output voltage of 1.3 kV is an evidence of such a limiting field. Thus, the maximum output pulsed power is limited by the switch to $P_{out} = (1.3\ \text{kV})^2/25\ \Omega = 67.6$ kW.

In conclusion, kilovolt square pulse generation by a DBL, a new inductive energy pulse forming line system, with a GaAs p-i-n diode PCSS has been demonstrated for the first

time. A simple method of pulsed current charging by a charged capacitor is employed, and the resultant staircase-like charging current waveform is observed. The maximum obtained power, which is limited by the switch in this experiment, is 67 kW.

ACKNOWLEDGMENT

The authors wish to thank A. Rosen of the David Sarnoff Research Center for providing the GaAs p-i-n diode switch.

REFERENCES

[1] A. Guenther, M. Kristiansen, and T. Martin, Eds. *Opening Switch*. New York: Plenum, 1987.

[2] K. H. Schoenbach, M. Kristiansen, and G. Schaefer, "A review of opening switch technology for inductive energy storage," *Proc. IEEE*, vol. 72, pp. 1019-1039, 1984.

[3] M. J. Rhee, T. A Fine, and C. C. Kung, "Basic circuits for inductive-energy pulsed power systems," *J. Appl. Phys.*, vol. 67, pp. 4333-4337, 1990.

[4] E. E. Funk, E. A. Chauchard, M. J. Rhee, and C. H. Lee, "80-kW Inductive Pulsed Power System with a Photoconductive Semiconductor Switch," *IEEE Photon. Technol. Lett.*, vol. 3, pp. 576-577, 1991.

[5] A. Rosen, P. J. Stabile, A. M. Gombar, W. M. Janton, A. Bahasadri, and P. Herczfeld, "100 kW DC-biased, all semiconductor switch using Si p-i-n diode and AlGaAs 2-D laser arrays," *IEEE Photon. Technol. Lett.*, vol. 1, pp. 132-134, 1989.

[6] F. J. Zutavern, G. M. Loubriel, M. W. O'Malley, L. P. Shanwald, W. D. Helgeson, D. L. McLaughlin, and B. B. McKenzie, "Photoconductive Semiconductor Switch Experiments for Pulsed Power Applications," *IEEE Trans. Electron Dev.*, vol. 37, pp. 2472-2477, 1990.

Appendix D

INDUCTIVE ENERGY STORAGE SYSTEMS AND PHOTOCONDUCTIVE SEMICONDUCTOR OPENING SWITCH

by

Chun Chieh Kung

Dissertation submitted to the Faculty of the Graduate School
of The University of Maryland in partial fulfillment
of the requirements for the degree of
Doctor of Philosophy
1992

Advisory Committee:

Professor Chi H. Lee, Chairman/Advisor
Professor Moon-Jhong Rhee, Co-Advisor
Professor Julius Goldhar
Professor James R. Anderson
Associate Professor Ping-Tong Ho

ABSTRACT

Title of Dissertation: INDUCTIVE ENERGY STORAGE SYSTEMS AND PHOTOCONDUCTIVE SEMICONDUCTOR OPENING SWITCH

Chun Chieh Kung, Doctor of Philosophy, 1992

Dissertation directed by: Dr. Chi H. Lee
Professor
Electrical Engineering Department

Because the energy storage element in an inductive system has a low resistance value in the dc regime, high charging current with a low charging voltage is expected. Thus, the problems of which a capacitive system suffers the most, such as high voltage insulation and requiring voltage stepup device, do not exist in the inductive system. Moreover, the energy density in current is higher than in voltage, so the size of an inductive system is smaller than that of a capacitive system. However, the switch in the inductive system, which is called the opening switch, is the key element retarding its development. This is owing to the switch requirements which are a low on-state resistance and a long conducting period to build up a high charging current as well as a fast opening time and high voltage hold-off ability for generating a high-power pulse. In this case, those conventional opening switches suffer at least one of the drawbacks such as single shot operation, triggering jitter, non-controllable conduction time, slow opening time, etc. Because of such a limited capability of the existing switches, the development of high power photoconductive semiconductor switches (PCSS's) in this application has been prompted.

Since the switch is laser activated, it can have a jitter free triggering. As the switch is turned off by terminating the laser illumination, its turn-off time can be determined by either the carrier recombination time inside the switch or the optical pulse fall-time, whichever is slower. Hence, its conduction period

is controllable and its opening time can be on the order of nanosecond. This makes the PCSS be the fastest opening switch among all the existing ones.

In this work, the pulse forming theories in the dual of the *LC* generator, the current charged transmission line (CCTL), and the dual of the Blumlein line (DBL) which are charged with a voltage source are discussed for the first time. Furthermore, we have demonstrated the feasibility of using a 5 mm cube GaAs p-i-n diode PCSS to generate multi-kilovolt pulses from the CCTL and the DBL. These experimental results clearly illustrate that the PCSS can be treated as an ideal opening switch when it is activated by a nearly square laser pulse. Also, the potential of employing the PCSS in these two inductive systems to obtain voltage/power gain through electrical pulse compression has been realized for the first time. By combining the experimental waveforms with an appropriate circuit model, the switch dynamic resistance during the closing and opening period has been computed and analyzed. The calculated results strongly suggest that the switch on-resistance can be as low as few ohms and the abnormal conduction of the switch during the opening stage might be related to the "lock-on" effect observed in the closing switch experiments. The details related to this abnormal conduction still requires further investigation.

ACKNOWLEDGEMENT

First, I like to thank my parents who gave me their encouragement and spiritual support unselfishly. In this work, I would like to thank everyone, especially Dr. Chi H. Lee and Dr. M. J. Rhee who served as my project advisor. I would also like to thank Dr. E. A. Chauchard who guided and taught me so much in the experimental work. Other staff in the laboratory as Dr. C. S. Chang, Dr. B. Thedrez, Dr. L. Yan, Dr. M. G. Li, Dr. W. L. Cao, Mr. E. E. Funk, Mr. D. Butler, Mr. Y. Q. Liu, Mr. P. S. Cho, Mr. S. L. Huang, Mr. S. Saddow, Mr. L. Golob, and Mrs. J. D. Ling who gave me a lot of valuable suggestions, I would like to thank them too. In these years, I have gained a lot of knowledge from the faculty members in my major and minors as well as have obtained tremendous assistance from the staff members in the Electrical Engineering Department, I would like to express my deepest appreciation to them.

The support of the electronic and machine shop which are run by Mr. R. Sumner, Mr. S. Mehrotra, Mr. V. Rinker, and Mr. R. Siebel were very helpful to my research work, I would like to show my gratitude to them. As for the title, I like to thank myself who have devotedly spent 6 full years to accomplish all the requirements towards this fantasy.

Finally, I would like to acknowledge Dr. A. Rosen at the David Sarnoff Research Center, who provided me the GaAs p-i-n diode switches. This research project were supported by the Air Force Office of Scientific Research and the Strategy Defense Initiative Organization/Office of Naval Research.

TABLE OF CONTENTS

LIST OF FIGURES

CHAPTER 1

Introduction and Historical Overview

A wide range of applications for high power electrical pulses has stimulated the rapid development of electrical pulsed power systems (PPS's) in the past few decades [1]-[3]. In order to compress the electrical pulse, long charging time to store the energy in the system and short discharging time to transfer the energy to the load are required. Thus, the switch plays an important role in the process of pulse formation. In 1972, the discovery of the picosecond photoconductive effect by Jayaraman and Lee [4] led to the development of ultrafast semiconductor switches. This development is due to the fact that the optically controlled photoconductive semiconductor switches (PCSS's), upon being activated by a well-defined laser pulse, can be precisely triggered and operated without jitter [5]. All other conventional switches, such as the spark gap, avalanche diode, and SCR, which are triggered by either a voltage pulse or a current pulse, always suffer from some degree of jitter. The unique characteristic of jitter free operation opens the door for a wide variety of applications. The PCSS's have been applied in two major categories. First, the PCSS is used to generate ultra-short pulses in the picosecond or femtosecond regime for high speed communication, waveform sampling, and system analysis purpose [6]-[8]. Second, the PCSS is used to generate high power pulses in the multi-kilowatt or even megawatt range for radar, microwave generation, and weaponry applications [9]-[11].

In the 70's, Si was the material commonly used in the PCSS [12]-[14]. However, due to its long carrier lifetime and serious thermal runaway problem, Lee pointed out that the Si switch was not suitable for high repetition rate and high power applications [15]. As discussed in the Ph.D. dissertation of C. S. Chang's [16], the Si PCSS was used in several pulse forming networks, such as the voltage charged line pulser, Blumlein line, and frozen wave pulse generator. In spite

of the drawbacks, the fabrication processes for Si switch are very mature and the physical properties are well understood. Hence, research on the Si PCSS continues [11],[17],[18]. Upon the discovery of the picosecond photoconductive switching effect in GaAs in 1977 [15], much research work shifted to developing GaAs PCSS's. As soon as Mourou et al. demonstrated that GaAs could be used as a high power switch [19], it was realized that GaAs was immune from thermal runaway owing to its short carrier lifetime and high dark resistivity. Thus, multi-kilovolt square pulse generation using the GaAs switch was pursued, and was first achieved by Lee et al in 1981 [20]. In 1984, Nunnally and Hammond reported that a 2.5-cm-long bar of single-crystal, high resistivity silicon with a 0.5 × 0.5 cm cross section was able to hold off 150 kV pulsed bias voltage. Upon activating the switch with nanosecond laser pulses, they could successfully generate 100-kV, 1.8-kA electrical pulses [21]. Due to this demonstration, the pulsed power community became aware of the capability and scalability of the PCSS's in high power switching application.

In addition to no jitter and scalability, PCSS's also possess other unique features such as low inductance, fast rise-time (closing time), high repetition rate, fast recovery time (fall-time, opening time), and bulk conducting for high current operation [10]. Because of these unique properties, research works relating to the PCSS's are enhanced. For example, the group at the Sandia National Laboratory is able to switch electrical pulses as high as 120 kV and 4 kA from silicon or GaAs switches [11]. In order to reduce the contact resistance and the leakage current, p-i-n diode switch was first suggested by Rosen et al. at the David Sarnoff Laboratory [22]. They reported that a Si p-i-n diode switch which was activated by a two-dimensional laser diode array was capable of switching out megawatt pulses. Other than semiconductor materials, wide bandgap but high mobility materials such as diamond and ZnSe were suggested by Ho, Lee, and Goldhar at the University of Maryland [23]-[27]. They demonstrated that diamond, which has very good thermal conductivity, can withstand a field

strength up to 1 MV/cm. They have also shown that polycrystalline ZnSe which is inexpensive can hold off at least 100 kV/cm. Unfortunately, short wavelength laser pulses, of which the techniques are still under development, are required to generate the carriers in diamond and ZnSe.

Regarding this research work, the main focus is on the high power application of the PCSS's. However, the work is unique in that the PCSS is not used in the conventional fashion to charge and discharge a capacitive energy storage system, but to charge and discharge an inductive energy storage system. In this case, the switch is called the opening switch and its function is to abruptly interrupt the charging current in the inductive element to generate a high voltage pulse. The advantages of the inductive energy storage system are its compactness and low charging voltage as compared to the capacitive energy storage system. In Chapter 2, some detailed descriptions of these two energy storage systems and their differences are presented. For the purpose of charging and discharging an inductive system efficiently, an ideal opening switch should have the following characteristics [28]:

1. long conduction time for charging the system,
2. large currents (low loss) during the charging cycle,
3. fast rise of impedance during the opening stage to obtain a high di/dt value,
4. jitter free,
5. high impedance when opened,
6. high hold-off voltage,
7. fast recovery (high repetition rate).

At present, the properties of existing opening switches fall far from these requirements. In fact, their greatest shortcomings are the fast rise of impedance and fast recovery. Also, they suffer from jitter problem to a certain degree. For illustrating these drawbacks, several conventional opening switches are briefly introduced and compared in Chapter 2. Furthermore, several important factors, which are from the circuit structure and the properties of PCSS's, are

used to justify the PCSS's as the most suitable candidate for the opening switch application.

Because of the slow rise in impedance and slow recovery of the conventional opening switch, one of the main objectives in this research is to demonstrate the fast opening capability of the PCSS in an inductive circuit. This results in using the material with a short carrier recombination time (carrier lifetime). In other words, this is the same switch requirement for generating ultra-short electrical pulses. In this case, the surface conducting effect is much more important than the bulk conducting effect and the switch efficiency is not the major concern. Therefore, single photon direct absorption which incurs a shallow penetration depth is more desirable than the absorption process accompanying with a deep penetration depth. In order to further decrease the carrier lifetime, the switch surface is usually bombarded with heavy neutrons [29] or protons [30] to increase the number of surface defects. Even though the results obtained from the pulse forming experiments display a 1-ns opening time, the efficiency of these switches is much less than our expectation. Hence, the main purpose of generating high power pulses can not be attained.

To overcome this shortcoming, effort has been devoted to investigating the switch efficiency. It is believed that the carrier mobility in the switch materials needs to be as high as possible. In addition, the bulk conducting effect is more favorable than the surface conducting effect. This leads to the usage of two photon direct absorption or single photon absorption by impurity states. In this case, the penetration depth of the laser light is deeper and the bulk conducting effect in the switch can be utilized. In order to preserve the carrier mobility, intrinsic materials are preferred in this application. The fundamental issues in switch physics, which are important to predicting the performance of an inductive system and in selecting suitable materials for this purpose, are discussed in Chapter 3.

According to the experimental results, the switch on-resistance can be $\sim$1

Ω. This prompts us to suspect that the contact resistance may be the primary factor affecting this resistance. Thus, minimizing the contact resistance through metal vapor deposition might be vital for maximizing the charging current in the inductive systems. The details regarding the evaporation procedure and some pertained benefits, such as engineering the electrode pattern and increasing the surface flash-over distance, are presented in Chapter 3. Other than these issues, several different switch materials, such as Si, GaAs, Cr:GaAs, diamond, polycrystalline ZnSe, high T_c superconductor, and graphite, are compared and discussed for this purpose as well.

Merely having the basic switch physics is not sufficient to determine the performance of inductive systems and to interpret the experimental data. In other words, we also need to understand the pulse forming theories in the inductive systems. In Chapter 4, possible output pulse shapes with different circuit parameters in three different lumped inductive systems are carefully derived and explained. These lumped circuits are the simple *RL* circuit, the parallel *RLC* circuit, and the dual of the *LC* generator [31]. For fast high voltage pulse generation, short-circuited transmission lines are used to replace inductors. In this work, two transmission line circuits, the current charged transmission line (CCTL) and the dual of the Blumlein line (DBL) [31], are discussed in great detail in Chapter 5. However, the inductive systems discussed in Chapter 4 and 5 are not charged with current sources but charged with voltage sources. Since the internal resistance of an ideal inductive element is zero, the final charging current in the circuit with an ideal switch is independent of the voltage source but depends on the switch closing time. If this closing time is long enough, the voltage pulse being switched out will be much higher than the voltage source and large amount of voltage gain will be achieved. This compactness in size with the potential of the electrical pulse compression is the major advantage of using the inductive energy storage system. In Chapter 5, this unique feature of the CCTL and the DBL is discussed and several differences between these two

circuits are brought up.

In the next three chapters, Chapters 6, 7, and 8, the experimental setups and the corresponding results of this research are presented. As mentioned before, most of the conventional opening switches suffer from slow rise of impedance and slow recovery, thus the first task in this research is to demonstrate nanosecond opening time of certain PCSS's in an inductive circuit. In this experiment, the laser system used was an Ar^+ laser at 514 nm wavelength. Since the photon energy is higher than the band gap energy, single photon direct absorption occurs and the surface conducting effect is utilized. According to the experimental results, we have demonstrated a 10-Hz operation by using several PCSS's with the opening time less than 1 ns [32]. The details regarding these experiments are discussed in Chapter 6.

However, these experiments have proven the inefficiency of using the surface conducting effect to lower the switch on-resistance and the importance of the laser pulse fall-time [33]. Since the switch on-resistance is the key factor in determining the charging current in the inductive circuit, much effort is focused on lowering the switch on-resistance. In this work, two important changes have been made to the original setup. The first change is to adopt a 1 μm wavelength pulsed laser in order to generate carriers deeper into the switch and to further lower the switch on-resistance. The second change is to employ bulk switches to replace microstrip line switches in order for high power handling capability. In this case, we are able to switch out kilovolt pulses from a voltage charged line pulser with the switch on-resistance as low as 1 Ω [34]. These experimental results are shown in Chapter 7.

With the success in lowering the switch on-resistance, the next task is to use a well-defined laser pulse shape at 1 μm wavelength to activate the switch. There are two requirements for this well-defined laser pulse shape. First, it has to be a few hundred nanoseconds or longer in duration in order to charge the inductive element in the circuit with sufficient current. Then, its fall-time has

to be few nanoseconds or shorter to interrupt the charging current in order to obtain a high di/dt value. Two Nd:Glass laser systems employing a Pockels cell to shorten the fall-time of the laser pulse are used so that these two requirements can be satisfied [35]-[40]. The detailed descriptions of the laser systems and the pulse forming experiments are in Chapter 8. Based on the experimental results, we are the first research group using the PCSS in a CCTL or a DBL to generate kilovolt output voltage pulses with a voltage gain. The highest voltage gain of ~6.5 is obtained with a 5-mm-cube GaAs p-i-n diode PCSS. The corresponding output peak power in this case is greater than 65 kW.

With this achievement, data analysis is as important as data acquisition. Three different methods are developed to estimate the switch resistance during the pulse forming stage. The first method is to place the switch in a capacitive circuit and then to use the output voltage pulse amplitude to calculate the switch resistance [35]. However, the switch performance in this circuit is different from that in the inductive circuit. Only little information can be obtained from this measurement. The second method is to take the current charged line as a lump inductor and use the series RLC circuit analysis to compute the switch on-resistance from the current waveform. Yet, this analysis fails to describe the dynamic process in the switch [36]. The third method is to combine the data from the charging current waveform and the output voltage waveform so that the dynamic switch resistance can be calculated [37],[38]. In this method, several dynamic switch parameters, such as power dissipation, electric field intensity, and carrier density, can also be calculated. The lowest switch on-resistance for this 5-mm-cube GaAs p-i-n diode switch is found to be ~2 Ω by using the last two methods. Through the data analysis, a switch latch-on effect has been observed in the high voltage pulse forming experiments. It seems related to the "lock-on" effect [11],[41],[42] observed by other groups in the capacitive energy storage systems (closing switch experiments/configurations). All these works regarding the data analysis are also described in Chapter 8.

For the future work, it may be necessary to understand the physics involved in the "lock-on" effect in order to overcome the problem of slow opening at high fields and to achieve higher output voltage. Furthermore, switches with much larger gap are required for scaling up the system to obtain the voltage pulse on the order of few tens of kilovolts or even megavolts. Accordingly, the laser system, which can provide optical pulses with a long duration and a fast fall-time to activate the switch, must be scaled up as well. In addition, switch materials other than GaAs and Cr:GaAs still require further investigation through direct experiments to prove their feasibility in this application. Also, new circuit systems used to generate high voltage pulses such as the dual of the Marx generator and the stack lines might be another direction worth looking into theoretically and experimentally in this future work. All of these issues will be presented in the last chapter.

CHAPTER 2

Pulse Forming Systems and Opening Switches

As mentioned in Chapter 1, the inductive energy storage system is more advantageous than the capacitive energy storage system. To emphasize this point, the simple circuit structure of these two systems is described and compared in the first section. By recognizing the duality between these two systems in circuit theory, the differences of the switch functions in these two systems can be realized. Hence, the difficulties of having an ideal opening switch to operate the inductive system can be clearly seen. In the next section, several conventional opening switches are briefly introduced. Through this introduction, the capability and drawbacks of these conventional opening switches can be comprehended. Thus, the capacitive energy storage systems are still widely utilized for high voltage pulse generation. In the last section, the issue of using high power PCSS's as the opening switches is brought up. The unique features of the PCSS in this application are described and compared to the requirements of an ideal opening switch. The progress and the difficults of this research are addressed in this section as well.

2.1 Basic pulse forming systems

Generally, the pulsed power systems can be categorized into two groups. One is the capacitive energy storage pulsed power system (CESPPS) which stores the energy in the form of an electric field [43]. The other is the inductive energy storage pulsed power system (IESPPS) which stores the energy in the form of a magnetic field [44]. For a relatively slow system, lumped circuit elements and model are used to construct and describe the system. Alternatively, the fast system is constructed with transmission lines and is described by transmission line theory. In terms of the circuit configuration, the IESPPS's are the duals of the CESPPS's [45], therefore one can construct the IESPPS's

directly from the CESPPS's by replacing a capacitance with an inductance, an inductance with a capacitance, a resistance with a conductance, a closing switch with an opening switch, a series connection with a parallel connection, a voltage source with a current source, and vice versa. In this type of overall transformation, the nodal voltage response in the dual circuit is the same as the loop current response in the original circuit, and vice versa.

Conventionally, CESPPS's are commonly used for generating high voltage pulses. They consist of a dc voltage source, a switch and a capacitive element. This capacitive element can be either a capacitor (Fig. 2.1(a)) or an open-circuited transmission line (Fig. 2.1(b)). Usually, the lumped capacitor circuit (Fig. 2.1(a)) is used for a relatively slow system. For example, it can drive a flashlamp for various applications, such as laser systems, copy machines, and cameras. On the other hand, the open-circuited transmission line (Fig. 2.1(b)) is used for square or fast pulse generation. These square or fast pulses are suitable for system analysis, waveform sampling, and microwave generation. As shown in Fig. 2.1, the capacitive element is slowly charged to voltage V_o at a rate determined by the charging resistor, R. The purpose of the charging resistor is to protect the high voltage power supply in case of capacitor failure. Also, it is used to prevent excessive current being drawn when the switch is first closed. During the switch closing period, the stored capacitive energy is transferred to the load resistance. In the lumped capacitor circuit, the output pulse amplitude is V_o and its duration is determined by the $R_L C$ time constant. In the open-circuited transmission line, if the load resistance is $R_L = Z_o$, the matched load, the output pulse amplitude will be $V_o/2$ and its duration will be $2l/v$, where $R \gg Z_o$ and v is the traveling wave propagation speed in the transmission line. Since the most important function of the switch is its closing action, the switch is called the closing switch. The requirements for an ideal closing switch are

1. fast closing time,

2. jitter free,

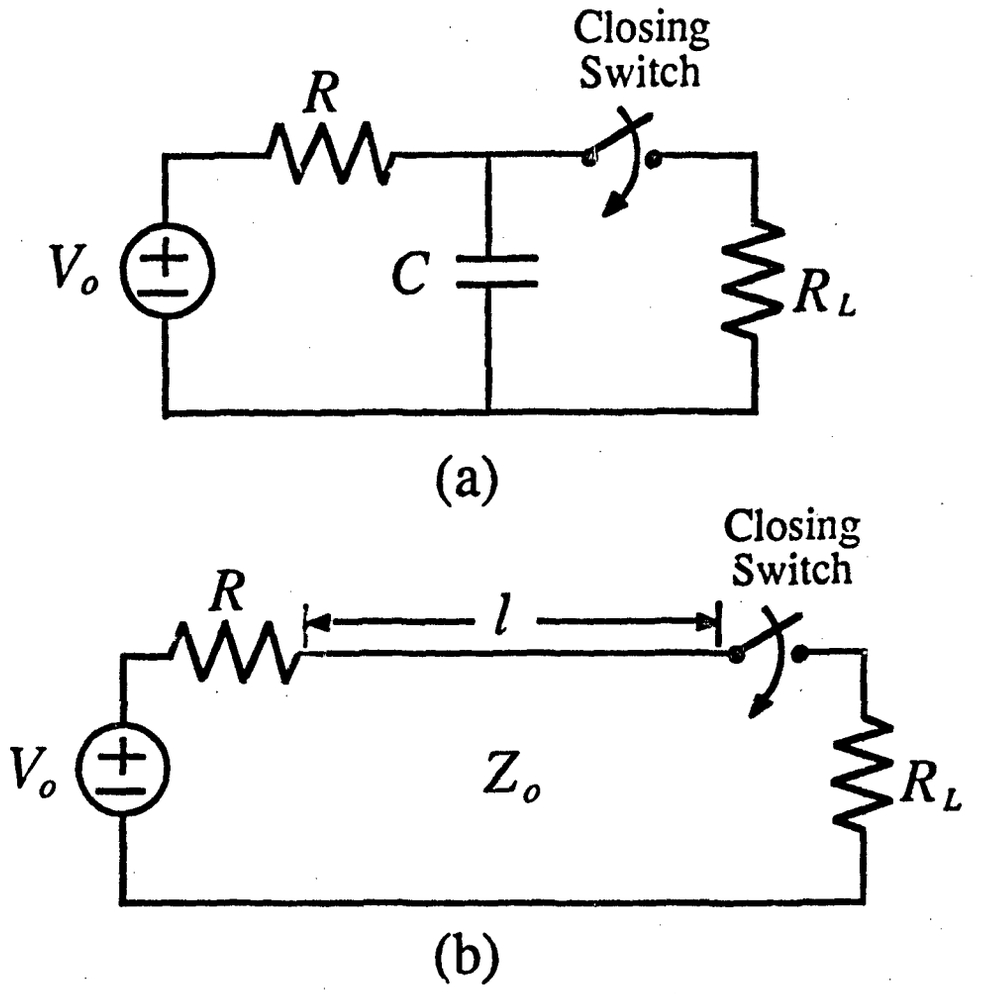

Fig. 2.1. Schematic diagram of a simple capacitive energy storage system. (a) lumped capacitor circuit, $R_L \ll R$; (b) voltage charged line, $R_L = Z_o \ll R$.

3. high hold-off voltage,
4. low on-resistance.

As for the dual of the CESPPS's, the IESPPS's consist of a current source, a switch and an inductive element. This inductive element can be either an inductor (Fig. 2.2(a)) or a short-circuited transmission line (Fig. 2.2(b)). In this configuration, the circuit is charged with current while the switch is closed. In order to generate a high voltage pulse or deliver the stored energy to the load, the switch must be opened as fast as possible to divert the charging current to the load resistance. Since the most important function of the switch is its opening action, the switch is called the opening switch [28],[45]. For the lumped inductor circuit (Fig. 2.2(a)), the maximum output current is the same as the final charging current I_o and the corresponding output voltage pulse amplitude is $I_o R_L$. The fall time of the output voltage pulse is determined by the L/R_L time constant. In contrast, the short-circuited transmission line (Fig. 2.2(b)) with a matched load, $R_L = Z_o$, can generate a square output voltage pulse with an amplitude of $I_o Z_o/2$ and a pulse duration of $2l/v$. This implies that an ideal opening switch should have the following characteristics [28]:

1. long conduction time for charging the system,
2. large currents (low loss) during the charging cycle,
3. fast rise of impedance during the opening stage to obtain a high di/dt value,
4. jitter free,
5. high impedance when opened,
6. high hold-off voltage,
7. fast recovery (high repetition rate).

Because the closing switch is mainly under the influence of a static electric field, it is relatively easy to find suitable dielectric materials and proper triggering methods to satisfy all the requirements listed before. On the contrary, the opening switch is required to sustain a large charging current during its long closing period and to hold off a high induced electric field at its fast opening

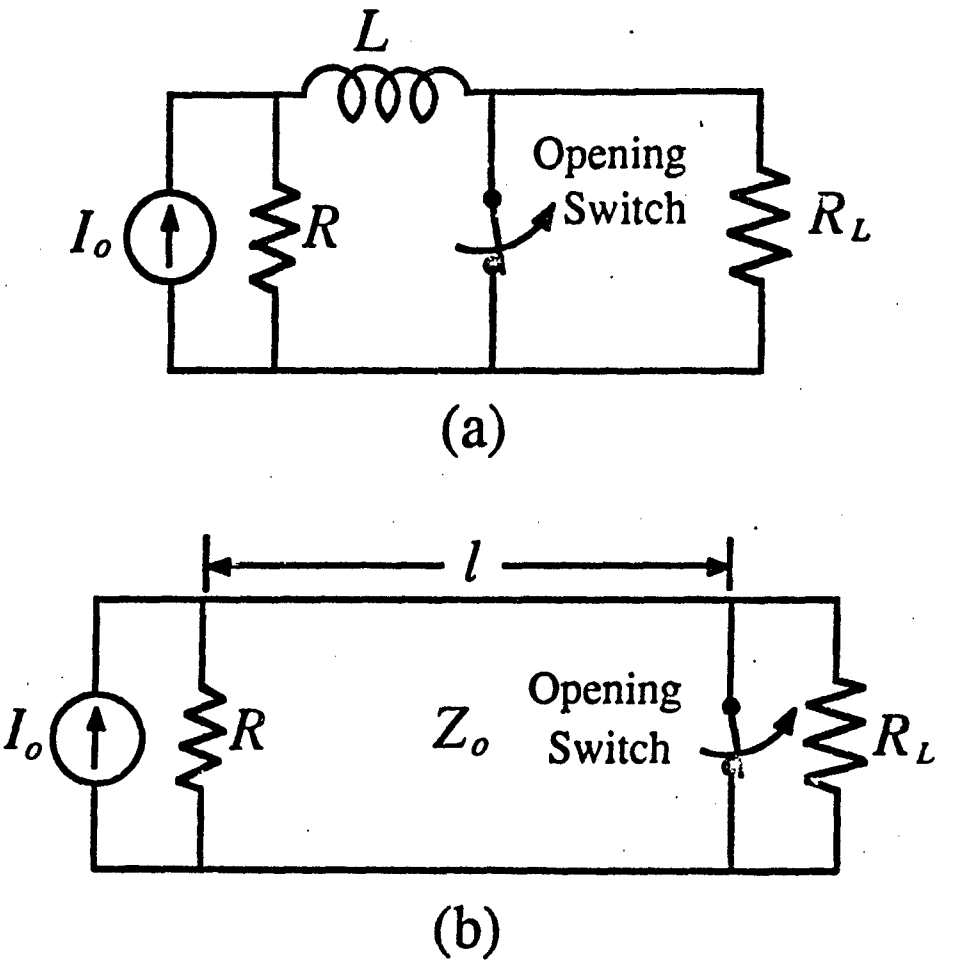

Fig. 2.2. Schematic diagram of a simple inductive energy storage system. (a) lumped inductor circuit, $R_L \gg R$; (b) current charged line, $R_L = Z_o \gg R$.

stage. These are the key factors which make the ideal opening switch difficult to find or manufacture. In the next section, several conventional opening switches are briefly introduced and their drawbacks are summarized at the end. Due to these technological problems in existing opening switches, conventional CESPPS's are still commonly used. However, there are three major disvantages for the CESPPS's; these disadvantages are as follows:

1. The systems are bulky in volume due to the size of the capacitor.
2. The required pulse voltage is usually much higher than a simple voltage source can supply. Thus a voltage stepup device such as a Marx generator, a Van de Graaff, or a high voltage transformer is needed to satisfy this demand.
3. High voltage transmission from the voltage source to the capacitor always complicates the problem of the system insulation.

If the IESPPS with an ideal opening switch can be found, these three problems can be easily solved. This is because the energy storage density of the IESPPS's is much higher than that of the CESPPS's by a scale of 10 to 100 times [28],[47]. In this case, the IESPPS's are much more efficient and less bulky than the CESPPS's. If a voltage source is used instead of a current source to charge the inductive system, the charging voltage can be very low (e.g. few hundred volts) to obtain a large charging current due to the low internal resistance of the inductive element. Accordingly, the voltage stepup device is not required and the problem of insulation for high voltage transmission is solved for the IESPPS's. The detailed analysis for these circuits with the voltage source is shown in Chapter 4 and 5.

In addition, inductive systems with voltage sources have the potential to multiply the peak output voltage/power through electrical pulse compression [35]-[40]. In contrast, the capacitive systems do not have such potential. This is because the output voltage pulse from a simple capacitive system can never exceed the charging voltage through electrical pulse compression. But for a

simple inductive system, as long as it is charged with sufficient current and the switch opening time is short enough, the di/dt value can be very large and most of the stored current can be transferred to the load to produce a giant voltage pulse. In this manner, the switch on-resistance must be as small as possible so that it does not limit the charging current. In order to direct the greatest amount of the charging current to the load in the least amount of time and to achieve the highest di/dt value, the rise of the switch off-resistance has to be very fast. In the ideal case, of zero switch on-resistance and instantaneous switch turn-off time, the charging current is independent of the charging voltage and voltage/power amplification can be very large.

2.2 Conventional opening switches

Based on the above arguments, the IESPPS's are superior to the CESPPS's. Yet the key element that hinders the development of the IESPPS's is the opening switch. In this section, several conventional opening switches are listed and their principle of operation is briefly described.

1. Mechanical circuit breakers

The basic structure of a mechanical opening switch consists of two separate contacts placed in an insulating medium which may be liquid, gas or vacuum. Due to the mechanical restrictions, it can not work at a high repetition rate. Also due to the electrical arcs during the opening stage, it can not have a very fast turn-off time (10's μs) [48].

2. Metal plasma arc switches

They are annular in shape with the cathode at the center and anode surrounding it. The mechanism of opening is based on the separation of its cathode and anode. An applied magnetic field is perpendicular to the paths of the electrons which are straight lines from the cathode to the anode. The purpose of this magnetic field is to bend the electron motion and extinguish the arc in order to decrease turn-off time at the opening stage. The opening time of the switch is in the microsecond range, but it is not very stable [49].

3. Fuses

Fuses are very cheap and easy to make, their interruption process can be as fast as 50 ns and conduction time is determined by the fuse material, dimension, and the surrounding media. Wires and foils embedded in vacuum or in gaseous, liquid, or solid media have been used. The opening mechanism is melting, boiling and vaporization of a metallic conductor to create a highly resistive channel of dense vapor through joule heating. The major drawback of this kind of opening switch is jitter and single shot operation. In other words, the fuse (the opening switch) has to be replaced after each shot [50],[51].

4. Explosive opening switches

In the explosive opening switch, the current is interrupted by using an explosive to break the conductor apart, the opening time is between 10 μs and 20 μs. The explosion is initiated with standard exploding bridgewire detonators. The jitter time is approximate 10 μs. The major disadvantage is single shot operation [52],[53].

5. Thermally driven opening switches

The fundamental principle of the thermally driven opening switch depends on the positive resistive increment with respect to temperature for all the metals. The opening procedure is to heat the switch (actually just a part of the wire) almost to, but slightly lower than, its melting point so as to increase its resistance and hence to interrupt the current. Due to the cooling problem and the variation of the metal characteristics under recycling of heating and cooling, these switches do not have either a high repetition rate or a fast opening time [54].

6. Diffuse discharge opening switches

In the diffuse discharge opening switches, a thermally activated or an optically activated cathode is used to generate electron plasma in order to keep the switch in the conducting state. By means of varying the voltage of the control grid or blocking the optical source, the plasma is interrupted and the switch is quickly turned off. The main advantage is its high repetition rate, but it is

not jitter free due to the ionization process. In addition, the opening time still fluctuates between 10 μs and 20 μs [55],[56].

7. The plasma erosion switch

The plasma erosion switch consists of an anode, a porous cathode, and a plasma-gun array. The plasma-gun array is placed behind the cathode. To turn on the switch, the emitted plasma from the gun array is injected into the switch region through the holes of the cathode. As soon as the plasma is in the switch region which is the space between the cathode and the anode. The plasma will experience a finite voltage gradient. This makes the whole switch behave like a planar diode. In this case, the switch operation can be explained by the Child-Langmuir Law. According to the Child-Langmuir Law, when the current increases, the minimum potential in the electron plasma, which can be lower than the cathode potential, may drop further. Hence the plasma density is decreased near the cathode due to the repellent force from the injected electron plasma. This effect can quickly increase the switch resistance to a limit that may interrupt the current. The main advantage of this type of switch is its opening and closing time which are in the range of 10 ns to 100 ns; but the switch works in an unstable region, jitter and inaccurate triggering problems are very severe [57],[58].

8. Reflex triode switch

The reflex triode switch is based on reflex triode physics. It comprises a primary cathode, a thin anode, and a secondary cathode. All of the electrons are emitted from the primary cathode, they moves back and forth through the anode between these two cathodes. An axial magnetic field is used to minimize the radial loss of electrons. Positive ions are accelerated from the anode to the primary cathode. The electron stream and the counterstreaming positive ion flow make the total current between the anode and the primary cathode much greater than the Child-Langmuir current in a vacuum diode. The switch impedance is thus lowered to a certain value. Turning off this switch can be

achieved by short-circuiting the anode with the secondary cathode in order to stop the back and forth movement of the electrons, this implies that the current flowing through the switch at the opening stage is dominated by the Child-Langmuir current as in a vacuum diode. However, the off-resistance is still quite low, hence the jitter and inaccurate triggering problems are still very crucial [59],[60].

Through the above descriptions, these conventional opening switches have at least one of the following drawbacks:

1. slow turn-off time (0.1 μs-10 μs),
2. single shot operation,
3. short closing period (50 ns-10 μs),
4. low repetition rate (less than 1 kHz),
5. inaccurate triggering.

Because of these existing drawbacks, the capacitive energy storage systems are still the favorite choice in most of pulse forming networks. In order to take the advantage of the inductive energy storage systems, the development of new high power opening switches has become one of the major research topics in the pulsed power community.

2.3 Advantages of photoconductive semiconductor opening switches

By comparing the drawbacks with the requirements of an ideal opening switch, the existing opening switches cannot compress the energy stored in the inductive energy storage systems efficiently. This prompted an immense study on the feasibility of using the PCSS's [11],[12],[21],[41],[61],[62] as the opening switches in IESPPS's. The reason for such an attraction, which is discussed in Chapter 1, is attributed to the prominent features of the PCSS's. In the following, it can be clearly seen that these features match well with the opening switch requirements.

As mentioned before, the principle of the PCSS operation is to use the photoconductive effect [4] in the semiconductor material. Since the switch is

a piece of bulk semiconductor, it can be turned on by illuminating with laser light to generate an electron-hole plasma. Because the electron-hole plasma in the switch behaves like free carriers, the switch is able to conduct current and, hence, the switch resistance is lowered. If the laser light which illuminates the switch is suddenly extinguished, the electron-hole plasma will recombine and the switch will be turned off. In order to have a fast turn-off, the electron-hole plasma must recombine rapidly. Due to the laser light activation through the photoconductive effect, the switch is jitter free. If the laser pulse duration is long enough, it can have a long conduction time to charge the system. In theory, most of the semiconductor materials have a high breakdown electric field and large power handling ability [19]-[21]. Thus the switch, which can be easily scaled up to satisfy the system requirements, is capable of withstanding high voltage and current. According to the experimental results, the turn-off time of the switches can be the same as the carrier recombination time of the semiconductor materials. If the switch were made of Cr:GaAs or Fe:InP, this turn-off time can be faster than 1 ns. As compared to those conventional opening switches mentioned before, this opening time is the fastest among them. Moreover, the switching process for the semiconductor materials is not destructive, the semiconductor switch can be operated immediately after the switching action. Hence, semiconductor switches can not only have an opening time on the order of a nanosecond or subnanosecond, but they also are suitable for high repetition rate applications [5],[15],[63]. The experimental results which demonstrate these properties are described in Chapter 6.

Regarding the PCSS resistance, we have demonstrated that it could change from hundreds of megaohms at the dark state to a few ohms when the switch was activated by a well defined laser pulse of a few millijoules energy at 1 μm wavelength [34]. The details of these experiments are in Chapter 7. Based on these experimental results, the materials which are suitable for this application are GaAs and Cr:GaAs. For example, we have shown that the current charged

transmission line (CCTL) and the dual of the Blumlein line (DBL) with a 5-mm-cube GaAs p-i-n diode switch can be charged to 75 A at 200 V charging voltage and switch out a 1.3 kV pulse for the first time. In this experiment, the estimated switch on-resistance is less than 2 Ω and the switch turn-off process is a fast change from 2 Ω to a few kilo-ohms or higher within tens of nanoseconds. Higher charging current and output voltage pulses have also been observed with higher charging voltages. These results clearly support the feasibility of electrical pulse compression and output voltage/power amplification by using the PCSS in an IESPPS [35]-[40]. These details are discussed in Chapter 8. With all of these experimental results, we can easily conclude that the features of the semiconductor opening switch satisfy all the requirements of the ideal opening switch and overcome most of the drawbacks of the conventional opening switch. In other words, the semiconductor materials are the most suitable candidates for the opening switch application.

2.4 Summary

Fundamental circuit structures of capacitive energy storage pulsed power systems and inductive energy storage pulsed power systems have been introduced. Because of the duality between these two pulsed power systems, they can be described by the same differential equations but with different circuit variables. Because the opening switch, the key element in an inductive energy system, is not well developed, the inductive systems are not widely applied to pulsed power systems, even though the inductive systems have several advantages over the capacitive systems. In order to take the advantage of the inductive systems, several opening switches have been reported in the literature. However, they all have some drawbacks and can not satisfy the requirements for an ideal opening switch. This leads to the development of the high power photoconductive semiconductor switches as the opening switches. The special features of the photoconductive semiconductor switch have been compared with the requirements of an ideal opening switch in this chapter. The experiments to verify

those arguments are discussed in the latter chapters.

CHAPTER 3

Photoconductive Semiconductor Switch

The advantages of using the photoconductive semiconductor switches (PCSS's) as opening switches have been discussed in Chapter 1 and 2. To fully utilize these advantages, fundamental semiconductor switch physics has to be understood. In the first section, the equation for the switch on-resistance is derived from the photoconductive effect. Because the laser pulse duration affects the on-resistance differently, the discussion is divided into two aspects. First, we consider using laser pulses of duration shorter than the carrier lifetime. Then we consider using a cw laser or laser pulses of duration much longer than the carrier lifetime. According to the derivation, the switch resistance is determined by different parameters in these two cases. The results show that the switch resistance is inversely proportional to the laser pulse duration in the former case and is inversely proportional to the carrier lifetime in the latter case. In addition, other effects that might affect the switch conductance are also discussed qualitatively.

As discussed in the previous chapter, the amount of the charging current in the inductive element is one of the major factors in determining the efficiency of an inductive energy storage system. Usually, this charging current is limited by the switch on-resistance. If this on-resistance were lower than a few ohms, it might come from the switch contact resistance. In this case, the contact resistance has to be as low as possible, otherwise the opening switch can adversely affect the performance of the inductive energy storage system. In order to reduce this resistance, metal vapor deposition may be the best solution. This is because the deposition can create a close contact between the metal electrode and the semiconductor surface. If the metal for the deposition is carefully selected, a low ohmic contact resistance can be easily obtained. The details of this

method are described in the second section. In the last section, the properties of several different switch materials are compared. Through the comparison, the materials chosen for the pulse forming experiments are GaAs and Cr:GaAs. The experimental results which demonstrate the potential of these two materials as the opening switch are discussed in Chapter 8. Materials other than these two have also been suggested either by us or by other research groups. However, the experimental results obtained are not very good and they are still under investigations for this application. Some information regarding these materials is briefly introduced in the last section as well.

3.1 Fundamental physics of photoconductive semiconductor switches

In solid state physics, it uses the width of the energy gap to group materials into metal (conductor), semiconductor, and insulator [64]. The energy gap, by definition, is the minimum energy separation between the conduction and valence band. In metal, because the conduction band overlaps the valence band, there is no energy gap and the electrons can move freely to conduct current. In contrast to metal, the energy gap of an insulator can be as wide as several electron volts, thus it is very difficult to excite electrons from the valence band to the conduction band to conduct current. As for semiconductors, their physical properties are between that of metal and insulator. For most of the important semiconductor materials, the energy gap is varying from a few tenths of an electronvolt to 2 eV, so the valence electrons can be excited to the conduction band leaving the holes in the valence band by absorbing either thermal or optical energy [65]. According to this model, the electrons and the holes always appear in pairs and they both behave like free carriers which are able to conduct current. Nevertheless, this is only valid for the intrinsic materials. For the extrinsic materials which are doped with either n- or p-type impurities, the energy absorption process may involve the impurity level. In this case, the free carriers are the majority carriers which are electrons for the n-type materials and holes for the p-type materials respectively. The process of absorbing optical energy

to generate electron-hole pairs or majority carriers to conduct current is known as photoconductivity, which is the basic principle of operation for a PCSS. The model which describes the photoconductive phenomenon is in the following.

Let h be the Planck's constant and ν be the photon frequency, the photon energy E_p is found to be

$$E_p = h\nu \,. \tag{3.1}$$

If this photon energy E_p is greater than the energy gap or the impurity level, the semiconductor can absorb the photon to generate either an electron-hole pair or a majority carrier. This process is referred to as single photon absorption. The only limitation of this process is the uncertainty principle, so it can be as fast as 10^{-15} sec or a few optical cycles [4],[66]. In this process, the conductivity σ of the semiconductor [6],[67] can be expressed as

$$\sigma = q(\mu_n n + \mu_p p) \,, \tag{3.2}$$

where q is the electronic charge, μ_n and μ_p are the mobilities of an electron and a hole respectively, and n and p are the electron and hole densities respectively. As shown in Fig. 3.1, the switch geometry is rectangular and its dimensions are $l \times a \times b$, where l is the switch gap length, a is the width and b is the thickness. In terms of the energy conservation and Ohm's law, the power dissipated in the switch can be expressed as

$$\frac{V^2}{R_{on}} = \int \vec{E} \cdot \vec{J} dv \,, \tag{3.3}$$

where V is the voltage across the switch gap, R_{on} is the switch on-resistance, $\vec{E}$ is the electric field, $\vec{J}$ is the current density, and v is the effective switch conduction volume. The effective switch conduction volume is

$$\mathrm{v} = l \times a \times \frac{1}{\alpha} \,, \tag{3.4}$$

where α is the optical absorption coefficient. Rewriting Eqn. (3.3) with

$$\vec{J} = \sigma \vec{E} \,, \tag{3.5}$$

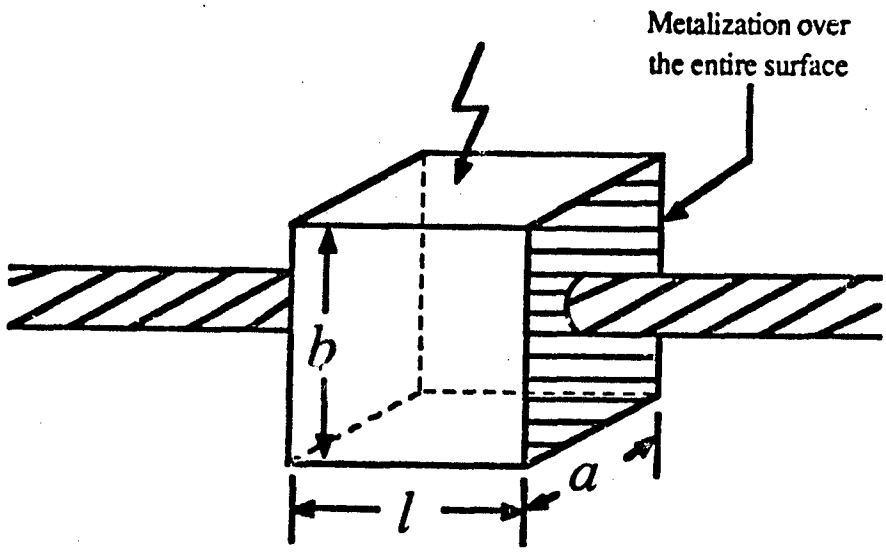

Fig. 3.1. Geometry of a bulk semiconductor switch.

the equation becomes

$$\frac{1}{R_{on}} = \frac{1}{V^2}\int \sigma|\vec{E}|^2 dv \,. \tag{3.6}$$

Assuming that the switch is under the low injection condition, the electric field $\vec{E}$ can be expressed as

$$|\vec{E}| = \frac{V}{l} \,. \tag{3.7}$$

Substituting Eqns. (3.2) and (3.7) into Eqn. (3.6) yields

$$\frac{1}{R_{on}} = \int \frac{q(\mu_n n + \mu_p p)}{l^2} dv \,. \tag{3.8}$$

If the laser pulse duration τ_d is shorter than the carrier lifetime τ_s, the optically generated carrier density N can be shown as

$$N = (1-\Gamma)\eta\alpha\tau_d \frac{W_{pi}(x,y)}{\hbar\omega}\exp(-\alpha z) = \begin{cases} n & \text{n-type material} \\ p & \text{p-type material} \\ n=p & \text{intrinsic material} \end{cases} , \tag{3.9}$$

where Γ is the reflectivity of the photoconductor surface, η is the quantum efficiency of the material at the specific laser wavelength, W_{pi} is the incident optical power per unit area, $\hbar\omega$ is the photon energy, $\hbar = h/2\pi$, and $\omega = 2\pi\nu$. Substituting Eqn. (3.9) into Eqn. (3.8) results in

$$\frac{1}{R_{on}} = (1-\Gamma)\eta\frac{q\tau_d}{\hbar\omega}\frac{\mu}{l^2}\int \alpha W_{pi}\exp(-\alpha z)dv \,, \tag{3.10}$$

where

$$\mu = \begin{cases} \mu_n & \text{n-type material} \\ \mu_p & \text{p-type material} \\ \mu_n + \mu_p & \text{intrinsic material} \end{cases} \tag{3.11}$$

is the dominated carrier mobility. Defining

$$P_{in} = \int \alpha W_{pi}\exp(-\alpha z)dv \tag{3.12}$$

as the total incident optical power, the number of generated carriers N_d by the laser pulse can be expressed as

$$N_d = \frac{(1-\Gamma)\eta P_{in}\tau_d}{\hbar\omega} = \begin{cases} n_i & \text{n-type material} \\ p_i & \text{p-type material} \\ n_i = p_i & \text{intrinsic material} \end{cases} , \tag{3.13}$$

where n_t and p_t are the total number of electrons and holes respectively. By combining Eqns. (3.10), (3.12), and (3.13), the switch on-resistance can be simply expressed as

$$R_{on} = \frac{l^2}{N_d q \mu} . \tag{3.14}$$

On the other hand, if the laser pulse duration is much longer than the carrier lifetime ($\tau_d \gg \tau_s$), the optical generation process will reach steady state [67],[68]. In this case, the generation rate is equal to the recombination rate, so the rate equation for the generated carriers can be expressed as

$$\frac{dN}{dt} = (1-\Gamma)\eta\alpha\frac{W_{pi}(x,y)}{\hbar\omega}\exp(-\alpha z) - \frac{N}{\tau_s} = 0 , \tag{3.15}$$

where N/τ_s is the recombination rate. Hence the carrier density becomes

$$N = (1-\Gamma)\eta\alpha\tau_s\frac{W_{pi}(x,y)}{\hbar\omega}\exp(-\alpha z) = \begin{cases} n & \text{n-type material} \\ p & \text{p-type material} \\ n = p & \text{intrinsic material} \end{cases} . \tag{3.16}$$

Compared with Eqn. (3.9), the only difference in Eqn. (3.16) is replacing τ_d with τ_s. Thus, Eqn. (3.10) can be changed to

$$\frac{1}{R_{on}} = (1-\Gamma)\eta\frac{q\tau_s}{\hbar\omega}\frac{\mu}{l^2}\int \alpha W_{pi}\exp(-\alpha z)dv \tag{3.17}$$

and the number of generated carriers N_s in the steady state becomes

$$N_s = \frac{(1-\Gamma)\eta P_{in}\tau_s}{\hbar\omega} = \begin{cases} n_t & \text{n-type material} \\ p_t & \text{p-type material} \\ n_t = p_t & \text{intrinsic material} \end{cases} . \tag{3.18}$$

This leads to the switch on-resistance R_{on} to be

$$R_{on} = \frac{l^2}{N_s q \mu} . \tag{3.19}$$

As shown in Eqns. (3.13) and (3.18), n_t or p_t is proportional to the total incident optical power P_{in}. This is only true in the condition of low optical intensity. If the optical intensity is strong enough to create a high carrier density, a non-linear effect such as Auger recombination [69] in the semiconductor materials

may severely affect the photoconductivity. In this case, Eqns. (3.13) and (3.18) are no longer valid.

Auger recombination consists of direct recombination between an electron and a hole at a high carrier concentration. Because this recombination is accompanied by transferring the energy to another free hole or free electron, the scattering process is enhanced and the carrier lifetime is reduced. Alternatively, this process can be treated as the inverse process of avalanche multiplication. The Auger lifetime τ_A can be expressed as

$$\tau_A = \frac{1}{GN^2} , \tag{3.20}$$

where G is the Auger coefficient. This Auger coefficient is found to be $\sim 10^{-31}$ cm^6/s for Si [67] and $\sim 10^{-29}$ cm^6/s for GaAs [70] and it is strongly temperature dependent. Including Auger recombination, the carrier lifetime τ_s becomes

$$\frac{1}{\tau_s} = \frac{1}{\tau_c} + \frac{1}{\tau_A} , \tag{3.21}$$

where τ_c is the carrier lifetime determined by the traps and the recombination centers in the material. This clearly suggests that the Auger recombination should be dominant when the carrier density in Si or in GaAs exceeds $\sim 10^{19}$ cm^{-3}. Hence, the switch on-resistance can not be further lowered under this condition.

Another key factor in determining n_t or p_t in Eqn. (3.13) and (3.18) is surface recombination [71]. Surface recombination is due to the high density of surface states at the semiconductor surface. This high density of surface states is directly from the discontinuity of the crystal structure at or near the surface. Since these surface states act like recombination centers for the free carriers, the carrier lifetime is decreased and the total number of free carriers is saturated; thus it is difficult to lower the switch on-resistance.

Experimental observation indicates that it is not possible to lower the on-resistance to less than 100 Ω [35] by using the laser with photon energy greater

than the energy gap (single photon direct absorption) to activate the switch, even though the quantum efficiency η reaches 100% and the optical intensity is very high. The reasons for this high switch on-resistance can be easily attributed to the shallow penetration depth ($1/\alpha \ll 1$ μm) of single photon absorption. Because the electron-hole pairs are only generated near or at the surface, the surface recombination effect is enhanced and the effective conduction volume v is reduced. Due to this confined volume, the carrier density might become so high that Auger recombination cannot be neglected. Thus, the switch on-resistance can remain high when the single photon direct absorption is used.

To ease the effect of surface recombination, long wavelength lasers with photon energy below the band gap energy are preferred [4],[20]. Since the laser intensity in the experiment is not enough to incur two photon direct absorption, the optical generation process is mainly dominated by the impurity levels in the semiconductor material. This implies that the quantum efficiency may be reduced while the penetration depth is drastically increased. As shown in Fig. 3.2, the penetration depth for GaAs at 1 μm laser wavelength can be as deep as a few millimeters [72]; therefore the effective switch conduction volume v would be increased. If the switch is few millimeters thick, the volume v, which can be considered as the switch volume, will become

$$\mathrm{v} = l \times a \times b \,. \tag{3.22}$$

Geometrically, this larger volume corresponds to a lower carrier density N and, therefore, less carrier-carrier scattering. Thus, Auger recombination can be totally neglected and surface recombination becomes very unimportant. Accordingly, the switch on-resistance can be sharply reduced to a few Ohms.

Beside the switch on-resistance, the switch opening time is also an important factor in determining the performance of an opening switch. In order to obtain a large di/dt value, the switch opening time must be as short as possible. For the PCSS, this time is determined by the lifetime of the photo-generated carriers after the laser light is extinguished. Since the equilibrium environment

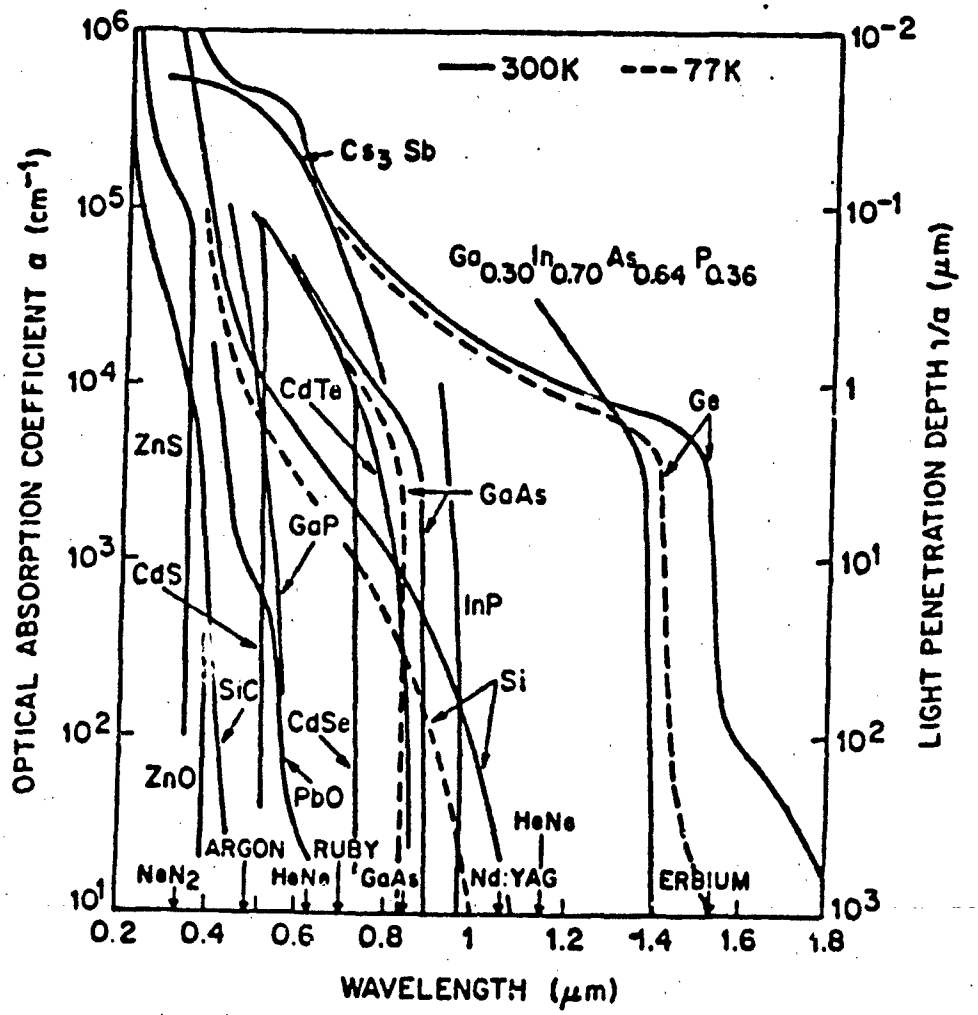

Fig. 3.2. Absorption coefficient of several semiconductor materials with respect to the optical wavelength [72].

has to be established between the lattice and the free carriers (electrons and holes), the recombination process is always much slower than the optical generation process [15],[20]. For example, the carrier lifetime of intrinsic Si is ~10 μs and of intrinsic GaAs is ~7 ns. In the first order approximation, it is assumed that the bulk conducting effect is dominated and the carrier density is relatively low. This implies that the recombination process is mainly governed by the traps and the recombination centers in the material. Surface recombination and Auger recombination in this case can be neglected. In other words, the carrier lifetime τ_s of the electron and hole in the material [67] can be estimated by

$$\tau_s = \tau_c = \frac{1}{N_t \sigma_c \langle v_{th} \rangle} , \tag{3.23}$$

where N_t is the density of the trap or the recombination center, σ_c is the capture cross section of the electron or hole, and $\langle v_{th} \rangle$ is the mean thermal velocity. As shown in Eqn. (3.23), the carrier lifetime τ_s is inversely proportional to N_t. Therefore, τ_s is decreased with higher N_t. This suggests that there are two methods which are frequently used for speeding up the recombination process. One is to introduce a moderate density of lattice defects in the semiconductor material through high energy particle irradiation. The other is to dope the semiconductor material with mid-energy gap impurities to increase the number of recombination centers. Moreover, one can even directly use materials with large densities of naturally occurring defects such as polycrystalline and amorphous semiconductors.

Other than the short switch opening time, a good opening switch also requires a long conduction time. To achieve this purpose, laser pulses much longer than the carrier lifetime are then needed for activating the PCSS. This implies the use of Eqns. (3.18) and (3.19) to describe the switch on-resistance. As shown in these two equations, the carrier lifetime τ_s is proportional to the generated carriers, N_s, and inversely proportional to the switch on-resistance, so this short carrier lifetime might detrimentally affect the switch on-resistance. This suggests that higher optical intensity is required to obtain a lower switch

on-resistance for materials with a large number of defects or high doping level of mid-gap impurity states. Based on the earlier discussion, the use of high optical intensity to activate the switch might result in invoking the side effect of Auger recombination. In order to achieve good switching performance, the carrier lifetime in the semiconductor material has to be optimized. In Chapter 7, the comparisons of the switch on-resistances between an intrinsic GaAs switch and a Cr:GaAs switch under the same optical intensity are carried out to support this argument.

3.2 Switch electrode design and fabrication procedures

In the structure of an inductive energy storage system, the energy storage device is a short-circuited element in the dc regime. In order to charge the system with as much current as possible, the switch must have a very long conduction time and zero on-resistance. However, finite switch on-resistance is always expected and thus limiting the amount of the charging current through Ohm's law. In Chapter 7, it will show that the on-resistance of a photoconductive semiconductor switch can be reduced down to a few ohms. In this case, the contact resistance between the wire and the unprocessed semiconductor surface might be the major contributor to this on-resistance [73]. To reduce this resistance, several methods have been employed.

The simplest way to bond the wire is to use silver paint or silver epoxy to glue the wire directly to the semiconductor surface. The silver paint (SC 12, Micro-Circuits Company) is a suspension of fine silver powder and banana oil, it can be dried in air within 40 minutes and the conductivity can be very high after being dried. If any mistakes were made while applying it to the surface, it could be easily washed away by acetone. However, the mechanical strength of the silver paint is very poor, any vibration may severely affect the attachment. In order to overcome this drawback, silver epoxy might be a better substitute, but it takes too long to cure and is difficult to remove after being dried. The major disadvantage for using this simple method is that the semiconductor surface

on-resistance for materials with a large number of defects or high doping level of mid-gap impurity states. Based on the earlier discussion, the use of high optical intensity to activate the switch might result in invoking the side effect of Auger recombination. In order to achieve good switching performance, the carrier lifetime in the semiconductor material has to be optimized. In Chapter 7, the comparisons of the switch on-resistances between an intrinsic GaAs switch and a Cr:GaAs switch under the same optical intensity are carried out to support this argument.

3.2 Switch electrode design and fabrication procedures

In the structure of an inductive energy storage system, the energy storage device is a short-circuited element in the dc regime. In order to charge the system with as much current as possible, the switch must have a very long conduction time and zero on-resistance. However, finite switch on-resistance is always expected and thus limiting the amount of the charging current through Ohm's law. In Chapter 7, it will show that the on-resistance of a photoconductive semiconductor switch can be reduced down to a few ohms. In this case, the contact resistance between the wire and the unprocessed semiconductor surface might be the major contributor to this on-resistance [73]. To reduce this resistance, several methods have been employed.

The simplest way to bond the wire is to use silver paint or silver epoxy to glue the wire directly to the semiconductor surface. The silver paint (SC 12, Micro-Circuits Company) is a suspension of fine silver powder and banana oil, it can be dried in air within 40 minutes and the conductivity can be very high after being dried. If any mistakes were made while applying it to the surface, it could be easily washed away by acetone. However, the mechanical strength of the silver paint is very poor, any vibration may severely affect the attachment. In order to overcome this drawback, silver epoxy might be a better substitute, but it takes too long to cure and is difficult to remove after being dried. The major disadvantage for using this simple method is that the semiconductor surface

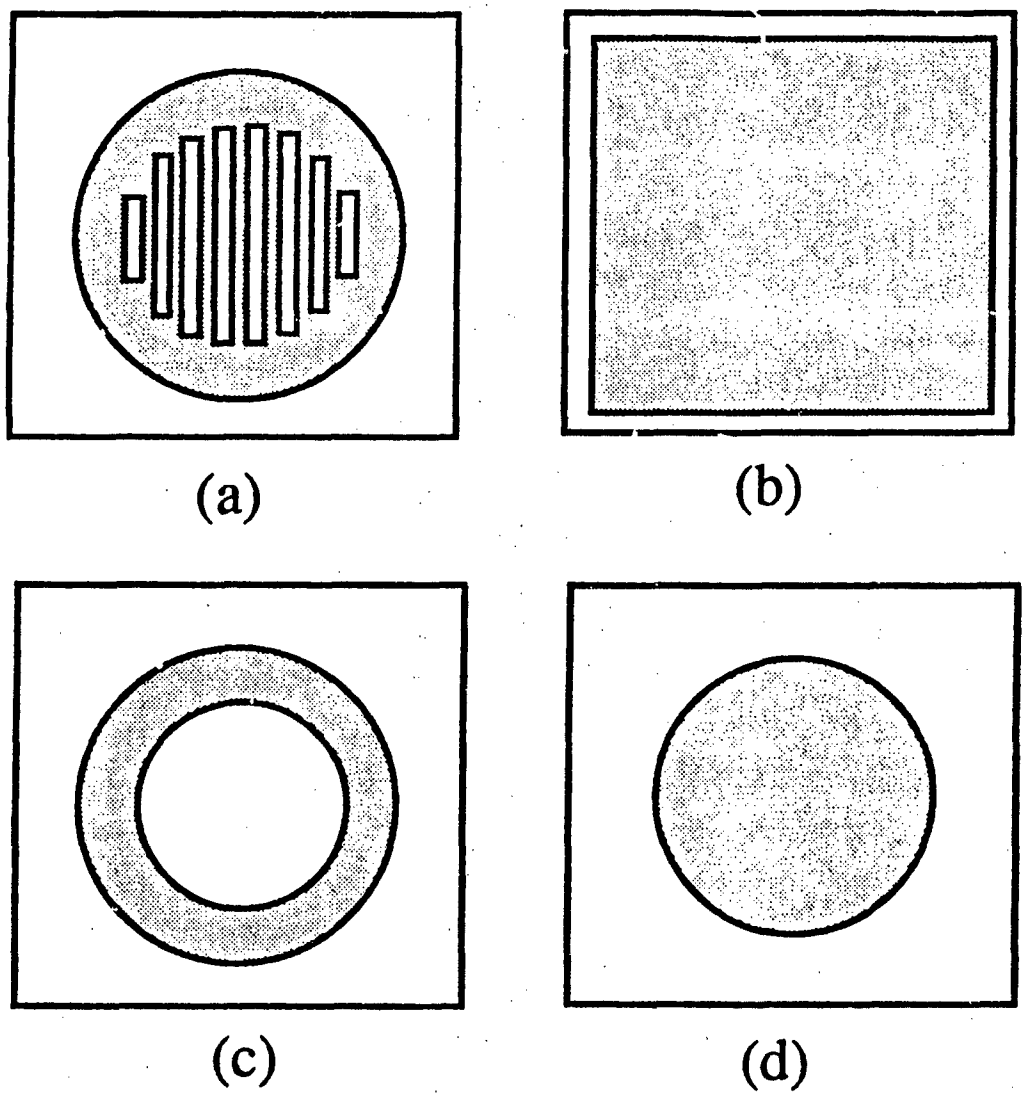

Fig. 3.3. Typical geometries for the switch electrode, the shaded area is deposited with gold. (a) gridded shape; (b) plain shape to cover the whole surface; (c) ring shape; (d) full circle shape.

following, the wafer is dipped in an HF solution (1:1 with water) to remove the oxide layer, and then rinsed with deionized water, and blown dry with N_2. If it is necessary, the wafer can be etched in sulfuric acid and hydroperoxide solution at this point. If the wafer is etched, it must be rinsed with deionized water and blown dry with N_2 again. Afterwards, the wafer is placed in an oven (preset to 130°C) for half an hour to bake out the residual water. The next step is to spin the photoresist on the wafer at an appropriate rate and duration, and then soft bake it in an oven at 90°C for half an hour. After the soft-bake, the wafer is placed under the mask on the mask aligner for exposure. Then we soak this exposed wafer in the developer to reveal the mask patterns on the wafer. Finally, the wafer can be put in the evaporator to deposit the thin metal film. Depending on the material, different metal compounds have to be prepared. For example, for Cr:GaAs or p-type GaAs, we must deposit ~150 Å of Cr first, then ~2000 Å of Au. In contrast, n-type GaAs requires ~750 Å of AuGe alloy first, then ~2000 Å of Au. The next process following the deposition is the lift-off. The lift-off process consists of dipping the wafer in acetone to remove the part of deposition attached to the photoresist so that the remaining gold is in the shape of the mask pattern. If the Au were firmly attached to the surface, the process is accomplished; if not, the whole process has to be repeated. In addition, for an n-type surface deposition, there is still another remaining step, that is surface annealing to alloy the crystal structure between Ge and GaAs. The reason for depositing Cr or AuGe prior to Au is to assure that the subsequent Au deposition can firmly attach to the surface and that an ohmic contact can be formed between these layers [74].

Once the process of deposition for both electrodes is done, the next step is to cut the wafer to the desired size so that it can be used as the switch. The switch leads, which are thin stripes of copper foil, are bonded to the electrodes with either silver paint or indium solder paste. For a gridded or a ring electrode (Fig. 3.3(a) and (c)), the laser light illuminates the switch in parallel with the electric

field which is across the switch (longitudinal illumination). The advantage of this scheme is a higher surface breakdown threshold and thus it can be used to study the internal breakdown phenomenon. The drawback is that the laser light is partially blocked by the electrode during the operation. It is found that the optimal opening [74] for a gridded electrode to maintain a uniform electric field between two electrodes and achieve the best switch performance is 50%. However, the opening for the ring electrode is 100 %; the electric field across the switch is not uniform, so the operation always takes place within a small portion of the ring. For a plain or a solid circle electrode (Fig. 3.3(b) and (d)), the laser light illuminates the switch perpendicular to the electric field between these two electrodes (transverse illumination). The advantage of this scheme is in fully utilizing the laser light. The drawback is in having a much lower surface breakdown threshold. In the following section, the internal breakdown threshold of some semiconductor materials are discussed. According to the discussion, their breakdown fields are all much higher than that of the air.

3.3 Selection of switch materials

As discussed in Chapter 2, a good opening switch should have low on-resistance, high off-resistance, fast opening time, and high voltage hold-off ability. Table I shows that the breakdown fields for the semiconductor materials which have been used as switches are all higher than the air breakdown field (29 kV/cm for dry air) by at least one order. Therefore, these semiconductor materials should be able to hold off high voltage. In this case, the cause of the switch failure can be attributed to surface flash-over and thermal runaway [61]. Surface flash-over, which results in an arc between the two switch electrodes, often occurs at an electric field strength less than the air breakdown field and the material breakdown field. The exact reasons for this low flash-over field are not well understood. Experimental work to investigate this phenomenon has been done by Donaldson et al at the University of Rochester. In their experiment, they tried to study this failure mechanism by placing the semiconductor switch

in a well controlled environment, so that the drastical field change during the flash-over process [75] can be registered and analyzed.

Thermal runaway is due to the leakage current caused by thermally generated carriers under the influence of an electric field. Since this leakage current generates joule heat and this joule heat creates more thermally generated carriers, an increase in leakage current can be expected and more heat would be generated to create yet higher current. Because of this positive feedback process, the switch will gradually lose its high voltage hold-off ability. Generally, this phenomenon might become very prominent when the repetition rate is high. This is because the dissipation of heat is always a slow process. If the repetition rate is high enough, the quick accumulation of heat with a slow heat dissipation can aggravate this thermal runaway problem very much. However, in our application, the repetition rate, which is limited by the charging time of the capacitor bank for the laser amplifier, is very low, only one operation every ~3 minutes. Hence, this phenomenon has not been observed in all the switches except in Si switch under a high charging voltage. The reason can be easily attributed to the low dark resistivity and long carrier lifetime of Si switch. If this phenomenon did become an important factor in affecting the switch performance, better cooling methods and pulsed bias would have to be considered for solving the problem. The work to overcome this thermal runaway problem in the Si switch for the pulsed power application has been discussed thoroughly in C. S. Chang's Ph.D. dissertation [16].

Based on the above discussion, Si is not the best candidate for the opening switch application due to its long carrier lifetime and a strong tendency toward thermal runaway [15]. Other than Si, those materials shown in Table I are all suitable for the opening switch application. This is because of their high dark resistivity and short carrier lifetime. As in Table I, this carrier lifetime can be in the picosecond or nanosecond regime. This implies that the switch made of these materials can have an opening time as fast as the carrier lifetime and its

off-resistance can increase to a few kilo-ohms or even few megaohms in this time period. However, the matched laser sources for lowering the on-resistance of a diamond and a ZnSe switch are not readily available due to their wide energy gap. Thus, more intense research is needed to prove the feasibility in the opening switch application for these materials.

Currently, Drs. Goldhar, Ho, and Lee in our group are engaged in the investigation of using diamond and polycrystalline ZnSe as photoconductive switches [23]-[27]. From their study on the nonlinear properties of ZnSe under the influence of a strong electric field, they predicted that electrical pulse compression and voltage multiplication can be achieved at a strong field. In this case, laser pulse shaping which requires the use of a Pockels cell is no longer necessary. As mentioned in Chapter 1, a Pockels cell is used to generate the laser pulse with a fast fall-time. Since the Pockels cell crystal and the driver are very expensive and low in repetition rate, it is more desirable to use a laser system for the opening switch without the need of a Pockels cell. Thus, ZnSe may be a good candidate for the opening switch application. Cho et al. at the University of Maryland have developed a simple circuit model to simulate the nonlinearity in the polycrystalline ZnSe at a strong electric field [76]. From the simulation, they found that the output voltage pulse under certain conditions could be greater than the charging voltage when the switch is in series with an inductance and is activated by a laser pulse with a relatively slow fall-time. This strongly implies that the increase of the switch off-resistance in time in ZnSe switch is faster than the laser pulse fall-time, hence the Pockels cell can be omitted in the laser system. Nevertheless, further experimental work has to be done to verify this switch model and the simulated results. In this respect, GaAs and Cr:GaAs in Table I become the most suitable candidates for making photoconductive semiconductor opening switches. Those experiments with the switches made of these two materials are discussed in Chapters 6, 7 and 8.

Materials other than those shown in Table I are also suggested either by

our group or other groups. They are graphite, high T_c superconductors, Au:Si, and Cu compensated Si doped GaAs. Among them, graphite and high T_c superconductor are suggested by our group. Preliminary experiments on graphite had been conducted. The graphite sample, which is called highly oriented pyrolytic graphite (HPOG), has a unique feature [77],[78]. This feature shows that the HPOG is in a highly conducting state without laser illumination; once it is illuminated by an intense laser pulse, it would undergo a phase transition to become highly insulated. Because its current density can be as high as 160 kA/cm^2 in the conducting state, this makes it an ideal candidate to be used as an opening switch [79]-[81]. For high T_c superconductor [82]-[84], our group is presently engaged in the investigation of its feasibility in this application. Au:Si is suggested by Zutavern et al [85],[86] at the Sandia National Laboratories. They demonstrated that Au:Si switch could withstand the field intensity up to 36.6 kV/cm and have an opening time as fast as 20 ns. Cu compensated Si doped GaAs is suggested by Schoenbach et al [62],[87],[88] of the Old Dominion University. They demonstrated that this material can have a conduction time on the order of microsecond by illuminating with a picosecond 1.064 μm laser pulse. In order to turn off this switch quickly, it has to be illuminated with a 1.3 μm laser pulse to preempty trap states, and hence initiate a fast carrier recombination which quenches the conductivity and changes the switch from the conducting state to the insulating state. However, there is still no major break-through with these materials in high power opening switch applications. On the other hand, GaAs and Cr:GaAs have already shown the potential of achieving voltage gain in either a current charged transmission line or a dual of the Blumlein line. Those details are discussed in Chapters 6, 7, and 8.

3.4 Summary

The basic photoconductive semiconductor switch physics has been discussed. The procedures for making the switch electrodes have been described. Different materials used in this application have been compared and two po-

tential mechanisms causing switch failure have been mentioned. Through the discussion and comparison, we see that GaAs and Cr:GaAs might be the most suitable candidates at present to be used as the high power photoconductive semiconductor opening switches.

Table I

Semiconductor Materials for Kilovolt Photoconductive Switches

Semiconductor Material	Energy Gap at 300°K (eV)	Carrier Lifetime (ns)	Dark Resistivity (Ω-m)	Breakdown Field (V/cm)
Si	1.124	10^4	5×10^4	3×10^5
GaAs	1.43	~10	$> 10^7$	3.5×10^5
Cr:GaAs	1.43	< 1	$> 10^7$	3.5×10^5
Diamond	5.5	< 1	$> 10^{16}$	10^6
ZnSe	2.7	< 1	$> 10^{12}$	$> 10^5$

CHAPTER 4

Pulse Forming in Lumped Inductive Circuits

The simplest inductive energy storage pulsed power system (IESPPS) would be the lumped inductive circuit, which has a variety of applications. For instance, the ballistic coil in a fluorescent light and the ignition coil in an auto engine are some typical examples from our daily life. During the early stage of this research, a lumped inductive circuit was used to determine the feasibility of employing the photoconductive semiconductor as an opening switch. Later in pulse forming experiments, the lumped inductive circuit model is always cited for a rough estimation of the switch performance. Therefore, we must understand pulse forming theory of the lumped inductive circuits in order to predict the possible output pulse shapes.

In the first section of this chapter, a simplified model for a lumped inductive circuit, which can be merely a parallel connection of an inductance, a resistance, and a current source, is discussed. However, this circuit model fails to explain some of the details of the circuit response. In Chapter 6, some experimental results clearly prove this point. This is because those results strongly suggest a parasitic capacitance in the circuit. Thus, the stray capacitance between the inductance and the load resistance has to be included in the circuit analysis. With this modification, the circuit model becomes a parallel connection of an inductance L, a capacitance C, and a resistance R. Since an ideal current source for the pulse forming purpose is difficult to find, a voltage source, which is connected in series with the parallel RLC circuit through an opening switch, is used instead. The detailed description and analysis of this RLC circuit appear in the second section. In the analysis, different circuit parameters leading to different types of response such as overdamp, critical damp, and oscillatory are discussed separately. If the capacitance value is small enough and the capacitive

effect is negligible, it is possible to treat the circuit as a parallel RL circuit with a voltage source. The corresponding circuit response is described at the end of this section.

In the last section, a new circuit, which is directly derived from the LC generator by using the duality property in the circuit analysis, is introduced. This new circuit is called the dual of the LC generator and it features an output current which is twice the charging current under a certain combination of circuit parameters. The possible output waveforms and the circuit analysis to justify this feature are also shown in this section.

4.1 Simplified model for the lumped inductive circuit

The basic lumped inductive circuit, which is comprised of a current source, an opening switch, and an inductance, is shown in Fig. 4.1. The R_{Th}, which is appeared in parallel with the current source in this figure, is the internal resistance of the source and it is always much greater than the load resistance R_L. In the analysis, it is assuming that the switch is ideal, R_{Th} approaches infinite, and there is no stray capacitance in the circuit. At $t < 0$, the switch has been closed long enough so that the circuit has reached the steady state. This implies that the charging current I_o provided by the current source only flows through the inductance L and there is no current passing through R_{Th} and R_L, and thus the output voltage across R_L is zero. Upon opening the switch at $t = 0$, the circuit performance can be described in terms of Kirchhoff's voltage law along the loop of L and R_L, and be expressed as a first order differential equation [89] with the initial condition $I(0) = I_o$. This equation is written as

$$L\frac{dI(t)}{dt} + R_L I(t) = 0\,, \tag{4.1}$$

where L is the inductance, R_L is the load resistance, and $I(t)$ is the current flowing through the inductance and the resistance when the switch is opened at $t = 0$. The corresponding solution for Eqn. (4.1) at $t > 0$ is

$$I(t) = A\exp\left(-\frac{R_L}{L}t\right), \tag{4.2}$$

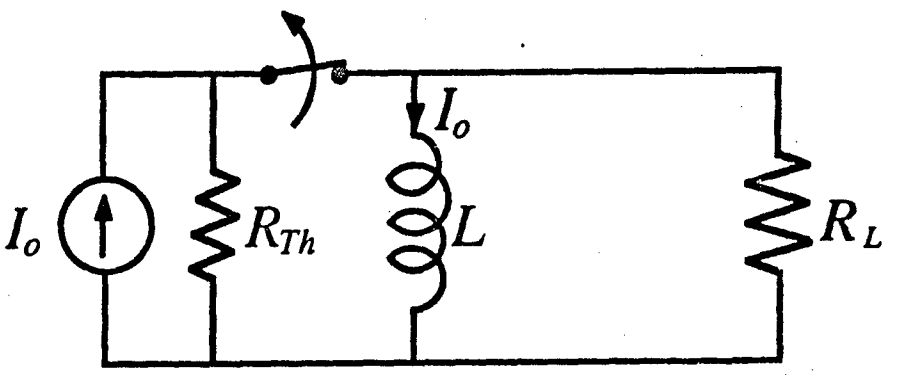

Fig. 4.1. A simple inductive lumped circuit with a current source.

where A can be determined from the initial current. Hence, Eqn. (4.2) becomes

$$I(t) = I_o \exp\left(-\frac{R_L}{L}t\right) , \tag{4.3}$$

where I_o is the initial current. Thus, the output voltage waveform $V_{out}(t)$ for $t > 0$ can be found as

$$V_{out}(t) = I(t)R_L = -L\frac{dI(t)}{dt} = I_o R_L \exp\left(-\frac{R_L}{L}t\right) \tag{4.4}$$

and is plotted in Fig. 4.2.

4.2 Parallel RLC model for the lumped inductive circuit

As mentioned earlier, the simple circuit model discussed in the previous section does not apply to a practical circuit. In order to predict the correct output voltage waveform, extra factors must be considered in this circuit model. These factors are the finite switch resistance, and the stray capacitance in the system. Also, since a current source is not commonly used as a power supply, a voltage source is used instead in this modified circuit model.

In the derivation, let V_o be the charging voltage, R_L the load resistance, L the inductance, C the stray capacitance, and R_{on} and R_{off} the switch on- and off-state resistances respectively. Assuming the stray capacitance, C, is in parallel with the inductance, L, this suggests that the modified lumped inductive circuit becomes a simple parallel RLC circuit. The circuit diagram is shown in Fig. 4.3. At $t < 0$, the switch has been on for a long time and the circuit has reached the steady state. This implies that the inductance is charged with current V_o/R_{on}, there is no charge stored in C, and there is no current flowing through R_L. At $t = 0$, the switch is turned off. By applying Norton's theorem to convert the voltage source to a current source (Fig. 4.4), the output voltage waveform, V_{out}, which is measured across the load resistance, R_L, can be obtained by solving the following equation [31],[89]:

$$\frac{V_{out}(t)}{R_L} + \frac{V_{out}(t)}{R_{off}} + C\frac{dV_{out}(t)}{dt} + \frac{1}{L}\int_0^t V_{out}dt = \frac{V_o}{R_{off}} . \tag{4.5}$$

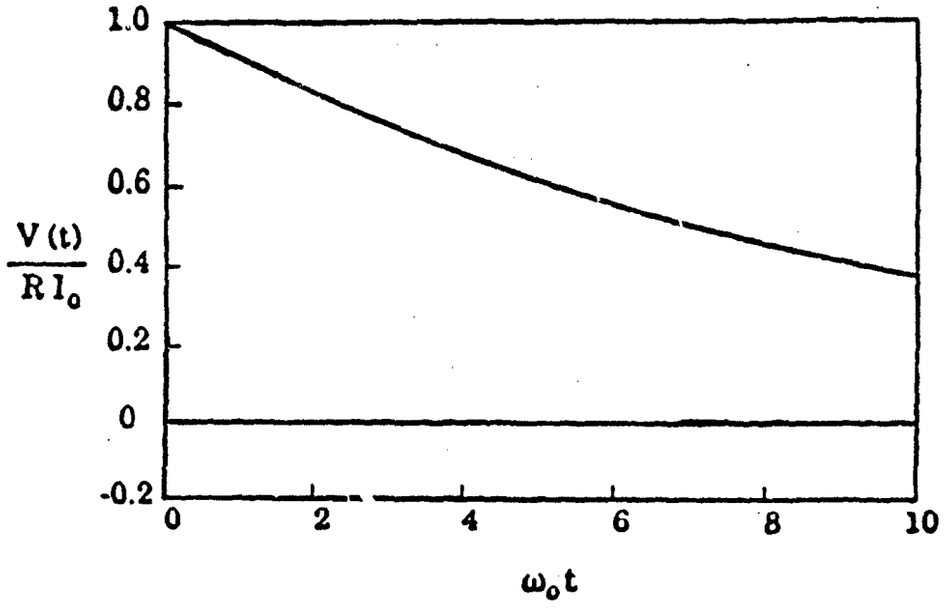

Fig. 4.2. Typical output waveform from a simple inductive lumped circuit, where V(t)=$V_{out}(t)$, R=R_L, and $\omega_o = 0.1L/R$.

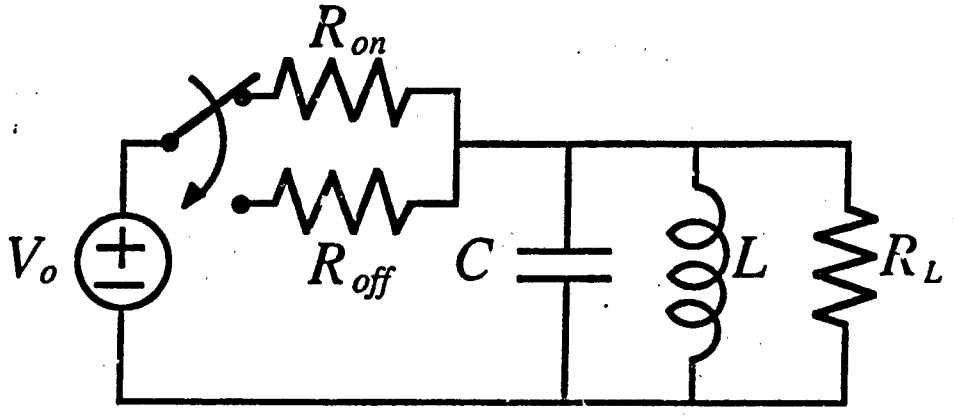

Fig. 4.3. Equivalent circuit diagram for an inductive lumped circuit with a voltage source and a non-ideal switch.

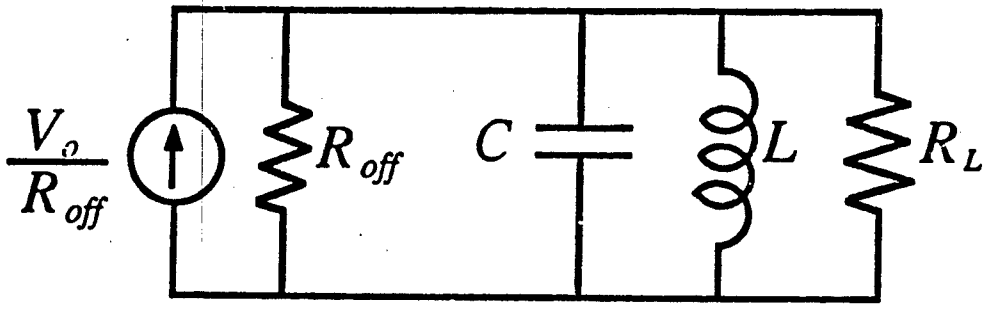

Fig. 4.4. Norton's equivalent circuit for the inductive lumped circuit when the switch is off.

Assuming R_{off} is constant, Eqn. (4.5) becomes

$$C\frac{d^2V_{out}(t)}{dt^2} + \left(\frac{1}{R_{off}} + \frac{1}{R_L}\right)\frac{dV_{out}(t)}{dt} + \frac{V_{out}(t)}{L} = 0\,. \tag{4.6}$$

By letting

$$\frac{1}{R'} = \frac{1}{R_{off}} + \frac{1}{R_L}\,, \tag{4.7}$$

the solution to Eqn. (4.6) can be written as

$$V_{out}(t) = A\exp(S_1 t) + B\exp(S_2 t) \tag{4.8}$$

where

$$S_1 = -\frac{1}{2R'C} + \sqrt{\Delta}\,, \tag{4.9}$$

$$S_2 = -\frac{1}{2R'C} - \sqrt{\Delta}\,, \tag{4.10}$$

$$\Delta = (\frac{1}{2R'C})^2 - \frac{1}{LC}\,. \tag{4.11}$$

By applying the first initial condition $V_{out}(0) = 0$, the constants A and B in Eqn. (4.8) must satisfy

$$A = -B\,. \tag{4.12}$$

Using the other initial condition, $I_L(0) = V_o/R_{on}$, where $I_L(t)$ is the current flowing through the inductance L at $t > 0$, leads to

$$\frac{V_o}{R_{off}} = \frac{0}{R_L} + \frac{0}{R_{off}} + C(S_1 A - S_2 A) + \frac{V_o}{R_{on}}\,. \tag{4.13}$$

Thus, the constants can be obtained as

$$A = -B = \frac{I_o}{C(S_1 - S_2)} = \frac{I_o}{2C\sqrt{\Delta}}\,, \tag{4.14}$$

where

$$I_o = V_o\left(\frac{1}{R_{off}} - \frac{1}{R_{on}}\right)\,. \tag{4.15}$$

Substituting them into Eqn. (4.8), the final result becomes

$$V_{out}(t) = \frac{I_o}{2C\sqrt{\Delta}}[\exp(S_1 t) - \exp(S_2 t)]\,. \tag{4.16}$$

Accordingly, the current flowing through the load resistance R_L can be easily expressed as

$$I(t) = \frac{V_{out}(t)}{R_L} = \frac{I_o}{2R_LC\sqrt{\Delta}}[\exp(S_1t) - \exp(S_2t)]. \tag{4.17}$$

Two types of response can be described by Eqn. (4.17):

1. $\Delta > 0$, the overdamped case

S_1 and S_2 are real numbers, no oscillation occurs (Fig. 4.5). Eqn. (4.17) can be rewritten as

$$I(t) = \frac{I_o}{R_LC\sqrt{\Delta}} \exp\left(-\frac{t}{2R'C}\right) \sinh(\sqrt{\Delta}t) \, . \tag{4.18}$$

The slope of the current waveform can be obtained as

$$\frac{dI(t)}{dt} = \frac{I_o}{R_LC\sqrt{\Delta}} \exp\left(-\frac{t}{2R'C}\right) [\sqrt{\Delta}\cosh(\sqrt{\Delta}t) - \frac{1}{2R'C}\sinh(\sqrt{\Delta}t)] \, . \tag{4.19}$$

At $t = 0$, the slope is

$$\left.\frac{dI(t)}{dt}\right|_{t=0} = \frac{I_o}{R_LC} \, , \tag{4.20}$$

thus the stray capacitance value can be found as

$$C = \frac{I_o/R_L}{dI(t)/dt|_{t=0}} \, . \tag{4.21}$$

By setting $dI(t)/dt = 0$, the time, t_{max}, at which the output current reaches its maximum value can be determined, that is

$$t_{max} = \frac{1}{\sqrt{\Delta}} \tanh^{-1}(2R'C\sqrt{\Delta}) = \frac{1}{2\sqrt{\Delta}} \ln\left(\frac{1+2R'C\sqrt{\Delta}}{1-2R'C\sqrt{\Delta}}\right) \, . \tag{4.22}$$

Substituting this value into Eqn. (4.18) results in

$$I_{max} = \frac{I_o\sqrt{LC}}{R_LC}\left(\frac{1-2R'C\sqrt{\Delta}}{1+2R'C\sqrt{\Delta}}\right)^{\frac{1}{4R'C\sqrt{\Delta}}} \, , \tag{4.23}$$

so the peak amplitude of the output voltage pulse is

$$V_p = I_{max}R_L = I_o\sqrt{\frac{L}{C}}\left(\frac{1-2R'C\sqrt{\Delta}}{1+2R'C\sqrt{\Delta}}\right)^{\frac{1}{4R'C\sqrt{\Delta}}} \, . \tag{4.24}$$

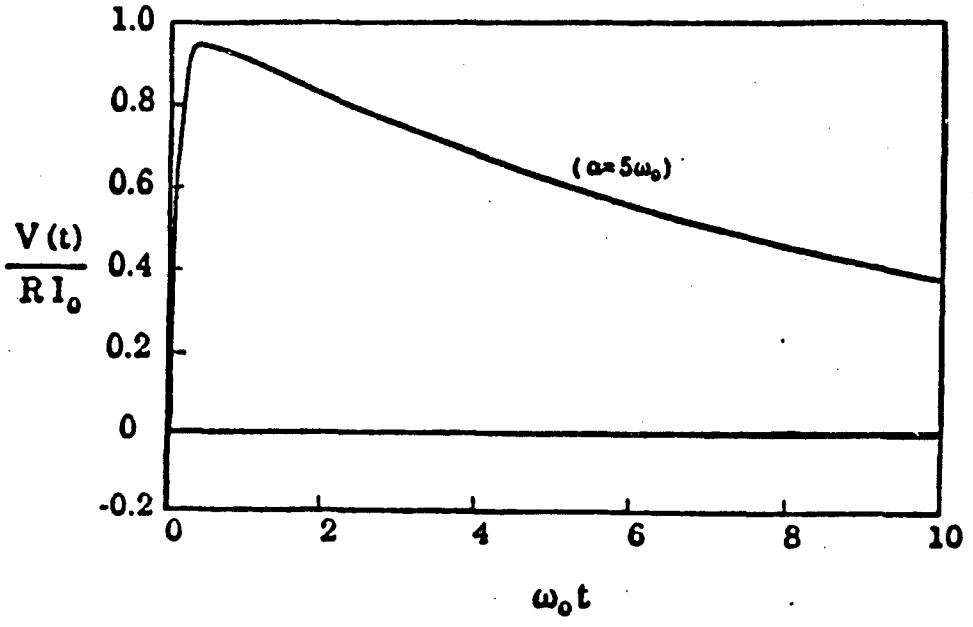

Fig. 4.5. Typical output waveform for the overdamped case ($\Delta > 0$), where V(t)=$V_{out}(t)$, R=R_L, $\alpha = (2R'C)^{-1}$, and $\omega_o = 1/\sqrt{LC}$.

2. $\Delta < 0$, the oscillatory case

In tnis case, $\sqrt{\Delta}$ is an imaginary number, and S_1 and S_2 are complex conjugates. Eqn. (4.17) can be rewritten as

$$I(t) = \frac{I_o}{R_L C\sqrt{-\Delta}} \exp\left(-\frac{t}{2R'C}\right) \sin(\sqrt{-\Delta}t) \,. \tag{4.25}$$

Thus, the current waveform is oscillating with a damping time constant $\tau = 2R'C$ and the period $T = 2\pi/\sqrt{-\Delta}$. This is shown ir. Fig. 4.6. The slope of the current waveform is

$$\frac{dI(t)}{dt} = \frac{I_o}{R_L C\sqrt{-\Delta}} \exp\left(-\frac{t}{2R'C}\right) [-\frac{1}{2R'C} \sin(\sqrt{-\Delta}t) + \sqrt{-\Delta}\cos(\sqrt{-\Delta}t)] \,. \tag{4.26}$$

At $t = 0$, this leads to

$$\left.\frac{dI(t)}{dt}\right|_{t=0} = \frac{I_o}{R_L C} \,,$$

which is the same as Eqn. (4.20) in the overdamped case. By setting $dI(t)/dt = 0$, t_{max} can be expressed as

$$t_{max} = \frac{1}{\sqrt{-\Delta}} \tan^{-1}(2R'C\sqrt{-\Delta}) \,. \tag{4.27}$$

Substituting it into Eqn. (4.25), the maximum output current is obtained as

$$I_{max} = \frac{I_o\sqrt{LC}}{R_L C} \exp\left(-\frac{\tan^{-1}(2R'C\sqrt{-\Delta})}{2R'C\sqrt{-\Delta}}\right) \,. \tag{4.28}$$

The corresponding peak amplitude of the output voltage pulse is

$$V_p = I_{max}R_L = I_o\sqrt{\frac{L}{C}} \exp\left(-\frac{\tan^{-1}(2R'C\sqrt{-\Delta})}{2R'C\sqrt{-\Delta}}\right) \,. \tag{4.29}$$

If $\Delta = 0$, the critically damped case,

$$S_1 = S_2 = -\frac{1}{2R'C} \tag{4.30}$$

and the solution of Eqn. (4.6) becomes

$$V_{out}(t) = (A + Bt)\exp\left(-\frac{t}{2R'C}\right) \,. \tag{4.31}$$

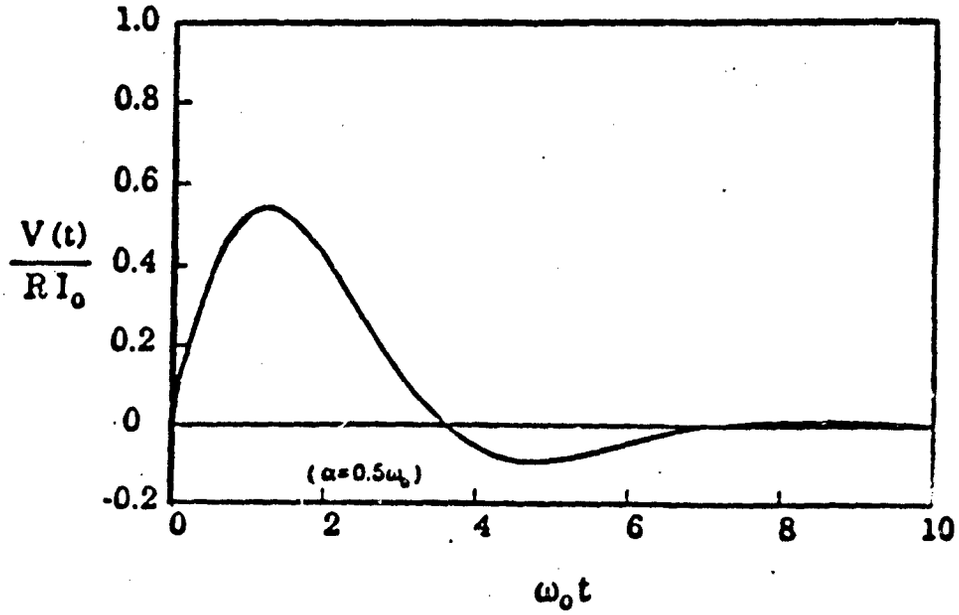

Fig. 4.6. Typical output waveform for the underdamped case ($\Delta < 0$), where V(t)=$V_{out}(t)$, R=R_L, $\alpha = (2R'C)^{-1}$, and $\omega_o = 1/\sqrt{LC}$.

Applying the initial conditions leads to

$$A = 0$$

and

$$\frac{V_o}{R_{off}} = \frac{0}{R_{off}} + \frac{0}{R_L} + \frac{V_o}{R_{on}} + CB. \tag{4.32}$$

Hence,

$$B = \frac{V_o}{C}\left(\frac{1}{R_{off}} - \frac{1}{R_{on}}\right) = \frac{I_o}{C} \tag{4.33}$$

and the final result is

$$V_{out}(t) = \frac{I_o t}{C}\exp\left(-\frac{t}{2R'C}\right) . \tag{4.34}$$

In this case, the current flowing through the load resistance is

$$I(t) = \frac{I_o t}{R_L C}\exp\left(-\frac{t}{2R'C}\right) \tag{4.35}$$

and its slope is

$$\frac{dI(t)}{dt} = \frac{I_o}{R_L C}\exp\left(-\frac{t}{2R'C}\right)\left(1 - \frac{t}{2R'C}\right) . \tag{4.36}$$

At $t = 0$, the slope of the current waveform is still the same as Eqn. (4.20), that is

$$\left.\frac{dI(t)}{dt}\right|_{t=0} = \frac{I_o}{R_L C} .$$

The corresponding output current and voltage waveforms are depicted in Fig. 4.7. By setting $dI(t)/dt = 0$, we find that

$$t_{max} = 2R'C \tag{4.37}$$

and

$$I_{max} = 0.736 I_o \frac{R'}{R_L} . \tag{4.38}$$

This leads to the peak amplitude of the output voltage pulse to be

$$V_p = I_{max} R_L = 0.736 I_o R' . \tag{4.39}$$

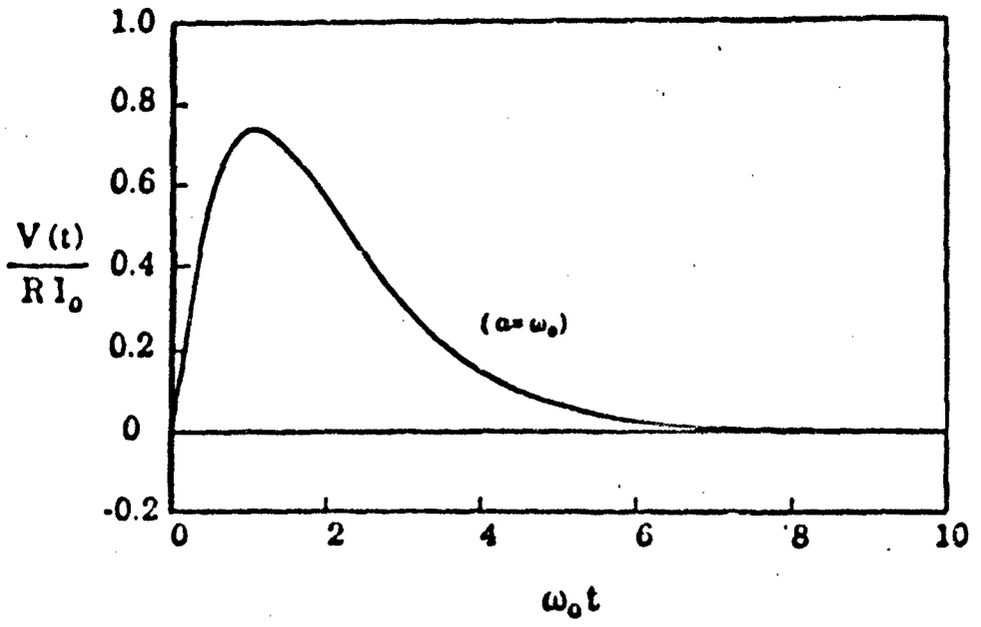

Fig. 4.7. Typical output waveform for the critically damped case ($\Delta = 0$), where V(t)=$V_{out}(t)$, R=R_L, $\alpha = (2R'C)^{-1}$, and $\omega_o = 1/\sqrt{LC}$.

Figs. 4.5, 4.6, and 4.7 clearly illustrate the effects of the stray capacitance on the output waveforms. In those waveforms, the most significant parts are the zero voltage at $t = 0$ and the long fall-time. These can be attributed to the capacitive voltage response which lags behind the current response. If the stray capacitance is negligible due to a large $dI(t)/dt|_{t=0}$ value in Eqn. (4.21), the output waveforms can not be determined directly by letting $C = 0$ in Eqns. (4.18), (4.25), and (4.35). On the contrary, Eqn. (4.6) has to be simplified to a first order differential equation in order to obtain the output waveform. The simplified equation is

$$\frac{1}{R'}\frac{dV_{out}}{dt} + \frac{V_{out}}{L} = 0 . \tag{4.40}$$

The corresponding solution is

$$V_{out}(t) = A \exp\left(-\frac{R'}{L}t\right) . \tag{4.41}$$

The circuit diagram is shown in Fig. 4.8. By applying the initial condition $I_L(0) = V_o/R_{on}$, the circuit equation becomes

$$\frac{V_o}{R_{off}} = V_{out}(0)\left(\frac{1}{R_{off}} + \frac{1}{R_L}\right) + \frac{V_o}{R_{on}} . \tag{4.42}$$

Rewriting Eqn. (4.42) leads to

$$I_o = \frac{A}{R'} ,$$

where I_o and R' are defined in Eqn. (4.15) and Eqn. (4.7). Therefore, $A = I_o R'$ and the solution becomes

$$V_{out}(t) = I_o R' \exp\left(-\frac{R'}{L}t\right) . \tag{4.43}$$

In this case, the current flowing through the load resistance is found to be

$$I(t) = \frac{V_{out}(t)}{R_L} = I_o \frac{R'}{R_L} \exp\left(-\frac{R'}{L}t\right) . \tag{4.44}$$

This is identical to Eqn. (4.3) by setting $R' = R_L$, so the output voltage and current waveforms will have the same shape as shown in Fig. 4.2.

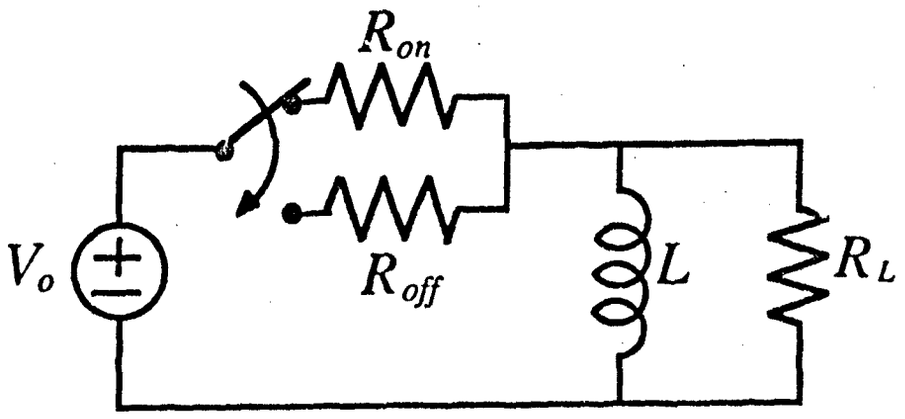

Fig. 4.8. A simple inductive lumped circuit without the stray capacitance.

4.3 Dual of the LC generator

The schematic circuit structure of the LC generator is shown in Fig. 4.9. In order to roughly estimate the circuit performance, one can assume that the switch in the LC generator is opened long enough so that the steady state has been reached. In this case, the voltage V_o appears across both capacitances, C, and no current flows through the inductance, L, and the load resistance, R_L. Upon closing the switch, both capacitances will discharge toward the inductance and the load resistance. If the load resistance is large enough to have an R_LC time constant much longer than the LC resonance period, $\sqrt{LC}$, the output voltage will vary between V_o and $2V_o$ in the first few resonant cycles. This suggests that the peak output voltage from this circuit can be as high as $2V_o$ depending on the circuit parameters. However, the output waveform will always be oscillatory.

In an effort to obtain an output amplitude twice the input, we can transform the LC generator into its dual circuit, the dual of the LC generator [31]. The circuit diagram is shown in Fig. 4.10. In this circuit, the two inductances L are used to replace the function of the capacitances in the LC generator and the closing switch is changed to an opening switch. While the switch is closed, putting the circuit in the steady state, the current I_o only flows through those two inductances, L, and there is no voltage appearing across the load resistance, R_L, and the capacitance, C. As soon as the switch is opened, the charging current in the inductances is diverted to the capacitance and the load resistance. If the load resistance is small enough so that the L/R_L time constant is much larger than the LC resonance period, $\sqrt{LC}$, it will be possible to obtain a peak output current amplitude which is twice the charging current I_o under certain combinations of the circuit parameters. Like the LC generator, the output waveform is also oscillatory. In the following analytical derivation, this oscillatory output waveform can be clearly understood.

Since a current source is seldom used as a power supply, a voltage source

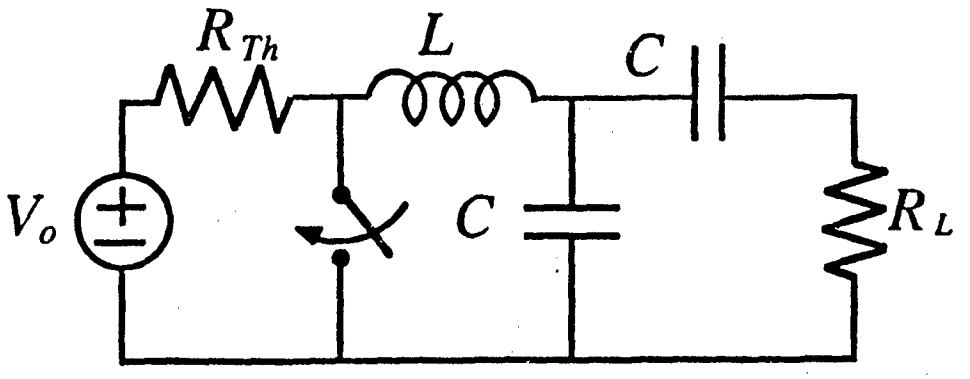

Fig. 4.9. Schematic diagram of an LC generator.

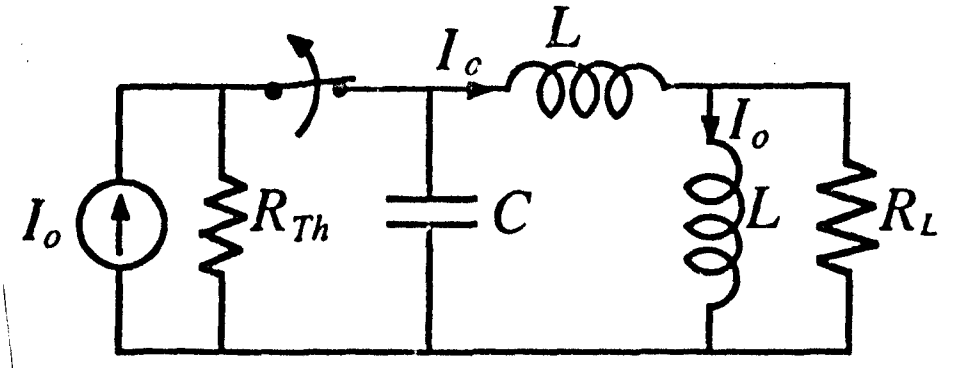

Fig. 4.10. Schematic diagram of a dual of the LC generator.

is used instead in the circuit analysis. By taking the switch resistance into consideration, the modified circuit diagram is shown in Fig. 4.11. Before opening the switch, the switch has been closed for a long period of time and the circuit has reached the steady state. This sets the initial conditions for the circuit to be $I_{L1}(0) = I_{L2}(0) = V_o/R_{on}$ and $V_C(0) = 0$, where I_{L1} and I_{L2} are the current flowing through each inductance as shown in Fig. 4.11, V_C is the voltage appearing across the capacitance, and R_{on} and R_{off} are the switch on- and off-resistance respectively. At $t = 0$, the switch is flipped from the on-state to the off-state so that the charging current in the inductances, L_1 and L_2, is diverted to the capacitance, C, and the load resistance, R_L. The analytical solutions are shown in the following derivation.

By using Norton's theorem to convert the circuit (Fig. 4.12), applying Kirchhoff's law, and letting $L_1 = L_2 = L$, the following equations are obtained:

$$\frac{V_o}{R_{off}} = \frac{V_C(t)}{R_{off}} + C\frac{dV_C(t)}{dt} + I_{L1}(t)\,, \tag{4.45}$$

$$V_C(t) = L\frac{dI_{L1}(t)}{dt} + L\frac{dI_{L2}(t)}{dt} = L\frac{dI_{L1}(t)}{dt} + I(t)R_L\,, \tag{4.46}$$

$$I_{L1}(t) = I(t) + I_{L2}(t)\,, \tag{4.47}$$

where $I(t)$ is the current flowing through the load resistance, R_L, after the switch is opened. By substituting Eqn. (4.46) and Eqn. (4.47) into Eqn. (4.45), we obtain

$$\frac{V_o}{R_{off}} = LC\frac{d^2}{dt^2}[I(t) + 2I_{L2}(t)] + \frac{L}{R_{off}}\frac{d}{dt}[I(t) + 2I_{L2}(t)] + I(t) + I_{L2}(t)\,. \tag{4.48}$$

Then differentiating Eqn. (4.48) and using

$$V_{out}(t) = L\frac{dI_{L2}(t)}{dt} = I(t)R_L \tag{4.49}$$

lead to a third order differential equation, that is

$$\frac{d^3I(t)}{dt^3} + \left(2\frac{R_L}{L} + \frac{1}{R_{off}C}\right)\frac{d^2I(t)}{dt^2} + \left(1 + 2\frac{R_L}{R_{off}}\right)\frac{1}{LC}\frac{dI(t)}{dt} + \frac{R_L}{L^2C}I(t) = 0. \tag{4.50}$$

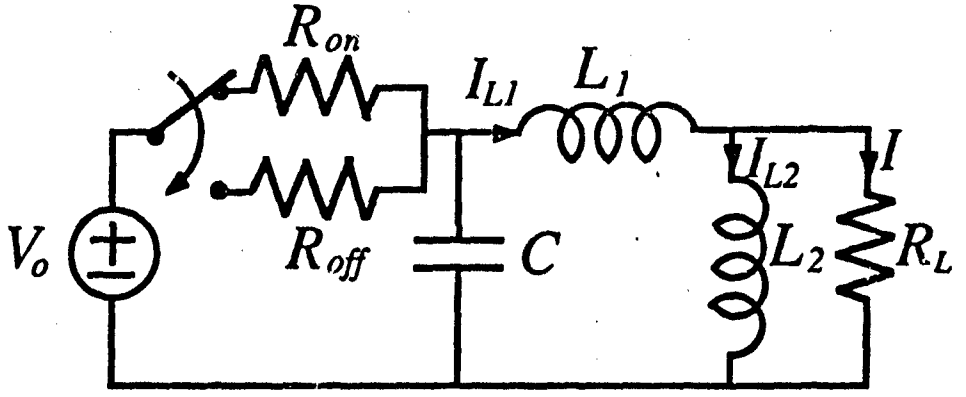

Fig. 4.11. A modified circuit diagram of the dual of the LC generator with $L_1 = L_2 = L$, a voltage source, and a non-ideal switch.

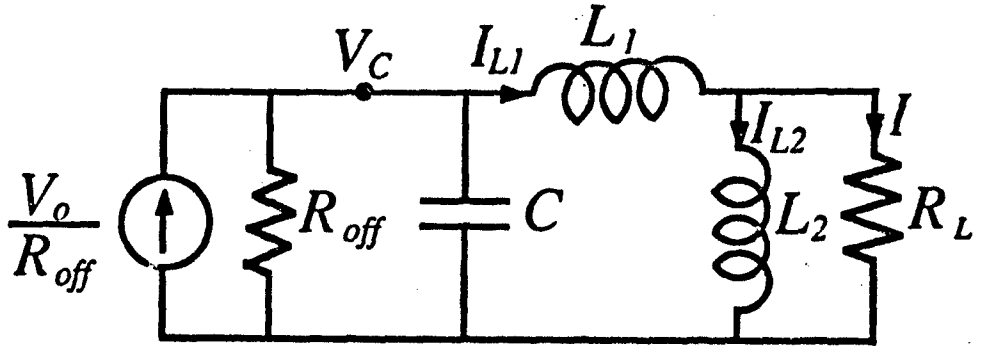

Fig. 4.12. Norton's equivalent circuit for the dual of the LC generator when the switch is off.

The determination of the initial conditions, the detailed derivation, and a discussion of Eqn. (4.50) are included in Appendix I. According to that analysis, the output current $I(t)$ is found to be

$$I(t) = \frac{I_o}{LC[(\alpha-\beta)^2+\omega^2]}\{e^{-\alpha t} - e^{-\beta t}[\cos(\omega t) - \frac{\alpha-\beta}{\omega}\sin(\omega t)]\} \qquad (4.51)$$

and the corresponding output voltage V_{out} is

$$V_{out}(t) = \frac{I_o R_L}{LC[(\alpha-\beta)^2+\omega^2]}\{e^{-\alpha t} - e^{-\beta t}[\cos(\omega t) - \frac{\alpha-\beta}{\omega}\sin(\omega t)]\}\ , \qquad (4.52)$$

where I_o is defined in Eqn. (4.15), and

$$\alpha = \frac{1}{3}\left(\frac{2R_L}{L} + \frac{1}{R_{off}C}\right) - (r+d)^{1/3} - (r-d)^{1/3}, \qquad (4.53)$$

$$\beta = \frac{1}{2}[(r+d)^{1/3} + (r-a)^{1/3}] + \frac{1}{3}\left(\frac{2R_L}{L} + \frac{1}{R_{off}C}\right)\ , \qquad (4.54)$$

$$\omega = \frac{\sqrt{3}}{2}[(r+d)^{1/3} - (r-d)^{1/3}]\ , \qquad (4.55)$$

$$d = (q^3 + r^2)^{1/2}\ , \qquad (4.56)$$

$$q = \frac{1}{9}\left(\frac{3}{LC} + \frac{2R_L}{R_{off}LC} - \frac{4R_L^2}{L^2} - \frac{1}{R_{off}^2C^2}\right)\ , \qquad (4.57)$$

$$r = -\frac{R_L}{6L^2C} - \frac{8R_L^3}{27L^3} + \frac{R_L}{R_{off}LC}\left(\frac{2R_L}{9L} + \frac{1}{9R_{off}C} + \frac{1}{6R_LC}\right)\ . \qquad (4.58)$$

Apparently, the behavior of this solution depends heavily on the circuit parameters, R_L, L, and C. Three different cases with the same $(LC)^{-1/2} = 10^6$ but different L/R_L values are plotted in Fig. 4.13, Fig. 4.14, and Fig. 4.15. The corresponding values of $L/R_L = 10^{-4}$, 10^{-5}, and 10^{-6} are used respectively. As shown in Fig. 4.13, the output peak current amplitude can really reach twice the charging current amplitude if $L/R_L \gg (LC)^{1/2}$. Also, those three plots clearly display the oscillatory output waveforms as predicted in the very beginning of this section.

4.4 Summary

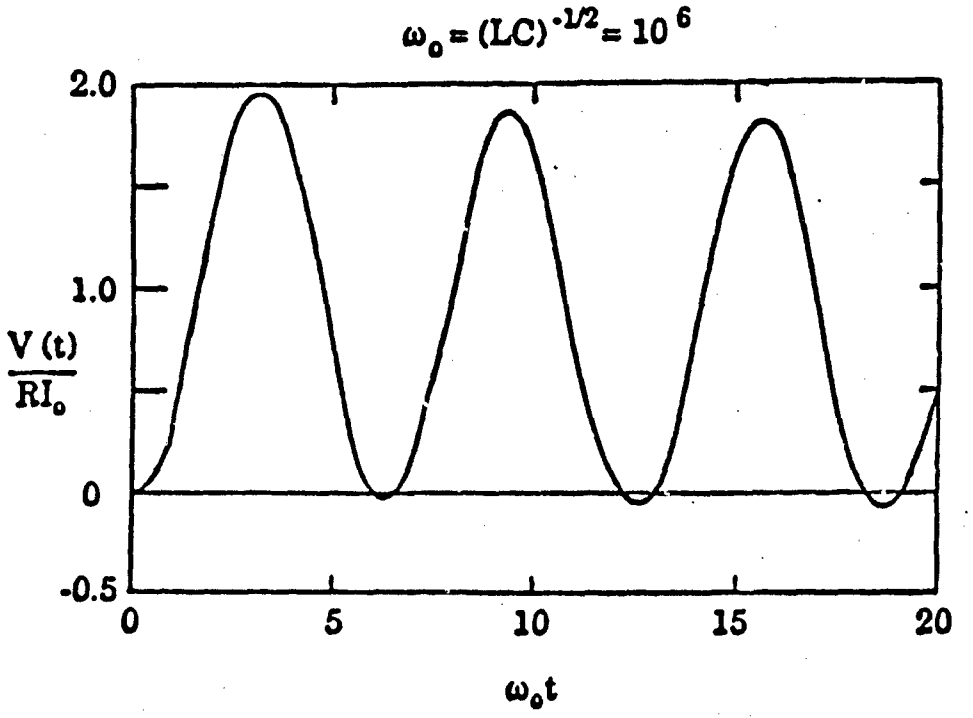

Fig. 4.13. Typical output waveform for $\sqrt{LC} = 10^{-6}$ and $L/R_L = 10^{-4}$, where V(t)=$V'_{out}(t)$ and R=R_L.

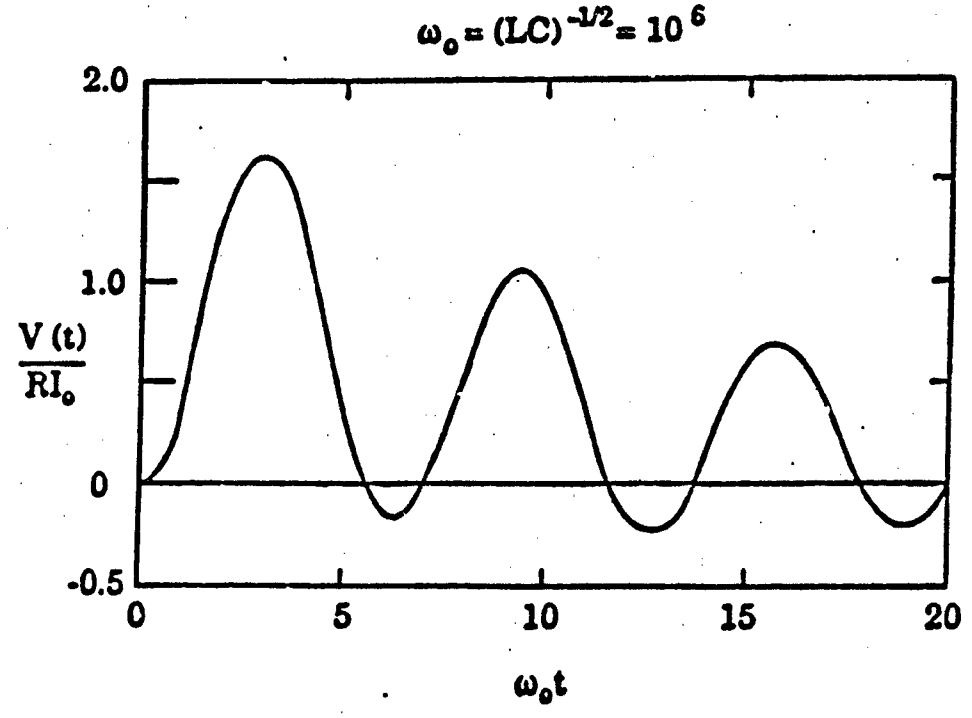

Fig. 4.14. Typical output waveform for $\sqrt{LC} = 10^{-6}$ and $L/R_L = 10^{-5}$, where V(t)=$V'_{out}(t)$ and R=R_L.

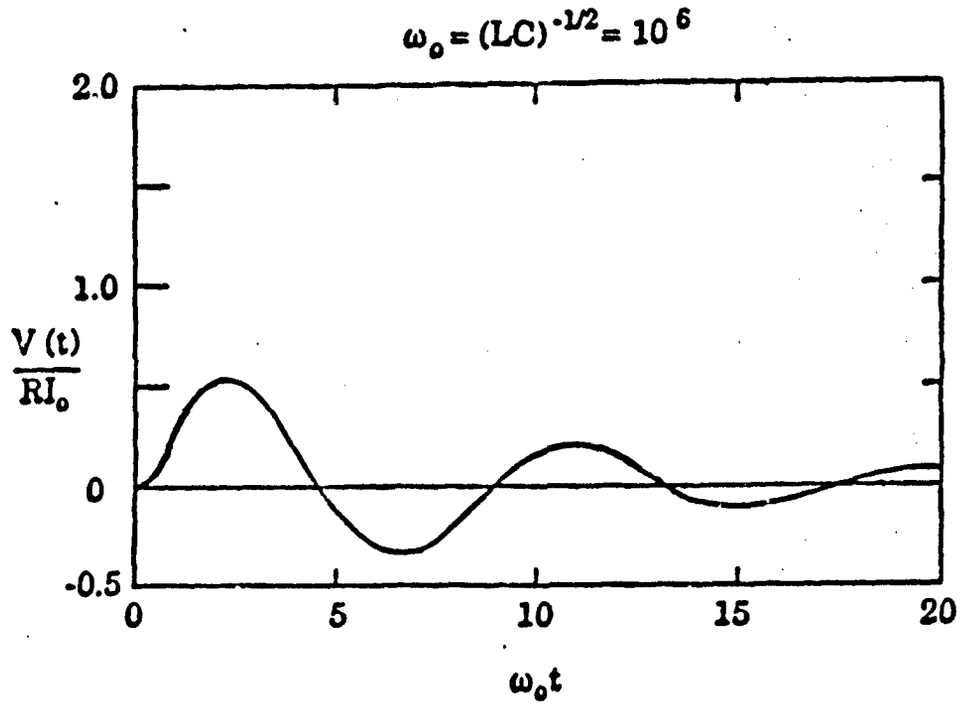

Fig. 4.15. Typical output waveform for $\sqrt{LC} = 10^{-6}$ and $L/R_L = 10^{-6}$, where V(t)=$V_{out}(t)$ and R=R_L.

Pulse forming mechanisms in different types of lumped inductive circuits have been discussed in great detail. In order to generate a high voltage pulse without ringing or oscillation from an *RLC* circuit, circuit parameters have to be chosen carefully. In spite of the ringing or the oscillation, the output current from the *RLC* circuit can never exceed the charging current which depends heavily on the switch on-resistance. Thus, the switch on-resistance has to be as low as possible in order to have the output voltage pulse much higher than the charging voltage. According to the circuit analysis, the main advantage of the dual of the *LC* generator over the simple lumped inductive circuit is that it is possible to provide the load resistance with a current amplitude twice the initial charging current. However, the unwanted ringing or oscillation in the output waveforms of this circuit can never be avoided due to the nature of this circuit structure.

CHAPTER 5

Pulse Forming in Current Charged Line and Dual of the Blumlein Line

In order to simplify the system analysis and make the system more efficient, fast pulses are preferred in many applications. For example, high power fast pulses can be used in a particle accelerator for studying fundamental particle physics, in a microwave cavity for generating high power microwave pulses, and in a Q-switched laser system for controling a Pockels cell to obtain high power laser pulses. In contrast, low power fast pulses are also very useful. Generally, they are suitable for analyzing high frequency microwave circuits (e.g. monolithic microwave intergrated circuits) [7].

Conventionally, capacitive energy storage pulsed power systems, such as the voltage charged line pulser and the Blumlein line, are used for this fast pulse generation. If the inductive energy storage pulsed power systems were employed for this purpose, short-circuited transmission lines would have to be used as the energy storage device instead of an inductor in the lumped circuit. This is because the response of the lumped inductive circuits, which is limited by the L/R time constant, is always very slow. The details have been shown in the previous chapter already. In this case, it is impossible for them to generate pulses with a fast rise-time or a fast fall-time.

In order to use the short-circuited transmission lines for generating fast pulses, basic energy propagation concepts in the transmission line must be understood. Those details are discussed in the first section of this chapter. Through the discussion in this section, the concepts of voltage and current waves are introduced. Since the boundary conditions can significantly affect wave propagation, the transmission and reflection coefficient of the waves are introduced as well. By using these equations, pulse forming phenomenon in a current charged

transmission line (CCTL) with an ideal opening switch can be analyzed. The discussion is in the following section of this chapter. In this pulse forming discussion, the current build-up during the switch closing period and the fast voltage pulse generation during the switch opening period are derived. Different voltage waveforms corresponding to different load impedances are discussed in detail as well. The experimental results which verify the theoretical derivation are shown in Chapters 7 and 8. The possibility of observing the ideal waveforms is due to the fast closing and opening of the photoconductive semiconductor switch in this circuit. If the conventional opening switches which are described in Chapter 2 are used, these types of theoretical waveforms cannot be observed due to their slow closing and opening times.

In the third section, a new circuit, the dual of the Blumlein line (DBL), is introduced. In this circuit, the current build-up waveform and the output fast voltage pulse shape are very different from the CCTL. Derivation and discussion of these pulse shapes are covered in detail. The experimental results which verify the theories by using a fast photoconductive semiconductor switch are shown in Chapter 8. Since these two current charged lines have several common features according to the experimental results shown in Chapter 8, this makes the comparisons of these two systems with an ideal switch become necessary. These theoretical comparisons, which include the key differences, advantages, and the pulse forming effects on the switch, are described in the last section. As for the pulse forming effects on the switch, two respects are covered. The first one is under the condition of the same total length of the charging line. The other one is under the condition of the same output pulse duration.

5.1 Energy propagation in the transmission line

The simple geometry of the transmission line is two parallel conductors with a constant cross-sectional area. Hence, the transmission line can be treated as a distributed LC circuit. However, since coaxial cables are amply used in the pulse forming experiment, the following analysis mainly focuses on this type of

concentric structure (Fig. 5.1).

In the analysis, assuming that the coaxial transmission line is lossless, its distributed capacitance (C, Farad per unit length) and inductance (L, Henry per unit length) can be calculated directly from its geometrical parameters [90]. They are

$$C = \frac{2\pi\epsilon}{\ln(b/a)} \tag{5.1}$$

and

$$L = \frac{\mu \ln(b/a)}{2\pi} , \tag{5.2}$$

where b is the radius to the outer conductor, a is the radius of the inner conductor, ϵ is the permittivity, and μ is the permeability of the dielectric material between these two conductors. The characteristic impedance, Z_o, of the transmission line can be determined by

$$Z_o = \sqrt{\frac{L}{C}} = \sqrt{\frac{\mu}{\epsilon}} \frac{\ln(b/a)}{2\pi} . \tag{5.3}$$

The distributed-circuit representation of a lossless transmission line is shown in Fig. 5.2. Based on this circuit structure, one can obtain

$$\frac{\partial^2 V}{\partial z^2} = LC \frac{\partial^2 V}{\partial t^2} . \tag{5.4}$$

and

$$\frac{\partial^2 I}{\partial z^2} = LC \frac{\partial^2 I}{\partial t^2} . \tag{5.5}$$

It is clear that these two equations are basic wave functions and their solutions are

$$V(z,t) = V^+(z - vt) + V^-(z + vt) \tag{5.6}$$

and

$$I(z,t) = I^+(z - vt) + I^-(z + vt) , \tag{5.7}$$

where

$$v = \frac{1}{\sqrt{LC}} = \frac{1}{\sqrt{\mu\epsilon}} \tag{5.8}$$

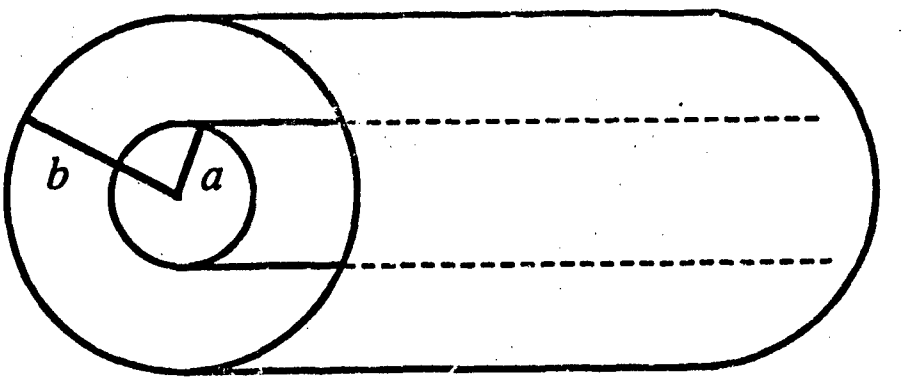

Fig. 5.1. A cross-sectional view of a coaxial transmission line.

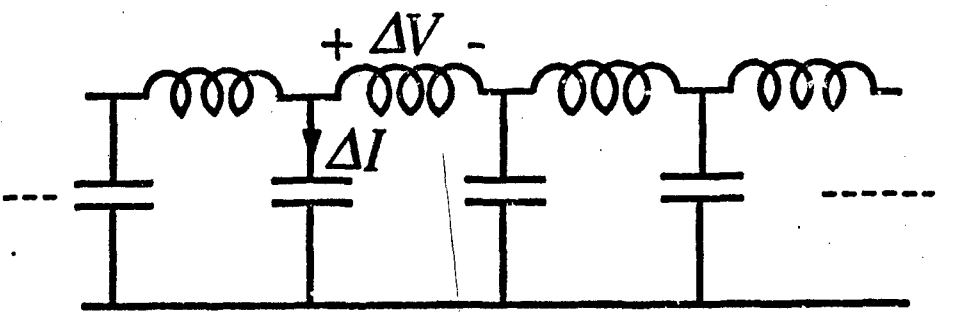

Fig. 5.2. Distributed-circuit representation of a lossless transmission line.

is the wave velocity propagating in the transmission line, and '+' and '−' represent the positive-going and negative-going traveling wave respectively. The relationships between the voltage and current traveling waves are

$$\frac{V^+(z,t)}{I^+(z,t)} = Z_o \tag{5.9}$$

and

$$\frac{V^-(z,t)}{I^-(z,t)} = -Z_o \,. \tag{5.10}$$

If there is a circuit element in the transmission line to change the boundary conditions, reflection and transmission will occur at this junction. The voltage traveling wave reflection coefficient Γ_V and the transmission coefficient T_V can be expressed as

$$\Gamma_V = \frac{Z_L - Z_o}{Z_L + Z_o} \tag{5.11}$$

and

$$T_V = \frac{2Z_L}{Z_L + Z_o} \,, \tag{5.12}$$

where Z_L is the effective load impedance at this junction. By applying the duality relationship from circuit theory, the current traveling wave reflection coefficient Γ_I and transmission coefficient T_I are

$$\Gamma_I = \frac{Y_L - Y_o}{Y_L + Y_o} \tag{5.13}$$

and

$$T_I = \frac{2Y_L}{Y_L + Y_o} \,, \tag{5.14}$$

where $Y_L = 1/Z_L$ and $Y_o = 1/Z_o$.

In the pulsed forming lines, two extreme cases, open-circuited and short-circuited load, are frequently encountered. Detailed discussions of these two cases are as follows:

I. The open-circuited load, $Z_L = 1/Y_L = \infty$

In this case, the reflection coefficients are $\Gamma_V = 1$ and $\Gamma_I = -1$ and the transmission coefficients are $T_V = 2$ and $T_I = 0$. Thus, we see that the energy is

totally reflected at the opened end with an in-phase reflection for the reflected voltage traveling wave and an out-of-phase reflection for the reflected current traveling wave. By applying the superposition theorem, the voltage and the current in the transmission line can be expressed as the sum of the incident ('+') and the reflected ('−') traveling waves. In order to satisfy the boundary conditions, the sum of the voltage and the current waves at the boundaries becomes

$$V^+ + V^- = V_o \tag{5.15}$$

and

$$I^+ + I^- = 0 \tag{5.16}$$

respectively, where V_o is the voltage across the transmission line. With the in-phase reflection, $V^+ = V^-$, and the out-of-phase reflection, $I^+ = -I^-$, as well as using Eqns. (5.9) and (5.10), they yield

$$V^+ = V^- = \frac{V_o}{2} \tag{5.17}$$

and

$$I^+ = -I^- = \frac{V_o}{2Z_o}\,. \tag{5.18}$$

II. The short-circuited load, $Z_L = 1/Y_L = 0$

With this load impedance, the reflection coefficients are $\Gamma_V = -1$ and $\Gamma_I = 1$ as well as the transmission coefficients are $T_V = 0$ and $T_I = 2$. Hence, the energy is totally reflected at the shorted end and the equations to satisfy the boundary conditions are

$$V^+ + V^- = 0 \tag{5.19}$$

as well as

$$I^+ + I^- = I_o \tag{5.20}$$

at the boundaries, where I_o is the current flowing in the transmission line. Considering the in-phase reflection of the current waves, $I^+ = I^-$, and the out-of-phase reflection of the voltage waves, $V^+ = -V^-$, and using Eqns. (5.9) and

(5.10), we find that

$$I^+ = I^- = \frac{I_o}{2} \tag{5.21}$$

and

$$V^+ = -V^- = \frac{I_o Z_o}{2} \,. \tag{5.22}$$

Table II

Dual Relationships in the Transmission Line

Voltage Based Analysis	Current Based Analysis
$I^+(z) = V^+(z)/Z_o$	$V^+(z) = I^+(z)/Y_o$
$I^-(z) = -V^-(z)/Z_o$	$V^-(z) = -I^-(z)/Y_o$
$\Gamma_V = (Z_L - Z_o)/(Z_L + Z_o)$	$\Gamma_I = (Y_L - Y_o)/(Y_L + Y_o)$
$T_I = 2Z_L/(Z_L + Z_o)$	$T_V = 2Y_L/(Y_L + Y_o)$
$V(z) = V^+(z) + V^-(z)$	$I(z) = I^+(z) + I^-(z)$
$I(z) = I^+(z) + I^-(z)$	$V(z) = V^+(z) + V^-(z)$
$= (V^+(z) - V^-(z))/Z_o$	$= (I^+(z) - I^-(z))/Y_o$
Open Circuited End	**Short Circuited End**
$I^+ + I^- = 0$	$V^+ + V^- = 0$
$V^+ + V^- = V_o$	$I^+ + I^- = I_o$
$V^+ = V^- = V_o/2$	$I^+ = I^- = I_o/2$
$I^+ = -I^- = V_o/2Z_o$	$V^+ = -V^- = I_o/2Y_o$
$\Gamma_V = 1$	$\Gamma_V = -1$
$\Gamma_I = -1$	$\Gamma_I = 1$
$T_V = 2$	$T_V = 0$
$T_I = 0$	$T_I = 2$

According to the above discussion, all the equations in this section clearly show the dual relationships between the voltage traveling waves and the current traveling waves in the transmission lines. These relationships are summarized in Table II. By applying these fundamental relationships between the voltage traveling wave and the current traveling wave in the transmission line, the electrical pulse compression and energy storage principles in a current charged transmission line and in a dual of the Blumlein line can be easily understood. The details are discussed in the following two sections.

5.2 Pulse forming in the current charged transmission line

A current charged transmission line (CCTL) [31],[33],[47] is composed of a short-circuited transmission line, a load resistance, a switch, and a power supply. Since a current source is not available for charging the system, a voltage source is used instead as the power supply. The schematic circuit diagram of a CCTL with a voltage source is shown in Fig. 5.3. It shows that the switch is located between the voltage source and the short-circuited transmission line. The length of the transmission line is l and the characteristic impedance is Z_o. The load resistance, R, is inserted between the common ground and the switch end on the transmission line side.

In the analysis, it is assuming that the switch and the voltage source are ideal. In other words, the switch has a null on-resistance, an infinite off-resistance, and an instantaneous switch-closing and switch-opening time, and the voltage source has a zero internal resistance. As soon as the switch is closed, the voltage source provides the energy to the system in the form of current traveling wave. Because the load impedance seen by the voltage source in the transient state is the parallel connection of R and Z_o, the amplitude of the current wave is limited to $V_o(R + Z_o)/RZ_o$ initially. Since the load resistance, R, is next to the voltage source, the amplitude of the current wave flowing through R at this time is V_o/R. Therefore, the amplitude of the current wave propagating down the short-circuited transmission line is V_o/Z_o. Upon reaching the short-circuited end, in-phase total reflection of the current wave ($\Gamma_I = 1$) and out-of-phase total reflection of the associated voltage wave ($\Gamma_V = -1$) occur. Theoretically, no energy can cross the short-circuited end. However, the current flowing through this end is $2V_o/Z_o$ due to $T_I = 2$ and the voltage appearing across this end is zero due to $T_V = 0$. When the reflected wave arrives at the voltage source end, total reflection occurs again due to the zero internal resistance of the voltage source. At this moment, the positive-going current traveling wave, the current wave which is propagating down the transmission

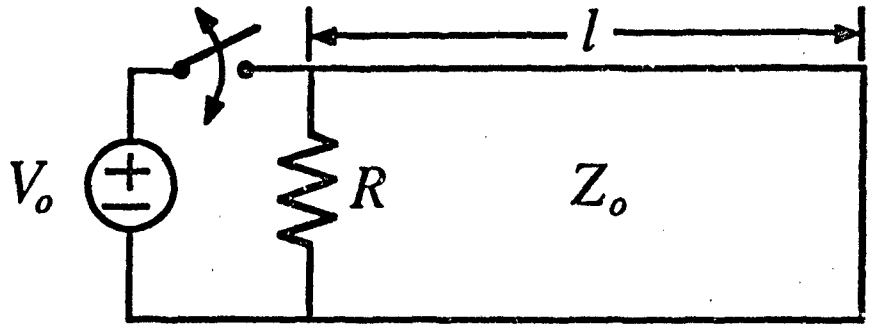

Fig. 5.3. Schematic circuit diagram of a current charged transmission line with a voltage source.

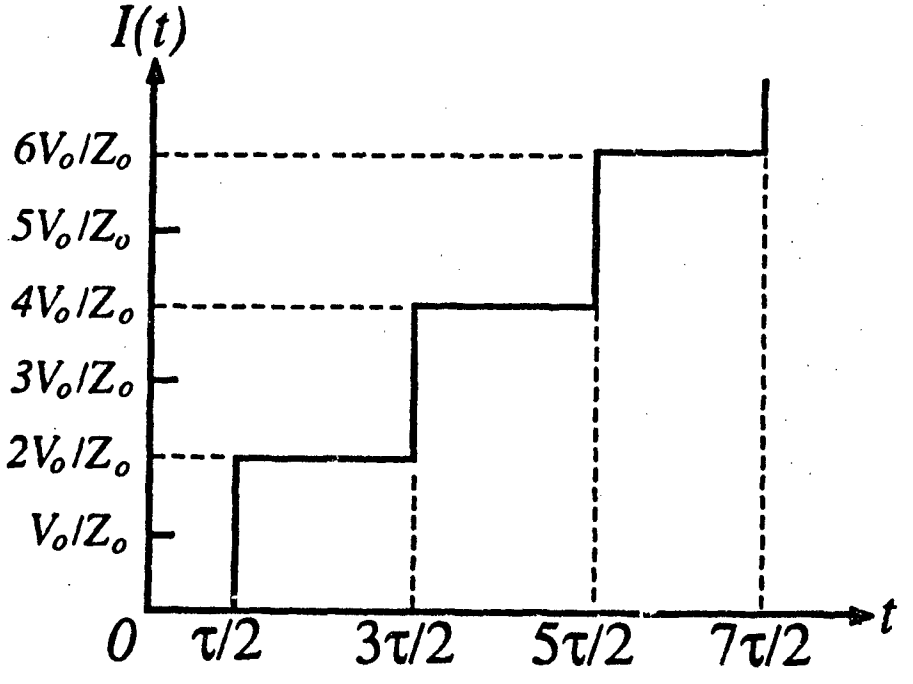

Fig. 5.4. Ideal charging current waveform at the shorted end for a current charged transmission line with a voltage source.

line, becomes the sum of this reflected wave and the continuous incoming wave from the voltage source. Hence, the amplitude of the positive-going current wave is $2V_o/Z_o$. The amplitude of the current wave which flows through R remains V_o/R. Once the wave hits the shorted end the second time, the current flowing through that end becomes $4V_o/Z_o$ and the voltage appearing across the end remains zero. With this scenario, the current waveform in the system forms a staircase-like structure while the switch is closed. This is shown in Fig. 5.4. According to this thought experiment, the amplitude of each step at the shorted end should be

$$I_s = 2V_o \frac{R+Z_o}{RZ_o} \frac{R}{R+Z_o} = \frac{2V_o}{Z_o} \tag{5.23}$$

and the duration of the step should be the round-trip time of the traveling wave in the short-circuited transmission line, that is

$$\tau = \frac{2l}{v} . \tag{5.24}$$

The factor of two in Eqn. (5.23) is due to the total reflection of the traveling wave at the shorted end ($T_I = 2$). The value of the current flowing in the transmission line appears as the sum of the positive and the negative going current traveling wave. The amplitude of the prepulse, which is the voltage V_{pre} appearing across the load while the switch is closed, is

$$V_{pre} = \frac{V_o(R+Z_o)}{RZ_o} \frac{Z_o}{R+Z_o} R = V_o . \tag{5.25}$$

If the system charging time, which is equal to the switch closing time, is t_{ch}, the charging current I_o at the end of t_{ch} will be

$$I_o = \frac{t_{ch}}{\tau} I_s = \frac{t_{ch}}{2l/v} \frac{2V_o}{Z_o} . \tag{5.26}$$

This can indirectly represent the energy stored in the transmission line. The corresponding voltage and current traveling waves which are propagating in the z-direction are shown in Fig. 5.5(a) and (b). The amplitude of these traveling waves can be clearly described by Eqns. (5.21) and (5.22). Upon opening the

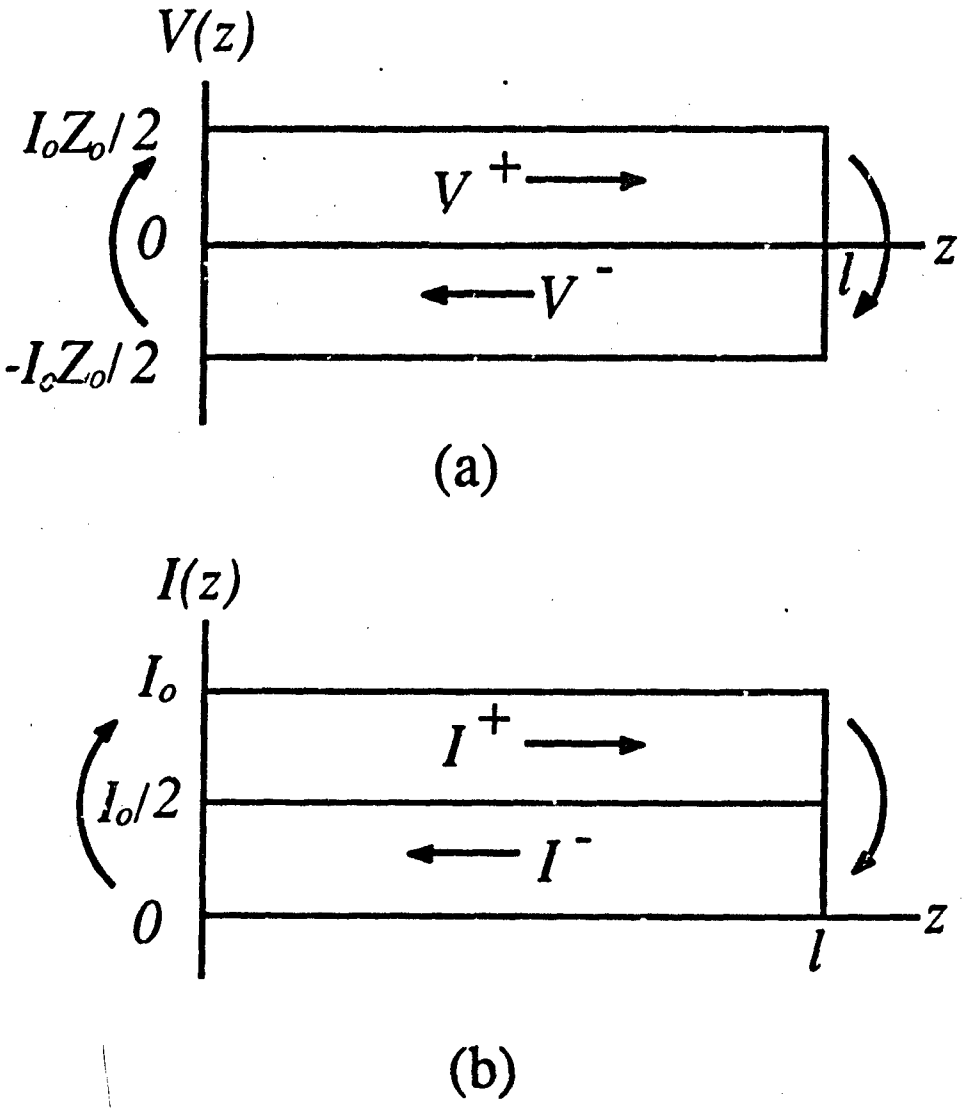

Fig. 5.5. Steady state standing wave patterns in the current charged transmission line which is charged to current I_o. (a) superposition of the voltage waves, where $V^+ + V^- = 0$; (b) superposition of the current waves, where $I^+ + I^- = I_o$.

switch, the boundary conditions at the switch end are changed and the stored energy proceeds toward the load resistance, R, to form an output voltage pulse. Since the negative-traveling wave moves toward the load first (Fig. 5.6(a) and (b)), the polarity of the output voltage waveform is opposite of the charging voltage, V_o. Depending on the load resistance, R, this waveform is in one of the following three categories:

1. $R > Z_o$, $\Gamma_V = \dfrac{R - Z_o}{R + Z_o} > 0$ and $T_V = \dfrac{2R}{R + Z_o} > 1$

This implies that partial energy is transmitted to the load resistance, R, and the rest is reflected. The reflected traveling wave at the load end is bounced back from the other end (the shorted end) without losing energy. When this traveling wave moves back to the load end, the same phenomenon of partial reflection and partial transmission occurs again. Accordingly, the output waveform consists of a series of postpulses after the main pulse with gradually reducing amplitudes. At the load end, the phase of the reflected voltage traveling wave is not altered since $\Gamma_V > 0$; yet at the other end (shorted end) where $\Gamma_V = -1$, a 180^o phase shift is introduced. This causes a change in polarity of adjacent pulses. The output voltage waveform is shown in Fig. 5.7. The duration of each pulse is equal to the round-trip time, τ, and the amplitude of the nth postpulse is given by

$$V_{out}^n = -\frac{(-\Gamma_V)^n T_V Z_o I_o}{2} = -R Z_o I_o \frac{(Z_o - R)^n}{(Z_o + R)^{n+1}}, \qquad (5.27)$$

where $n = 0$ corresponds to the main pulse.

2. $R = Z_o$, $\Gamma_V = 0$ and $T_V = 1$

No reflection occurs at the load end, all of the energy is transmitted to the load resistance, R. The output voltage waveform is shown in Fig. 5.8. The pulse duration is equal to the round-trip time, τ, and the pulse amplitude is

$$V_{out} = -\frac{Z_o I_o}{2}. \qquad (5.28)$$

3. $R < Z_o$, $\Gamma_V = \dfrac{R - Z_o}{R + Z_o} < 0$ and $T_V = \dfrac{2R}{R + Z_o} < 1$

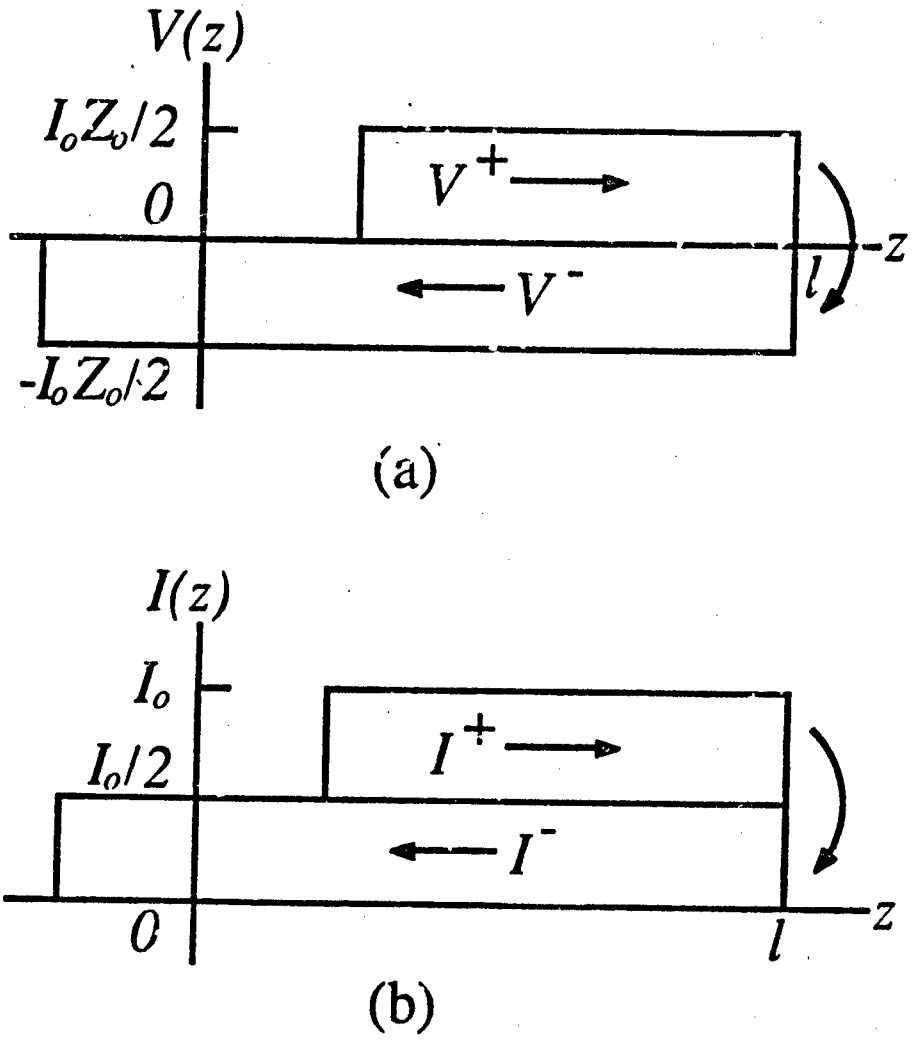

Fig. 5.6. Traveling waves in the current charged transmission line propagating in the z-direction after the switch is opened. (a) spatial distribution of the voltage waves; (b) spatial distribution of the current waves.

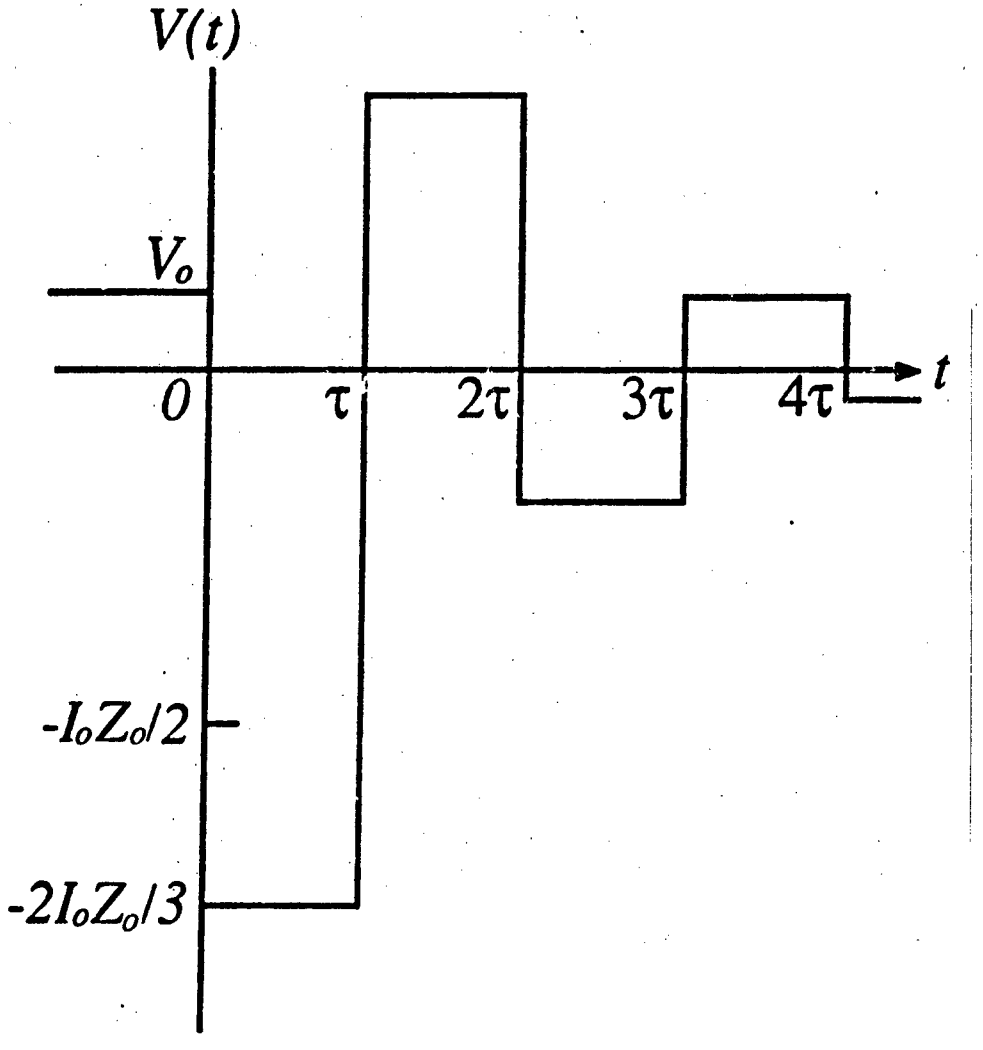

Fig. 5.7. Typical output voltage waveform from the current charged transmission line with a mismatched load, $R > Z_o$ ($R = 2Z_o$).

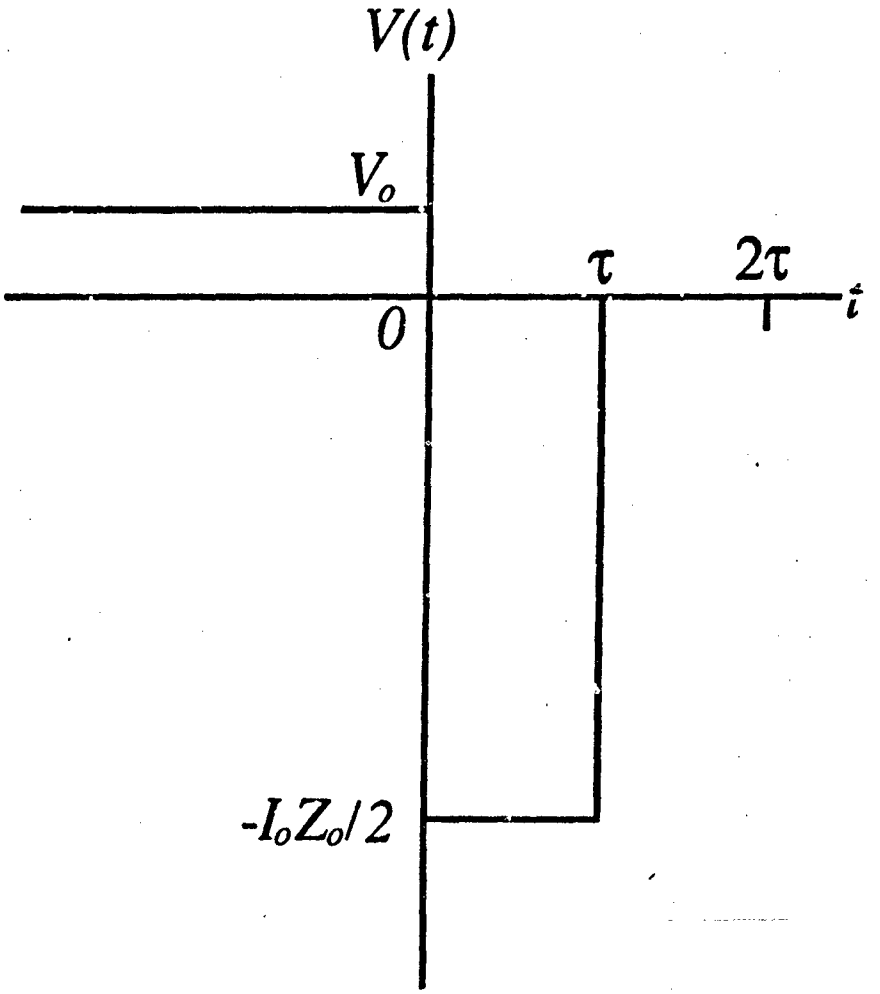

Fig. 5.8. Typical output voltage waveform from the current charged transmission line with a matched load, $R = Z_o$.

The result in this case is similar to case 1. However, the adjacent pulses do not change polarity. This is due to $\Gamma_V < 0$ at the load end and $\Gamma_V = -1$ at the shorted end causing the total phase shift to be 360° for the energy transmitted to the load resistance. The output voltage waveform is shown in Fig. 5.9. The duration of each pulse is equal to τ and the amplitude of each pulse can be described by Eqn. (5.27).

5.3 Pulse forming in the dual of the Blumlein line

A Blumlein line consists of a switch, a load resistance, R, a voltage source, V_o, and two equal length transmission lines of characteristic impedance, Z_o. As shown in Fig. 5.10, the length of each transmission lines is l; the load resistance, R, is connected in series with these two transmission lines. The end of one transmission line is opened and the other is connected to the voltage source through the charging resistor, R_{Th}. The switch is situated between the ground and the junction of R_{Th} and the transmission line. Assuming that the condition of $R_{Th} \gg Z_o$ is satisfied and the switch is constantly opened, this suggests that in-phase total reflection of the voltage traveling wave occurs at the switch end as soon as the steady state is reached and the transmission line is charged with voltage V_o. At this moment, zero voltage appears across the load resistance, R. Once the switch is closed, out-of-phase total reflection of the voltage traveling wave occurs at the switch end. Due to this change, the amplitude of the voltage pulse appearing across R can be V_o if a matched load, $R = 2Z_o$, is used in this case. The corresponding pulse duration is equal to the round trip time of the traveling wave in one transmission line i.e. $2l/v$.

By using this analogy and duality to convert the Blumlein line, the dual of the Blumlein line (DBL) is obtained [31],[36],[40]. This is shown in Fig. 5.11. Basically, the DBL is achieved by changing the series connection of the load resistance, R, and the transmission lines to a parallel connection, substituting the voltage source, V_o, with a current source, I_o, and replacing the open-circuited transmission line with a short-circuited one. The switch, in this case, becomes

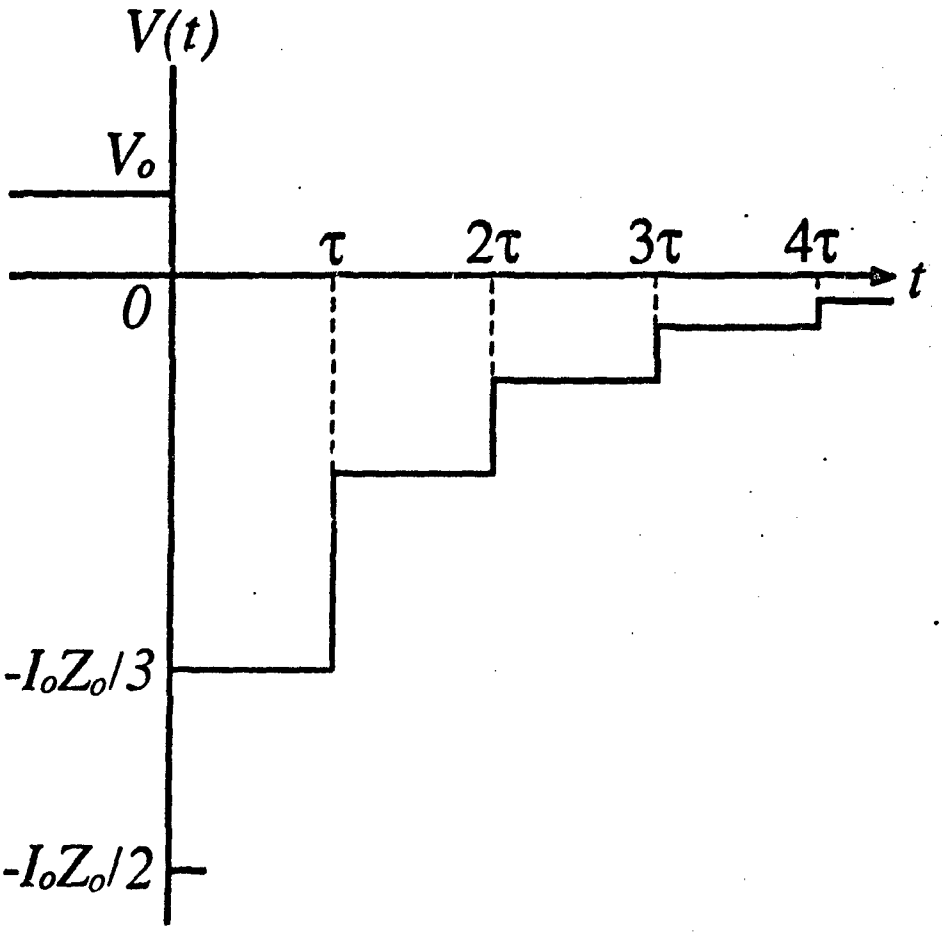

Fig. 5.9. Typical output voltage waveform from the current charged transmission line with a mismatched load, $R < Z_o$ ($R = 0.5Z_o$).

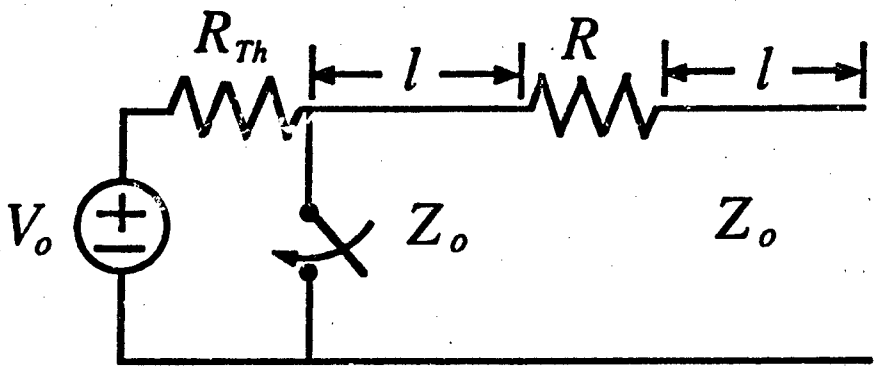

Fig. 5.10. Schematic circuit diagram of a Blumlein line with a voltage source.

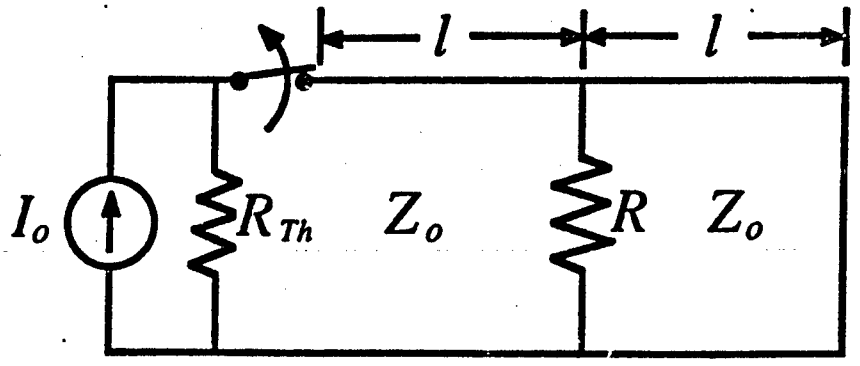

Fig. 5.11. Schematic circuit diagram of a dual of the Blumlein line with a current source.

connected in series and is left closed. Because the charging resistance, R_{Th}, becomes connected in parallel to the current source, the condition of $R_{Th} \ll Z_o$ must be met. We require $R_{Th} \ll Z_o$ in order to have an in-phase total reflection for the current traveling wave at the switch end while the steady state is reached. Upon opening the switch, the output current pulse is expected to have an amplitude of I_o and a pulse duration of $2l/v$, where the matched load, $R = Z_o/2$, is used in the circuit.

If a random load resistance, R, and a zero series connected charging resistance ($R_{Th} = 0$) are used, we can proceed with a general analysis of the DBL. Since a current source is rarely used in a pulse forming system, a voltage source is used in this analysis of the DBL. In addition, it is assuming that the switch and the voltage source used in the system are ideal. This modified circuit diagram is depicted in Fig. 5.12. As soon as the switch is closed, the energy in the voltage source is transferred to the system in the form of current traveling wave. Since the load resistance, R, is at the junction of these two transmission lines, partial reflection and partial transmission occur at the junction. By letting $Y = 1/R$ and $Y_o = 1/Z_o$ and using Eqns. (5.13) and (5.14) with $Y_L = Y + Y_o$, the reflection coefficient at the load is found to be

$$\Gamma_I = \frac{Y + Y_o - Y_o}{Y + Y_o + Y_o} = \frac{Y}{Y + 2Y_o} = \frac{Z_o}{Z_o + 2R} \; ; \tag{5.29}$$

the transmission coefficient, T_I, for the current wave across the junction to the other transmission line is found to be

$$T_I = \frac{2(Y + Y_o)}{Y + Y_o + Y_o} \frac{Y_o}{Y + Y_o} = \frac{2Y_o}{Y + 2Y_o} = \frac{2R}{Z_o + 2R} \; ; \tag{5.30}$$

and the transmission coefficient, T_R, for the current wave into the load resistance to form the prepulse while the switch is closed is found to be

$$T_R = \frac{2(Y + Y_o)}{Y + Y_o + Y_o} \frac{Y}{Y + Y_o} = \frac{2Y}{Y + 2Y_o} = \frac{2Z_o}{Z_o + 2R} \; . \tag{5.31}$$

The reason for having $Y_L = Y + Y_o$ is attributed to the parallel connection of the load resistance and the transmission line. The multiplication factors appearing

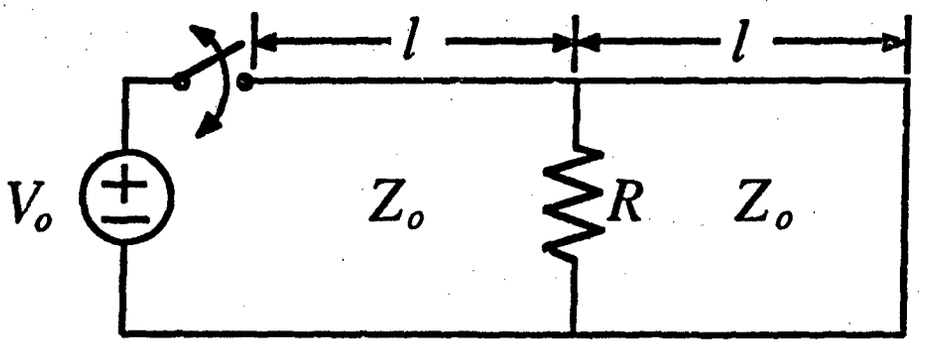

Fig. 5.12. Schematic circuit diagram of a dual of the Blumlein line with a voltage source.

in Eqns. (5.30) and (5.31) are due to treating this parallel connection as a current divider, hence the correct portion of the current wave propagating to each segment is predicted. Using Eqns. (5.29), (5.30), (5.31), and considering total reflection at the voltage source end and the shorted end where $\Gamma_V = -1$ and $\Gamma_I = 1$, the current waveform and the prepulse in this system can be obtained by iteration. This iteration process, which takes the discontinuity of the transmission line at the load junction into consideration, is described below.

At $t = 0$, the switch is closed and a current wave of amplitude V_o/Z_o propagates along the transmission line. Upon reaching the load junction at $t = l/v$, the transmitted and reflected portion of the wave can be determined by Eqns. (5.29), (5.30) and (5.31). They are

$$I_{sw}^{-}(t) = \frac{V_o}{Z_o}\frac{Z_o}{Z_o + 2R} = \frac{V_o}{Z_o + 2R} \tag{5.32}$$

for the amplitude of the reflected wave,

$$I_{sh}^{+}(t) = \frac{V_o}{Z_o}\frac{2R}{Z_o + 2R} \tag{5.33}$$

for the amplitude of the wave transmitted to the shorted line, and

$$I_L(t) = \frac{V_o}{Z_o}\frac{2Z_o}{Z_o + 2R} = \frac{2V_o}{Z_o + 2R} \tag{5.34}$$

for the amplitude of the wave transmitted to the load resistance, where I_{sw} and I_{sh} represent the current traveling wave in the transmission line before and after the load resistance respectively, and I_L is the current flowing through the load resistance. When $t > l/v$, the transmitted part proceeds to the shorted end and the reflected part moves toward the source end. Since these two lines are of equal length, the part reaching the shorted end at $t = 2l/v$ is synchronized with the part returning to the voltage source end. This suggests that total reflection occurs at these two ends simultaneously. In this case, the current wave at the source end, $I_{sw}^{+}(t)$, becomes the sum of the reflected wave and the wave leaving the voltage source. The corresponding amplitude at $t > 2l/v$ becomes

$$I_{sw}^{+}(t) = \frac{V_o}{Z_o}\left(1 + \frac{Z_o}{Z_o + 2R}\right) = \frac{V_o}{Z_o}\frac{2(Z_o + R)}{Z_o + 2R}\,. \tag{5.35}$$

At $t = 3l/v$, this wave reaches the load junction simultaneously with the wave reflected from the shorted end. At this instance, Eqns. (5.29), (5.30), and (5.31) have to be used for both traveling waves again. This makes the amplitudes of the traveling waves at the junction for $t > 3l/v$ become

$$I_{sw}^{-}(t) = \frac{V_o}{Z_o}\frac{2(Z_o^2 + RZ_o + 2R^2)}{(Z_o + 2R)^2}\,, \tag{5.36}$$

$$I_{sh}^{+}(t) = \frac{V_o}{Z_o}\frac{2(3RZ_o + 2R^2)}{(Z_o + 2R)^2}\,, \tag{5.37}$$

and

$$I_L(t) = \frac{4V_oZ_o}{(Z_o + 2R)^2}\,. \tag{5.38}$$

In brief, Eqns. (5.36) and (5.37) are obtained from the sum of the wave reflected from the same line and the wave transmitted from the other line, and Eqn. (5.38) is obtained from the sum of the wave transmitted from both lines. Since the voltage source is able to continuously provide energy to the system, the amplitude of the positive current traveling wave will increase by a step whenever the total reflection occurs at the voltage source end. Since total reflections at both ends and both partial reflection and transmission at the load junction occur after every round trip of the traveling wave in each transmission line of the length l, the charging current will accumulate in a staircase-like structure with a step duration of

$$\tau = \frac{2l}{v}\,. \tag{5.39}$$

The detailed analysis of this current accumulation and the prepulse is shown in Appendix II.

According to the previous analysis, the increment of the charging current in the transmission line to the right of the load junction is always one step lower than that in the line to the left of the load junction. Depending on the load resistance, R, the charging current waveform and the output voltage waveform can be classified into one of the following three categories:

1. $R > Z_o/2$

Due to the partial reflection and the partial transmission at the load, the steps of the staircase-like current waveform are not of the same amplitude. We assume that the switch closing time, which is equal to the system charging time, is t_{ch}. As the step duration is $2l/v$, the number of steps in this charging process is found to be

$$n = \frac{t_{ch}}{\tau} = \frac{t_{ch}}{2l/v} . \tag{5.40}$$

By extending the above discussion to the nth round trip, the equations for I_{sw}^{+}, I_{sw}^{-}, I_{sh}^{+}, and I_{sh}^{-} can be obtained. By using

$$I_{sw} = I_{sw}^{+} + I_{sw}^{-} \tag{5.41}$$

and

$$I_{sh} = I_{sh}^{+} + I_{sh}^{-} , \tag{5.42}$$

the corresponding charging current flowing through the switch at the end of t_{ch} is given by

$$I_{sw} = \frac{nV_o}{Z_o} + \frac{V_o}{4}\left(\frac{Z_o - 2R}{RZ_o}\right)\left[1 - \left(\frac{Z_o - 2R}{Z_o + 2R}\right)^{n-1}\right] \tag{5.43}$$

and the current flowing across the shorted end is given by

$$I_{sh} = \frac{(n-1)V_o}{Z_o} - \frac{V_o}{4}\left(\frac{Z_o - 2R}{RZ_o}\right)\left[1 - \left(\frac{Z_o - 2R}{Z_o + 2R}\right)^{n-1}\right] . \tag{5.44}$$

The prepulse which is strongly influenced by the load resistance, R, is found to be

$$V_{pre} = \frac{V_o}{2}\left[1 - \left(\frac{Z_o - 2R}{Z_o + 2R}\right)^{n}\right] ; \tag{5.45}$$

this is not a constant voltage as in the CCTL. The detailed derivations of these three equations are shown in Appendix II. If t_{ch} is long enough such that $n \gg 1$, the difference between I_{sw} and I_{sh} in Eqns. (5.43) and (5.44) can be neglected and the amplitude of the prepulse in Eqn. (5.45) gradually approaches $V_o/2$. Thus, it is possible to treat the system with a uniformly distributed current,

I_o, at the end of t_{ch}, that is $I_o \simeq I_{sw} \simeq I_{sh}$. The corresponding voltage and current traveling waves propagating in z-direction are shown in Fig. 5.13(a) and (b). The prepulse across the load resistance and the charging current waveform observed at the shorted end are shown in Fig. 5.14(a) and (b).

As soon as the switch is opened at the time of t_{ch}, the boundary conditions at the switch end are changed to $\Gamma_I = -1$ and $\Gamma_V = 1$. In this case, the reflected voltage traveling wave does not change its polarity, but the reflected current traveling wave does. Hence, the positive traveling wave moving toward the load from the switch end becomes $I_{sw}^+ = -I_o/2$ and $V_{sw}^+ = -I_o Z_o/2$ due to the reflection (Fig. 5.15(a) and (b)). As shown in Fig. 5.15(b), when this current wave meets the negative traveling wave reflecting from the shorted end with an unchanged polarity, i.e. $I_{sh}^- = I_o/2$, the main pulse of the output current flowing through the load resistance becomes

$$I_{out} = (I_{sw}^+ - I_{sh}^-)\left(\frac{2Z_o}{Z_o + 2R}\right) = \left(-\frac{I_o}{2} - \frac{I_o}{2}\right)\left(\frac{2Z_o}{Z_o + 2R}\right) = -\frac{2I_o Z_o}{Z_o + 2R} \tag{5.46}$$

and the pulse duration is the round trip time of the traveling wave propagating in one transmission line, that is $\tau = 2l/v$. The reason for choosing $I_{sw}^+ - I_{sh}^-$ in Eqn. (5.46) is discussed in Appendix II. Since this is not a matched load, a series of postpulses follow the main pulse. The amplitude of the mth postpulse can be expressed as

$$V_{out}^m = -2RZ_o I_o \frac{(Z_o - 2R)^m}{(Z_o + 2R)^{m+1}}, \tag{5.47}$$

where $m = 0$ corresponds to the main pulse. Since $(Z_o - 2R) < 0$ in this case, adjacent postpulses have opposite polarities. The output voltage pulse shape is shown in Fig. 5.16. Notice that the adjacent pulses are separated by a time of $\tau = 2l/v$. This is very different from the results in a CCTL, where there is no interpulse separation. The reason for this separation can be understood intuitively. The spacing occurs because the dual of the Blumlein line has one end open-circuited and the other end short-circuited at this time. Owing to the

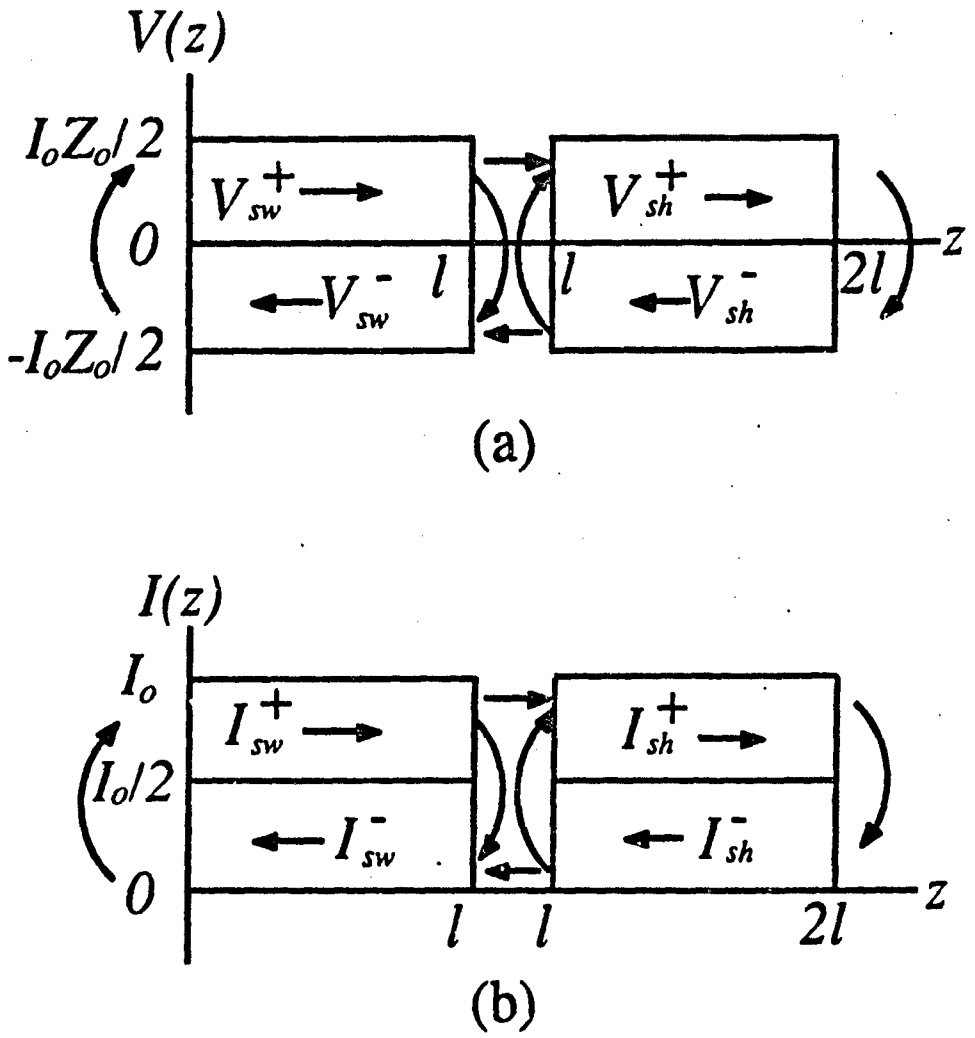

Fig. 5.13. Steady state standing wave patterns in the dual of the Blumlein line which is charged to current I_o, the arrows at the load junction represent the directions of partial transmission and partial reflection. (a) superposition of the voltage waves, where $V_{sw}^+ + V_{sw}^- = 0$ and $V_{sh}^+ + V_{sh}^- = 0$; (b) superposition of the current waves, where $I_{sw}^+ + I_{sw}^- = I_o$ and $I_{sh}^+ + I_{sh}^- = I_o$.

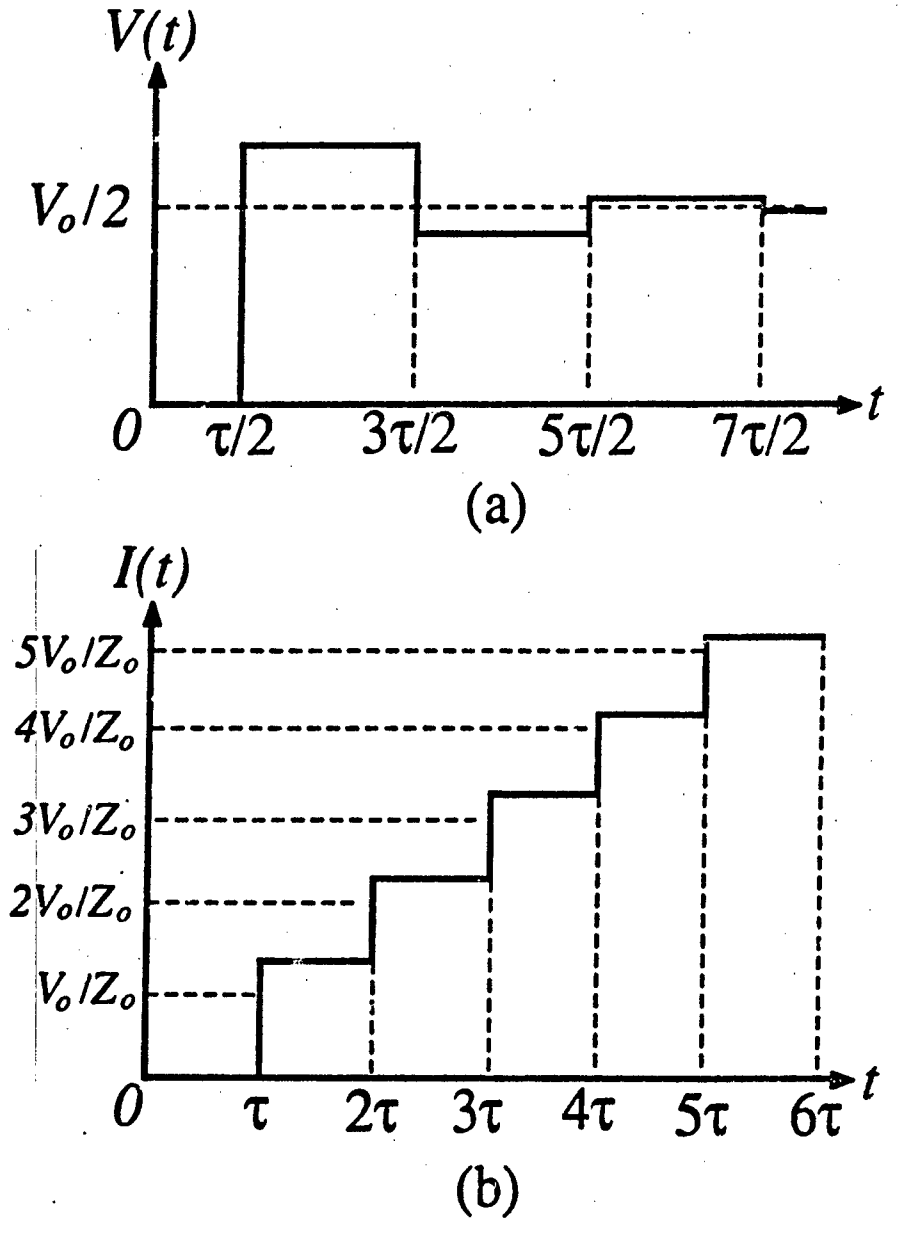

Fig. 5.14. Typical waveforms from the dual of the Blumlein line with a mismatched load, $R > Z_o/2$ ($R = Z_o$), when the switch is closed. (a) the prepulse; (b) the charging current waveform at the shorted end with an ideal switch.

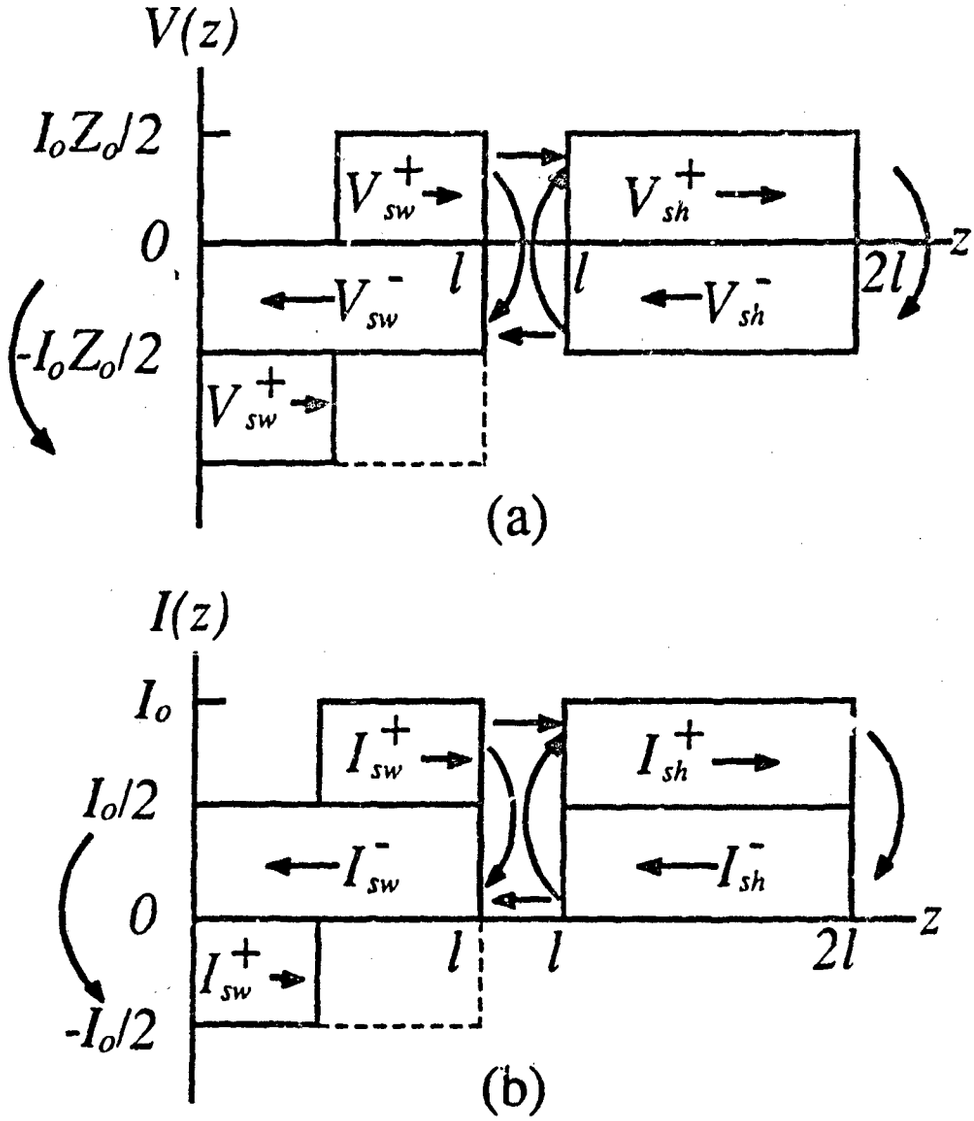

Fig. 5.15. Traveling waves in the dual of the Blumlein line propagating in the z-direction after the switch is opened, the arrows at the load junction represent the directions of partial transmission and partial reflection. (a) spatial distribution of the voltage waves; (b) spatial distribution of the current waves.

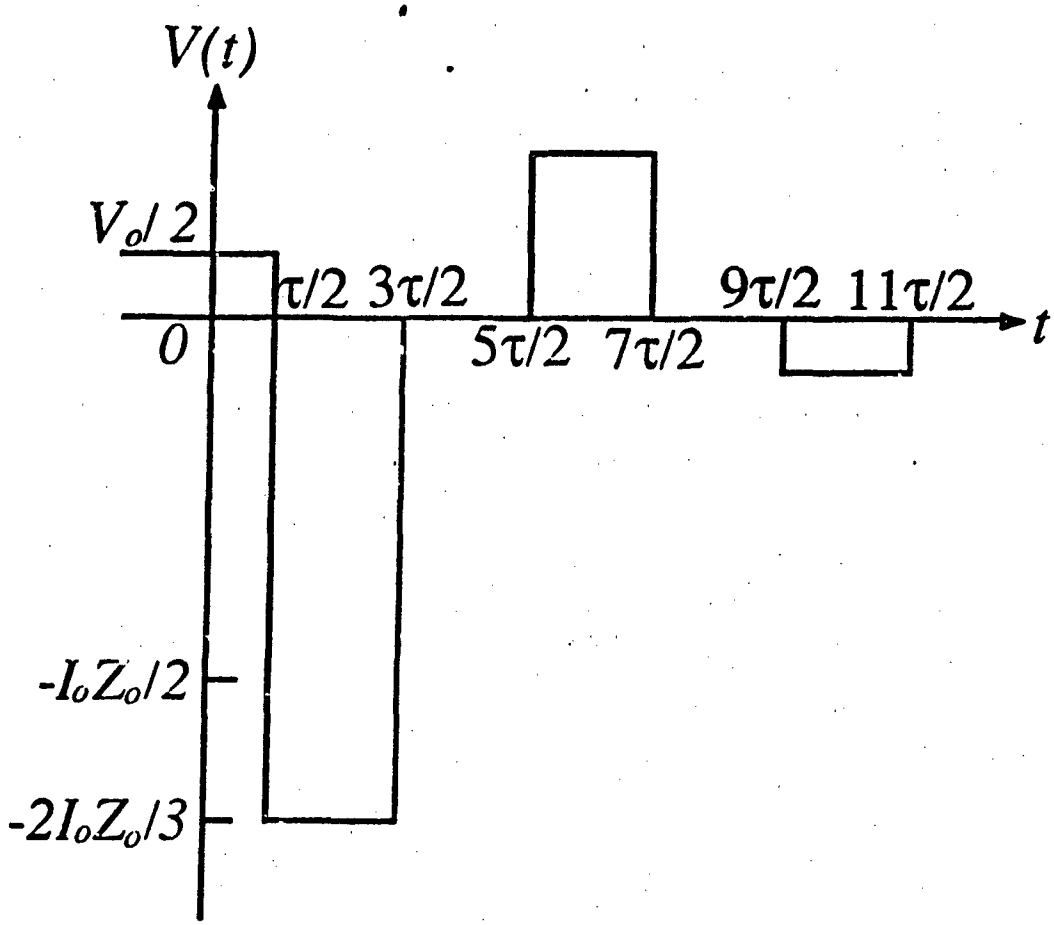

Fig. 5.16. Typical output voltage waveform from the dual of the Blumlein line with a mismatched load, $R > Z_o/2$ ($R = Z_o$).

out-of-phase total reflection of the current traveling wave at the opened end, the current traveling waves add up with each other and appear across the load resistance as the main pulse. Then, the reflected energy propagates toward both ends. Another out-of-phase total reflection of the current traveling wave occurs at the opened end (the switch end). Since this is the second time reflected from this opened end, the total phase difference between the reflection from the opened end and that from the shorted end disappears in this duration. Hence, these two current traveling waves cancel each other out as soon as they reach the load resistance, and thus the output voltage becomes zero. In this manner, the $2l/v$ interpulse separation is automatically generated.

2. $R = Z_o/2$

Here, the load is matched to the system, therefore all of the equations discussed in the previous case can be simplified to concise expressions. For instance, the staircase-like charging current waveform will have a constant step amplitude V_o/Z_o and the prepulse will be a constant value $V_o/2$. The charging current at the end of t_{ch} will be $I_{sw} = nV_o/Z_o$ on the switch side and $I_{sh} = (n-1)V_o/Z_o$ across the shorted end. The voltage and current traveling waves propagating in z-direction are the same as shown in Fig. 5.13(a) and (b) as well as Fig. 5.15(a) and (b). The prepulse across the load resistance and the charging current waveform observed at the shorted end are shown in Fig. 5.17(a) and (b). The amplitude of the output current pulse in this case becomes

$$I_{out} = I_{sw}^{+} - I_{sh}^{-} = -\frac{I_o}{2} - \frac{I_o}{2} = -I_o \qquad (5.48)$$

under the assumptions that $n = t_{ch}/\tau \gg 1$ and $I_o \simeq I_{sw} \simeq I_{sh}$. Since the load is matched to the system, no partial reflection and transmission occur at the load resistance when the switch is opened. This suggests that the stored energy is fully transferred to the load resistance, R, in the main pulse and no postpulses come after the main pulse. The corresponding output voltage pulse with an amplitude of $V_{out} = -I_o Z_o/2$ and a duration of $\tau = 2l/v$ is shown in Fig. 5.18.

3. $R < Z_o/2$

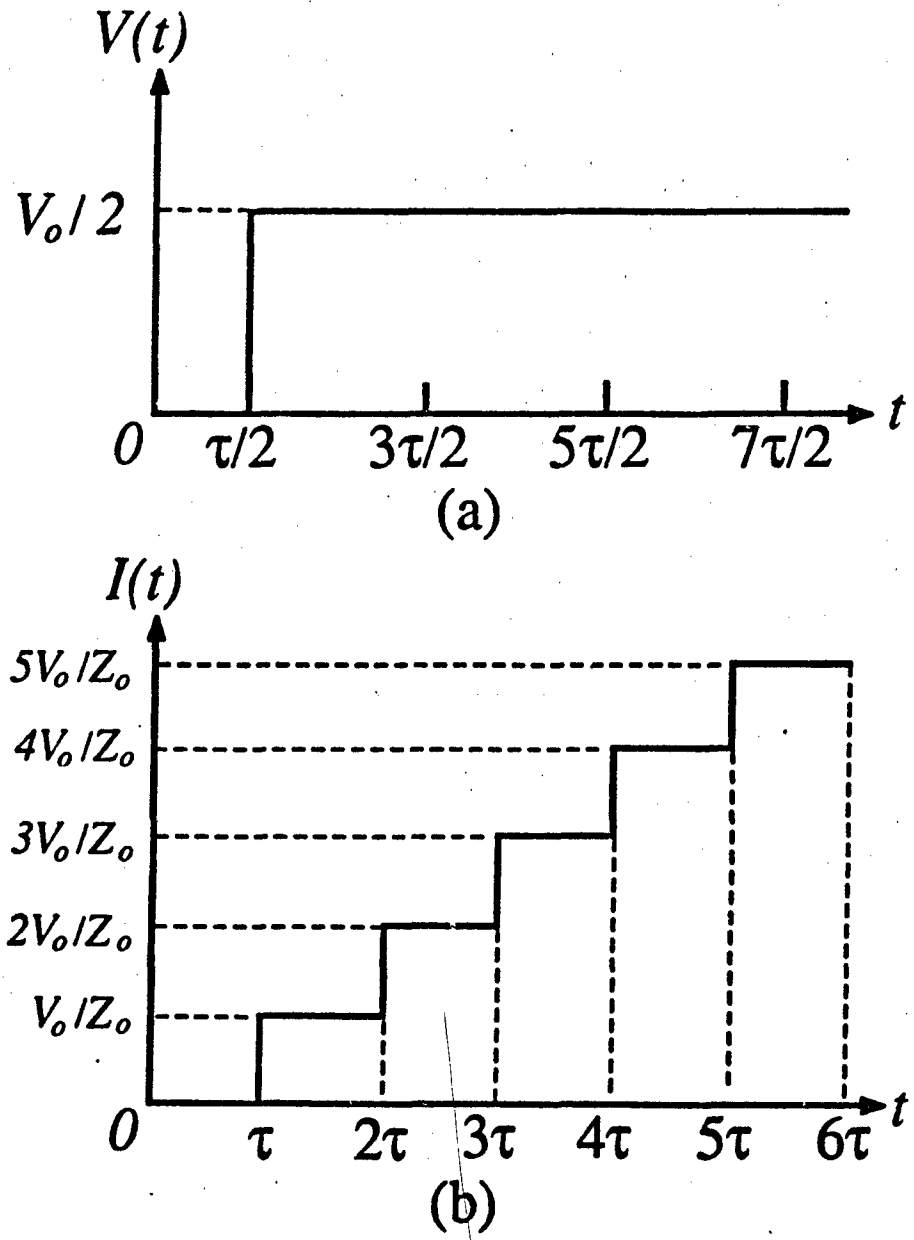

Fig. 5.17. Typical waveforms from the dual of the Blumlein line with a matched load, $R = Z_o/2$, when the switch is closed. (a) the prepulse; (b) the charging current waveform at the shorted end with an ideal switch.

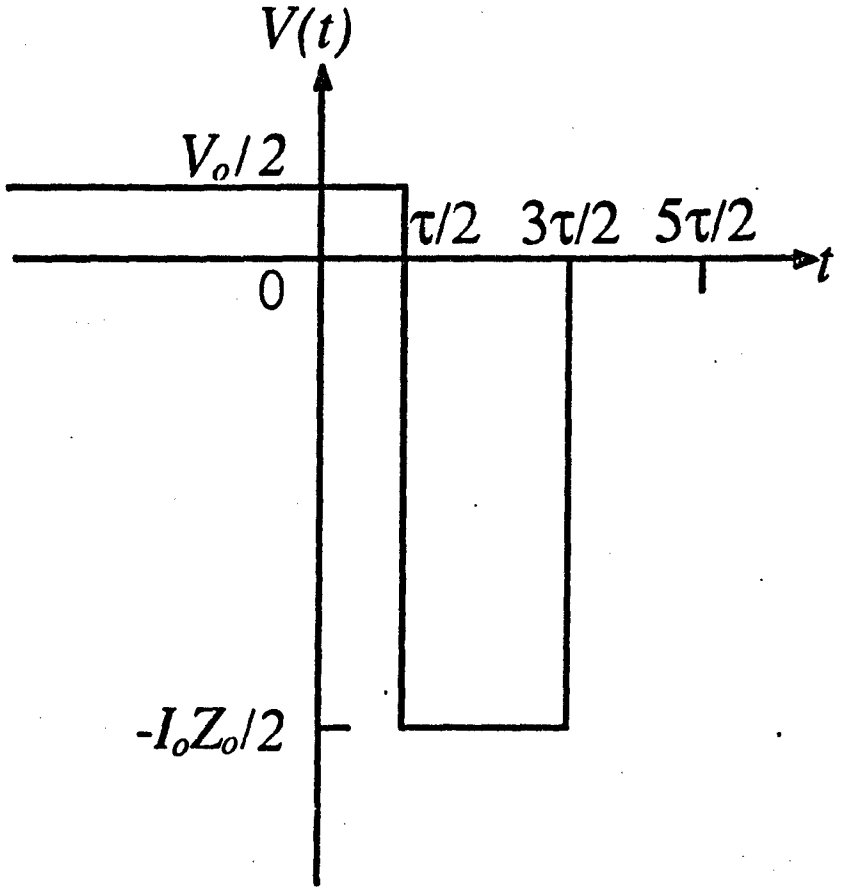

Fig. 5.18. Typical output voltage waveform from the dual of the Blumlein line with a matched load, $R = Z_o/2$.

All of the equations discussed in case 1 can be applied to this case. However, because of $(Z_o - 2R) > 0$, the pulse shape is very different from case 1. Assuming $n \gg 1$ and $I_o \simeq I_{sw} \simeq I_{sh}$, the voltage and current traveling waves propagating in z-direction can still be pictured by Fig. 5.13(a) and (b) as well as Fig. 5.15(a) and (b). The prepulse appearing across the load resistance and the charging current flowing through the shorted end are shown in Fig. 5.19(a) and (b). The output voltage waveform which has the same polarity for all of the postpulses is shown in Fig. 5.20.

5.4 Comparison between the current charged transmission line and the dual of the Blumlein line

Through the discussion in Sections 5.2 and 5.3, the differences between a CCTL and a DBL can be immediately found by assuming that the total length of the charging line are the same. That is $l = 2l'$ for the CCTL and $l = l'$ for the DBL. Geometrically, the major difference between these two circuits is the position of the load resistance. By comparing Figs. 5.3 and 5.12, we see that the DBL can be obtained from the CCTL by merely moving the load resistance at the switch end to the center of the transmission line. Since some conventional opening switches discussed in Chapter 2 often employ a strong magnetic and/or electric field to decrease the switch opening time, the environment adjacent to the switch is certainly full of electromagnetic interference. Since the load resistance in the DBL is far away from the opening switch, this interference to the output waveforms can be reduced by choosing an appropriate length of the line and by using a carefully designed geometrical configuration.

In addition to the geometrical difference, the output waveforms are also very different. The first difference is the prepulse, V_{pre}; that is $V_{pre} = V_o$ for the CCTL, but is $V_{pre} \simeq V_o/2$ for the DBL if $t_{ch} \gg 2l'/v$ with an arbitrary load resistance R. The second difference is the charging current waveform. In the CCTL, the amplitude of each step is $I_s = 2V_o/Z_o$ and the duration is $4l'/v$ for $l = 2l'$. As discussed in Section 5.2, the step amplitude in the CCTL is

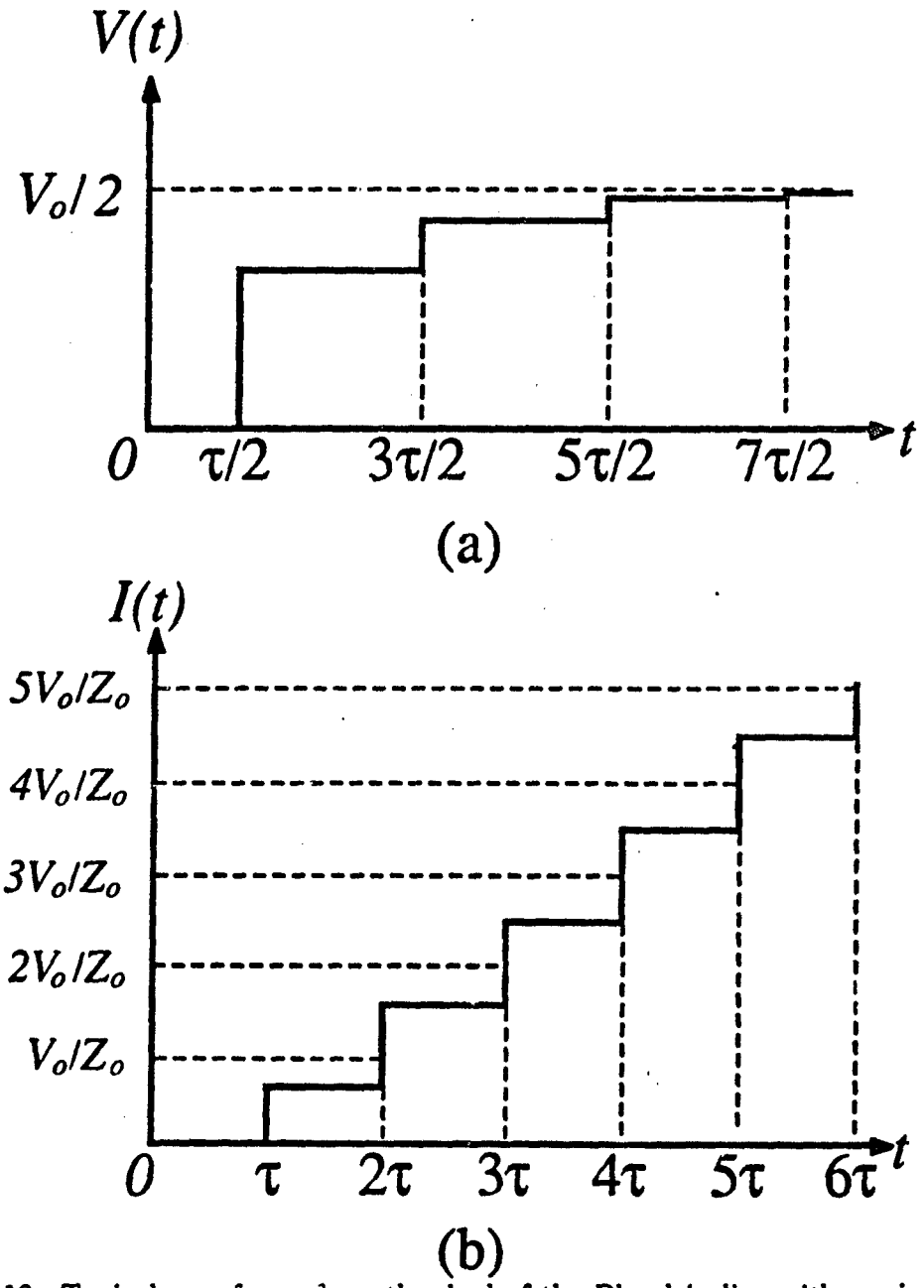

Fig. 5.19. Typical waveforms from the dual of the Blumlein line with a mismatched load, $R < Z_o/2$ ($R = 0.25Z_o$), when the switch is closed. (a) the prepulse; (b) the charging current waveform at the shorted end with an ideal switch.

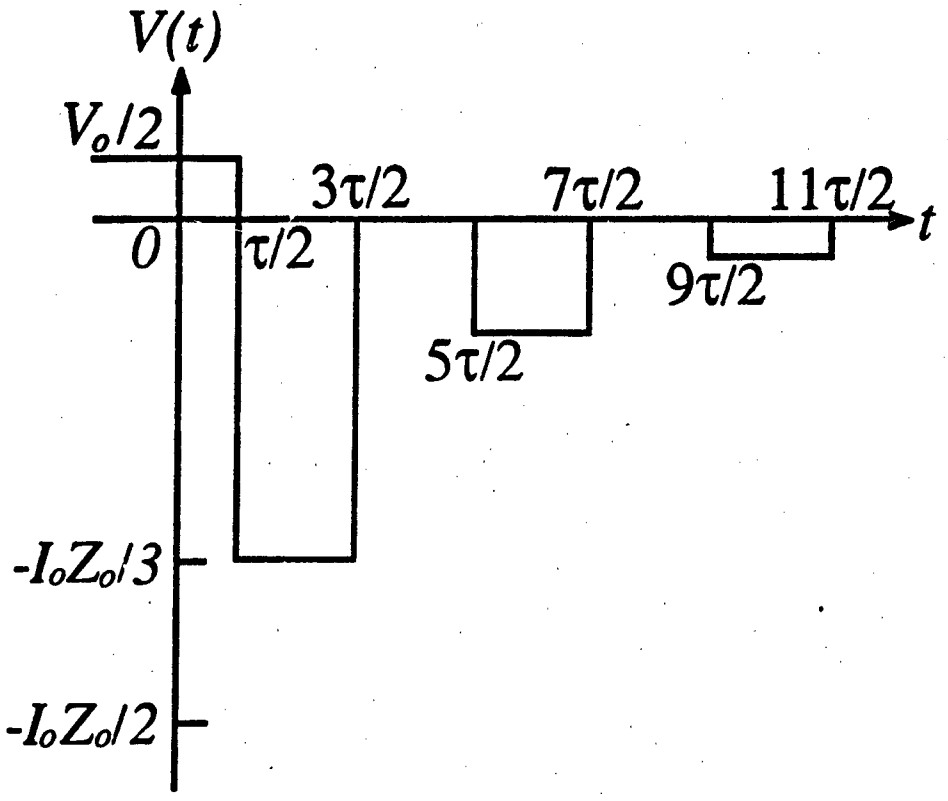

Fig. 5.20. Typical output voltage waveform from the dual of the Blumlein line with a mismatched load, $R < Z_o/2$ ($R = 0.25Z_o$).

independent of the load resistance. On the other hand, the amplitude of each step in the DBL is varying according to the load resistance, R, and the duration is $2l'/v$ which is half of that in the CCTL. If $t_{ch} \gg 2l'/v$, the charging current in the DBL would be

$$I_o \simeq I_{sh} \simeq \left(\frac{t_{ch}}{2l'/v}\right)\left(\frac{V_o}{Z_o}\right) , \tag{5.49}$$

which is the same as the charging current in the CCTL,

$$I_o = \left(\frac{t_{ch}}{4l'/v}\right)\left(\frac{2V_o}{Z_o}\right) = \left(\frac{t_{ch}}{2l'/v}\right)\left(\frac{V_o}{Z_o}\right) . \tag{5.50}$$

If $R = Z_o/2$, the matched load in the DBL, the amplitude of each step in the DBL would be V_o/Z_o which is half of that of the CCTL. Since the amount of the charging current in these two systems is identical for $t_{ch} \gg 2l'/v$, this implies that the number of steps in the DBL should be twice as many as that in the CCTL.

Under the matched load condition, $R = Z_o$ in the CCTL and $R = Z_o/2$ in the DBL, the output voltage pulse amplitude from both the DBL and the CCTL is $I_oZ_o/2$, hence,

$$V_{out} = \frac{I_oZ_o}{2} = \left(\frac{t_{ch}v}{4l'}\right)V_o . \tag{5.51}$$

We define the voltage gain G_V as the ratio of the peak output voltage pulse V_{out} to the input charging voltage V_o, that is

$$G_V = \frac{V_{out}}{V_o} = \frac{I_oZ_o}{2V_o} = \frac{t_{ch}v}{4l'} . \tag{5.52}$$

Both the CCTL and DBL have the same voltage gain. However, the pulse duration is $2l'/v$ for the DBL and $4l'/v$ for the CCTL. The peak power from the CCTL is

$$P_{CCTL} = \left(\frac{I_o}{2}\right)^2 Z_o = \left(\frac{t_{ch}v}{4l'}\right)^2\left(\frac{V_o^2}{Z_o}\right) \tag{5.53}$$

and the peak power from the DBL is

$$P_{DBL} = I_o^2\left(\frac{Z_o}{2}\right) = 2\left(\frac{t_{ch}v}{4l'}\right)^2\left(\frac{V_o^2}{Z_o}\right) . \tag{5.54}$$

By Comparing Eqns. (5.53) and (5.54), we see that the output peak power from the DBL is twice of that from the CCTL with the same total length of the charging line. This does not imply the DBL is more desirable than the CCTL. We must also consider the voltage across the switch during the opening stage. As the total reflection of the voltage traveling wave at the switch end does not change polarity during the opening stage, the voltage across the switch, V_{DBL}, in the DBL is

$$V_{DBL} = V_o + V^+ + V^- = V_o + \frac{I_o Z_o}{2} + \frac{I_o Z_o}{2} = V_o + I_o Z_o \qquad (5.55)$$

and the voltage across the switch, V_{CCTL}, in the CCTL is

$$V_{CCTL} = V_o + V^- = V_o + \frac{I_o Z_o}{2} . \qquad (5.56)$$

By comparing Eqns. (5.55) and (5.56), the voltage across the switch in the DBL is greater than that in the CCTL by $I_o Z_o/2$. This implies that the limiting output voltage from the DBL can not be as high as that in the CCTL due to the earlier breakdown of the switch with a higher charging voltage.

If the total length of the CCTL is half that of the DBL, that is l for the CCTL and $2l$ for the DBL. The duration of the output voltage pulse, which is $2l/v$, would be the same for both of them. Yet the amount of the charging current is different by a factor of two in these two systems; the current in the CCTL is

$$I_{CCTL} = \left(\frac{t_{ch} v}{l}\right) \frac{V_o}{Z_o} \qquad (5.57)$$

and in the DBL is

$$I_{DBL} = \left(\frac{t_{ch} v}{2l}\right) \frac{V_o}{Z_o} . \qquad (5.58)$$

In this case, the output current I_{out} and the voltage across the switch V_{sw} during the opening stage are the same, that is

$$I_{out} = I_{DBL} = \left(\frac{t_{ch} v}{2l}\right) \frac{V_o}{Z_o} \qquad (5.59)$$

and

$$V_{sw} = V_{DBL} = V_{CCTL} = V_o + I_{out}Z_o \,. \tag{5.60}$$

The corresponding output voltage pulse amplitude and the voltage gain from the CCTL are

$$V_{out} = \frac{I_{CCTL}Z_o}{2} = I_{out}Z_o = \left(\frac{t_{ch}v}{2l}\right)V_o \tag{5.61}$$

and

$$G_V = \frac{t_{ch}v}{2l} \tag{5.62}$$

respectively. The corresponding quantities obtained from the DBL are

$$V_{out} = \frac{I_{DBL}Z_o}{2} = \frac{I_{out}Z_o}{2} = \frac{1}{2}\left(\frac{t_{ch}v}{2l}\right)V_o \tag{5.63}$$

and

$$G_V = \frac{1}{2}\frac{t_{ch}v}{2l} \tag{5.64}$$

respectively. According to Eqns. (5.61), (5.62), (5.63), and (5.64), the output voltage pulse amplitude and the voltage gain of the CCTL are twice of that of the DBL in this configuration. In addition, another key feature which is worth noticing in this configuration is the output peak power; the output peak power from the CCTL is

$$P_{CCTL} = \left(\frac{t_{ch}v}{2l}\right)^2 \frac{V_o^2}{Z_o} \,, \tag{5.65}$$

while the power from the DBL is

$$P_{DBL} = \frac{1}{2}\left(\frac{t_{ch}v}{2l}\right)^2 \frac{V_o^2}{Z_o} \,, \tag{5.66}$$

which is only half that from the CCTL.

For the case of mismatched load, $R \neq Z_o$ for the CCTL and $R \neq Z_o/2$ for the DBL, the output voltage waveform would be very different from the matched case. In this case, there is no interpulse separation between adjacent postpulses obtained from the CCTL, but there is a time separation corresponding to the round-trip time, $\tau = 2l/v$, of one transmission line in the DBL between adjacent postpulses.

According to the above discussions, the DBL has several advantages over the CCTL. The first one is that in the DBL the switch is far away from the load resistance, so that the load is physically separated from the magnetic or electric field interference in the switch which may occur during the opening stage. The second advantage is that the DBL is suitable for systems with a lower load resistance. Also in contrast to its dual circuit, the Blumlein line, the DBL is capable of connecting directly to the load impedance without having a grounding problem. Unlike the Blumlein line, it requires either triple-layer parallel plates or triple-concentric coaxial cables to intricately avoid the grounding problem.

5.5 Summary

Pulse forming principles in two types of inductive pulse forming lines, the current charged transmission line and the dual of the Blumlein line, have been discussed in great detail. The dual of the Blumlein line with a matched load is able to generate a square pulse with the peak current amplitude equal to the charging current; this is twice of that of a simple current charged transmission line. Another notable feature of the DBL is that the opening switch is located at the end of the transmission line, thus, the output voltage pulse is not affected by the interference of the switch during the opening process. In contrast to the Blumlein line, the DBL is capable of directly connecting to a lower impedance system without suffering the grounding problem.

CHAPTER 6

Fast Photoconductive Semiconductor Opening Switches

Through the discussions in the last three chapters, one can understand the basic photoconductive semiconductor switch physics and the pulse forming theories in different inductive energy storage systems. With this knowledge, the next step is to demonstrate the feasibility of employing the photoconductive semiconductor switch (PCSS) as an opening switch in an inductive energy storage system. As mentioned in Chapter 2, conventional opening switches have rather long opening times. Therefore, the first step in this research was to demonstrate that the opening time of the PCSS is much faster than any of the conventional opening switches.

Based on this guideline, short carrier recombination time materials become the primary candidates. The experimental work which is accomplished with the switches of short carrier recombination time is discussed throughout this chapter. In the first section, we discuss the results from a lumped inductive circuit. Then, the following section centers on the works with a current charged transmission line. The experimental results in these two sections clearly demonstrate that the opening time of the PCSS can be as fast as 1 ns and the repetition rate can be up to 10 Hz. The switches used are of microstrip line structure. The main purpose of using the microstrip line structure is to maintain the continuity of the transmission line and to preserve the high speed/frequency response in the circuit. Furthermore, the laser system used to activate the switches was a cw Ar^+ laser at 514 nm wavelength. Because this photon energy exceeds the band gap energy of those switches used, single photon direct absorption and surface conductivity are the dominated effects in determining the switch on-resistance. In this case, the fast opening requirements were easily satisfied by using the

microstrip line switch and Ar^+ laser.

However, the switch efficiency is too low to observe any voltage gain from the inductive energy storage system. In order to understand this, the on-resistance of the switches used in the pulse forming experiment were measured under various laser powers at 514 nm wavelength. The experimental results are shown in the last section of this chapter. According to these measurements, the switch on-resistance can only be reduced to the range of few hundred ohms even with the tightest focus of the cw laser light beam at a few watts of power. Hence, it is impossible to have a low enough switch on-resistance to observe the voltage gain. From this study, we concluded that lowering the switch on-resistance to a few ohms would become the next major goal in this research. For this purpose, different laser systems at a longer wavelength were employed. The experimental works and the results are discussed in the next chapter.

6.1 Signal response in the lumped inductive circuit

The main objective of this experiment is to demonstrate the feasibility of using the PCSS as an opening switch in a lumped inductive circuit. Since the opening time of those conventional opening switches listed in Chapter 2 is in the range of microseconds, this is too slow for high power fast pulse generation. Thus, the first approach in this research was to use the materials with a short carrier recombination time in order to obtain a fast opening time. In other words, the switch design is very critical in preserving high speed/frequency response. In order to satisfy this high speed/frequency requirement, all of the switches used in this experiment are of the microstrip line structure which can maintain the fast response with geometric continuity of the transmission line and impedance matching. In this case, the switch geometry is then either a simple strip line gap (Fig. 6.1(a)) or an interdigitated gap (Fig. 6.1(b)).

The laser system used to activate the switch also had to meet the fast opening requirement. As mentioned in Chapter 3, the semiconductor surface is always rich in surface states due to the discontinuity of the crystal structure.

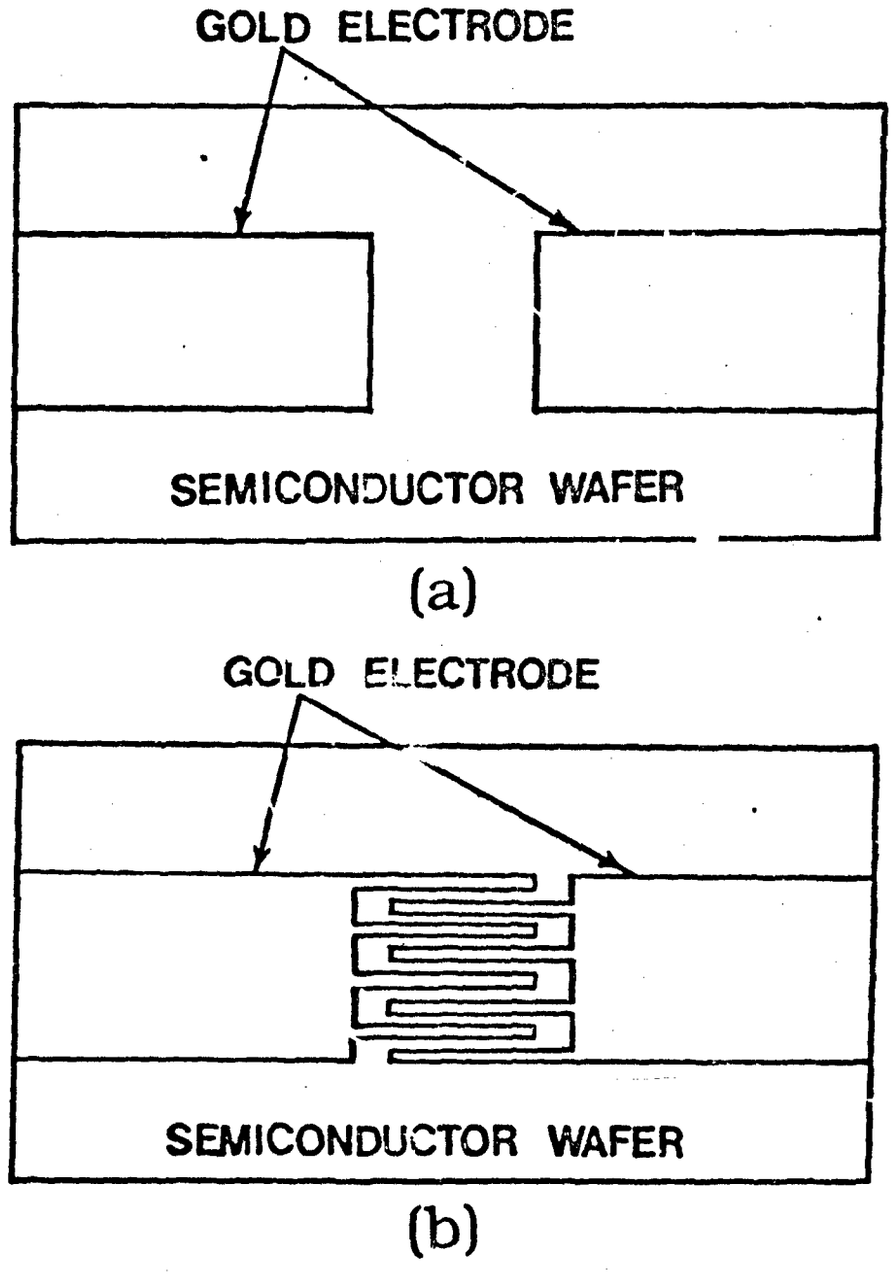

Fig. 6.1. Geometries used for the switch gap. (a) simple strip line gap; (b) interdigitated gap.

Because those surface states behave like recombination centers, they effectively shorten the recombination time. Thus, we can take the advantage of this surface phenomenon by using the laser light of single photon direct absorption wavelength, which is accompanied by a shallow penetration depth, to obtain a fast opening of the switch. Furthermore, a long conduction time of the switch is required to charge the inductive energy storage system. This strongly suggests the use of a cw laser system to achieve this requirement.

Based on the above statement, a 6.4 W cw Ar^+ laser (Spectral Physics, Model 171) was used to activate the switch in the experiment. The wavelength used was 514 nm, this corresponds to 2.4 eV per photon. This is higher than the band gap energy of those semiconductor materials listed in Table I. Hence, the switch on-resistance is mainly determined by single photon direct absorption and surface conducting effect. In the pulse forming experment, the switch was continuously illuminated with cw laser light for charging the inductive energy storage system. In order to discharge the inductive system effectively, the switch had to be opened as quickly as possible. This implies that the cw laser light must be interrupted on a nanosecond or shorter time scale. For this purpose, a Pockels cell sandwiched between two polarizers was used in the experimental setup. This is shown in Fig. 6.2. Because the Pockels cell is an electro-optic crystal, it is able to rotate the polarization of the incoming light to a certain angle by applying an appropriate voltage in the z-direction [68]. In this setup, the orientation of the polarizer and the analyzer were in parallel to allow the 514 nm vertically polarized green light to pass through. Since the output of the Ar^+ laser was vertically polarized, the light could continuously shine on the switch to lower the resistance. The fast interruption of the light was then achieved by applying the half-wave voltage, which was ~4.3 kV for 514 nm green light, across the Pockels cell. A Lasermetrics 8612C high voltage pulse generator was used to provide a 200-ns-long half-wave high voltage pulse.

In other words, the light to the switch was interrupted for 200 ns due to

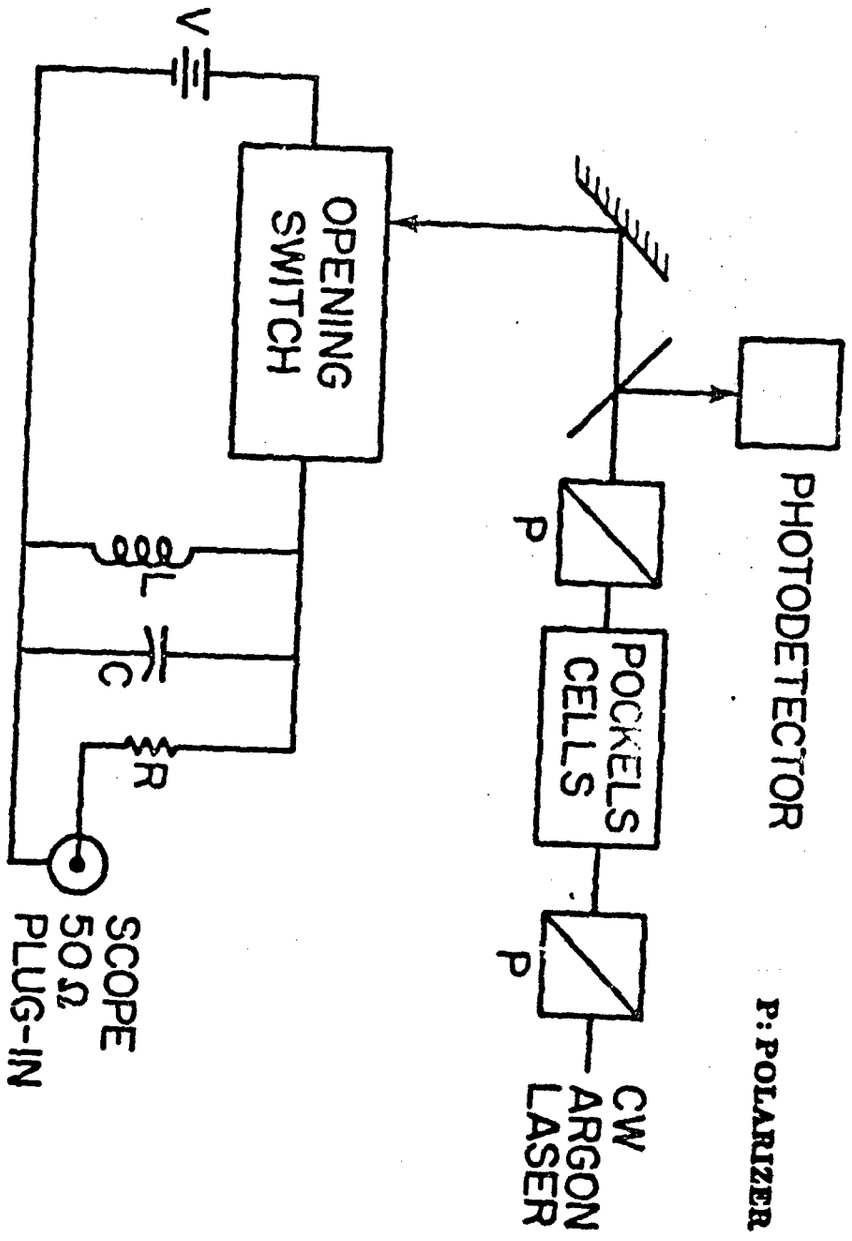

Fig. 6.2. Experimental setup for the inductive energy storage circuit.

a 90° rotation of its polarization. As shown in Fig. 6.3(a) which shows the optical pulse detected by an HP photopindiode, the interruption of the laser light was very fast (1 ns) and very efficient (contrast ratio > 200). The change of the current $I(t)$ flowing through the resistor due to the change of the switch resistance from the on-state to the off-state was observed and registered on the oscilloscope. As shown in Fig. 6.2, the 50 Ω oscilloscope amplifier plug-in was in series with a known resistor to form the load resistance for the lumped inductive circuit. Thus, the response signal, $V(t)$, would be $V(t) = I(t) \times 50$. By using the equations discussed in Chapter 4, all the circuit variables can be calculated from the output current $I(t)$. In this experiment, the observed signal rise-time is restricted by three factors:

1. carrier recombination time in the switch,
2. Pockels cell response time (~ 1 ns),
3. Oscilloscope response time (~ 1 ns),

so it is impossible to observe a signal which is faster than 1 ns.

Because of the electromagnetic noise emitted from the high voltage pulse generator, the circuit was built in a shielded box. Since no capacitance was used in the lumped inductive circuit, the capacitive effect shown in the results was due directly to the parasitic capacitance in the transmission line, in the semi-rigid coaxial cable, and in the switch. The value of this capacitance can be evaluated from the experimental measurements by using Eqn. (4.23). The results which are reported by E. A. Chauchard et al [5] are quoted in the following. The switches used were a GaAs switch with a 200 μm simple strip line gap and a Fe:InGaAs switch with a 4 μm interdigitated gap. The measured dark resistances, R_{off}, were 2 MΩ for the GaAs switch and 150 kΩ for the Fe:InGaAs switch. A 2-W cw Ar^+ laser focused on the switch gaps was used to keep the switch closed. The corresponding switch on-resistances, R_{on}, were 10 kΩ for the GaAs switch and 150 Ω for the Fe:InGaAs switch.

The results obtained with the GaAs switch under the conditions of differ-

ent circuit parameters are shown in Fig. 6.3(b)-(e). Fig. 6.3(b) displays the oscillatory case, that is $\Delta < 0$. The result in Fig. 6.3(d) is still the oscillatory case but it is close to the critical damped case ($\Delta = 0$). By using the damping time constant and the oscillatory period in these two results, the parasitic capacitance is found to be 22 pF. The overdamped cases, $\Delta > 0$, are shown in Fig. 6.3(c) and (e). In Fig. 6.3(c), the parasitic capacitance is almost negligible when it is compared with other circuit parameters. Therefore, it is possible to calculate the fall time of the signals by assuming that there is no capacitance in the circuit and still obtain a good agreement with the experimental results. The calculated and observed fall time from Fig. 6.3(c) is 400 ns. The corresponding switch on-resistance in this case is found to be 12.5 kΩ. By measuring the slope of the rising current at $t = 0$ and then using Eqn. (4.21), we estimate the parasitic capacitance to be ~30 pF for the result shown in Fig. 6.3(e). This leads to a calculated fall time of $\tau = 260$ ns which is in a good agreement with the observed value.

Due to the slow recombination time in the intrinsic material, the result of the fastest opening time which was observed with the GaAs switch was ~5 ns (Fig. 6.3). But with the Fe:InGaAs switch with 300-ps recombination time, the switch turn-off time was limited by the Pockels cell rise-time (1 ns), and the signal rise-time was restricted by the oscilloscope response time (1 ns). As shown in Fig. 6.4, this 1 ns switch opening time was indeed observed with this switch. According to this result, it is possible to conclude that the switch opening time is limited by the longer of the following times: the Pockels cell rise-time (1 ns), and the carrier recombination time in the semiconductor. The possible jitter in these two experimental results is then also determined by the longer of these two times. Since these two times are within a nanosecond time scale, the time jitter is almost negligible when it is compared to the time scale of the output waveforms and thus the jitter free operation is demonstrated. For example, the output waveforms shown in Fig. 6.3 demonstrated a response at the instant

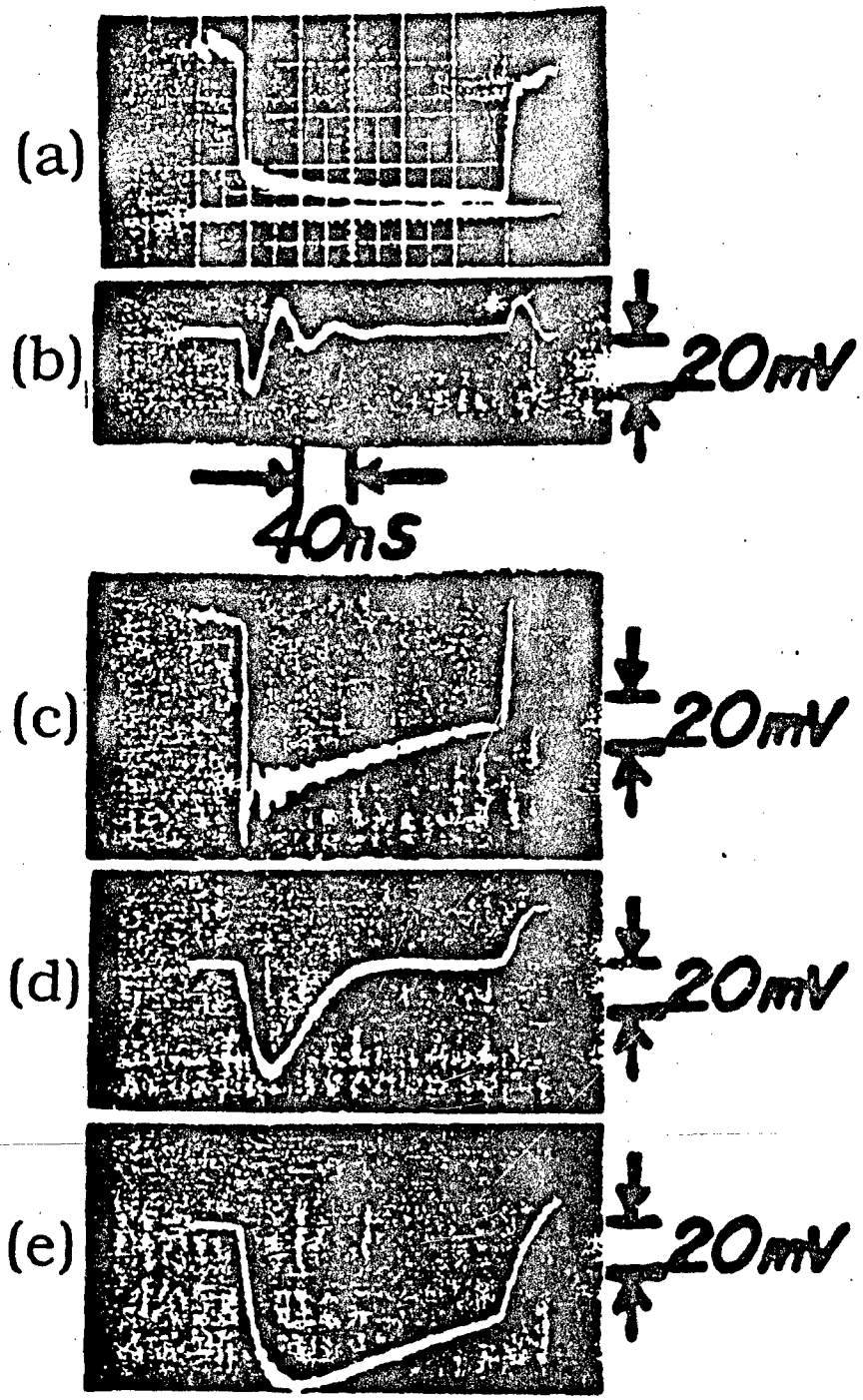

Fig. 6.3. (a) 200-ns-long cut-off of the light. (b)-(e) output voltage waveforms obtained with the GaAs switch at $V = 20$ V, $R_{on} = 12.5$ KΩ and $R_{off} = 85$ KΩ, no capacitance is used. (b) $R_L = 573\ \Omega$, $L = 1.8\ \mu$H; (c) $R_L = 50\ \Omega$, $L = 20\ \mu$H; (d) $R_L = 573\ \Omega$, $L = 20\ \mu$H; (e) $R_L = 573\ \Omega$, $L = 156\ \mu$H.

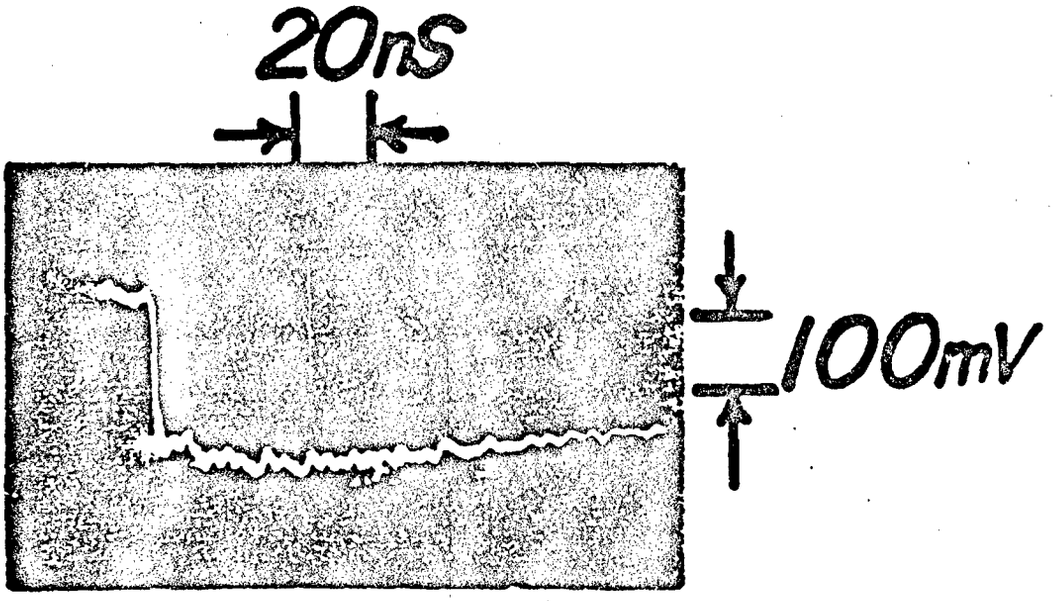

Fig. 6.4. Output voltage waveform obtained with the Fe:InGaAs switch at $R_L = 50\ \Omega$ and $L = 20\ \mu$H showing a 1-ns rise-time.

when the laser light was interrupted.

Another important feature which was demonstrated in this experiment was the high current density. By employing the absorption depth of GaAs ($\sim 0.1\ \mu$m) at this wavelength and the width of the electrode (~ 0.5 mm), the cross-sectional area of the current profile A is found to be 5×10^{-11} m^2. Since the voltage across the GaAs switch was 20 V and the switch resistance at the on-state was 12.5 kΩ, the current flowing through the switch can then be obtained by using Ohm's law. That is

$$I = \frac{V}{R_{on}} = 1.6 \text{ mA} . \tag{6.1}$$

Thus, the current density J was calculated to be

$$J = \frac{I}{A} = 3.2 \text{ kA/cm}^2 . \tag{6.2}$$

Since the estimated current density was on the order of 3 kA/cm^2, it seems very promising to apply this type of opening switch to high current systems as long as the dimensions of the switch are enlarged.

In conclusion, due to the fast signal response time and high current density, this semiconductor opening switch is suitable for high repetition rate and high power systems. Because it is activated by laser light via the photoconductive effect, it is jitter free during the switch closing stage. Since the carrier recombination time in the switch can be less than 1 ns, there is a negligible output signal jitter during the switch opening stage. As mentioned in Chapter 1 and 2, the main purpose of the inductive energy storage circuit is to generate high voltage pulses. Especially when a voltage source is used to charge the system, voltage gain should be observed. However, the output voltage obtained from this experiment were all much less than the charging voltage. This can be attributed to the high switch on-resistance, R_{on}=12.5 kΩ, which limits the charging current in the inductor during the charging period. This suggests that low switch on-resistance is also a key parameter for a successful opening switch.

6.2 Pulse generation in the current charged transmission line

Because the response times of the lumped inductive circuits are limited by the L/R time constant, they can only generate pulses with an exponential fall-time. If fast pulses or square pulses in the nanosecond or picosecond scale are preferred for the applications, the current charged transmission line (CCTL) will be the most suitable candidate. In this square pulse generation experiment, two major goals were achieved. One is to demonstrate the capabilities of the PCSS's to be used in the CCTL for the purpose of fast pulse generation. The other is to reveal the potential of repetitive operation by using a PCSS in an inductive energy storage system. Since the high voltage pulse generator for the Pockels cell was manually triggered in the previous experiment, all the results displayed were obtained with the single shot operation. In order to operate the system repetitively, two modifications have been made to the experimental setup shown in Fig. 6.2. This modified experimental setup is shown in Fig. 6.5.

As in the figure, the first modification was to use a mechanical chopper in the laser path to chop the cw Ar^+ laser at 10 Hz. The pulse duration of the laser light which was determined by the geometry of the chopper disc was ~35 ms. The main purpose of using this chopper was to reduce the laser illumination time on the switch. This is because the switch on-resistance, which is discussed in Chapter 3, is determined by the incident optical power and is not related to the optical pulse duration as long as this duration is much longer than the carrier lifetime. In addition, the experimental results and the analysis discussed later in this section show that the system charging time only lasts for one round-trip time of the traveling wave in the transmission line. This is due to the high switch on-resistance limiting the amount of the charging current during the charging process. In this case, long illumination time can not further charge the inductive system but might heat the switch to generate more thermal carriers. Since thermal dissipation is always a slow process, the excess heat in the material might prolong the carrier recombination time and increase the switch opening time. In other words, the switch illumination time must be properly adjusted to

PD: PHOTODETECTOR

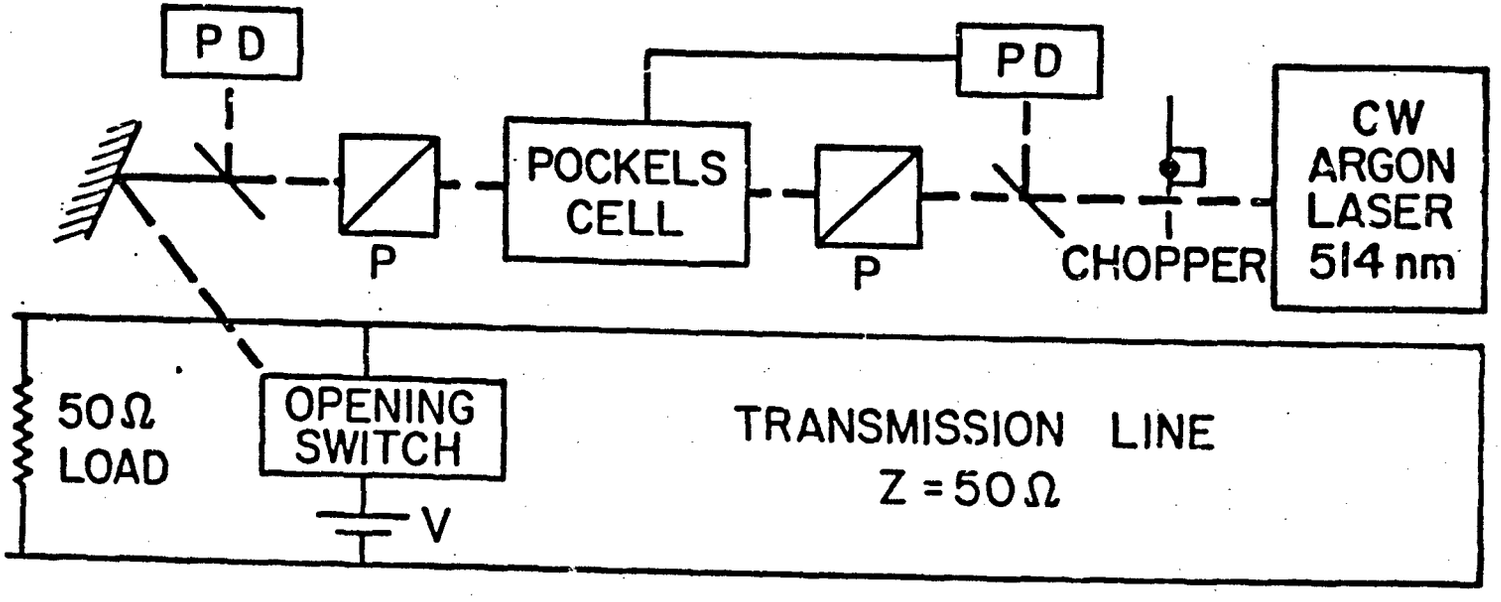

Fig. 6.5. Experimental setup for the current charged transmission line.

balance between the charging time and the thermal integration time. Practically speaking, some results show that this 35 ms illumination time at 10 Hz is long enough to make at least one switch suffer from this thermal effect. This implies that shorter illumination time for higher repetition rate operation might be required for all of the switch materials.

Because the chopper was chopping the laser light at 10 Hz, the synchronization between the laser light to the switch and the trigger for the Pockels cell must be established in order to obtain meaningful output waveforms. This requirement leads to the second modification, which was placing a home-made delay circuit in the experimental setup to trigger the 8612C high voltage pulse generator. The key function of this circuit was to delay the trigger signal to the pulse generator between 5 ms and 20 ms from the rising edge of this 35-ms-long laser pulse. By using this circuit, the system charging time can now be varied from 5 ms to 20 ms after the switch was activated by the laser light. Furthermore, the triggering process was no longer manual as shown in the previous section, it could now be automatically accomplished at a repetition rate of 10 Hz. The timing of this triggering process is shown in Fig. 6.6.

In this pulse forming experiment, the high voltage pulse generator for the Pockels cell was able to provide a 300-ns-long high voltage pulse and the CCTL was a 6-meter long RG-58 coaxial cable with one end shorted. The other end of this cable was connected to a voltage source through an opening switch. The load resistance, which was matched to the characteristic impedance of the transmission line, was the 50 Ω plug-in of a Tektronix 7A24 amplifier and was connected in parallel with the CCTL. The schematic circuit diagram is also shown in Fig. 6.5. From the pulse forming theory of the CCTL which is discussed in Chapter 5, it can be understood that there is no reflection occuring at the matched load end when the switch is suddenly opened due to the interruption of the laser light for 300 ns.

Four switches were used in this CCTL. They are

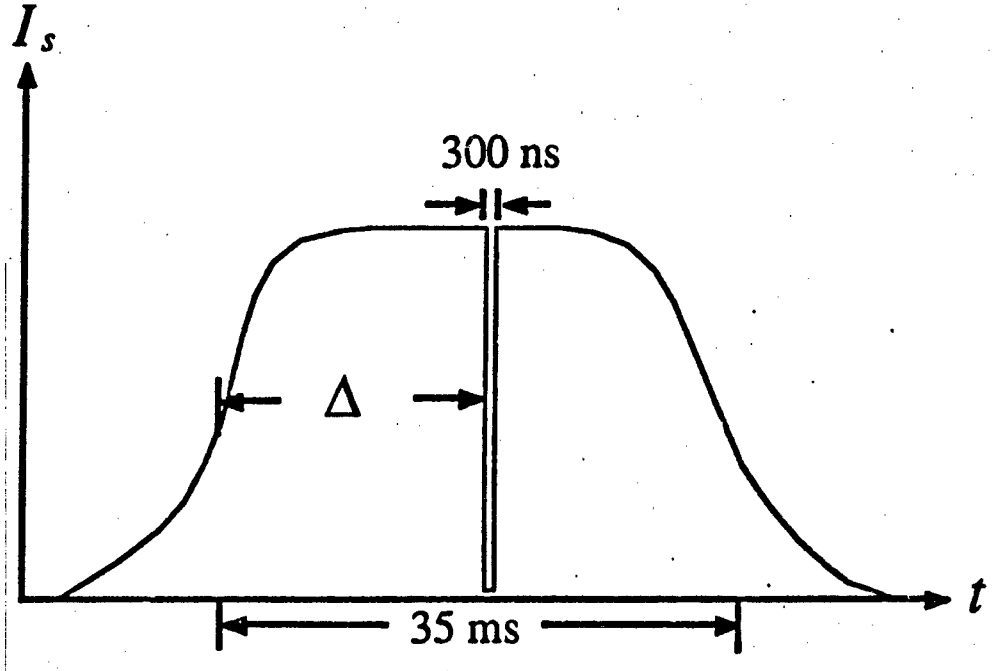

Fig. 6.6. Description of the laser pulse shape and the triggering process, where Δ can be varied from 5 ms to 20 ms.

1. GaAs switch with a 21 μm simple strip line gap,
2. Cr:GaAs switch with a 30 μm simple strip line gap,
3. Fe:InGaAs switch with a 3 μm simple strip line gap,
4. Fe:InGaAs switch with a 6 μm interdigitated gap.

Because the switch gaps were all very small, the cw Ar^+ laser power, which was focused on the gap to keep the switch on, was kept at less than 0.5 W in the experiment to avoid damaging the switches. The ideal output waveform displayed on the oscilloscope should be a 60-ns-long square pulse which is equal to the round-trip time of the traveling wave in this 6-meter-long transmission line. The amount of the charging current, I_o, in the CCTL would be limited by the switch on-resistance, R_{on}, and the charging voltage, V_o. This yields

$$I_o = \frac{V_o}{R_{on}} . \tag{6.3}$$

Since the switch off-resistance is much higher than the load resistance (50 Ω), not much energy is dissipated by the switch. Thus the efficiency of the energy transferred to the load, which can be defined as the ratio of the output energy to the stored energy in the CCTL, should be 100%. In this case, the charging current, I_o, can be derived from the output voltage amplitude, V_p, of the square pulse displayed on the oscilloscope, that is

$$I_o = \frac{2V_p}{50} . \tag{6.4}$$

By combining Eqn. (6.3) and (6.4), the switch on-resistance is found to be

$$R_{on} = 50\frac{V_o}{2V_p} . \tag{6.5}$$

The square pulses obtained with these four switches are shown in Fig. 6.7. The slightly noisy appearance of the leading edge of the pulses is due to the mode beating of the Ar^+ laser at a frequency of 100 MHz corresponding to its cavity length. In order to prevent the interference of the noise emitted by the pulse generator, the switch was put in a shielded box during the experiment.

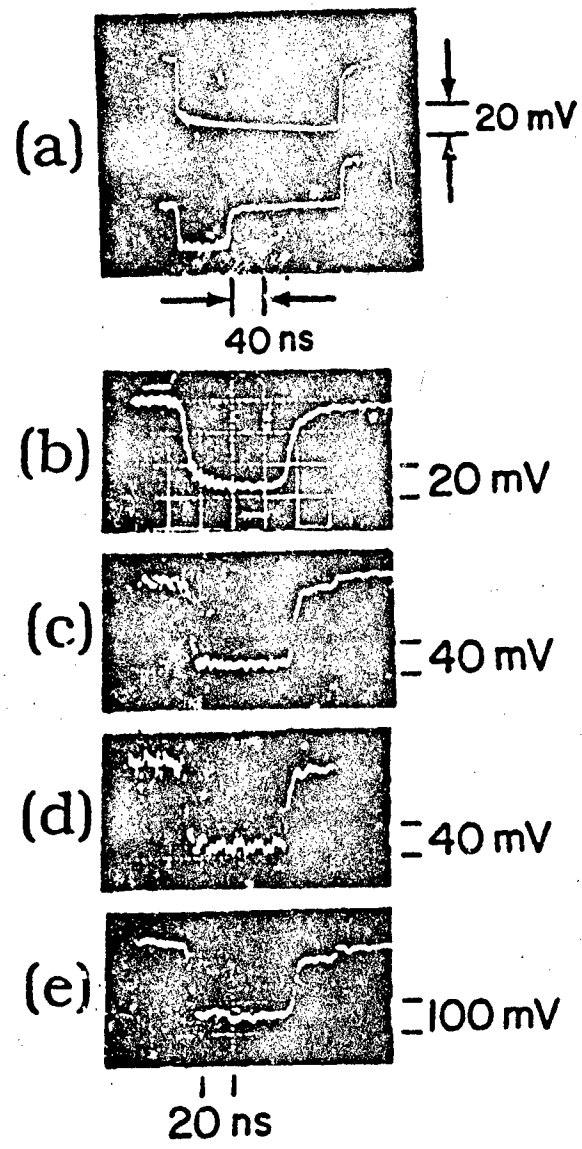

Fig. 6.7. (a) Top, 300-ns-long cut-off of the light; bottom, general output waveform obtained from the current charged transmission line. Following square pulses are obtained with (b) switch 1, 5 V bias voltage (c) switch 2, 15 V (d) switch 3, 4 V (e) switch 4, 2 V; these switches are listed in page 117.

According to the results (Fig. 6.7), the fastest rise-time was obtained with the Cr:GaAs switch with a 30 μm gap as well as the Fe:InGaAs switch with a 3 μm gap. We believe that the 1-ns rise-times displayed in the results are due to the limit of the Pockels cell rise-time and the oscilloscope response time. Only the opening time of the GaAs switch, which is limited by the carrier recombination time (~5 ns), was observed on the oscilloscope. The results also show that the Fe:InGaAs switch with an interdigitated gap is not suitable for 10 Hz operation. This is because the heat accumulation in the switch after a few minutes generates too many excessive carriers degrading the recombination time up to 10 ns. The square pulse shown in Fig. 6.7(e) was obtained with this switch under single shot operation.

As mentioned before, the charging current which determines the output voltage is inversely proportional to the switch on-resistance. By using the experimental results and Eqn. (6.5), the corresponding on-resistances can be estimated. The on-resistances are 2.27 kΩ for GaAs switch (switch 1), 3.57 kΩ for Cr:GaAs switch (switch 2), 909 Ω for Fe:InGaAs switch with a 3 μm gap (switch 3), and 100 Ω for Fe:InGaAs switch with a 6 μm gap (switch 4) respectively. These on-resistances are all greater than a few hundred ohms or even in the few thousand ohms range. This is expected based on the experimental results obtained from the lumped inductive circuit. Therefore, it is impossible to observe any voltage gain through electrical pulse compression in this experiment.

As discussed in the previous chapter, the charging current waveform for the CCTL with an ideal switch should be a staircase-like structure and the corresponding prepulse height should be equal to the charging voltage. However, if the switch on-resistance is large enough, this on-resistance has to be considered in the circuit analysis. In this case, the effective reflection coefficient for the current wave at the load and switch end becomes

$$\Gamma_I = \frac{Y + Y_{on} - Y_o}{Y + Y_{on} + Y_o} = \frac{R_{on}Z_o + RZ_o - RR_{on}}{R_{on}Z_o + RZ_o + RR_{on}}, \qquad (6.6)$$

and the coefficient T_R for the current wave transmitted to the load resistance

becomes

$$T_R = \frac{2Y}{Y + Y_{on} + Y_o} = \frac{2R_{on}Z_o}{RR_{on} + R_{on}Z_o + RZ_o}\,, \tag{6.7}$$

where $R = 1/Y$ is the load resistance, $R_{on} = 1/Y_{on}$ is the switch on-resistance, and $Z_o = 1/Y_o$ is the characteristic impedance of the transmission line. Alternatively, this suggests that the effective impedance for the traveling waves is the parallel connection of the switch on-resistance and the load impedance. As soon as the switch is closed, the amplitude, I_s, of the positive-going current wave propagating down the transmission line can be found to be

$$I_s = \frac{V_o}{R_{on} + \dfrac{RZ_o}{R + Z_o}} \frac{R}{R + Z_o} = \frac{V_o R}{RR_{on} + R_{on}Z_o + RZ_o}\,, \tag{6.8}$$

where V_o is the charging voltage. Since the voltage source can continuously provide energy to the system, the amplitude, I^+, of the positive-going current wave after each round-trip time, $2l/v$, is always the sum of I_s and the negative-going current wave reflected at the load and switch end. By using iteration and due to the partial reflection and transmission at the load and switch end, the amplitude increment of the positive-going current wave in this case becomes a geometrical series in the reflection coefficient Γ_I. That is

$$I^+ = I_s(1 + \Gamma_I + \Gamma_I^2 + \Gamma_I^3 + \cdots + \Gamma_I^n) \tag{6.9}$$

after the nth round-trip time. This implies that the charging current I_o observed at the shorted end, where in-phase total reflection of the current wave occurs, is

$$I_o = 2I^+ = 2I_s(1 + \Gamma_I + \Gamma_I^2 + \Gamma_I^3 + \cdots + \Gamma_I^n)\,. \tag{6.10}$$

The prepulse in this condition can be determined by the addition of the transmitted voltage waves from the source and from the negative-going (reflected) wave. This can be expressed as

$$V_{pre} = V_o \frac{\dfrac{RZ_o}{R + Z_o}}{R_{on} + \dfrac{RZ_o}{R + Z_o}} + V^- \frac{2\dfrac{RR_{on}}{R + R_{on}}}{\dfrac{RR_{on}}{R + R_{on}} + Z_o} = I_s Z_o + V^- T_R \frac{R}{Z_o}\,. \tag{6.11}$$

Applying $V^- = -I^- Z_o$, Eqn. (6.11) becomes

$$V_{pre} = I_s Z_o - I^- T_R R = I_s[Z_o - (1 + \Gamma_I + \Gamma_I^2 + \Gamma_I^3 + \cdots + \Gamma_I^{n-1})T_R R] \,. \quad (6.12)$$

Since the traveling wave leaving the switch end needs one round-trip time to return to the same end, the factor of $n-1$ in Eqn. (6.12) represents the prepulse after the nth round-trip time and the prepulse in the first round-trip time is as simple as $V_{pre} = I_s Z_o$.

By using the above equations with $R = Z_o = 50\ \Omega$, Eqns. (6.6), (6.7) (6.10), and (6.12) become

$$\Gamma_I = \frac{Z_o}{Z_o + 2R_{on}} \,, \quad (6.13)$$

$$T_R = \frac{2R_{on}}{Z_o + 2R_{on}} \,, \quad (6.14)$$

$$I_o = \frac{2V_o}{Z_o + 2R_{on}}(1 + \Gamma_I + \Gamma_I^2 + \cdots + \Gamma_I^n) \,, \quad (6.15)$$

$$V_{pre} = \frac{V_o Z_o}{Z_o + 2R_{on}}[1 - (1 + \Gamma_I + \Gamma_I^2 + \cdots + \Gamma_I^{n-1})T_R] \,. \quad (6.16)$$

As most of the results in Fig. 6.7 clearly show $R_{on} \gg Z_o$, this leads to $\Gamma_I \approx 0$ and $T_R \approx 1$. In this case, Eqns. (6.15) and (6.16) result in $I_o = V_o/R_{on}$ and $V_{pre} = 0$ after the first round-trip time of the traveling wave in this short-circuited transmission line. In other words, the prepulse only lasts for one round-trip time and the pulse amplitude is $\sim V_o Z_o/(2R_{on})$ which is equal to the output pulse amplitude, V_p.

In Fig. 6.7(a), the output voltage pulse shape, which is the bottom trace, indicates that the prepulse lasts only 60 ns as soon as the laser light reactivates the switch at the end of the 300-ns laser interruption time. This 60-ns duration is equal to the round-trip time of the traveling wave propagating in this 6 m long transmission line and is also equal to the duration of one step in the charging current waveform. According to the above discussion, this outcome is expected. Alternatively, the shape of the prepulse can be explained as the charging process reaching the steady state in one round-trip time due to the high switch on-resistance. Thus, the current wave no longer propagates to the load resistance

to form the prepulse. These results strongly suggest that the 5 ms to 20 ms delay introduced by the delay circuit is long enough to charge up the transmission line as soon as the switch is turned on by the laser light. Because the duty cycle of the chopper is 0.35, the switch illumination time is slightly greater than 1/3 of the operation time. Thus, the heating problem which might prolong the recombination time in the switch was only observed in switch 4.

In order to increase the charging current, the switch on-resistance must be further lowered. This is impossible to achieve with the Ar^+ laser, because the optically induced layer of electron-hole plasma is too shallow ($\sim$0.1 μm at 514 nm) to lower the switch on-resistance. The experiments to determine the on-resistance at different laser powers and the possible explanations for these high values are discussed in the following section. Despite that, the efficiency of the energy transferred from the CCTL to the load is close to 100% and the output pulse shape from the CCTL is nearly square. In contrast, the lumped inductive circuit can only generate the pulse with an exponential decay. From the theoretical point of view, the fast square pulse is much better for testing and analyzing a high speed circuit. With this unique characteristic and the advantages of the photoconductive semiconductor opening switch, the CCTL is an excellent energy storage system for the purpose of generating fast pulses.

6.3 Switch resistance measurement

The obtained switch on-resistances in the last two sections vary from a hundred ohms to a few kilo-ohms. These resistances are all too high to be used in charging the inductive system with a sufficient current. As discussed in Chapter 3, the switch on-resistance is determined by the photoconductive effect and can be estimated by Eqns. (3.18) and (3.19). Since $\hbar\omega$ = 2.4 eV is greater than the bandgap energy, single photon direct absorption dominates in the experiment and it is reasonable to assume that the quantum efficiency η is $\sim$100%. Because the switch's dielectric constant varies from 13 to 15, the reflectivity can be calculated as Γ = 0.32. Based on Dr. E. Chauchard's

measurement, the carrier recombination time, τ_s, for switch 2 is 200 ps and for switch 3 and 4 is 100 ps [32]. As for switch 1, the recombination time is ~5 ns due to the intrinsic GaAs. Using μ=9000 cm^2/V-s for switch 1 and 2 and μ=15000 cm^2/V-s for switch 3 and 4, the calculated switch on-resistances at 0.5 W cw laser power are 0.7 Ω for switch 1, 35 Ω for switch 2, 0.4 Ω for switch 3, and 1.7 Ω for switch 4. Apparently, the experimental values are much higher than the calculated values. This implies that other higher order effects discussed in Chapter 3 must also be taken into considerations to determine the switch on-resistance.

Thus, experiments were carried out to measure the switch on-resistance as a function of the laser power. In the experiment, the maximum cw Ar^+ laser power applied to the switch varied between 1 W and 3 W depending upon its gap size. In order to lower the switch resistance, the switch was continuously illuminated with the laser light. As the power of the laser light varied, the change of the switch resistance was recorded by reading an ohm-meter. Due to the narrow gap size of switch 3 and 4, the internal voltage of the ohm-meter might cause them to break down. In order to prevent the breakdown, an ammeter is used to measure the current, I_R, flowing through the switch and a volt-meter is used to measure the voltage, V_R, across the switch under the bias voltage which would not cause surface breakdown. Then the switch resistance can be directly calculated from the measured voltage and current by using Ohm's law.

Those four switches listed in the previous section and used in the CCTL experiment were measured with one of these two methods. Their results which are plotted on the linear scale and the log-log scale are shown in Fig. 6.8 and 6.9 respectively. According to the analysis presented in Chapter 3, the switch on-resistance, R_{on}, is inversely proportional to the number of photons, N_s, (Eqn. (3.18)) and this N_s is proportional to the laser power, P_{in}, (Eqn. (3.11)). Thus, the slope of the first order approximation on the log-log scale has to be -1, where the abscissa corresponds to the laser power and the ordinate corresponds

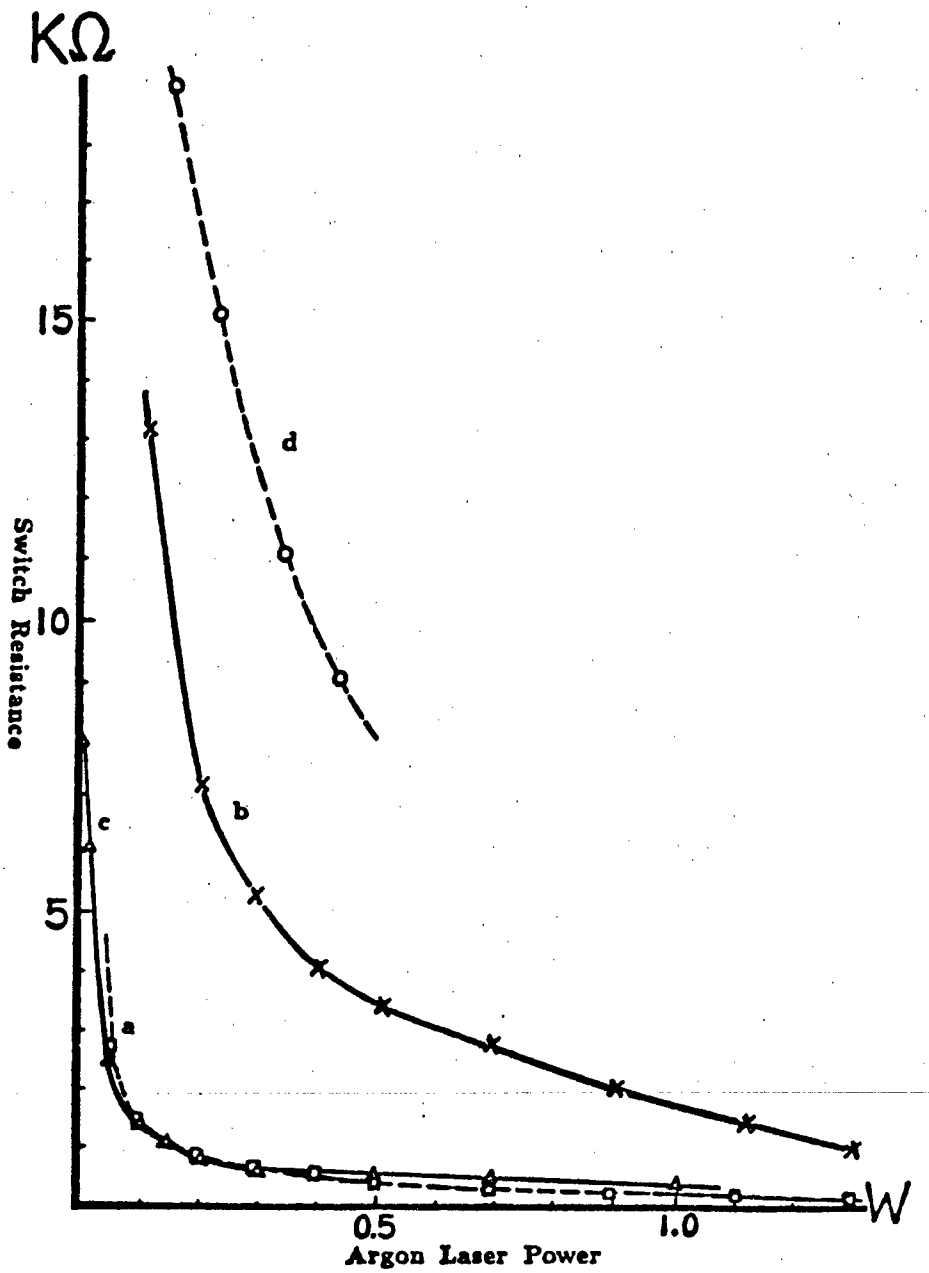

Fig. 6.8. Switch resistance variation in terms of cw Ar^+ laser power. (a) switch 1; (b) switch 2; (c) switch 3; (d) switch 4; these switches are listed in page 117.

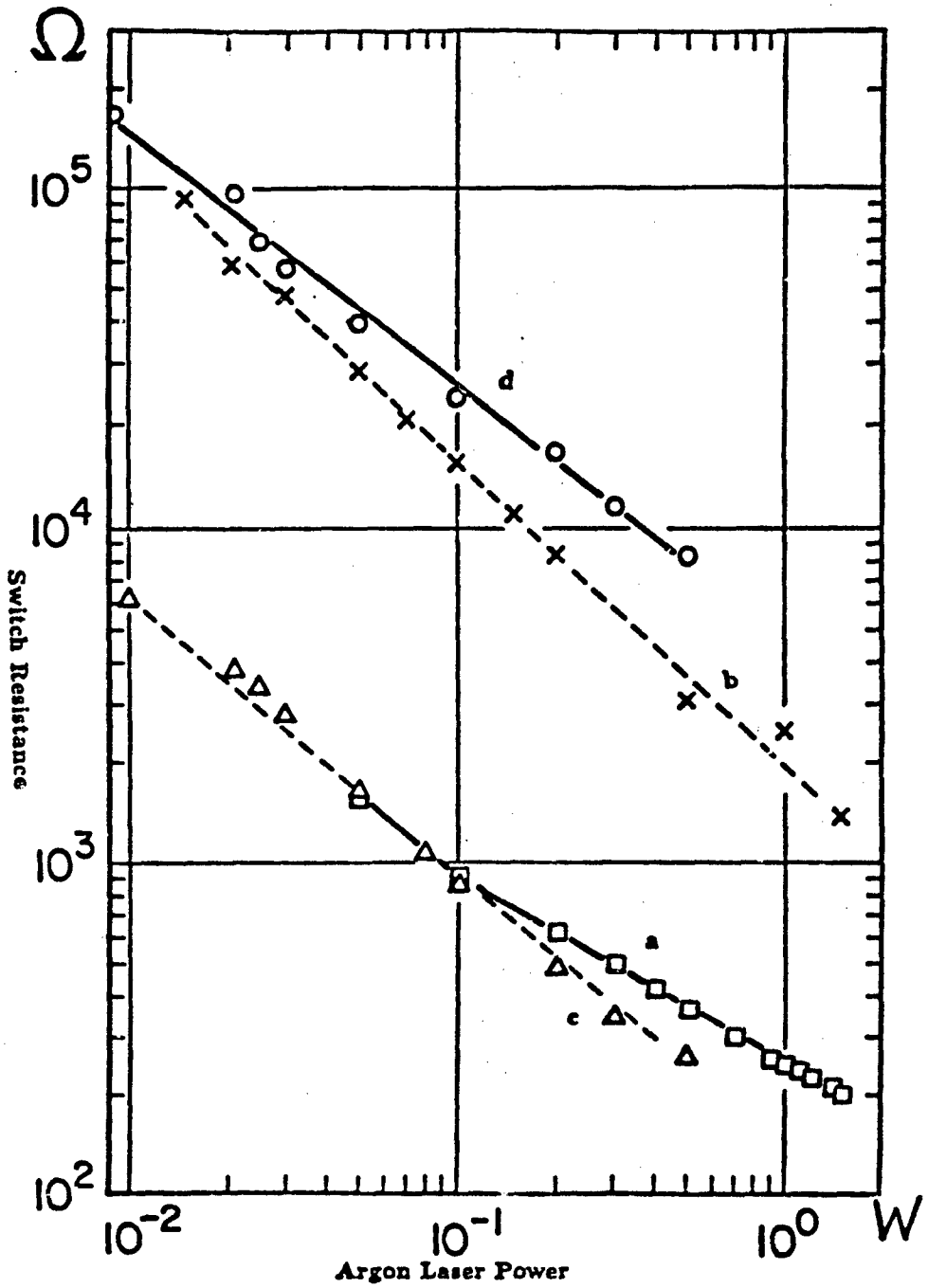

Fig. 6.9. Replot of Figure 6.8 on the log-log scale.

to the switch resistance. However, this statement is not true for the results shown in Fig. 6.9, the slopes of those four switches vary between -0.56 and -1. The reasons for such an apparent variation and high switch on-resistance are discussed below.

As discussed in Chapter 3, if the photon energy were above the energy gap, the induced layer of the electron-hole plasma would be very shallow and the resistance of the switch could not be further lowered. For instance, the absorption depth of GaAs at 514 nm wavelength is only $\sim$0.1 μm [65]. Since the electrode width of these four switches is either close to or less than 0.5 mm, this results in a small cross-sectional area, A. Even the largest area is only $\sim 5\times10^{-7}$ cm^2. In terms of these geometrical measurements, the switch resistance can also be expressed as

$$R_{sw} = \frac{l}{\sigma A}\ , \tag{6.17}$$

where l is the gap size of the switch and σ is the on-state conductivity. Hence, this small cross-section area has a strong impact on determining the switch resistance. Furthermore, the effective conduction volume for the photo-generated carriers which is discussed in Sec. 3.1 also becomes very small. The volume of the GaAs switch with a 21 μm simple strip line gap (switch 1), is 21 μm$\times$0.1 μm $\times$0.05 cm $\sim10^{-9}$ cm^3. Using 100% for the quantum efficiency, η, 5 ns for the carrier lifetime, τ_s, 32% for the surface reflectivity, Γ, and 1 W for the incident laser power, P_{in}, in Eqn. (3.18), the number of the calculated photo-generated carriers is 8.8×10^9. This corresponds to a free carrier density of $\sim 10^{19}$ cm^{-3}. In this regime, the Auger recombination process cannot be neglected [69]. Also, the increased probability of the scattering process leads to a decrease in the carrier mobility and lifetime, and thus dropping the effective conductivity. With these effects included in Eqn. (6.17), the switch on-resistance can be severely affected.

In addition, the shallow penetration depth also makes surface recombination and surface roughness become the major factors leading to a high switch

on-resistance. In brief, this surface recombination directly originates from the discontinuity of the crystal structure. Since this discontinuity is always rich in surface states which behave like recombination centers, the mobility and the conductivity close to the semiconductor surface will always be seriously degraded. Moreover, surface roughness, which is usually $\sim$0.1 μm, is on the order of the penetration depth at 514 nm wavelength. Thus, surface roughness can further decrease the mobility of the photo-generated carriers and the conductivity of the semiconductor material within this 0.1 μm penetration depth. With these two factors affecting the conductivity, σ, in Eqn. (6.9), high switch on-resistance is expected.

In conclusions, the density of photo-generated carriers at or near the surface under certain laser intensities is large enough to decrease the carriers recombination time via Auger recombination. Because of the shallow penetration depth of the laser light, surface roughness and surface recombination become important in determining the switch on-resistance. Due to these effects, the free carrier mobility μ and the effective conductivity σ drop and thus the switch resistance becomes higher. In other words, if there is no bulk conducting effect in these switches, their on-resistance cannot be lowered to less than a few hundred ohms even when they are illuminated with one watt cw laser power as shown in Fig. 6.8. Besides, these switches of microstrip line configuration are only suitable for low power, fast pulse generation. They are not good for the purpose of high voltage/power, fast pulse forming. Since the primary objective of this research is to generate high voltage pulses, this requires lower switch on-state resistance to charge the inductive system and larger switch dimension to withstand high voltage/power during the pulse forming stage. In order to reach this objective, large dimension bulk switches that are activated by a longer wavelength laser light might be the right choice. Because longer wavelength laser light can penetrate deeper into the semiconductor switch, thus the bulk conducting effect can be utilized. However the quantum efficiency might become lower and the switch

opening time might become longer. In the following chapter, we will see that the field strength across the switch can reach up to 15 kV/cm and the switch on-resistance can be as low as one ohm by illumination with a laser pulse of 1 mJ energy at 1.06 μm wavelength.

6.4 Summary

Some basic results of using the PCSS's in the IESPPS's to generate high speed voltage pulses are demonstrated. They show that the PCSS's can be used in either a lumped inductive circuit or a current charged transmission line to produce the expected waveforms. According to the experimental results, opening time faster than 1 ns and 10 Hz repetition rate are achieved with this type of opening switch. The results also show that the on-resistance of the PCSS can not be lowered down to a few ohms due to the shallow penetration depth of the laser light at 514 nm wavelength. In this case, the charging current cannot be increased further to generate high voltage pulses. Even though the switch on-resistance is too high in the experiment, the 1-ns opening time is the fastest among all the existing opening switches and 10 Hz operation is not the limit for the PCSS's. Higher repetition rate is possible if the laser system can be operated at a higher rate. In order to overcome the problem of high switch on-resistance, other approaches must be used. From the pulse compression and voltage gain point of view, it is much more important to obtain a low switch on-resistance than to achieve a fast opening time. It has also been suggested that the switch dimensions have to be scaled up to satisfy the requirements for high stand-off voltage. In the following chapter, we will focus on these issues.

CHAPTER 7

Bulk Photoconductive Semiconductor Opening Switches

Experimental results presented in the last chapter clearly demonstrate the feasibility of obtaining a 1-ns opening time at a 10-Hz repetition rate in an inductive energy storage system by using the photoconductive semiconductor switch. However, these results also reveal the inefficiency of employing the 514 nm wavelength laser light to lower the on-resistance of the semiconductor switches. Furthermore, those switches with microstrip line configurations are not suitable for high voltage/power pulse generation. In order to satisfy the requirements for generating high voltage pulses via electrical pulse compression, the main goal should be focused on obtaining a low switch on-resistance and a high charging current. In this chapter, investigation relating to this objective will be discussed.

As discussed in the previous chapter, the high switch on-resistance is attributed to the strong surface conducting effect at 514 nm wavelength. In this case, employing the bulk conducting effect instead of the surface conducting effect may be necessary to lower the on-resistance of semiconductor opening switches. Thus, longer wavelength laser light with a deep penetration depth into semiconductor material might be preferred for this purpose. In order to fulfill the requirement of higher voltage stand-off during the pulse forming stage, a larger dimension bulk semiconductor might be more suitable for this application. Thus, several bulk materials of few millimeters gap size were prepared to be used as opening switches.

Prior to using these bulk switches as opening switches, basic characteristics of these switches operated with a long wavelength laser must be investigated. Conventionally, the simplest and the most straightforward method for measuring

the dynamic switch resistance and determining the voltage hold-off capability of the switch is the closing switch experiment (pulse forming from a capacitive energy storage system). The circuit used to calibrate the switches is described in the first section. In this experiment, the laser system employed was a commercially available nanosecond Nd:YAG laser at 1.064 μm wavelength. Since its corresponding photon energy is below the band gap energy of the semiconductor materials, the process of two photons direct absorption and/or single photon absorption via the impurity/defect level in the material may be responsible for the generation of the free carriers. As shown in the experimental results, the switch on-resistance can be as low as 1 Ω at 1 mJ pulsed laser energy. We believe that the peak laser power at this energy level is too weak for the process of two photons direct absorption to be very significant.

Other than low switch on-resistance, the results obtained from the closing switch experiment also reveal that the switch is able to withstand an electric field greater than 15 kV/cm during the opening stage. The details regarding this work are presented in the first section also. The next step in this research work is then to observe the current build-up in the current charged transmission line (CCTL). As discussed in Chapter 5, the current build-up in the CCTL is the key element in achieving the voltage gain. For this purpose, experiments were designed to observe this staircase-like current build-up waveform. In order to observe the staircase-like waveform, the switch in the CCTL must be closed quickly and remain closed for a long time. Otherwise the slow switch closing time can smooth the rising edge of the charging current waveform and the short duration of the closing time may limit the number of steps in the staircase structure. Therefore, high power picosecond laser pulses which could completely saturate the photo-generated carriers in the switch to provide a longer closing time were used in this experiment. The detailed description of this experiment is in the second section.

7.1 Closing switch experiments

According to the experimental results shown in the previous chapter, the on-resistance of the switch is too high to charge the inductive system with a sufficient current. This is due to the illumination with the 514 nm green light which leads to a shallow penetration depth. Since longer wavelength laser pulses can penetrate deeper into the semiconductor materials, this prompts the idea of using such a laser pulse to activate the switches. Based on this idea, a commercial Quanta-Ray DCR Nd:YAG laser was used in the experiment. This system is a Q-switched laser and is able to produce optical pulses with a 10-ns pulse width (FWHM) at the wavelength of 1.064 μm. The repetition rate of this laser system can be changed continuously from 2 Hz to 10 Hz. There are two laser heads in this system, both are flashlamp pumped and water cooled. The front head is the oscillator which can generate ~100 mJ Q-switched pulses; the rear head is the amplifier which can boost the laser pulse energy to ~200 mJ. The Q-switched laser pulse shape is shown in Fig. 7.1.

In order to measure the on-resistance of the bulk switches, a closing switch experiment was carried out. The schematic circuit diagram of this experiment is sketched in Fig. 7.2. As shown in this figure, the circuit, which is a voltage charged line pulser, comprises a transmission line of length l and of characteristic impedance Z_o. One end of the transmission line is in series with an inductor, L, and a resistor, R, which are directly connected to a high voltage power supply. The other end of the transmission line is connected to the load impedance, R_L, through a photoconductive semiconductor switch.

Before the arrival of the laser pulse in the pulse forming experiment, the switch is opened and the transmission line is gradually charged to the voltage V_o by the power supply. Once the transmission line is charged, the inductor, L, and the resistor, R, which serve as a high impedance buffer, can isolate the transmission line from the power supply. In this case, a standing wave pattern is established in terms of voltage traveling waves due to the total reflection at either the switch or the buffer end. At this instant, the switch must withstand

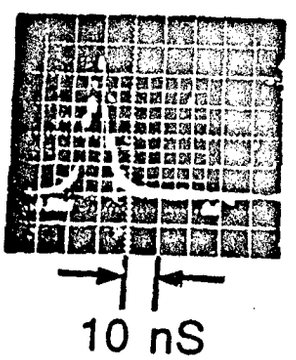

Fig. 7.1. Q-switched Nd:YAG laser pulse shape.

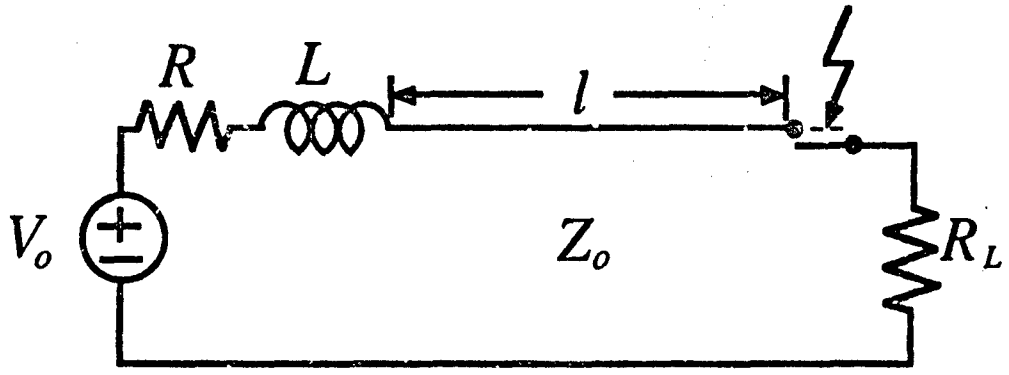

Fig. 7.2. Schematic circuit diagram for the closing switch experiment.

the high voltage to maintain the standing wave pattern. Therefore the switch's capability of withstanding high voltage at the opening stage is directly tested with this circuit configuration. Upon closing the switch with the laser pulse, the voltage traveling wave proceeds to the load. Since the positive-going wave moves to the load first, the polarity of the output voltage pulse is positive. If the load is mismatched ($R_L \neq Z_o$), partial reflection and transmission will always occur at the load end after each round-trip time of the traveling wave ($\tau = 2l/v$). This suggests that the output pulse consists of a main pulse and a series of postpulses. By using Eqn. (5.11) and (5.12), the amplitude of the output voltage pulse for the mismatched case can be expressed as

$$V_{out} = \frac{V_o}{2} \frac{2R_L}{R_L + Z_o} \left(\frac{R_L - Z_o}{R_L + Z_o} \right)^n , \qquad (7.1)$$

where n represents the nth postpulse and $n = 0$ is the main pulse. The duration of the main pulse and each postpulse is $2l/v$. If the load is matched, total transmission will occur at the load end. In this case, the amplitude of the output voltage pulse is $V_o/2$ and the pulse duration is $2l/v$. The possible output voltage pulse shapes from the voltage charged line pulser are plotted in Fig. 7.3.

In the experiment, the value of the charging resistor was $R = 10$ kΩ and the value of the inductor was L=50 mH. The length, l, of the transmission line was varied from 1 m to 20 m. Since the transmission line used was RG-58 coaxial cable with a dielectric breakdown of ~1500 V, this set the limit of the charging voltage to this breakdown voltage. Even though charging voltages as high as 2000 V have been applied, the data was not very reliable at this voltage due to the breakdown. There were two switches used in this experiment, both of them were bulk semiconductor materials. One was a 3 mm cube of GaAs and the other was a piece of bulk Cr:GaAs with dimensions of 2.15 mm×2.15 mm×1.4 mm, of which the gap size is 2.15 mm. Thin copper foils, which were used as the electric leads for these two switches, were in direct contact with the semiconductor surface. Silver paint was used to improve the conductivity between these two materials. There were no metal vapor deposition electrodes

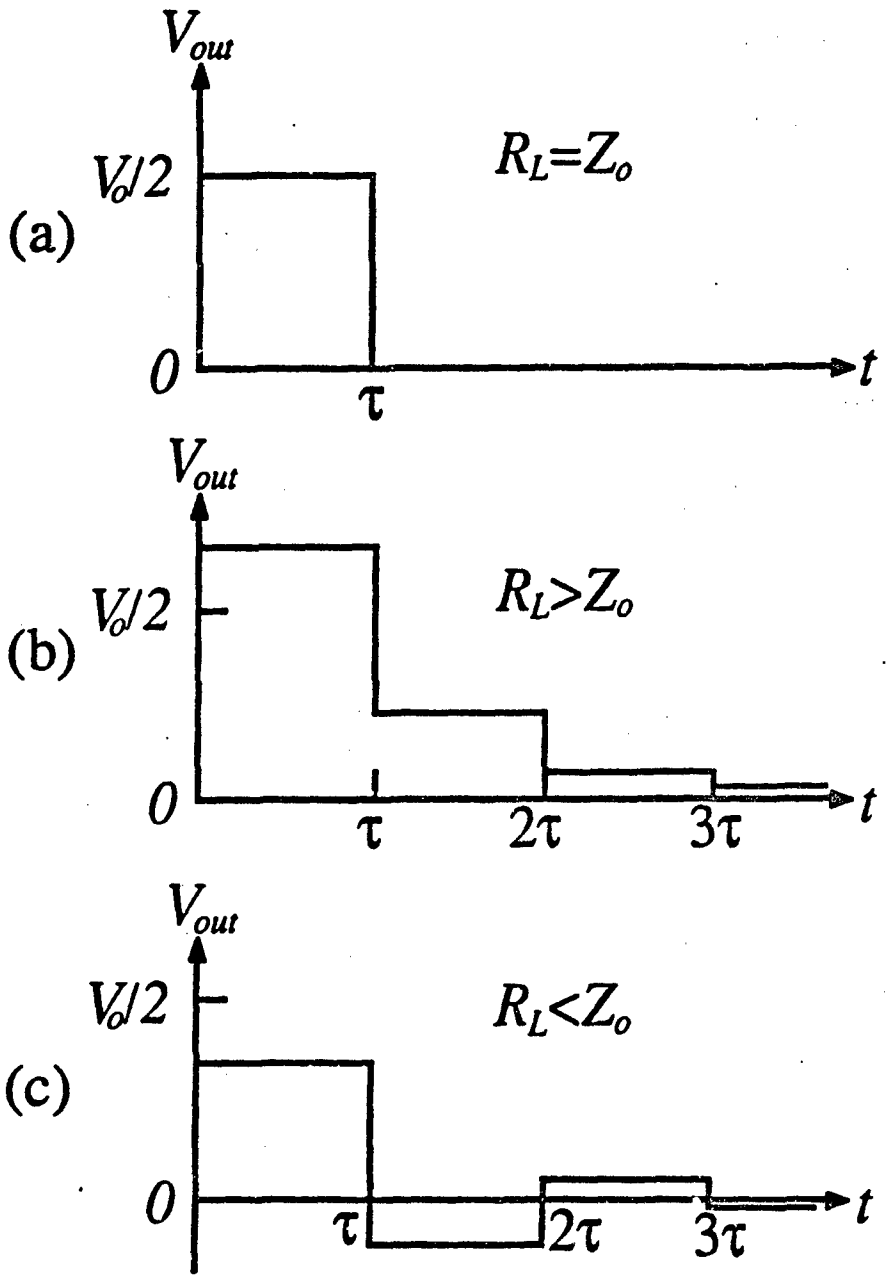

Fig. 7.3. Possible output waveforms from a voltage charged line pulser. (a) $R_L = Z_o$, the matched load; (b) $R_L > Z_o$; (c) $R_L < Z_o$.

for these two switches.

The photon energy at 1.064 μm is 1.17 eV, which is less than the band gap energy of GaAs and Cr:GaAs. Hence, free carriers could only be generated by absorbing photons via mid band gap impurity and/or defect levels. As mentioned in the very beginning of this chapter, two photon direct absorption is insignificant at this peak laser power level. The main advantage of this wavelength is that it can penetrate deeply into the bulk to generate bulk carriers and thus can lead to a low switch on-resistance [4],[71]. As shown in Fig. 7.1, the laser pulse duration is ~10 ns. If the round-trip time, $2l/v$, of the voltage traveling wave in the transmission line is longer than this duration, the output voltage pulse duration will be limited to either the laser pulse fall-time or the carrier lifetime and the postpulse will not appear at the load end due to the opening of the switch. For RG-58 coaxial cable ($Z_o = 50\ \Omega$), this 10-ns corresponds to the round-trip transit time in a 1-m long cable. The results displayed in Fig. 7.4 were obtained with the 3-mm cube GaAs switch at $l = 20$ m and V_o =1500 V under the condition of several different laser pulse energies. The load resistance used was the oscilloscope amplifier plug-in ($R_L = 50\ \Omega$) and the laser pulse energy was adjusted with a set of neutral density filters. The results in Fig. 7.4(a)-(c) were obtained with a laser pulse energy above 1 mJ. All of the pulses last much longer than 10 ns. This indicates that the photo-generated carriers in the switch are heavily saturated at a laser pulsed energy greater than 1 mJ [34],[91]. When the laser pulse energy is less than 100 μJ, the switch responses closely matches the laser pulse shape. These pulse shapes are shown in Fig. 7.4(d) and (e).

By using Eqn. (7.1) with $n = 0$ and considering the switch on-resistance as a part of the load, the amplitude of the output voltage pulse, V_{out}, displayed on the oscilloscope can be found as

$$V_{out} = \frac{V_o}{2}\left(\frac{2(R_{sw}+R_L)}{(R_{sw}+R_L)+Z_o}\right)\left(\frac{R_L}{R_L+R_{sw}}\right) = \frac{R_L}{R_L+Z_o+R_{sw}}V_o\,. \quad (7.2)$$

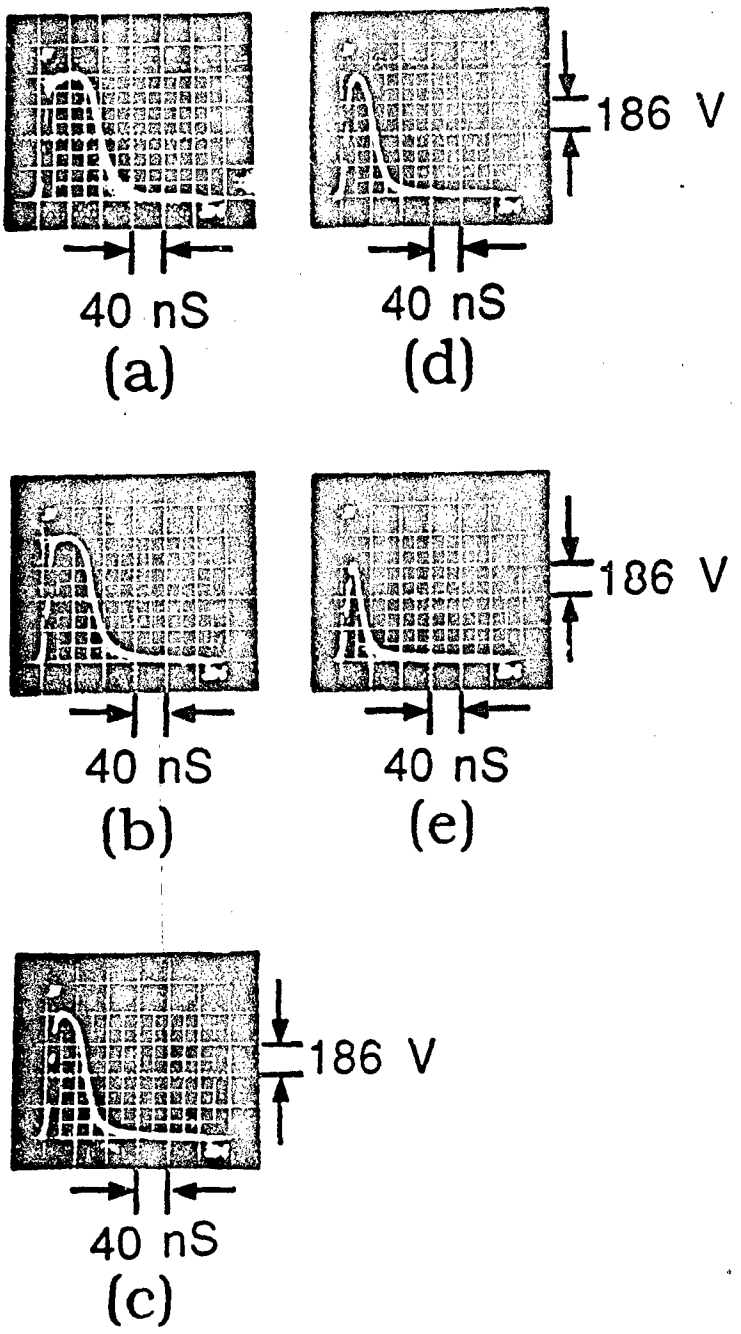

Fig. 7.4. Output voltage pulse shapes from a 3 mm cube GaAs switch in the closing switch configuration under different laser pulse energies, where l=20 m and V_o=1500 V. (a) 103 mJ; (b) 9.32 mJ; (c) 1.13 mJ; (d) 450 μJ; (e) 116 μJ.

This yields the switch on-resistance, R_{sw}, to be

$$R_{sw} = (\frac{V_o}{V_{out}} - 1)R_L - Z_o \ . \tag{7.3}$$

With $R_L = Z_o = 50\ \Omega$ in this circuit configuration, Eqn. (7.3) becomes

$$R_{sw} = 50 \times (\frac{V_{out}}{V_o} - 2) \ . \tag{7.4}$$

By using the output voltage pulse amplitudes under different laser pulse energies in Eqn. (7.4), the switch on-resistance as a function of the laser pulse energy can be calculated. The results are plotted in Fig. 7.5. As shown in Fig. 7.5(a), the lowest on-resistance for the 3-mm cube GaAs switch at $l = 20$ m and $V_o = 1500$ V can be less than 1 Ω with $\sim$1 mJ laser pulse energy. The on-resistance for the bulk Cr:GaAs switch with a 2.15-mm gap size under the same conditions is plotted in Fig. 7.5(b). It shows that the lowest on-resistance is $\sim$14 Ω at $\sim$100 mJ laser pulse energy.

By using Eqns. (3.13), (3.14), (3.18), and (3.19), the photo-resistance at 1 mJ laser pulse energy with a 10-ns pulse duration can be estimated according to the experimental conditions. In this estimation, it is assumed that the quantum efficiency is $\eta \approx 10\%$. Also, other parameters used in Eqns. (3.13) and (3.18) for both switches are the reflectivity $\Gamma = 32\%$ and the mobility $\mu = 9000$ cm^2/V-sec. Because the $\sim$5-ns carrier lifetime of the 3-mm cube GaAs switch is close to the laser pulse duration, it is possible to use $P_{in}\tau_d = 1$ mJ in Eqn. (3.13). By employing Eqn. (3.14), the calculated resistance value is 0.17 Ω. This is close to the measured value of 0.8 Ω. For the Cr:GaAs switch, we must use Eqn. (3.18) and Eqn. (3.19) to estimate the resistance due to its $\sim$300 ps carrier lifetime which is much shorter than the 10 ns laser pulse duration. This leads to $P_{in}\tau_s$=1 mJ$\times\tau_s/\tau_d$ in Eqn. (3.18). Substituting the N_s into Eqn. (3.19), the calculated resistance is found to be 4.4 Ω. This is very different from the measured result of 70 Ω. The discrepancy between these two results for this Cr:GaAs switch might be due to the higher contact resistance and the enhanced scattering process in

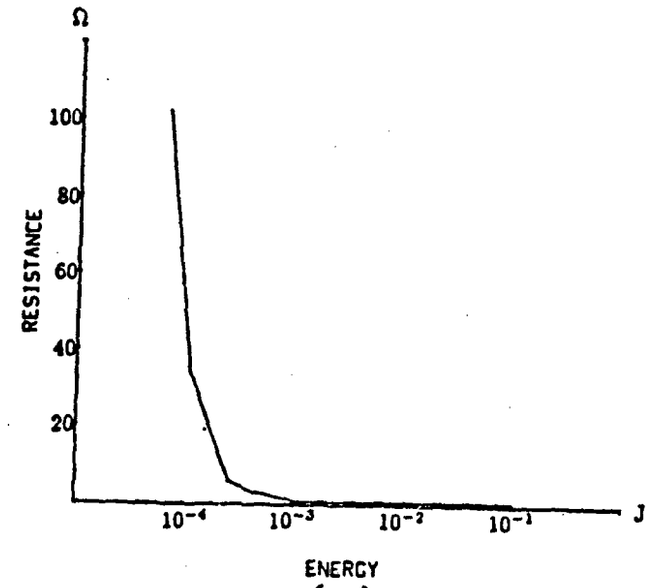

(a)

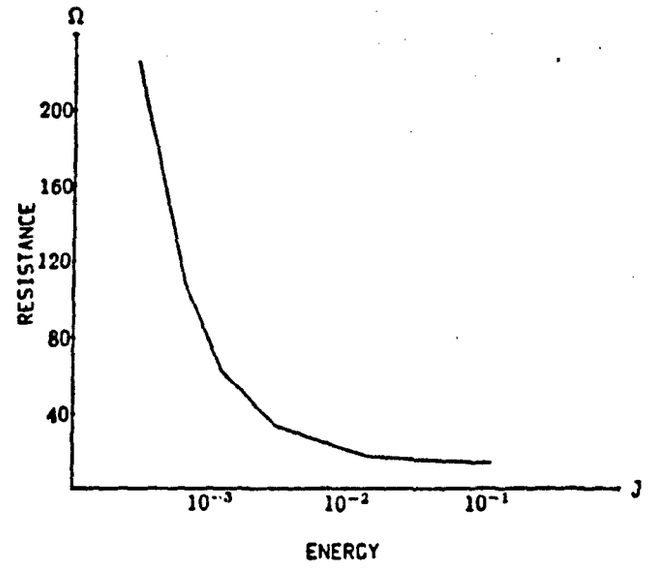

(b)

Fig. 7.5. Switch resistance with respect to the laser pulse energy in the closing switch configuration, where l=20 m and V_o=1500 V. (a) 3 mm cube GaAs switch; (b) 2.15 mm×2.15 mm×1.4 mm bulk Cr:GaAs switch.

the steady state. Because of this enhanced scattering process, a shorter carrier collision time, which can lead to a lower free carrier mobility, is expected. Thus, the mobility used for the Cr:GaAs switch might be overestimated. In conclusion, the calculated values and the experimental results clearly imply that Cr:GaAs needs higher laser intensity to increase the conductivity due to its fast carrier recombination time.

Beside measuring the photo-resistance of these two switches, their dark resistance and their capability of withstanding high voltage were also tested. Both switches were found to have dark resistances higher than 20 MΩ when they were measured with an ohm meter. In order to have a more accurate measurement, the switch is directly connected to a high voltage power supply through a resistor R_s with the value of a few mega-ohms. The purposes of this resistor is to protect the high voltage power supply from being damaged when the switch breaks down. Moreover, this resistor can serve as a voltage divider to increase the accuracy of the measurement. The bulk Cr:GaAs switch with a 2.15 mm gap size was found to have a dark resistance as high as ~200 MΩ at the electric field intensity of 15 kV/cm. When the field intensity is greater than 15 kV/cm, the switch dark resistance drops very fast. Since this field intensity is comparable to the air breakdown intensity, it might be just due to surface breakdown through the air or surface flashover. In spite of this breakdown, the switch dynamic range, which corresponds to the resistance changing from 100 MΩ to less than 1 Ω between the off- and on-state, is already greater than 10^8. This is the highest among all of the conventional opening switches. Because of this feature, photoconductive semiconductor switch is very promising in the opening switch application.

7.2 Observation of current build-up in the current charged transmission line

Current increasing in a staircase-like waveform in a current charged transmission line (CCTL) has been predicted in Chapter 5. As mentioned in Chapters

2 and 5, this current build-up process is crucial in determining the amount of energy stored in the inductive system and for the possibility of observing the voltage gain through electrical pulse compression. In this section, the main objective is to discuss the experimental approach used to verify this current build-up process. The circuit used to observe the current build-up waveform is depicted in Fig. 7.6. It is different from the circuit structure discussed in Chapter 5. The reasons for these differences are described below.

The capacitor, C, which is in parallel with the voltage power supply serves as an ideal voltage source when the switch is closed. The current viewing resistor (CVR, 0.1 Ω) which is inserted at the end of the transmission line to replace the short circuit is used to monitor the charging current waveform. Upon closing the switch, the current waveform is viewed on the oscilloscope through a 50 Ω amplifier plug-in which is in parallel with the CVR. Two switches have been used in this experiment; one was the 3 mm cube GaAs switch and the other was a Si switch. The dimensions of the Si switch are 1.5 mm$\times$1.0 mm$\times$1.0 mm and its gap size is 1.0 mm. These two switches were used due to their long carrier lifetime. Especially, the carrier lifetime of the Si switch can be as long as a few microseconds. According to Chapter 5, the amount of charging current and the number of steps in the current waveform are determined by the switch closing time. This strongly suggests that a switch with a long carrier lifetime, which corresponds to a long switch closing time, can provide a better chance of observing the staircase-like structure. That was why the Cr:GaAs switch of 300 ps carrier lifetime was not used in this experiment.

Theoretically, the switch closing time is identical to the rise-time of the laser pulse. In order to observe the staircase-like structure, the switch closing time must be much shorter than the round-trip time of the traveling wave in the transmission line. Since the rise-time of the Q-switched nanosecond Nd:YAG laser pulse is $\sim$10 ns, it is too slow to clearly display the fine staircase-like structure of the charging current waveform. Hence, a home-made passive and

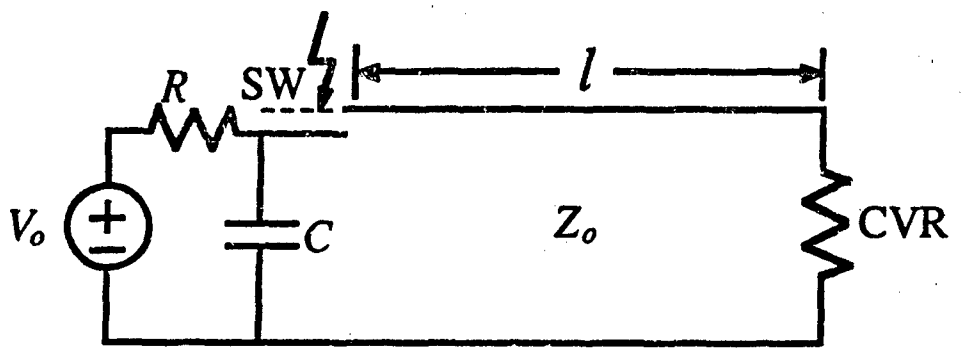

Fig. 7.6. Schematic circuit diagram for observing the charging current waveform in the current charged transmission line; CVR: Current Viewing Resistor (0.1 Ω).

active mode-locked picosecond Nd:YAG laser was used instead for this purpose. The layout of the laser system is shown in Fig. 7.7. In this system, a pulse train is generated by a passive and active mode-locked Nd:YAG laser oscillator. The mode-locked scheme is accomplished with the saturated absorber (Kodak-9860 concentrated dye solution) and an intracavity acoustic-optical modulator (Model ML-75W, Intraaction Corp.). In the stage following the oscillator, a single pulse is selected from this pulse train by using an optically triggered Pockels cell (Lasermetrics 8901B). Then, this pulse is sent to a spatial filter which consists of a diamond pin hole and a set of lenses to correct its spatial pattern. Afterwards, double pass amplification is achieved by passing the pulse through a thin film polarizer and a quarter wave plate twice. The laser heads of the Nd:YAG oscillator and amplifier are made by Quantel Co. Fig. 7.8 shows the selected laser pulse from the pulse train (Fig. 7.8(a)) and the amplified laser pulse shape (Fig. 7.3(b)). The duration (FWHM) of the amplified laser pulse is ~40 ps and the pulse energy is ~1 mJ. The repetition rate of this system is 1 Hz.

Due to the long carrier lifetime (several microseconds) of the Si switch, the Si switch can be driven into a deep saturation of photo-generated carriers and remain on for a long time after being illuminated by the picosecond laser pulse of ~1 mJ energy. Because the switch closing time is very close to the laser pulse rise-time, the fine structure of the staircase-like current waveform can be clearly observed. These results which were obtained with a capacitor C=10 nF and an RG-58 coaxial cable of length l = 6 m at a charging voltage of V_o=15 V are shown in Fig. 7.9. As in the figure, the duration of each step is 60 ns which is equal to the round-trip time of the traveling wave in this 6-m-long transmission line as predicted theoretically. However, the amplitude of each step is decreasing (Fig. 7.9(a)), not a constant as the theory predicts. This is attributed to two reasons. The first one is the finite value of the capacitor, of which the charging voltage is dropping due to losing its stored charges. Thus, a lower step amplitude is

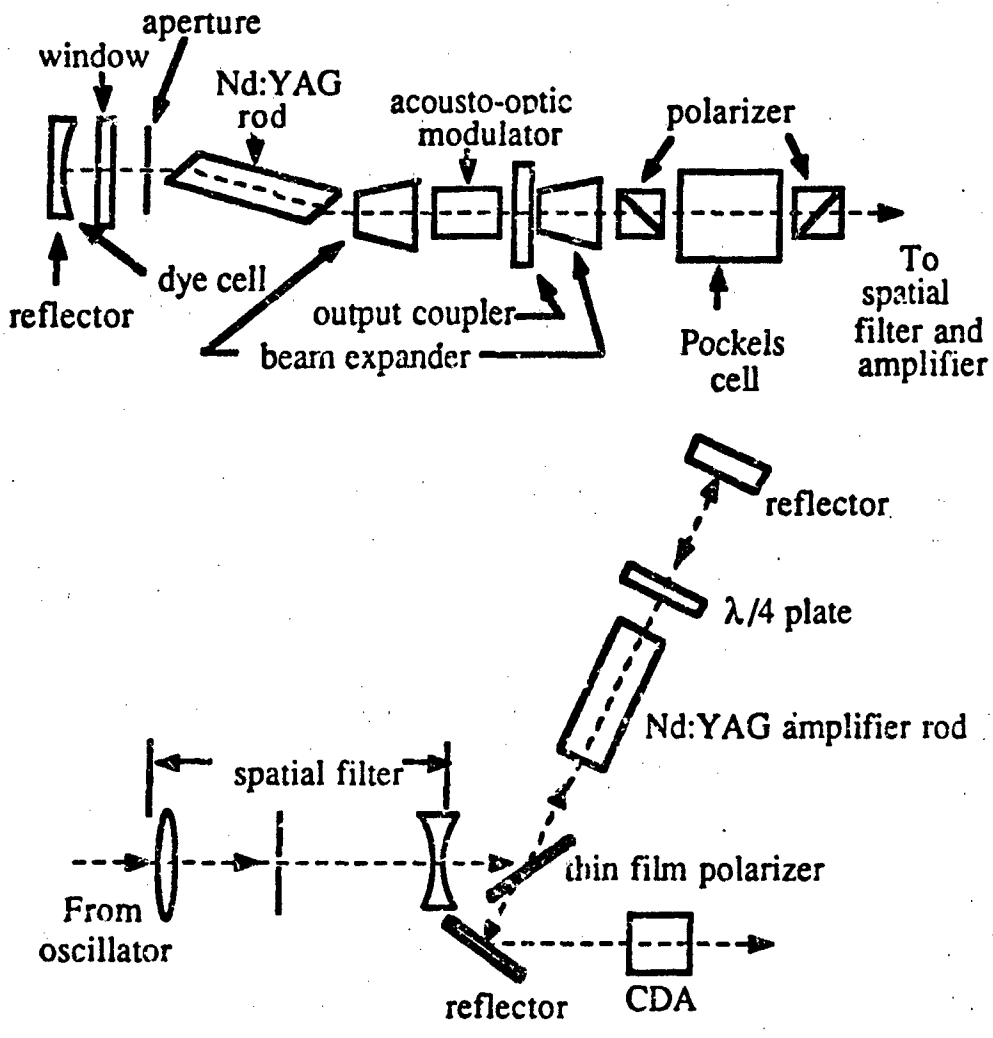

Fig. 7.7. Layout of the Nd:YAG passive and active mode-locked laser.

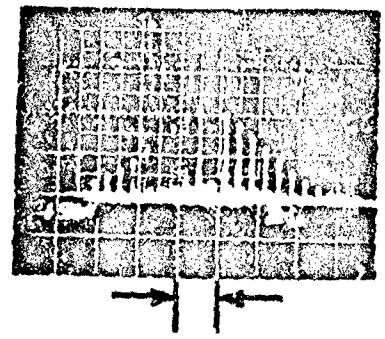

(a)

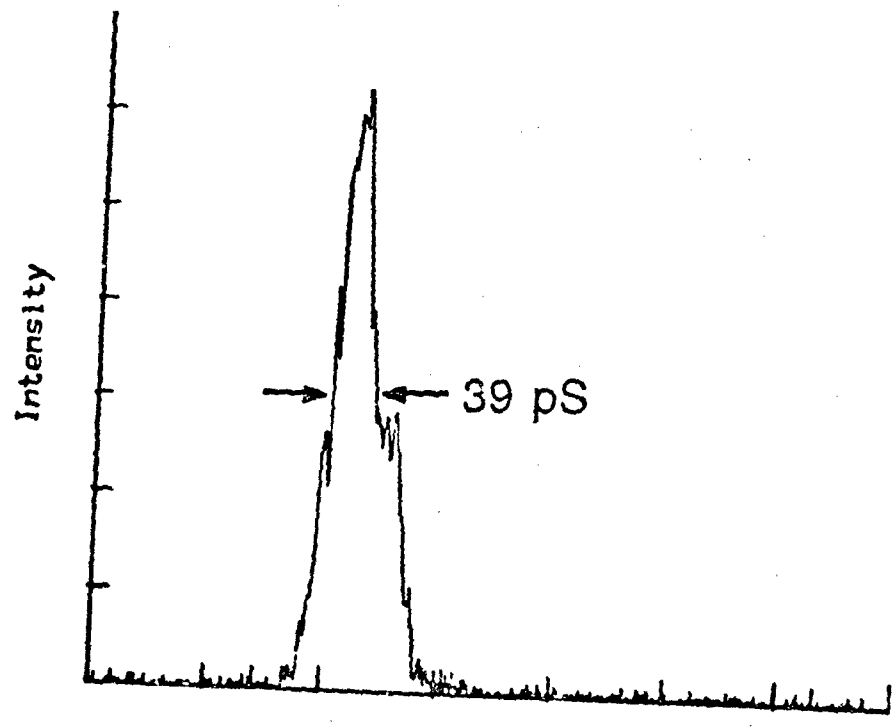

(b)

Fig. 7.8. Laser pulse shape of the passive and active mode-locked Nd:YAG laser. (a) the missing pulse or the selected pulse in the laser pulse train. (b) the amplified laser pulse shape.

expected. The second one is the finite switch on-resistance. This can be proven by the amplitude of the first step which reaches only 0.4 A. That is less than the theoretical value, which is $2V_o/Z_o = 2 \times 15/50$=0.6 A. Nevertheless, the result (Fig. 7.9(b)) shows that the maximum charging current in this circuit reaches 3.5 A in 2.2 μs. This suggests that there are at least ~35 steps in this current waveform while the switch is closed, and strongly implies that a long conduction time corresponds to a high charging current. This proves the importance of having a long conduction time for the switch to charge an inductive energy storage system.

Since the Si switch does not have a fast opening time due to its long carrier lifetime, it can not be used as an opening switch on the nanosecond time scale. This suggests that observing the current build-up in a switch with a short carrier lifetime such as GaAs is very essential. In order to have more than one round-trip time for the traveling wave during this short carrier lifetime, a shorter transmission line has to be used in conjunction with this type of switch. The result shown in Fig. 7.10 was obtained with the 3-mm cube GaAs switch with the carrier lifetime of ~5 ns. In the experiment, the transmission line used was an RG-58 cable of length l = 30 cm, the value of the capacitor used was C = 2.2 nF, and the charging voltage was V_o=200 V. Because this GaAs switch was in a deep saturation of photo-generated carriers after being activated by the picosecond Nd:YAG laser pulse of ~1 mJ pulse energy, four steps of 3-ns duration per step were observed before the switch opened and the maximum charging current in this configuration was 11 A. In addition, the fall-time of the current waveform was ~10 ns, this is closely related to the carrier lifetime in the intrinsic GaAs. The conclusion from this experiment is that it is necessary to have a long laser pulse to keep the switch on so that the inductive energy storage system can be fully charged with current. In order to have a fast opening time for the switch, a shorter carrier lifetime material has to be used in conjunction with a fast fall-time laser pulse.

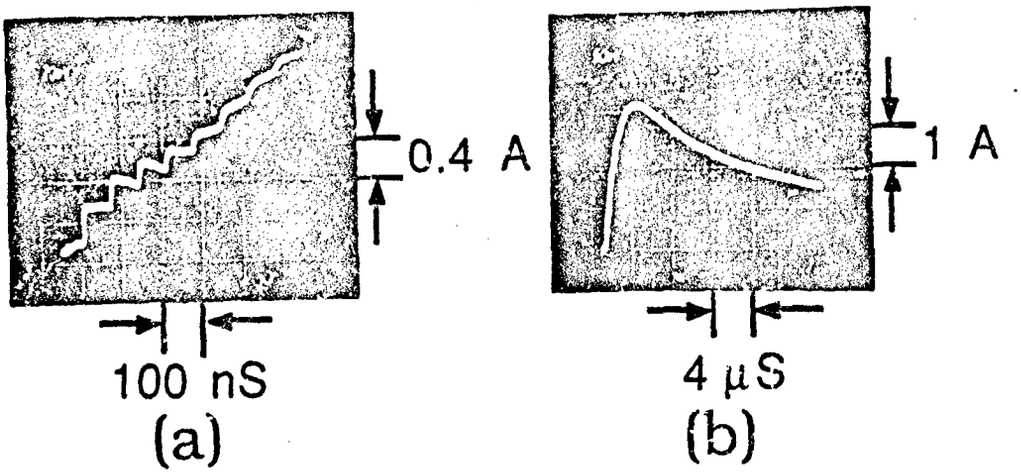

Fig. 7.9. Typical charging current waveform from the Si switch with C=10 nF and l=6 m at V_o=15 V. (a) the early charging stage; (b) the entire charging cycle during the switch closing period.

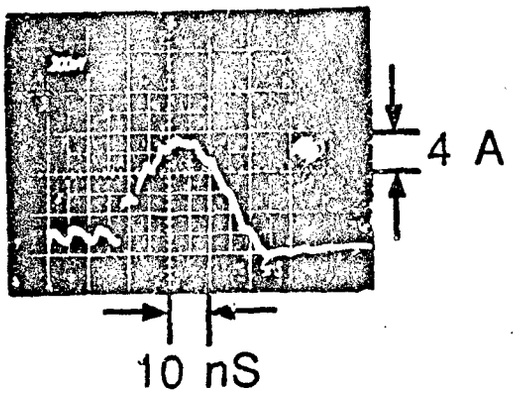

Fig. 7.10. Typical charging current waveform from the GaAs switch with C=2.2 nF and l=30 cm at V_o=200 V.

7.3 Summary

Bulk photoconductive semiconductor switch resistances lower than 1 Ω are obtained by illuminating a 10-ns-long 1.064 μm laser pulse of energy less than 1 mJ. Since the switch dark resistance is on the order of 100 MΩ, the dynamic range of the switch between the on- and the off-state is greater than 10^8. Current build-up in a current charged transmission line is observed. From these two experimental results, it is concluded that the laser pulse used to activate the switch should be capable of keeping the switch on for a long time to fully charge the system and then having a fast fall-time to turn off the switch on the order of its carrier lifetime. In order to achieve a voltage gain in the current charged transmission line, switch materials such as GaAs or Cr:GaAs with a short carrier lifetime should be used to provide a high di/dt value during the energy delivering and the pulse forming stage.

CHAPTER 8

High Voltage Pulse Forming

Based on the discussions in Chapter 5, the current charged transmission line (CCTL) and the dual of the Blumlein line (DBL) are able to compress an electrical pulse effectively if the switch is closed for a long enough time and is opened in the period much shorter than the round-trip time of the traveling wave in the transmission line. However, the experimental results described in Chapter 6 did not reveal this electrical pulse compression feature due to the high switch on-resistance during the charging stage. This leads to the experimental works discussed in Chapter 7. In those works, it was proven that 1 mJ of laser light at 1 μm wavelength can effectively lower the resistance of a GaAs switch to 1 Ω. Moreover, it has also been shown that long switch closing time is important for ensuring high charging current and that short switch opening time is vital for effectively delivering the energy to the load for achieving a voltage gain. From the conclusions in the last two chapters, it is clear that a new laser system, which can provide a light pulse with both a long duration and a fast falling edge, must be developed. The long duration is necessary to keep the switch closed long enough so that the inductive energy system can be charged up to a sufficient current. The fast falling edge is needed to open the switch fast enough so that the stored electrical energy can be effectively compressed and delivered to the load.

Two Nd:Glass laser systems were developed to satisfy these requirements. The first laser utilizes the leakage light from a cavity dumped Nd:Glass regenerative amplifier. Its laser pulse shape features a slow rise-time (~200 ns) and a fast fall-time (~10 ns). Since the laser pulse energy was too weak to effectively activate the switches of a few millimeter gap size, a Nd:Glass laser amplifier was built to enhance the laser pulse energy to ~2 mJ. With this ~2 mJ laser pulse

energy, several switches could potentially provide the voltage gain in a CCTL. The best result, which was obtained with a GaAs p-i-n diode switch with 0.5 mm gap size, shows that the output voltage pulse can be as high as 360 V at 100 V charging voltage. To further increase the laser pulse energy to ~4 mJ, the end mirror in the regenerative amplifier was changed to a mirror of lower reflectivity. By using this ~4 mJ pulse energy, a 5-mm cube GaAs p-i-n diode switch was able to generate a 2-kV electrical pulse from a CCTL at 500 V charging voltage.

In order to further improve the results, it is very important to understand the dynamic resistance of the switch in the pulse forming circuit. Two methods were used to investigate this dynamic evolution of the switch. The first method is to use the voltage and current waveforms obtained from the CCTL; the other method is to employ the output voltage waveforms obtained in the closing switch configuration. By comparing these two sets of results, it is found that the switch opening time in the CCTL is much faster than the opening time in the closing switch configuration. We will discuss these interesting results in the first section.

Because of the slow rise-time of the laser pulse, it is impossible to observe the staircase-like charging current waveform. Therefore, a new flashlamp pumped Nd:Glass laser system was developed. This system uses a Pockels cell outside of the cavity to shape the waveform and thus to tailor the laser pulse to have a fast rise- and fall-time. By passing this laser pulse through the same Nd:Glass amplifier used for the previous system, the laser pulse energy can reach ~12 mJ. Due to the fast rise-time, the staircase-like charging current waveform in a CCTL can be clearly observed. Similarly, pulse forming theory in the DBL has been successfully demonstrated. The best result obtained from the DBL was 1.3 kV output pulse voltage at 200 V charging voltage. Furthermore, the differences between the CCTL and the DBL are experimentally tested and compared by using the 5-mm cube GaAs p-i-n diode switch. These results are discussed in the second section.

During the pulse forming experiments with the CCTL and the DBL, an

abnormal conduction of the switches were observed during the switch opening stage, this might be related to the "lock-on" effect observed in the closing switch configuration by other groups. The fundamental phenomena of this effect, which are summarized by the researchers in the Sandia National Laboratory, are listed in the third section. Because their experimental conditions were totally different from ours, a comparison between their summary and our observation is conducted and discussed. This might help us to reach a conclusion that the switch failure in the CCTL and the DBL could be a new type of effect which is related to the "lock-on" effect. All of the details related to this effect are also presented in the third section.

8.1 Experimental results with the Nd:Glass laser pumped by Ar^+ laser

The results shown in Chapter 6 indicate that a well defined long laser pulse with a fast fall-time can efficiently discharge an inductive energy storage system to yield the expected output waveforms. In addition, they also imply that low switch on-resistance is very important for effectively charging the inductive system. This leads to the work which is presented in Chapter 7. The results clearly suggest that a laser pulse with energy falling between 1 mJ and 10 mJ at 1 μm wavelength can effectively lower the resistance of a GaAs switch. From the conclusions in Chapters 6 and 7, it is clear that a laser system which can provide long duration pulses with several millijoules energy at 1 μm wavelength is required for activating semiconductor switches. With these guidelines, an Ar^+ laser pumped Nd:Glass slab system, which is able to keep the switch on for few hundred nanoseconds and then turn off the switch in a few nanoseconds, was made for this purpose. In fact, this system was a modification of the laser designed by L. Yan [92]. Thus, it already exists in the laboratory. The schematic diagram of this laser system is depicted in Fig. 8.1. It shows that the system consists of an Ar^+ laser pumped oscillator and a two-stage amplifier. This oscillator was also used as a regenerative amplifier in other experiments.

In order to generate a laser pulse with a slow rise-time (~200 ns) and a

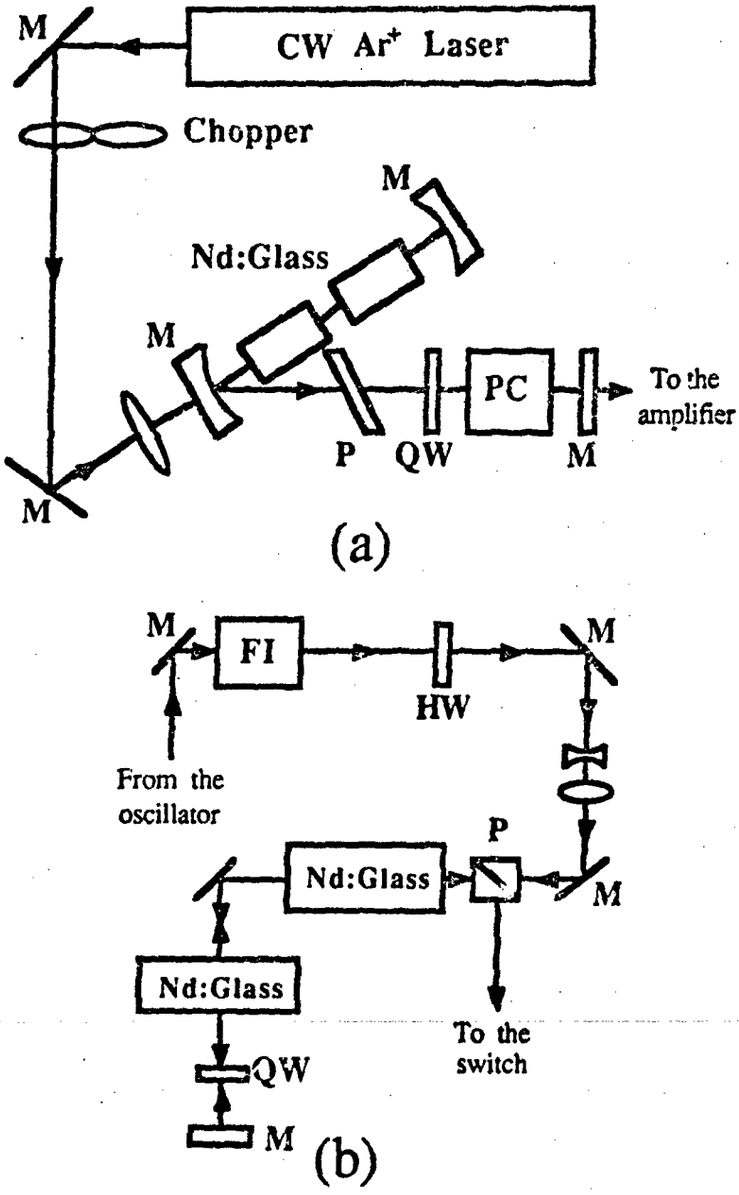

Fig. 8.1. Layout of the Ar^+ laser pumped Nd:Glass slab system. (a) the Nd:Glass oscillator; (b) the two stage flash lamp pumped glass amplifier; M: mirror, P: polarizer, QW: quarter wave plate, PC: Pockels cell, FI: Faraday isolator, HW: half wave plate.

fast fall-time (~10 ns), a chopper and a Pockels cell are utilized in the laser oscillator (Fig. 8.1(a)). The chopper, which chops the cw Ar^+ laser at 500 Hz, is controlled by the Pockels cell driver. When the Ar^+ laser passes through the chopper slit to pump the Nd:Glass slab, the Pockels cell acts as a quarter wave plate setting the cavity in a low loss state (high Q). This causes the laser light at 1.054 μm wavelength to be emitted from the output mirror with an intensity following the slowly rising pump beam of the Ar^+ laser. When this pulse reaches its peak intensity, the Pockels cell is switched on to act as a half wave plate. The timing is controlled by the Pockels cell driver electronics. At this moment, the cavity becomes very lossy (low Q), the lasing is quenched, and the output laser pulse has a fall-time on the order of the Pockels cell switching time. Since the output mirror is coated for high reflectivity (99.5%) at 1.054 μm, the energy of the output pulses at 500 Hz is only ~0.2 μJ. This energy is not enough to fully lower the switch on-resistance, so the laser pulse must be further amplified.

A two-stage flashlamp pumped glass rod amplifier (Fig. 8.1(b)) is built for the purpose of amplifying the laser pulse emitting from the oscillator. The injected laser pulse can traverse each stage of the amplifier twice by using a 0° mirror placing immediately after the second stage amplifier. The polarization of the reflected pulse is then rotated by 90° due to double-passing through a quarter wave plate, which is inserted between the mirror and the second stage amplifier. Thus, the energy stored in the glass rod is efficiently utilized. Also, the injected and reflected beam paths, which almost overlap, are orthogonally polarized. In this case, the amplified pulse can be deflected toward the switch by using a polarizing beamsplitter cube. The amplified pulse (Fig. 8.2) has an energy of ~2 mJ. According to the experimental results in Chapter 7, this pulse energy can efficiently lower the on-resistance of millimeter sized switches. In order to increase this pulse energy and to not severely affect the function of the oscillator as a regenerative amplifier for other on-going experiments in the laboratory, the output mirror is changed from 99.5% to 98% reflectivity at 1.054

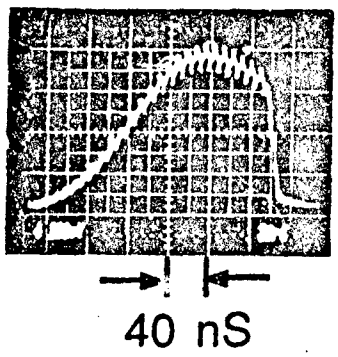

Fig. 8.2. The amplified laser pulse shape from the Ar^+ laser pumped system.

μm. This change increases the pulse energy to $\sim$4 mJ.

The schematic circuit diagram of a current charged transmission line (CCTL) is described in Fig. 8.3. The transmission line is a piece of RG-213 coaxial cable of length $l = 2.5$ m and characteristic impedance $Z_o = 50\ \Omega$. One end of the transmission line is shorted with a current viewing resistor (CVR, 0.1 Ω). A capacitor, C, which is charged to the voltage V_o initially, is connected to the other end of the transmission line through a photoconductive semiconductor switch (PCSS). As discussed in the previous chapter, this capacitor is used as an ideal voltage source in the pulse forming experiment. In order to further isolate the voltage source from the system, a charging resistor of $R = 2.7\ k\Omega$ is inserted in series with the voltage source before connecting to the capacitor and the switch. The matched load, which is a 50 Ω oscilloscope amplifier plug-in, is attached to the switch side of the CCTL via a 50 Ω transmission line.

Based on the discussion in Chapter 3 and the experimental results in Chapter 6 and 7, the switches used in the pulse forming experiments are all made of either GaAs or Cr:GaAs. Among them, two switches made of GaAs provide the best results. They are both of the p-i-n diode structure and were made by the David Sarnoff Research Center. The reasons for these good results can be easily attributed to the discussions in the paper of A. Rosen et al. on the Si p-i-n diode photoconductive switch [22]. In the conclusion of that paper, two distinct advantages for the p-i-n diode switch are discussed. The first advantage is that the reverse saturation current in the reverse biased condition is significantly lower than the bulk leakage current . This can greatly reduce the thermal run away problem. The second advantage is that the existence of the p^+ and n^+ layers at each surface can form a low ohmic contact resistance with the metal electrodes. In addition, it is reported that the Si p-i-n diode switch has the capability to hold off a field strength of 8 kV/cm [22]. Thus, we expect to obtain the best results from the GaAs p-i-n diode switches too.

For the GaAs p-i-n diode switches used in the experiment, the switch fab-

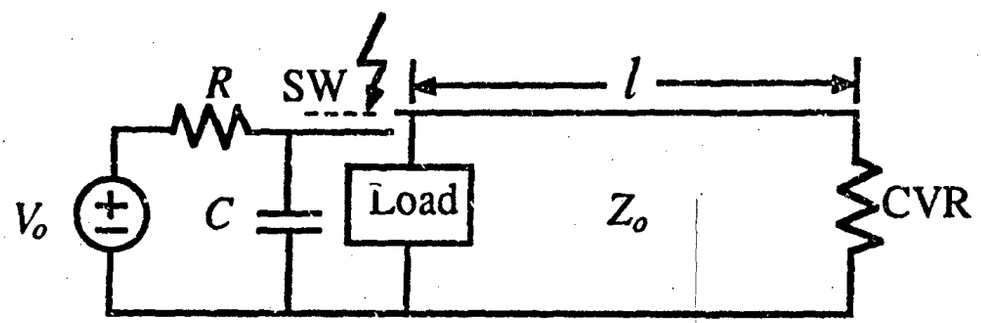

Fig. 8.3. Experimental circuit diagram for the current charged transmission line; CVR: Current Viewing Resistor (0.1 Ω), C: capacitor (0.1 μF), R: charging resistor (2.7 kΩ), Load: 50 Ω.

rication procedures, which are quoted below, are reported by A. Rosen, et al. As mentioned in the report, several 5-cm diameter undoped (100) LEC GaAs substrates are selected as the starting wafers prior to making the p^+ and n^+ layers. Then, a Be ion-implantation is used to form the p^+ layer on the top surface and a Si ion-implantation is used to form the n^+ layer on the bottom surface. After each ion-implantation, the wafer is annealed in a furnace with an AsH_3/H_2 atmosphere. Since the annealed temperature for the Si implant is higher than that for the Be implant, the n^+ layer is formed before the p^+ layer. Multiple-energy implant schedules are adopted to produce a flat doping profile. In order to form the ohmic contacts, AuZn is then applied to the p-side surface of the wafer by using photolithography and lift off, and AuGe-Ni-Au is directly applied to the n-side surface of the wafer. Afterwards, the wafer is diced into the wanted size.

The two switches used in the experiments have different designs. One is a 0.5 mm thick, 5×5 mm wafer, its electrode on the p-side surface is a ring-shape AuZn ohmic contact and its electrode on the n-side surface is a plain AuGe-Ni-Au ohmic contact. Silver paint bonds the copper foil stripes to these two electrodes. In this configuration, the pulsed laser beam, which illuminates the switch material from the center of the ring electrode, is in parallel with the electric field appearing across the switch. The other switch is a bulk switch of 5-mm cube, its electrode on the p-side surface is a solid-circle-shape AuZn ohmic contact and its electrode on the n-type surface is a plain AuGe-Ni-Au ohmic contact. The copper foil stripes are bonded to these two electrodes with the In solder paste. The pulsed laser beam illuminating the switch is perpendicular to the electric field across it. The carrier lifetime of these two switches is found to be ~5 ns by doing a closing switch experiment with a 14-ps optical pulse.

Both switches were reverse biased with the positive polarity of the charging voltage applied to the n-type surface in the pulse forming experiment. In fact, both switches showed that the output voltage pulses from the CCTL were sig-

nificantly lower when they are forward biased at a charging voltage less than 300 V. This poor result can be easily attributed to a large amount of the injected current under the forward biased condition during the switch opening stage. Since the 0.5 mm thick wafer switch broke down at 163 V charging voltage, there was no result above this voltage. However, the results obtained from the 5-mm cube bulk switch above 300 V charging voltage showed that there was little difference between these two biasing conditions. The reason for such little difference between these two conditions is due to the strong reverse biased condition enhancing the tunneling effect at the junction. Thus, the switching behavior was totally dominated by the intrinsic region and was not related to the biased condition.

In the pulse forming experiments, some of the best results are displayed and discussed in the following. Fig. 8.4 shows the results obtained with the 0.5 mm thick switch which was illuminated with the Ar^+ laser pumped Nd:Glass slab system [35],[39]. Upon activating the switch for 200-ns at the laser pulse energy of ~2 mJ (Fig. 8.2), the capacitive energy which was initially stored in the capacitor C=0.1 μF at a charging voltage V_o=100 V was transferred to the CCTL of inductance L = 0.63 μH. Due to this finite capacitance value, it is straightforward to treat the short circuited transmission line as a lumped inductor, and then to use the law of energy conservation,

$$\frac{1}{2}CV_o^2 = \frac{1}{2}LI_{max}^2 , \tag{8.1}$$

to estimate the maximum charging current. Assuming that the switch is ideal, the maximum current which can transfer to the CCTL would be

$$I_{max} = \sqrt{\frac{C}{L}}V_o = \sqrt{\frac{0.1}{0.63}} \times 100 = 40\text{A} \tag{8.2}$$

if the switch closing time is equal to $T/4$, where

$$T = 2\pi\sqrt{LC} = 2\pi\sqrt{0.63 \times 0.1} \times 10^{-6} = 1.6\ \mu\text{s} \tag{8.3}$$

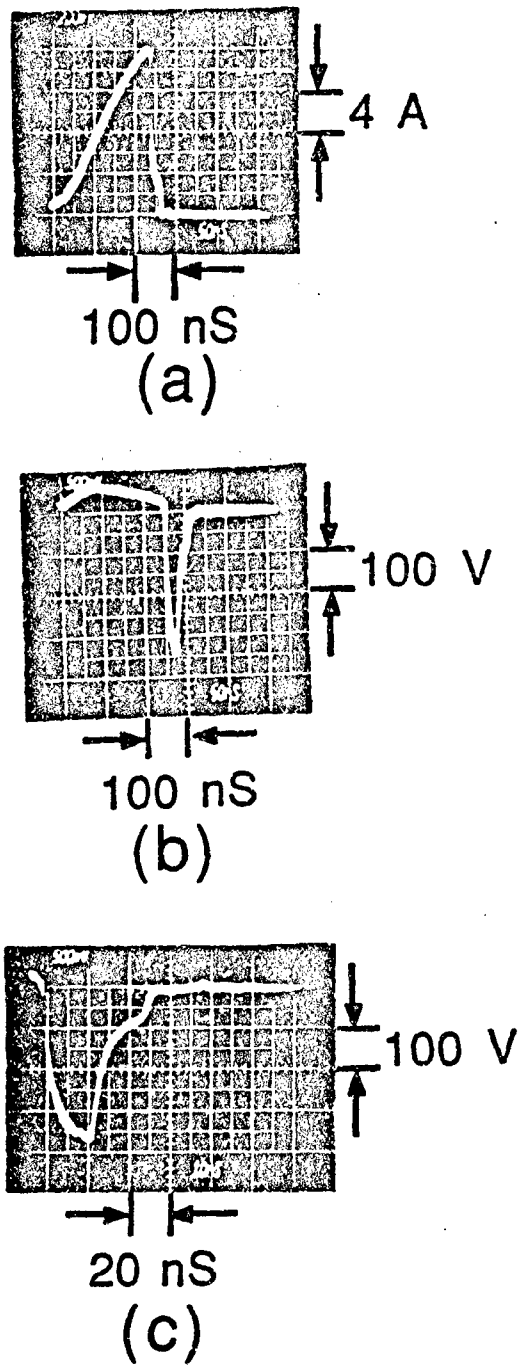

Fig. 8.4. Experimental results obtained from the 0.5 mm thick GaAs p-i-n diode switch in the current charged transmission line at 100 V charging voltage. (a) the charging current waveform monitored by the CVR; (b) and (c) output voltage waveform.

is the resonant period of this LC circuit. However, the charging current monitored by the 0.1 Ω CVR (Fig. 8.4(a)) only increased slowly up to 16 A in time, this was much less than the predicted value and the staircase-like build-up structure was not seen. The reason for this can be attributed to the switch closing time which is ~200 ns, shorter than $T/4 = 400$ ns, and the high switch on-resistance early in time when the laser pulse intensity is low. Though a shorter transmission line was used in the experiment to match the 200-ns-long switch closing time, the maximum current was still less than 16 A due to the high switch on-resistance early in time and the errors introduced in treating the short-circuited transmission line as a lumped inductor. In other words, this method only provides a rough estimation of the length of the CCTL. If an optimal length of the CCTL were desired, we would have to adjust the length several times during the experiment to achieve the optimal length. Other than this problem, the high switch on-resistance early in time also prevents us from using the equations discussed in Chapter 5 to predict the charging current waveform during the switch closing period.

As soon as the laser pulse was extinguished, the 0.5 mm thick switch was opened and the energy stored in the CCTL was transferred to the matched load, $R_L = 50\ \Omega$, to form a voltage pulse. If the switch resistance can increase to infinity instantaneously, the output voltage pulse amplitude will be $V_{out} = I_o Z_o/2 = 16 \times 50/2 = 400$ V and the pulse duration (discharging time of the CCTL) will be 25 ns. As compared to the experimental result, it shows that the peak output voltage pulse reaches V_{out} =360 V and the pulse duration is ~25 ns (Fig. 8.4(b) and (c)). This pulse shape is not far from the ideal pulse amplitude and duration. Thus, the result strongly implies that the switch off-resistance increased from few ohms to a few hundred ohms in a nanosecond time frame. Higher charging voltages were applied to the switch to produce higher output pulsed voltages, the highest output voltage achieved with this switch was 480 V at the charging voltage of V_o=150 V (Fig. 8.5). As discussed in Sec. 3.4, the

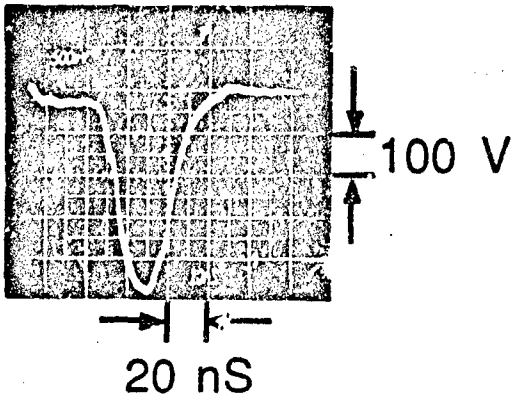

Fig. 8.5. The maximum output voltage pulse obtained from the 0.5 mm thick GaAs p-i-n diode switch in the current charged transmission line at 150 V charging voltage.

voltage across the switch during the pulse forming stage can be estimated by

$$V_{sw}(t) = I(t)R_{sw}(t) = V_C(t) - V_{out}(t) = V_o - \frac{1}{C}\int I(t)dt - V_{out}(t)\ , \quad (8.4)$$

where $V_C(t)$ is the remaining voltage across the capacitor and $I(t)$ is the charging current waveform. In this case, $V_C(t)$ can be directly estimated from the charge which the capacitor loses to the system during the charging cycle. Assuming $V_C(t) \simeq 0$, the peak electric field across the switch at 480 V was 9.6 kV/cm. The breakdown of this switch was observed at V_o=163 V. The physical damage consisted of a deep hole into the wafer where the laser pulse hit and an arc occured.

From this experimental result, the concept of electrical pulse compression is presented by using a CCTL in conjunction with a semiconductor opening switch. In brief, this compression concept can be realized by employing a long charging time to store the energy in a pulse forming network and then utilizing a short discharging time to transfer the energy to the load. This suggests that the opening switch has to be closed long enough to charge the CCTL with a sufficient current and then to be opened fast enough to transfer the stored current to the load resistance.

Moreover, this circuit configuration clearly demonstrates the potential of obtaining an output voltage pulse higher than the charging voltage through electrical pulse compression. Even though the stored current was much lower than the expected value and was limited by the switch on-resistance, it was already several times greater than the amplitude of one staircase, that is $2V_o/Z_o$ as discussed in Sec. 5.2. This achievement is due to the correct combination of laser pulse shape and switch material. Basically this 200-ns-long laser pulse with a 10-ns fall-time at 1.054 μm wavelength can activate the semiconductor switch such that it satisfies the requirements for an opening switch. As discussed in Chapters 1 and 2, those requirements are long charging time with a low switch on-resistance and a fast opening time with a high switch off-resistance. In fact, the results showed that the p-i-n diode switch was able to effectively compress

electrical pulse to have the output peak power 13 times greater than the input power.

In order to scale up the amplitude of the output voltage pulse, the 5-mm cube bulk switch was activated by a higher energy laser pulse in the pulse forming experiment. The results obtained from the CCTL with higher charging voltages are displayed in Fig. 8.6 [37],[38]. In these results, the laser pulse energy in the experiment was ~4 mJ and the charging voltage used was V_o=500 V. After this switch was turned on by the laser pulse, the charging current gradually rose to 105 A (Fig. 8.6(a)) which was much less than the value for the circuit with an ideal switch; that is $I_{max} = (0.1/0.63)^{1/2}500 = 200$ A. Once the switch was turned off at the termination of the laser pulse, the peak output voltage of $V_{out} = 2$ kV (Fig. 8.6(b) and (c)) was delivered across the 50 Ω matched load. This corresponded to a voltage gain of $G_V = 4$ and an output peak power of $P_{CCTL} = 80$ kW, which was the highest peak output power achieved from a PCSS in this type of inductive energy storage system. As expected, this was still less than the ideal value which was $I_o Z_o/2 = 105 \times 50/2 = 2625$ V. With higher charging voltages, higher output voltage pulses were obtained. Nevertheless, the pulse becomes very irregular and the peak amplitude was not far above 2 kV, hence the corresponding voltage gain dropped. If the peak electric fields at different charging voltages were analyzed by using Eqn. (8.4), it would be found that a severe unwanted conduction of this switch occured at or above the field intensity of ~5.0 kV/cm. Because this field intensity coincides with the "lock-on" field intensity, it is believed that this phenomenon might be related to the "lock-on" effect in the closing switch configuration [11],[83],[84]. Some descriptions related to the "lock-on" effect are presented in the third section.

In order to characterize the switch dynamic resistance (on- and off-resistance of the switch), two methods are employed. The first method involves using the circuit shown in Fig. 8.3, but with the CCTL being removed from the circuit. This circuit is a simple capacitive energy storage system. In this system, the

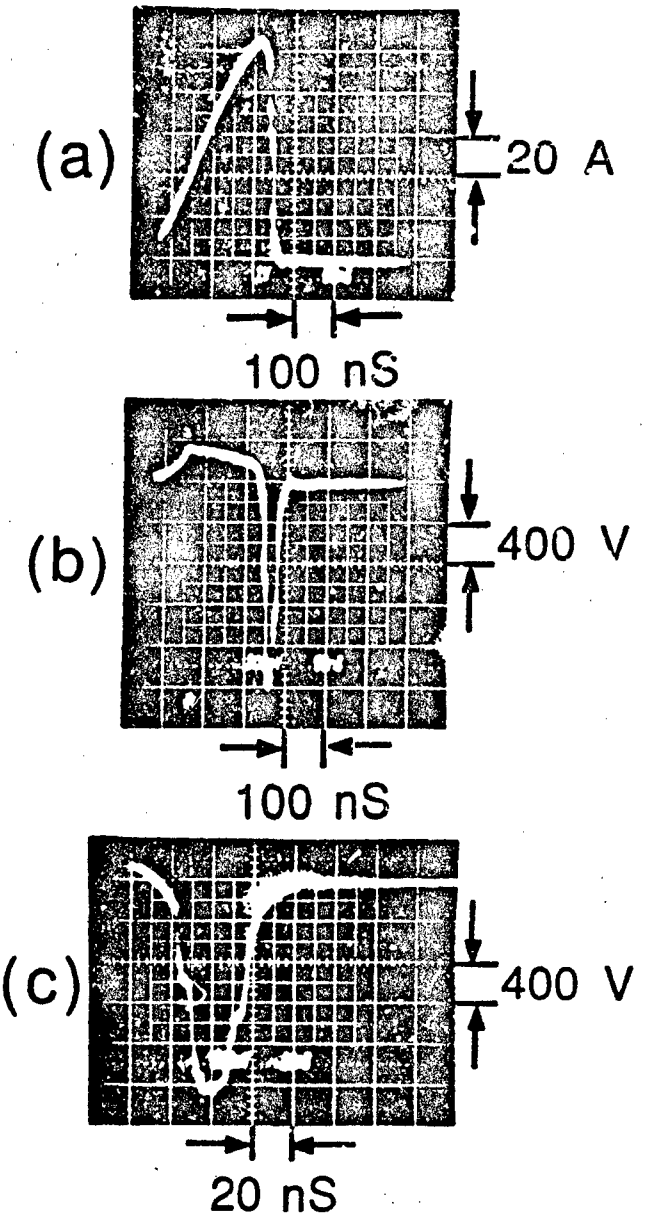

Fig. 8.6. Experimental results obtained from the 5 mm cube GaAs p-i-n diode switch in the current charged transmission line at 500 V charging voltage. (a) the charging current waveform monitored by the CVR; (b) and (c) output voltage waveform.

switch is connected in series with the load resistor, R_L. Thus, the circuit can be treated as a voltage divider. By analyzing the voltage waveform $V_{out}(t)$ across the 50 Ω matched load while the laser pulse is on and using the equation

$$R_{sw}(t) = 50 \times [V_o/V_{out}(t) - 1] , \tag{8.5}$$

the temporal variation of the switch resistance is obtained. The other method is to analyze the experimentally obtained waveform from the circuit shown in Fig. 8.3. Since the circuit response is very close to that of the series connection RLC circuit, it is straightforward to analyze the current waveform $I(t)$ obtained from the current viewing resistor and the voltage waveform $V_{out}(t)$ measured with the 50 Ω matched load together. The temporal variation of the switch resistance $R_{sw}(t)$ can be easily calculated from the equation

$$\frac{1}{C}\int I(t)dt + V_{out}(t) + I(t)R_{sw}(t) = V_o . \tag{8.6}$$

According to this analysis, the switch (the 5-mm cube GaAs p-i-n diode) behaved differently in these two different circuits. The results, which are obtained from these two circuits at V_o=700 V, are shown in Fig. 8.7. It shows that the lowest on-resistance is 6.0 Ω (Fig. 8.7(a)) in the capacitive circuit and is 3.4 Ω (Fig. 8.7(b)) in the CCTL circuit respectively. In the CCTL circuit, the switch resistance drops to a lower value during the closing phase and increases faster during the opening phase than those in the capacitive circuit. The reason for the lower on-resistance in the case of the CCTL circuit may be due to the higher thermal power dissipation while the charging current flowing through the switch is higher causing the switch on-resistance to drop further. As shown in the experimental results, the maximum charging current flowing through the switch is 100 A in the CCTL circuit and is 12.3 A in the capacitive circuit.

When the switch is turned off, the induced electric field across the switch in the CCTL circuit becomes higher and hence is in favor of sweeping out the excess carriers in the switch resulting in a faster opening. In fact, the analysis

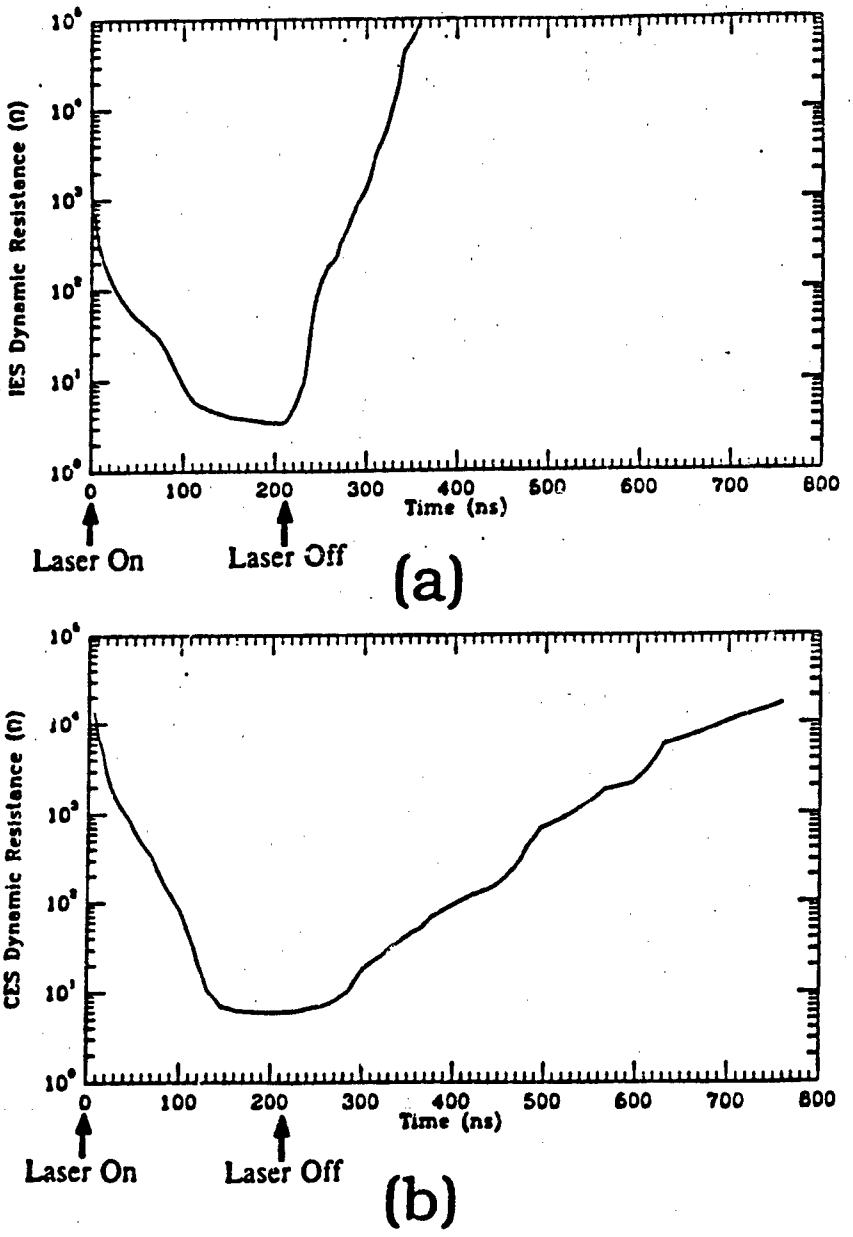

Fig. 8.7. The dynamic resistance of the 5 mm cube GaAs p-i-n diode switch in two different pulsed power systems at 700 V charging voltage. (a) the switch in the inductive energy storage pulsed power system; (b) the switch in the capacitive energy storage pulsed power system.

show that the maximum electric field across the switch in the CCTL circuit is 5.0 kV/cm, which occurs at the moment of the peak output voltage pulse. On the contrary, the maximum electric field across the switch in the capacitive circuit is 1.4 kV/cm, which occurs at the off-state of the switch. If the switch in the capacitive circuit is turned on, the electric field across the switch will drop significantly. Since the switch is heavily saturated with free carriers and there is lack of strong induced field to sweep out the excess carriers in the capacitive circuit, the switch opening time is thus severely prolonged. Fig. 8.7 clearly dispalys that the switch in the CCTL circuit can have a fast opening time due to the induced electric field. Also, we can see that the switch in the CCTL circuit is fully opened in 100 ns but in the capacitive circuit requires more than 500 ns to be opened. Furthermore, the experimental results obtained from the CCTL circuit with lower charging voltages show that the switch off-resistance can increase relatively faster to achieve a better voltage gain and power amplification as long as the induced field does not exceed the "lock-on" field (~5.0 kV/cm) [11],[82],[83].

8.2 Experimental results with the flashlamp pumped laser

Based on the experimental results obtained from the Ar^+ laser pumped system, it is impossible to observe the ideal charging current waveform and to increase the switch efficiency during the charging cycle due to the laser pulse shape. In order to overcome these drawbacks, a flashlamp pumped Nd:Glass rod system was developed by E. E. Funk in our laboratory. The unique feature of this flashlamp pumped Nd:Glass rod laser system is its nearly square laser pulse shape of 7-ns rise-time and fall-time. Thus, the switch efficiency is increased and the theoretical waveforms of the CCTL and the DBL which are discussed and compared in Chapter 5 can be observed and verified.

The system, which is shown in Fig. 8.8, is formed with an oscillator and an amplifier. The oscillator is a simple linear laser cavity pumped by a flash-lamp. In order to avoid self Q-switching and obtain only one long-duration,

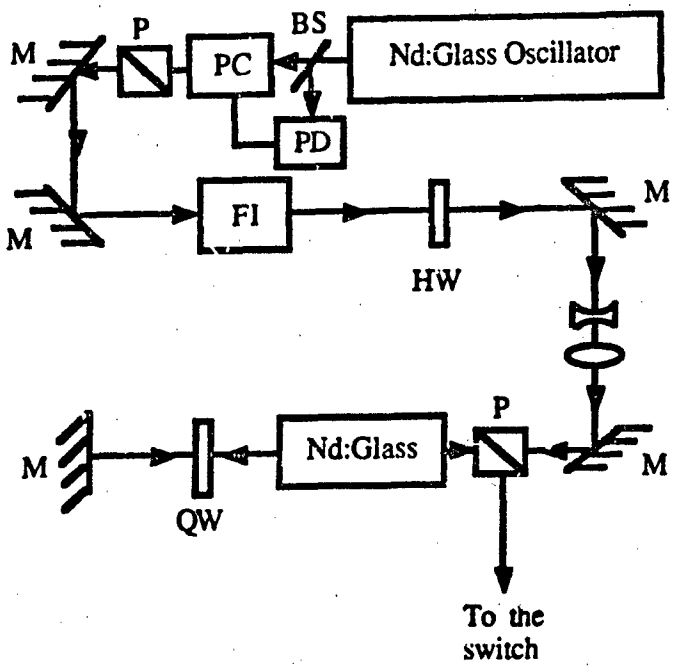

Fig. 8.8. Layout of the flashlamp pumped Nd:Glass rod system; BS: beam splitter, PD: photodetector, PC: Pockels cell, M: mirror, P: polarizer, QW: quarter wave plate, FI: Faraday isolator, HW: half wave plate.

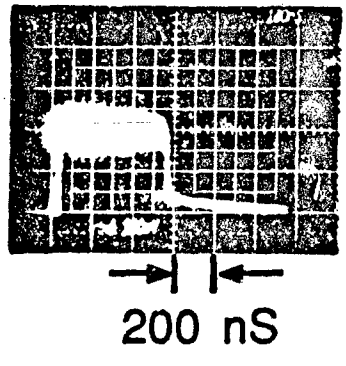

Fig. 8.9. The amplified laser p lse shape from the flashlamp pumped system.

Gaussian-profile laser pulse, the oscillator has to be operated just above the lasing threshold. The emitted laser pulse wavelength is 1.054 μm and the pulse duration is $\sim$2 μs (FWHM). By using a Pockels cell, a 540 ns long nearly square laser pulse is chopped from the middle of this long pulse. At this stage, the laser pulse energy is $\sim$2 μJ. This is not enough to fully lower the switch on-resistance, therefore a two-stage flashlamp pumped glass amplifier is used for further amplification. This glass amplifier is the same one used in the Ar^+ laser pumped system. As shown in Fig. 8.9, the amplified laser pulse has a $\sim$7 ns rise- and fall-time and an energy of $\sim$12 mJ.

With these features, the switch resistivity can drop quickly as soon as the laser pulse illuminates the switch. Thus, the switch efficiency is increased and it is possible to observe the staircase-like charging current waveform as long as the traveling wave round-trip time in the transmission line is longer than 7 ns. In this experiment, the switch used was the 5-mm cube GaAs p-i-n diode switch used before and the inductive energy storage systems used were the CCTL and the dual of the Blumlein line (DBL). Since this laser pulse width (540 ns, Fig. 8.9) was longer than the previous one ($\sim$200 ns) and the pulse energy was also higher, a larger capacitor could be used in the circuits to transfer more energy to the inductive energy storage systems [36],[40]. This approach can be justified by using Eqns. (8.2) and (8.3). Eqn. (8.3) implies that a larger capacitance and a longer transmission line can be used for the pulse forming experiment due to the longer laser pulse duration which can turn on the switch longer to attain a longer charging time. In this case, Eqn. (8.2) clearly suggests that a larger capacitance can produce higher charging current and that more energy can be compressed and switched out in the experiment.

The modified CCTL circuit was introduced in the previous section. In this section, the modified DBL circuit, which is different from the one discussed in Chapter 5, is depicted in Fig. 8.10. The modifications include the extra capacitor, C, placed next to the switch and the charging resistor, R, connected

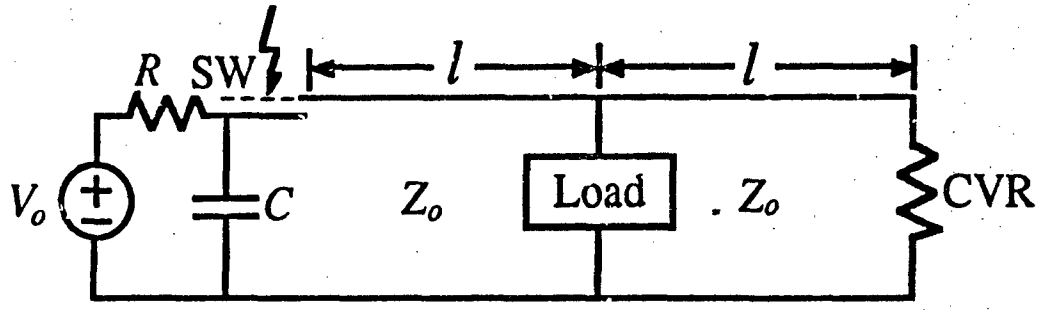

Fig. 8.10. Experimental circuit diagram for the dual of the Blumlein line; SW: switch, CVR: current viewing resistor (0.1 Ω), C: capacitor (1.1 μF), R: charging resistor (2.7 kΩ), Load: 25 Ω.

after the voltage source. The main purpose of the capacitor is to act as an ideal voltage source to the DBL, and the purpose of the charging resistor is to protect the voltage source and to isolate the voltage source from the DBL. In this configuration, the same concept of electrical pulse compression, which requires a long charging time to charge the pulse forming network and a short discharging time to transfer the energy to the load, applies again. The DBL, which is the pulse forming network in this experiment, comprises a parallel connection of two equal length transmission lines of characteristic impedance Z_o. The matched load, $Z_o/2$, is located at the junction of these two lines. The end of one transmission line is shorted with a current viewing resistor (CVR, 0.1 Ω), which is used for monitoring the charging current during the experiment. The end of the other transmission line is connected through the switch to a capacitor of value C=1.1 μF, which is larger than the previous one, 0.1 μF, and is initially charged to the voltage V_o. As mentioned before, the larger capacitor value is used because of the longer laser pulse duration corresponding to a longer conduction time of the switch.

The p-i-n diode switch was reverse biased in the experiment to achieve a better performance; that is with the positive polarity of the charging voltage applied to the n-type surface. The switch was illuminated perpendicularly to the electric field across the switch. Before the arrival of the laser pulse, the switch was in a high impedance state and the electrostatic energy was stored in the 1.1 μF capacitor. Upon activation of the switch by the laser pulse, the capacitively stored energy was transferred to the DBL, the inductive energy storage device, and was stored in the form of current. If the energy conservation concept is applied again, the maximum charging current I_{max} in the DBL will be related to the charging voltage V_o by the expression $(1/2)LI_{max}^2 = (1/2)CV_o^2$, where L is the inductance of the DBL with a total length of transmission line $2l$. The charging current waveform for $2l$=4 m, which corresponds to L = 1.0 μH, at V_o=200 V is shown in Fig. 8.11(a). It clearly displays a staircase-

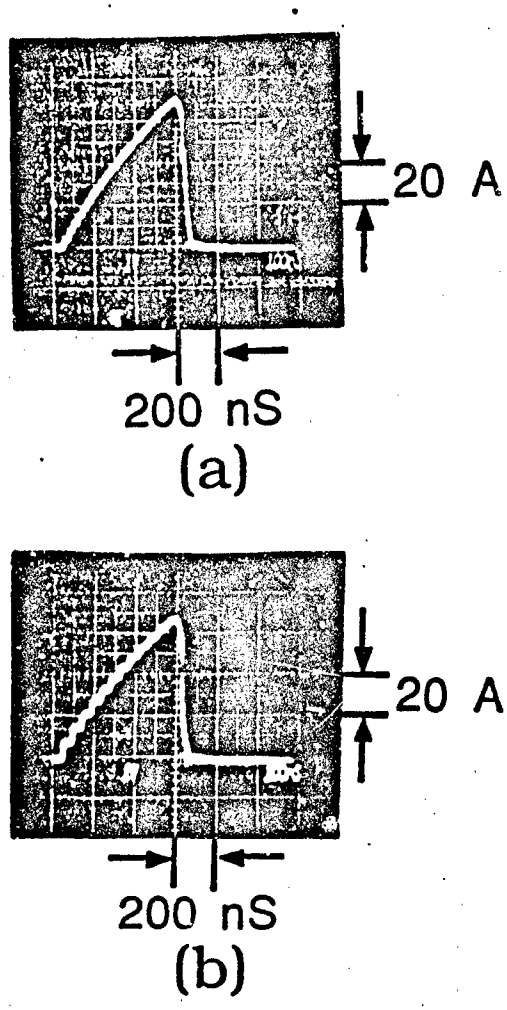

Fig. 8.11. The charging current waveforms obtained from the 5 mm cube GaAs p-i-n diode switch at 200 V charging voltage in two different circuits of 4-m-long charging line. (a) dual of the Blumlein line; (b) current charged transmission line.

like build-up waveform as being predicted. However, the maximum charging current, I_m 3 A, was much less than what was expected, that is $I_{max} = (C/L)^{1/2}V_o$ = (1.1 μF/1.0 μH)$^{1/2}$200 V=210 A. By considering the resonant period which is found to be $T = 6.3$ μs from Eqn. (8.3), one might conclude that the length of the DBL might be too long to reach the expected charging current. In fact, when the computed optimal length of the DBL having $T/4 = 540$ ns was chosen in the experiment, the result obtained was a current even less than 68 A. This may be attributed to the finite switch on-resistance during the charging cycle and the error in treating the DBL as a lumped inductance. In order to reduce the error in the lumped inductance model, the finite switch on-resistance must be considered in this estimation. In this case, the circuit has to be treated as a series connected *RLC* circuit during the charging cycle and using the best fit for the current waveform. Based on this estimation, the switch on-resistance is found to be $\sim$2 Ω. This is lower than 3.4 Ω, the resistance value discussed in the last section. This is because a higher laser pulse energy was used and should give a lower switch on-resistance. Hence, it is reasonable to have 2 Ω with 12 mJ pulse energy in contrast to 3.4 Ω with 4 mJ pulse energy.

Fig. 8.11(b) shows the charging current waveform for the CCTL with a total length of $2l = 4$ m and at V_o=200 V across the 1.1 μF capacitor. Notice that Fig. 8.11(a) and (b) exhibit the same pulse shape and pulse amplitude, but differ in the amplitude and the duration of each step. The same pulse shape and amplitude are the results of using the same length of short-circuited transmission lines which correspond to the same inductance value. The difference in the staircase structure was discussed in Sec. 5.4. It is from the position of the load impedance, where a discontinuity in the transmission line occurs. By combining the staircase structure and the lumped inductance model, the expected charging current waveform should be a series of steps with an envelope corresponding to an *RLC* circuit waveform under the oscillatory condition. Since the voltage in the capacitor is dropping, the corresponding height of each step is gradually

reduced after each round-trip time of the traveling wave. That is the reason why the envelope of the current waveforms shown in Figs. 8.11(a) and (b) are not straight lines, they are curved during the charging cycle. Thus, it had better to turn off the switch at the peak of the first quarter cycle of the current waveform to achieve the maximum energy transferring to the load impedance.

In terms of the staircase structure in the current waveforms, the amplitude of several early steps is close to $V_o/Z_o = 4$ A for the DBL (Fig. 8.11(a)) and $2V_o/Z_o = 8$ A for the CCTL (Fig. 8.11(b)) respectively. Besides, Fig. 8.11 also shows that the duration of each staircase step is ~20 ns for the DBL and that is ~40 ns for the CCTL. This suggests that the number of steps in the DBL charging current waveform is twice of that of the CCTL charging current waveform in order to transfer the same amount of current to the transmission lines. These results follow exactly the theory described in Chapter 5. This good agreement is the direct result of using a nearly square laser pulse to activate the switch and, thus, having a closing time which is much shorter than the round-trip time of the traveling wave in the current charging lines. This is in contrast to the results obtained from the Ar^+ laser pumped system. In those results, we could not observe these ideal charging current waveforms due to the slow rise of the laser pulse intensity. For this reason, the Ar^+ laser pumped Nd:Glass system was no longer used in the later experiments.

As just described, the inductive energy storage system was charged with current while the laser pulse was shining on the switch. Upon extinguishing the laser pulse, the switch was opened and the stored inductive energy was delivered to the resistive load. The output voltage waveforms from the DBL with the length of $2l$=3 m appeared as expected. The maximum charging current in this condition is $I_o = 75$ A. The output voltage waveform is shown in Fig. 8.12(a) and (b). It reveals that the peak voltage pulse reaches 1.3 kV, which is less than the expected value, $I_o Z_o/2 = 75 \times 50/2 = 1875$ V. This indicates that the switch gradually changes from the on-state (~ 2 Ω) to the off-state (few kΩ) within 10's

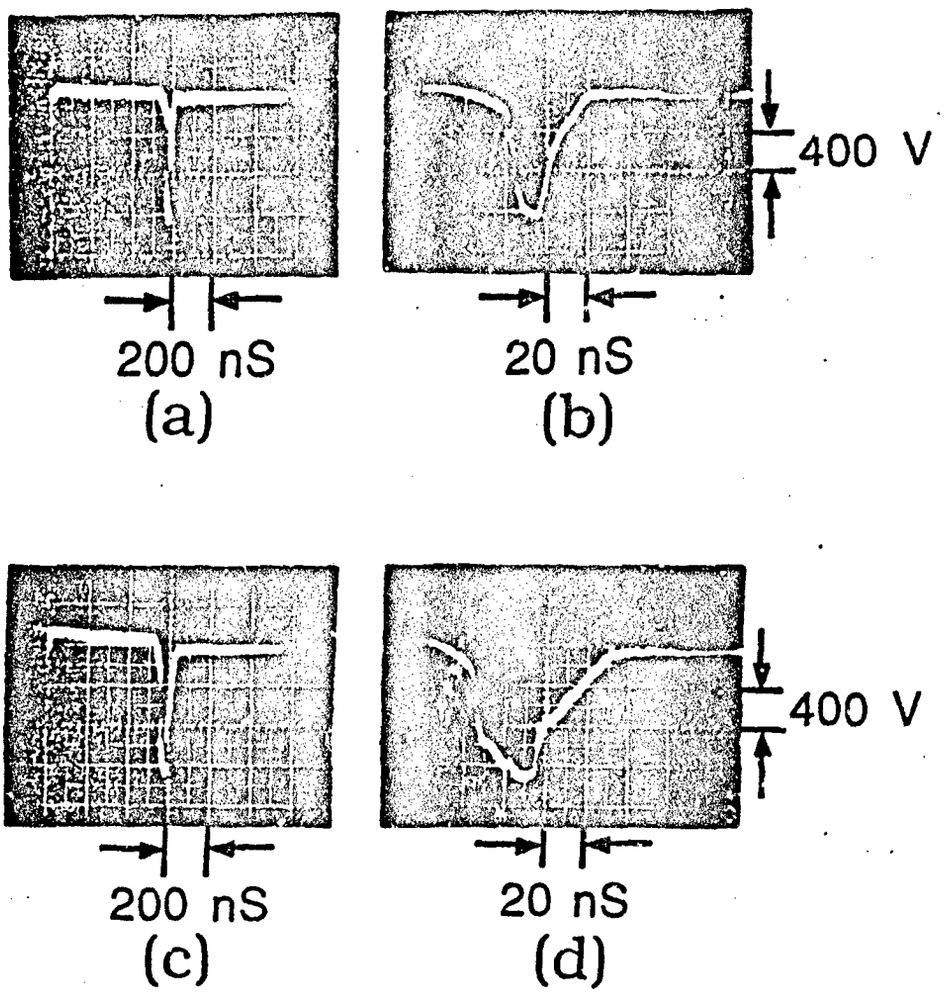

Fig. 8.12. The output voltage waveforms obtained from the 5 mm cube GaAs p-i-n diode switch at 200 V charging voltage in two different circuits of 3-m-long charging line. (a) and (b) dual of the Blumlein line; (c) and (d) current charged transmission line.

of nanoseconds. Comparing these results to the results obtained from the CCTL with a total length of $2l$=3 m and at V_o = 200 V (Fig. 8.12(c) and (d)), we see many similarities including the output voltage pulse amplitude and the pulse shape. The main differences between Fig. 8.12(a), (b) and (c), (d) come from the amplitude of the prepulse and the duration of the amplified negative pulse. The amplitude of the prepulse and the pulse duration of the amplified negative pulse obtained from the DBL are half of those obtained from the CCTL; this agrees perfectly with the theory discussed in Sec. 5.4.

Estimation of the voltage $V_{sw}(t)$ across the switch during the pulse forming stage has been discussed in Sec. 5.4. Since the reflection of the voltage traveling wave at the switch end does not change its polarity when the switch is opened, the voltage appearing across the DBL on the switch side should be twice that of the output voltage and $V_{sw}(t)$ can be expressed as

$$V_{sw}(t) = I(t)R_{sw}(t) = V_C(i) - 2V_{out}(t) = V_o - \frac{1}{C}\int I(t)dt - 2V_{out}(t)\ , \quad (8.7)$$

where $V_C(t)$ is the remaining voltage in the charging capacitor, C, and $I(t)$ is the charging current waveform. According to the experimental data from the CCTL, the maximum electric field across the switch without causing any pulse distortion is ~5.0 kV/cm. Thus, the maximum achievable output voltage from this 5-mm cube switch is ~1.25 kV in a DBL by assuming $V_C(t)$ = 0 V in Eqn. (8.7). In this case, 1.3 kV might be the highest output voltage which can be obtained from this switch in a DBL without causing any pulse distortion. If higher charging voltage is applied to the system, the switch failure will be observed and the output voltage pulse shape will become very irregular. As shown in Fig. 8.13, the distorted voltage pulse with a lower voltage gain is obtained from this switch by using l=2.5 m in a DBL at V_o=400 V, even though its 1.5 kV pulse height, which corresponds to a field strength of 6.0 kV/cm across the switch, is greater than that of 1.3 kV.

In spite of its failure at the higher charging voltage, the corresponding voltage gain from these two inductive energy storage systems at V_o = 200 V is

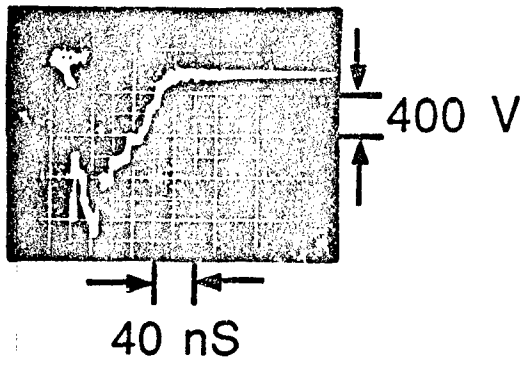

Fig. 8.13. Output voltage waveform obtained from the 5 mm cube GaAs p-i-n diode switch in the dual of the Blumlein line at 400 V charging voltage.

G_V=6.5, which is the highest among the results from all of the switches. The corresponding peak output power from the CCTL is P_{CCTL} = 33.8 kW and from the DBL is P_{DBL} = 67.6 kW. From these experimental results, the feasibility of compressing the electrical energy stored in a capacitor bank by utilizing an inductive energy storage circuit and an opening switch has been clearly demonstrated. Because of the fast response of the PCSS activated by a nearly square laser pulse, the ideal charging current waveform and the output voltage waveform discussed in Chapter 5 can be verified and understood experimentally. The issues related to the breakdown effect observed in the pulse forming experiments will be described in the following section. Those issues include the "lock-on" effect observed by other research groups and the discrepancies between their conclusions and ours.

8.3 Quasi-lock-on effect in the CCTL and the DBL

At present, the switch breakdown phenomenon and the "lock-on" effect are only experimental observations, and are not theoretically understood. There is still no very logical and self-consistent explanation. Because we employed the inductive energy storage systems in the pulse forming experiment, the switch function is totally different from the commonly used capacitive energy storage system. Hence, the "lock-on" effect we have observed might be different from other groups' observations. In this section, the characteristics of the "lock-on" effect which have been commonly observed by other research groups in the closing switch experiments are listed. By comparing our results with these characteristics, the differences between these two circuits can be seen. Those differences will be also discussed in this section.

As mentioned in the first section of this chapter, the switch resistance can be calculated by solving Eqn. (8.4) if the information of the charging current and the output voltage as a function of time were known. Computer codes which combine the charging current waveform and the output voltage waveform to solve for the switch resistance are developed. In this case, the dynamic switch

resistance and other parameters of the switch can be calculated. According to this analysis, the breakdown field for the GaAs switch is found to be close to the "lock-on" field observed by other groups in the closing switch configuration.

This "lock-on" effect of the GaAs switch was first observed by the Sandia National Laboratories groups. After the 1991 IEEE Pulsed Power Conference at San Diego, California, they collected the general information related to the "lock-on" effect which was observed by other research groups. According to their effort, these characteristics of the "lock-on" effect, which are commonly observed in the high voltage pulse forming experiments, are listed in the following [93]-[101]:

1. Electrical and optical thresholds must be exceeded. Non-linear switching occurs when (a) the field across the switch exceeds a threshold and (b) the switch is triggered with a sufficiently intense light or electron beam source. At least some types of GaAs do not switch spontaneously from thermal noise or from thermal run away (e.g. Cr doped for 30 minutes at 25 kV/cm).
2. A forward voltage drop is maintained. In the "on" state, the switch maintains a fixed electric field. This field, like the threshold field for initiation, is dependent on the semiconductor used and on its processing. It ranges from 4-9 kV/cm for standard types of GaAs and was extended to 55 kV/cm with neutron irradiation.
3. Gain is present. The switch current has been 300-1000 times larger than the linear photo-response for the trigger. This mode can support a current several orders of magnitude above the linear photocurrent if only the circuit can supply that current.
4. Initiation is rapid. For 1.5 cm long switches at high fields, conduction is established in less than 2 nanoseconds and may be as short as several hundred picoseconds following irradiation. This delay is even shorter in smaller switches.
5. Conduction persists. After being initiated, the switch continues to conduct

for as long as the circuit maintains the forward voltage drop (property 2). This has been tested to ~2 μs.

6. The current is filamentary. At low light levels, there is usually one filament. At higher fluence, many filaments are generated. The filaments change position from pulse to pulse and imply current densities of at least several hundred kiloamperes per square centimeter.

7. Types of semiconductors. High gain switching is seen in GaAs and in InP, but not in Si.

Due to the difference of the circuit structures, there are some similarities and disparities between our results and their empirical observations. In brief, the switch in our experiment needs a long-duration laser pulse with a fast fall-time and theirs requires a short laser pulse with a minimal energy to induce the phenomenon. Furthermore, the electrical field across the switch prior to the laser pulse is high and static in their experiment and is relatively low in our experiment. The only moment when the electrical field starts building up in our experiment is after the laser pulse during the switch opening and the pulse forming stage. This suggests that the field in our experiment is induced and dynamic. Thus, this results in our observation in opposition to some of the above characteristics. For example, the high gain mentioned in property 3 cannot be observed in our experiments and the optical threshold in property 1 does not exist in our observations. Also, the initiation in property 4 is difficult for us to observe during the switch opening stage.

However, we have observed some phenomena similar to the rest of the properties. For instance, the switch material we used in the experiment is GaAs, this immediately satisfies property 7 in the list. In addition, the data analysis for the 5-mm cube GaAs p-i-n diode switch shows that the switch has the tendency to maintain conduction at the field strength of ~5 kV/cm. These results coincide with property 5 and the field strength in property 2. Moreover, it is reported that the "lock-on" effect might be related to the Gunn effect due to the negative

differential resistivity exhibited by GaAs [11]. As shown in our data analysis, the switch also reveals this type of negative differential resistivity at ~5 kV/cm field strength. As for the current in property 6, we did observe the arcs across the switch during the opening stage. Nevertheless, the nature of these arcs which are either surface flash-over or filamentary in our experiments still needs further investigation. This is because we used our naked eyes to observe the phenomenon in the experiment. Thus, it is very possible to be misled or to jump to the wrong conclusions.

Based on the above discussion, the reason for limiting the output voltage pulse amplitude might be directly related to the "lock-on" effect in the closing switch configuration. Since there are some similarities and differences in the results obtained from these two circuit structures, which are inductive and capacitive circuits, we call the phenomenon we observed "quasi-lock-on" effect. However, it is still very important to understand the physics in the "lock-on" effect so that we can have more knowledge about the semiconductor switch in high power opening switch applications.

8.4 Summary

Due to the successful development of the laser systems, high power square pulses were produced with photoconductive semiconductor switches in the inductive energy storage systems, the CCTL and the DBL, for the first time. The highest output peak power, which is obtained with the 5-mm cube GaAs p-i-n diode switch in a CCTL activated by the Ar^+ laser pumped system, is 80 kW. The highest voltage gain obtained in both of the CCTL and the DBL with this 5-mm cube GaAs p-i-n diode switch activated by the flashlamp pumped system is 6.5. Because the laser pulse shape of this flashlamp pumped system is nearly square, many differences between the CCTL and the DBL, which are theoretically discussed in Sec. 5.4, can be experimentally compared and realized. In order to scale up the systems to achieve a higher output voltage, thicker switches and higher power laser pulses with a longer duration are required. The reasons

for the unwanted conduction of the switch at the opening stage, which limits the output voltage pulse amplitude, still needs further investigation. Even though some evidence of this unwanted conduction seem related to the "lock-on" effect in the closing switch configuration, further experimental data are still required due to the difference of our circuit structure. Perhaps, this may be a type of new effect for the semiconductor material under the influence of an intense electric field.

CHAPTER 9

Conclusions and Future Work

For the first time, voltage multiplication and electrical pulse compression are achieved with photoconductive semiconductor opening switches in the inductive energy storage pulsed power systems. The switches used are made of GaAs or Cr:GaAs with the opening time on the order of a nanosecond or subnanosecond. This opening time is the fastest among all the existing opening switches. Two Nd:Glass laser systems used to activate the switches are specially designed, they both emit at 1.054 μm wavelength and have a fall-time in the nanosecond regime. Since this fall-time is comparable to the carrier lifetime of the switch, the switch can be opened in this time scale. Due to the successful development of the laser systems, a new realm in the fast opening switch, which demonstrates the capability of electrical pulse compression, is attained. The inductive energy storage pulsed power systems employed in the pulse forming experiments are the current charged transmission line and the dual of the Blumlein line. The corresponding pulse forming theories in these two systems with an ideal opening switch and a voltage source were discussed in great detail. Lumped inductive energy storage pulsed power systems such as the simple *RLC* circuit and the dual of the *LC* generator were discussed in detail as well.

With the aide of a computer, dynamic switch resistance and other accompanied parameters in the switch can be calculated. In this case, the switch operation can be fully understood. Based on the experimental results, the threshold field for the GaAs switch to sustain an unwanted conduction is found to be close to the "lock-on" field observed by other groups in the closing switch configuration. According to their empirical observations and compared to our experimental results, there are a great deal of discrepancies due to the testing circuit configurations. In spite of this "lock-on" effect, it is still very promising

to employ the photoconductive semiconductor switches in inductive energy storage pulsed power systems to generate high voltage pulses. As mentioned and demonstrated, the photoconductive semiconductor switches have the following characteristics:

1. jitter free,
2. potential for high repetition rate,
3. very fast turn-off time,
4. low switch on-resistance,
5. high switch off-resistance.

In the future, there are several directions worth looking into. One direction is to study the abnormal conduction effect in the semiconductor switch. In order to understand how much it is related to the "lock-on" effect and the physics behind it, experiments with different switches of different materials and dimensions are required to reach a decisive conclusions. Presently, only one GaAs p-i-n diode switch revealing this effect is not sufficient to support a general argument. The other direction is to develop new laser systems which can provide the laser pulses with a higher pulsed power, a longer duration time, a fast rise-time, and a fast fall-time [102],[103]. The longer duration time is required to keep the semiconductor switch on long enough so that the inductive system can be charged with more current. The fast rise- and fall-time of the laser pulse are needed for operating the switch efficiently so that the inductive system performance may be diagnosed. Especially, the switch opening time which is determined by the carrier lifetime in the switch and/or the laser pulse fall-time is very critical in producing a fast voltage pulse with a voltage gain from an inductive system. As a matter of fact, the voltage pulses presently in use for pulsed power purpose are in the range of few hundred kilovolts to several megavolts, this is about two orders of magnitude larger than the best results obtained in this work. Thus, larger dimension switches which can hold off higher charging voltages and produce higher output voltage pulses are necessary for

scaling up the system to satisfy the practical usage requirements. Since a larger dimension switch has to be used for this purpose, this implies that a higher laser power is required to lower the switch on-resistance in order to fully charge the inductive system with current.

In addition to the switch physics and the laser system, designing the switch electrode and the switch geometry might be an interesting area to look into. The main goal is to obtain the lowest contact resistance and to increase the breakdown threshold, thus higher output voltage pulses may possibly be switched out. Also, testing the switches in different experimental environments and searching for some new switch materials are very important in improving the present results. As mentioned before, those new switch materials which still require experimental work to demonstrate their feasibility in an inductive system include high T_c superconductor, graphite, ZnSe, diamond, etc. Regarding the new experimental environments, some future experiments might have to immerse the switches in insulating fluids rather than in the air in order to reduce the probability of surface breakdown and to increase the output pulse voltage. Because all of the present experiments are performed in the open air, it is difficult to determine the cause of the breakdown in some results which are close to the air breakdown field. Finally, it is worth trying some new and different types of inductive energy storage pulsed power systems. In order to discover new inductive energy circuits, the duality between the inductive systems and the capacitive systems in circuit theory can be used to convert presently existing capacitive energy circuits, such as the Marx generator, to its dual circuit. For such a conversion, new theories have to be derived and new experiments have to be designed. For further improvement, the inductors in the new systems can be replaced with short-circuited transmission lines. As an example, one can expand the dual of the Blumlein line from two transmission lines in parallel to $2n$ transmission lines in parallel. This is shown in Fig. 9.1(a). In this configuration, n opening switches and n power supplies are required. The matched

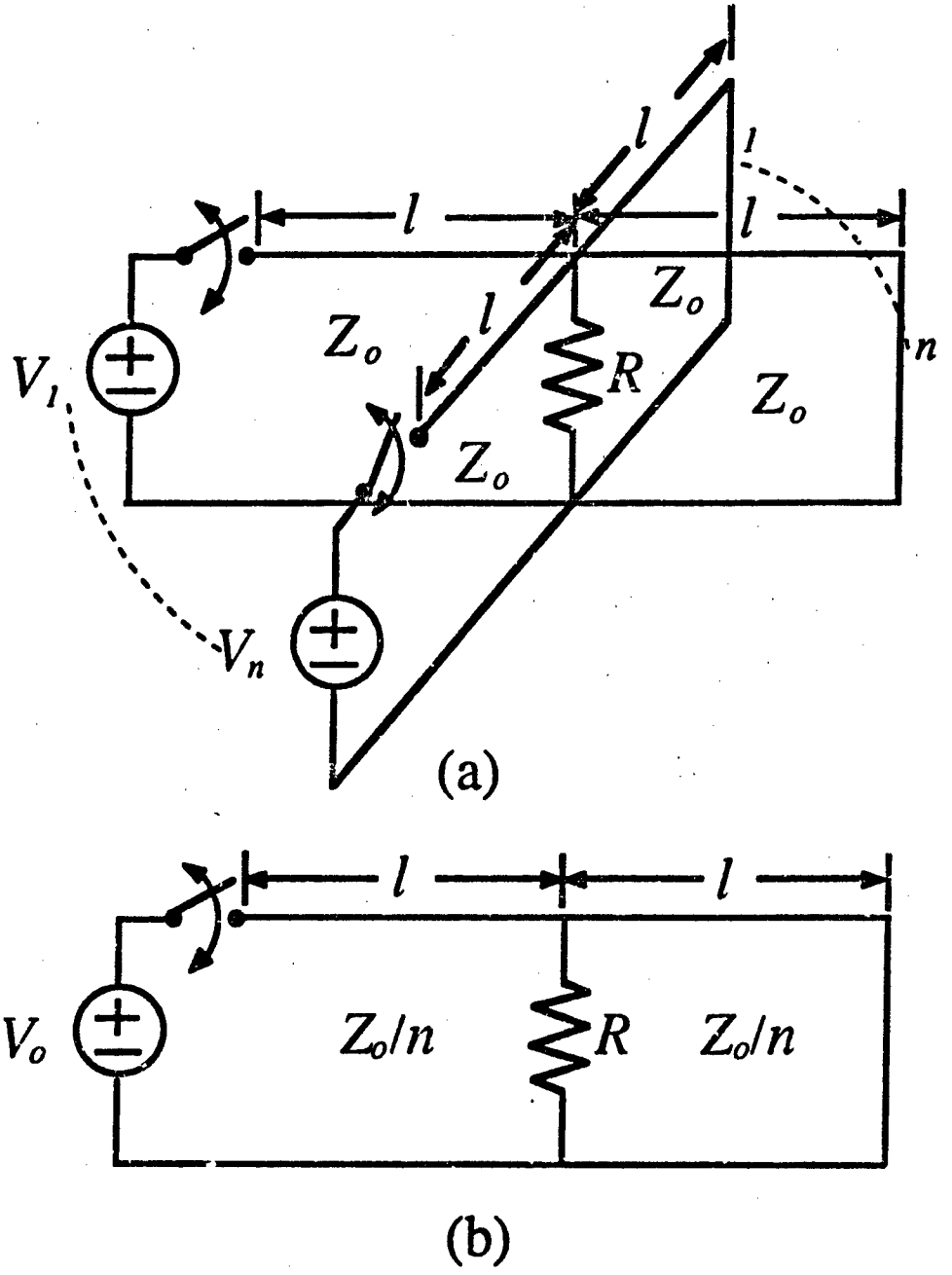

Fig. 9.1. (a) $2n$ transmission lines of characteristic impedance Z_o are in parallel with n power supplies and n opening switches. (b) The circuit can be simplified to a DBL system with the characteristic impedance of the transmission line Z_o/n.

load in the system is reduced to $Z_o/2n$ and the output peak current becomes ΣI_i, where I_i is the current flowing out of the ith power supply at the end of the charging cycle. In fact, this configuration can be simplified to a DBL system (Fig. 9.1(b)) with a characteristic impedance Z_o/n and the power supplies can be combined into a main power supply by using the superposition theorem. By the same token, the structure of n short-circuited transmission lines connected in parallel, which is shown in Fig. 9.2(a), can be reduced to a CCTL with a Z_o/n characteristic impedance (Fig. 9.2(b)). In addition, some other new circuits can be derived from this parallel connection. For example, two transmission lines of different length are in parallel connection and the load impedance is at the junction of these two lines. If the other end of these two lines is shorted (Fig. 9.3), it will look like an asymmetric DBL system. On the contrary, if the other end of these two lines is opened (Fig. 9.4), there will be no system really related to this structure. However, it is very interesting to theoretically and experimentally present the possible output waveforms from these two circuits. The details about these two circuit structures still need further study.

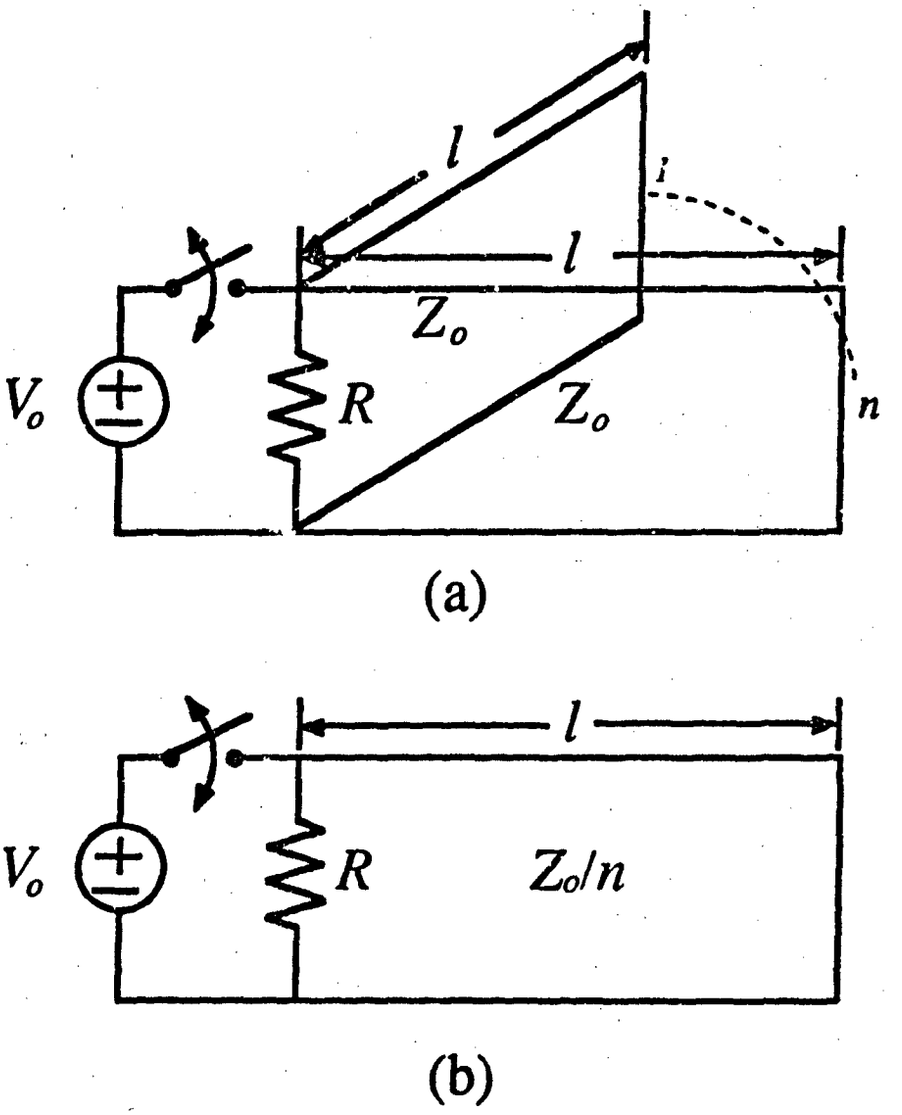

Fig. 9.2. (a) n transmission lines of characteristic impedance Z_o are connected in parallel. (b) The circuit can be simplified to a CCTL system with the characteristic impedance of the transmission line Z_o/n.

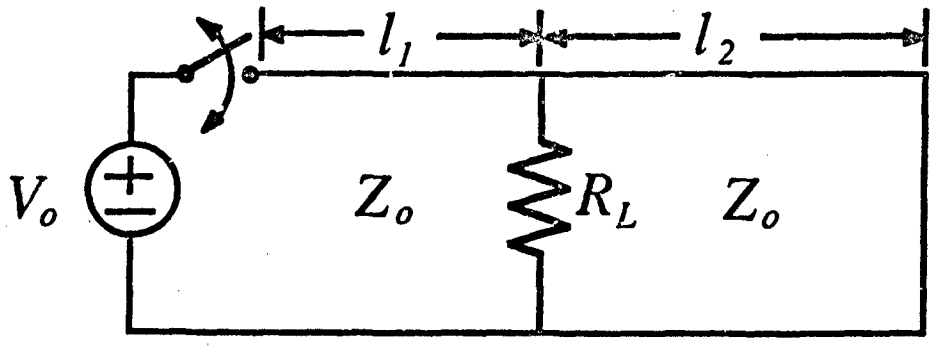

Fig. 9.3. Asymmetric DBL structure, where $l_1 \neq l_2$.

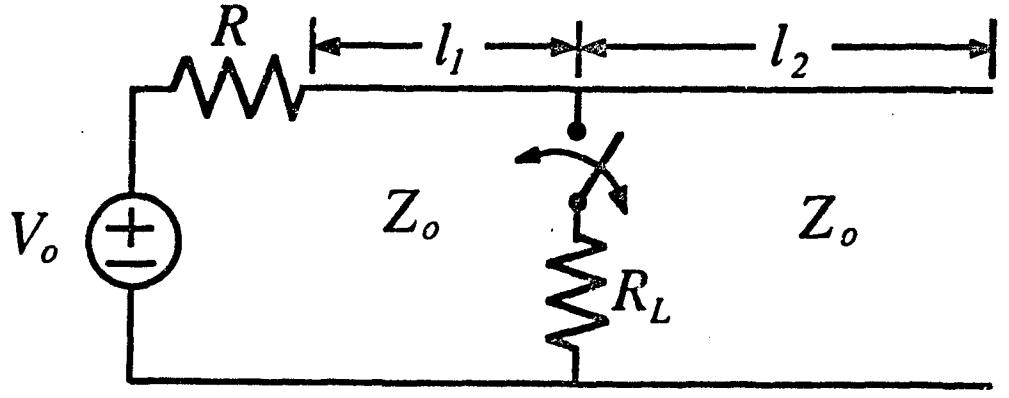

Fig. 9.4. Modified asymmetric DBL structure with one end opened and with the other end connected to a voltage source through the charging resistor R, where $R \gg Z_o$.

APPENDIX I

Initial Conditions and Solutions to the Dual of the LC Generator

As shown in Section 4.3, the response of a dual of the LC generator can be described by the following equations:

$$\frac{V_o}{R_{off}} = \frac{V_C(t)}{R_{off}} + C\frac{dV_C(t)}{dt} + I_{L1}(t)\,, \tag{A1.1}$$

$$V_C(t) = L\frac{dI_{L1}(t)}{dt} + L\frac{dI_{L2}(t)}{dt} = L\frac{dI_{L1}(t)}{dt} + I(t)R_L\,, \tag{A1.2}$$

$$I_{L1}(t) = I(t) + I_{L2}(t)\,, \tag{A1.3}$$

$$\frac{V_o}{R_{off}} = LC\frac{d^2}{dt^2}[I(t)+2I_{L2}(t)] + \frac{L}{R_{off}}\frac{d}{dt}[I(t)+2I_{L2}(t)] + I(t) + I_{L2}(t)\,, \tag{A1.4}$$

$$V_{out}(t) = L\frac{dI_{L2}(t)}{dt} = I(t)R_L\,, \tag{A1.5}$$

where $I(t)$ is the current flowing through the load resistance, R_L, and $V_{out}(t)$ is the voltage across R_L after the switch is opened. Rearranging the above equations, the third order differential equation for the dual of the LC generator is obtained as

$$\frac{d^3I(t)}{dt^3} + \left(2\frac{R_L}{L} + \frac{1}{R_{off}C}\right)\frac{d^2I(t)}{dt^2} + \left(1 + 2\frac{R_L}{R_{off}}\right)\frac{1}{LC}\frac{dI(t)}{dt} + \frac{R_L}{L^2C}I(t) = 0. \tag{A1.6}$$

The initial conditions and the possible solutions for this third order differential equation are derived and discussed below. By employing $I_{L1}(0) = I_{L2}(0)$ in Eqn. (A1.3), the zeroth order initial condition is determined as

$$I(0) = 0\,. \tag{A1.7}$$

Using $V_C(0) = 0$ in Eqn. (A1.2) results in

$$\left.\frac{dI_{L1}(t)}{dt}\right|_{t=0} = -\left.\frac{dI_{L2}(t)}{dt}\right|_{t=0}. \tag{A1.8}$$

Differentiating Eqn. (A1.3) and then using Eqn. (A1.8) leads to

$$\left.\frac{dI_{L1}(t)}{dt}\right|_{t=0} = \frac{1}{2}\left.\frac{dI(t)}{dt}\right|_{t=0} . \qquad (A1.9)$$

Substituting Eqn. (A1.9) into Eqn. (A1.2) gives

$$V_C(0) = 0 = \frac{L}{2}\left.\frac{dI(t)}{dt}\right|_{t=0} + I(0)R_L = \frac{L}{2}\left.\frac{dI(t)}{dt}\right|_{t=0} + 0 . \qquad (A1.10)$$

Thus, the first order initial condition is

$$\left.\frac{dI(t)}{dt}\right|_{t=0} = 0 . \qquad (A1.11)$$

Differentiating Eqn. (A1.5), one obtains

$$L\left.\frac{d^2I_{L2}(t)}{dt^2}\right|_{t=0} = \left.\frac{dI(t)}{dt}\right|_{t=0} R_L = 0 . \qquad (A1.12)$$

Then differentiating Eqn. (A1.2) and using Eqn. (A1.12) give

$$\left.\frac{dV_C(t)}{dt}\right|_{t=0} = L\left.\frac{d^2I_{L1}(t)}{dt^2}\right|_{t=0} . \qquad (A1.13)$$

Utilizing Eqn. (A1.1) leads to

$$\frac{V_o}{R_{off}} = \frac{0}{R_{off}} + C\left.\frac{dV_C(t)}{dt}\right|_{t=0} + \frac{V_o}{R_{on}} , \qquad (A1.14)$$

therefore

$$\left.\frac{dV_C(t)}{dt}\right|_{t=0} = \frac{1}{C}\left(\frac{V_o}{R_{off}} - \frac{V_o}{R_{on}}\right) = \frac{I_o}{C} , \qquad (A1.15)$$

where I_o is defined in Eqn. (4.15). Differentiating Eqn. (A1.3) twice and using the results in Eqns. (A1.12), (A1.13), and (A1.15), one can obtain the second order initial condition, that is

$$\left.\frac{d^2I(t)}{dt^2}\right|_{t=0} = \left.\frac{d^2I_{L1}(t)}{dt^2}\right|_{t=0} - 0 = \frac{1}{L}\left.\frac{dV_C(t)}{dt}\right|_{t=0} = \frac{I_o}{LC} . \qquad (A1.16)$$

The solution to Eqn. (A1.6) can be written as

$$I(t) = A_1\exp(-\alpha t) + A_2\exp[-(\beta + j\omega)t] + A_3\exp[-(\beta - j\omega)t] , \qquad (A1.17)$$

where

$$\alpha = \frac{1}{3}\left(\frac{2R_L}{L} + \frac{1}{R_{off}C}\right) - (r+d)^{1/3} - (r-d)^{1/3}, \qquad (A1.18)$$

$$\beta = \frac{1}{2}[(r+d)^{1/3} + (r-d)^{1/3}] + \frac{1}{3}\left(\frac{2R_L}{L} + \frac{1}{R_{off}C}\right), \qquad (A1.19)$$

$$\omega = \frac{\sqrt{3}}{2}[(r+d)^{1/3} - (r-d)^{1/3}], \qquad (A1.20)$$

$$d = (q^3 + r^2)^{1/2}, \qquad (A1.21)$$

$$q = \frac{1}{9}\left(\frac{3}{LC} + \frac{2R_L}{R_{off}LC} - \frac{4R_L^2}{L^2} - \frac{1}{R_{off}^2C^2}\right), \qquad (A1.22)$$

$$r = -\frac{R_L}{6L^2C} - \frac{8R_L^3}{27L^3} + \frac{R_L}{R_{off}LC}\left(\frac{2R_L}{9L} + \frac{1}{9R_{off}C} + \frac{1}{6R_LC}\right), \qquad (A1.23)$$

and A_1, A_2, and A_3 are the constants which can be determined from the initial conditions.

Intuitively, there are four different circuit responses for this third order differential equation:

1. $\alpha = \beta$ and $\omega = 0$, critical damping with one time constant, α

Using $\alpha = \beta$ and combining Eqns. (A1.18) and (A1.19), one can obtain

$$(r+d)^{1/3} + (r-d)^{1/3} = 0. \qquad (A1.24)$$

As $\omega = 0$ leads to $d = 0$, this results in $r = 0$ in Eqn. (A1.24). However, since $R_{off} \gg LC/R_L$ is generally true, Eqn. (A1.23) can be simplified to

$$r = -\frac{R_L}{6L^2C} - \frac{8R_L^3}{27L^3} \neq 0. \qquad (A1.25)$$

Apparently, these two outcomes contradict each other. The circuit cannot be critically damped with $\alpha = \beta$ in this case.

2. $\alpha \neq \beta$ and $\omega = 0$, critical damping with two time constants, α and β

With $\omega = 0$ yielding $d = 0$ as well as $R_{off} \gg LC/R_L$ and $R_{off} \gg 1/C$, Eqn. (A1.21) can be rewritten as

$$q^3 + r^2 = \frac{1}{729}\left(\frac{3}{LC} - \frac{4R_L^2}{L^2}\right)^3 + \left(-\frac{R_L}{6L^2C} - \frac{8R_L^3}{27L^3}\right)^2 = 0. \qquad (A1.26)$$

This yields

$$32\left(\frac{R_L^2C}{L}\right)^2 - 13\left(\frac{R_L^2C}{L}\right) + 4 = 0\,. \qquad (A1.27)$$

In this case, the quadratic equation can be solved as

$$\frac{R_L^2C}{L} = \frac{13 \pm j\sqrt{343}}{64}\,. \qquad (A1.28)$$

Because R_L^2C/L must be a real number, it is impossible to have this type of circuit response.

3. $\alpha \neq \beta$ and ω is imaginary, damping without oscillation

Comparing Eqns. (A1.18), (A1.19), and (A1.20), one can reach the conclusion that $(r+d)^{1/3}$ and $(r-d)^{1/3}$ have to be complex conjugates. Since r is a real number as shown in Eqn. (A1.23), d must be purely imaginary. At this point, employing the assumptions for R_{off} in the previous two cases can change Eqn. (A1.21) to

$$d^2 = q^3 + r^2 = \frac{1}{729}\left(\frac{3}{LC} - \frac{4R_L^2}{L^2}\right)^3 + \left(-\frac{R_L}{6L^2C} - \frac{8R_L^3}{27L^3}\right)^2 < 0\,. \qquad (A1.29)$$

With rearrangement, it becomes

$$32\left(\frac{R_L^2C}{L}\right)^2 - 13\left(\frac{R_L^2C}{L}\right) + 4 < 0\,. \qquad (A1.30)$$

This equation can be rewritten as

$$\left[4\left(\frac{R_L^2C}{L}\right) - \frac{13}{16}\right]^2 + \frac{343}{256} < 0\,. \qquad (A1.31)$$

Apparently, Eqn. (A1.31) is self-contradictory and its solution does not exist, therefore the circuit cannot respond in this manner either.

4. $\alpha \neq \beta$ and ω is real, damping with oscillation

This is the only case in which the circuit can response. In order to solve Eqn. (A1.5) with these three initial conditions, Eqn. (A1.17) can be changed to

$$I(t) = A_1\exp(-\alpha t) + \exp(-\beta t)[A_2\cos(\omega t) + A_3\sin(\omega t)]\,. \qquad (A1.32)$$

Applying the zeroth order initial condition, $I(0) = 0$, leads to

$$A_2 = -A_1 \ . \tag{A1.33}$$

By using the first order initial condition, $dI(t)/dt|_{t=0} = 0$, Eqn. (A1.32) becomes

$$\left.\frac{dI(t)}{dt}\right|_{t=0} = -\alpha A_1 + \beta A_1 + \omega A_3 = 0 \ . \tag{A1.34}$$

This results in

$$A_3 = \left(\frac{\alpha - \beta}{\omega}\right) A_1 \ . \tag{A1.35}$$

Employing the third order initial condition, $d^2I(t)/dt^2|_{t=0} = I_o/LC$, and substituting Eqns. (A1.33) and (A1.35) into Eqn. (A1.32) yield

$$\left.\frac{d^2I(t)}{dt^2}\right|_{t=0} = \alpha^2 A_1 + \beta^2(-A_1) - 2\beta\omega\left(\frac{\alpha - \beta}{\omega}\right) A_1 - \omega^2(-A_1) = \frac{I_o}{LC} \ . \tag{A1.36}$$

So the constants are solved as

$$A_1 = \frac{I_o}{LC[(\alpha - \beta)^2 + \omega^2]} \ , \tag{A1.37}$$

$$A_2 = -\frac{I_o}{LC[(\alpha - \beta)^2 + \omega^2]} \ , \tag{A1.38}$$

$$A_3 = \left(\frac{\alpha - \beta}{\omega}\right) \frac{I_o}{LC[(\alpha - \beta)^2 + \omega^2]} \ . \tag{A1.39}$$

Accordingly, the output current becomes

$$I(t) = \frac{I_o}{LC[(\alpha - \beta)^2 + \omega^2]}\{e^{-\alpha t} - e^{-\beta t}[\cos(\omega t) - \frac{\alpha - \beta}{\omega}\sin(\omega t)]\} \tag{A1.40}$$

and the output voltage becomes

$$V_{out}(t) = \frac{I_o R_L}{LC[(\alpha - \beta)^2 + \omega^2]}\{e^{-\alpha t} - e^{-\beta t}[\cos(\omega t) - \frac{\alpha - \beta}{\omega}\sin(\omega t)]\} \ , \tag{A1.41}$$

Apparently, the behavior of this solution depends heavily on the circuit parameters, R_L, L, and C.

APPENDIX II

Current Accumulation and Prepulse in the Dual of the Blumlein Line

The schematic circuit diagram of the dual of the Blumlein line is shown in Fig. 5.12. By letting $Y = 1/R$ and $Y_o = 1/Z_o$ and using Eqn. (5.13) and (5.14) with $Y_L = Y + Y_o$, the reflection coefficient at the load junction is

$$\Gamma_I = \frac{Y + Y_o - Y_o}{Y + Y_o + Y_o} = \frac{Y}{Y + 2Y_o} = \frac{Z_o}{Z_o + 2R} ,$$

the transmission coefficient T_I for the current wave to propagate across the load resistance to the other transmission line is

$$T_I = \frac{2(Y + Y_o)}{Y + Y_o + Y_o} \frac{Y_o}{Y + Y_o} = \frac{2Y_o}{Y + 2Y_o} = \frac{2R}{Z_o + 2R} ,$$

and the coefficient T_R for the current wave transmitted to the load resistance to form the prepulse while the switch is closed is

$$T_R = \frac{2(Y + Y_o)}{Y + Y_o + Y_o} \frac{Y}{Y + Y_o} = \frac{2Y}{Y + 2Y_o} = \frac{2Z_o}{Z_o + 2R} .$$

These three fundamental equations have been shown in Eqn. (5.29), (5.30), and (5.31). Since one end of the dual of the Blumlein line is short-circuited and the other end is connected to an ideal voltage source through an ideal opening switch, total reflection of the traveling waves with $\Gamma_V = -1$ and $\Gamma_I = 1$ occurs every round trip time, $2l/v$, of the traveling wave in one transmission line at these two ends. The schematic description of all these parameters is shown in Fig. A2.1. With the equations and boundary conditions, the current waveform and the prepulse in the dual of the Blumlein line can be obtained by using iteration.

In the analysis, I_{sw} (V_{sw}) and I_{sh} (V_{sh}) represent the current (voltage) traveling waves propagating in the transmission line before and after the load

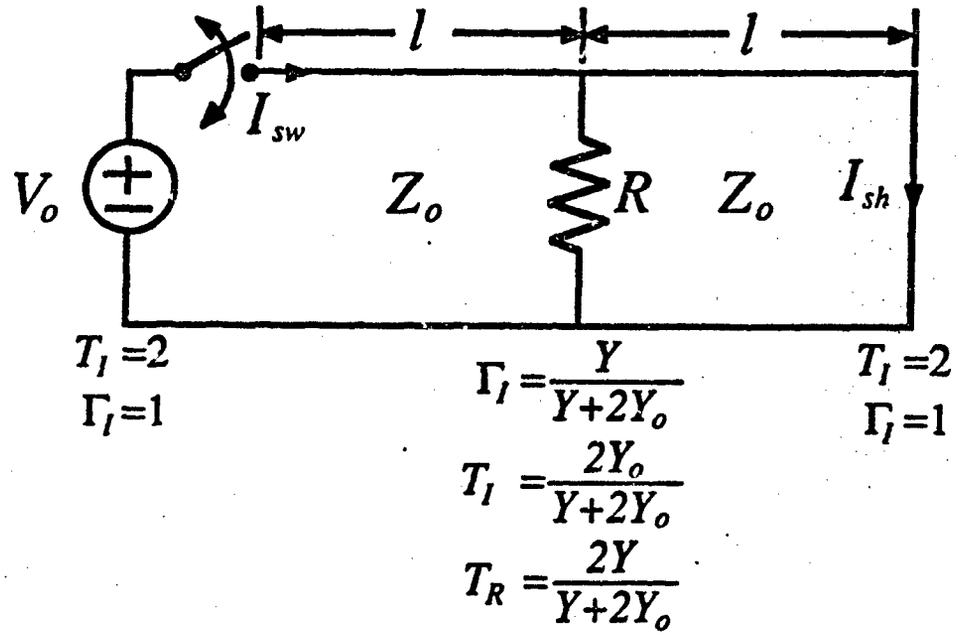

Fig. A2.1. Schematic circuit diagram of a dual of the Blumlein line, where Γ_I is the reflection coefficient of the current wave, T_I is the transmission coefficient of the current wave to the other side of the transmission line, T_R is the transmission coefficient of the current wave to the load impedance R, $Y = 1/R$, and $Y_o = 1/Z_o$.

junction respectively. Also, I_L is the current flowing through the load resistance, V_{pre} is the prepulse, and V_{out} is the output voltage pulse. While the switch is closed ($0 < t < t_{ch}$), the prepulse is determined by

$$V_{pre} = I_L(t)R \; . \qquad (A2.1)$$

Upon opening the switch ($t \geq t_{ch}$), the output pulse amplitude is

$$V_{out} = I_{out}(t)R = I_L(t)R \; . \qquad (A2.2)$$

Thus, it is important to know how to determine the current $I_L(t)$ during the pulse forming process. As shown in Fig. 5.13(a), I_L is determined by V_{sw}^+ and V_{sh}^- when they are propagating across the load junction. According to the previous discussion, the effective load impedance at the junction is $Z_L = Y_L^{-1} = RZ_o/(R + Z_o)$. In this case, the voltage traveling wave transmission coefficient T_V at the junction is

$$T_V = \frac{2Z_L}{Z_L + Z_o} = \frac{2R}{Z_o + 2R} \qquad (A2.3)$$

by using Eqn. (5.12). Since R is shunted in the transmission line, the amplitude of the voltage traveling wave propagating toward R and the other side of the transmission line must be equal. Alternatively, the voltage, V_R, appearing across the load resistance, R, can be expressed as

$$V_R = V_{sw}^+ T_V + V_{sh}^- T_V = (V_{sw}^+ + V_{sh}^-)\frac{2R}{Z_o + 2R} \; , \qquad (A2.4)$$

where $V_R = V_{pre}$ for $0 < t < t_{ch}$ and $V_R = V_{out}$ for $t \geq t_{ch}$. By using Eqns. (5.9) and (5.10), one can obtain $V_{sw}^+ = I_{sw}^+ Z_o$ and $V_{sh}^- = -I_{sh}^- Z_o$. Substituting them into Eqn. (A2.4) results in

$$V_R = I_L R = (I_{sw}^+ - I_{sh}^-)\frac{2RZ_o}{Z_o + 2R} \; , \qquad (A2.5)$$

and

$$I_L = (I_{sw}^+ - I_{sh}^-)\frac{2Z_o}{Z_o + 2R} = (I_{sw}^+ - I_{sh}^-)T_R \; . \qquad (A2.6)$$

In order to analyze the charging current waveform and the prepulse, the amplitude of the traveling waves must be calculated after every single trip time, l/v, after the switch is closed at $t = 0$. This is shown in the following:
In the period of $0 \leq t < l/v$, the current wave of amplitude V_oY_o is propagating along the transmission line toward the load resistance R. The amplitudes of all the current traveling waves can be expressed as

$$I_{sw}^{+} = V_oY_o \,, \tag{A2.7}$$

$$I_{sw}^{-} = 0 \,, \tag{A2.8}$$

$$I_{sh}^{+} = 0 \,, \tag{A2.9}$$

$$I_{sh}^{-} = 0 \,. \tag{A2.10}$$

The current flowing through the switch is

$$I_{sw} = I_{sw}^{+} + I_{sw}^{-} = V_oY_o \,, \tag{A2.11}$$

and through the short-circuited end is

$$I_{sh} = I_{sh}^{+} + I_{sh}^{-} = 0 \,, \tag{A2.12}$$

while the voltage appearing across the load resistance is

$$V_{pre} = 0 \,. \tag{A2.13}$$

Notice that $I_{sw}^{+} = 0$ and $I_{sh}^{-} = 0$ at the load junction when $t < l/v$.
In the period of $l/v \leq t < 2l/v$,

$$I_{sw}^{+} = V_oY_o \,, \tag{A2.14}$$

$$I_{sw}^{-} = V_oY_o\Gamma_I = V_oY_o\frac{Y}{Y + 2Y_o} \,, \tag{A2.15}$$

$$I_{sh}^{+} = V_oY_oT_I = V_oY_o\frac{2Y_o}{Y + 2Y_o} \,, \tag{A2.16}$$

$$I_{sh}^{-} = 0 \,. \tag{A2.17}$$

The current flowing through the switch is

$$I_{sw} = I_{sw}^{+} + I_{sw}^{-} = V_o Y_o \ , \qquad (A2.18)$$

and through the short-circuited end is

$$I_{sh} = I_{sh}^{+} + I_{sh}^{-} = 0 \ , \qquad (A2.19)$$

while the voltage appearing across the load resistance is

$$V_{pre} = (I_{sw}^{+} - I_{sh}^{-})\frac{T_R}{Y} = V_o Y_o \frac{2}{Y + 2Y_o} \ . \qquad (A2.20)$$

Notice that $I_{sw}^{-} = 0$ at the switch end and $I_{sh}^{+} = 0$ at the short-circuited end when $t < 2l/v$.

In the period of $2l/v \leq t < 3l/v$,

$$I_{sw}^{+} = V_o Y_o (1 + \frac{Y}{Y + 2Y_o}) = V_o Y_o \frac{2Y + 2Y_o}{Y + 2Y_o} \ , \qquad (A2.21)$$

$$I_{sw}^{-} = V_o Y_o \Gamma_I = V_o Y_o \frac{Y}{Y + 2Y_o} \ , \qquad (A2.22)$$

$$I_{sh}^{+} = V_o Y_o T_I = V_o Y_o \frac{2Y_o}{Y + 2Y_o} \ , \qquad (A2.23)$$

$$I_{sh}^{-} = V_o Y_o \frac{2Y_o}{Y + 2Y_o} \ . \qquad (A2.24)$$

The current flowing through the switch is

$$I_{sw} = I_{sw}^{+} + I_{sw}^{-} = V_o Y_o \frac{3Y + 2Y_o}{Y + 2Y_o} \ , \qquad (A2.25)$$

and through the short-circuited end is

$$I_{sh} = I_{sh}^{+} + I_{sh}^{-} = V_o Y_o \frac{4Y_o}{Y + 2Y_o} \ , \qquad (A2.26)$$

while the voltage appearing across the load resistance is

$$V_{pre} = (I_{sw}^{+} - I_{sh}^{-})\frac{T_R}{Y} = V_o Y_o \frac{2}{Y + 2Y_o} \ . \qquad (A2.27)$$

Notice that $I_{sw}^{+} = V_o Y_o$ and $I_{sh}^{-} = 0$ at the load junction when $t < 3l/v$.
In the period of $3l/v \leq t < 4l/v$,

$$I_{sw}^{+} = V_o Y_o (1 + \frac{Y}{Y + 2Y_o}) = V_o Y_o \frac{2Y + 2Y_o}{Y + 2Y_o} , \qquad (A2.28)$$

$$I_{sw}^{-} = V_o Y_o \frac{2Y + 2Y_o}{Y + 2Y_o} \Gamma_I + V_o Y_o \frac{2Y_o}{Y + 2Y_o} T_I = V_o Y_o \frac{2(Y^2 + YY_o + 2Y_o^2)}{(Y + 2Y_o)^2} , \qquad (A2.29)$$

$$I_{sh}^{+} = V_o Y_o \frac{2Y + 2Y_o}{Y + 2Y_o} T_I + V_o Y_o \frac{2Y_o}{Y + 2Y_o} \Gamma_I = V_o Y_o \frac{2(3YY_o + 2Y_o^2)}{(Y + 2Y_o)^2} , \qquad (A2.30)$$

$$I_{sh}^{-} = V_o Y_o \frac{2Y_o}{Y + 2Y_o} . \qquad (A2.31)$$

The current flowing through the switch is

$$I_{sw} = I_{sw}^{+} + I_{sw}^{-} = V_o Y_o \frac{3Y + 2Y_o}{Y + 2Y_o} , \qquad (A2.32)$$

and through the short-circuited end is

$$I_{sh} = I_{sh}^{+} + I_{sh}^{-} = V_o Y_o \frac{4Y_o}{Y + 2Y_o} , \qquad (A2.33)$$

while the voltage appearing across the load resistance is

$$V_{pre} = (I_{sw}^{+} - I_{sh}^{-}) \frac{T_R}{Y} = V_o Y_o \frac{4Y}{(Y + 2Y_o)^2} . \qquad (A2.34)$$

Notice that $I_{sw}^{-} = V_o Y_o Y/(Y + 2Y_o)$ at the switch end and $I_{sh}^{+} = V_o Y_o (2Y_o)/(Y + 2Y_o)$ at the short-circuited end when $t < 4l/v$.
In the period of $4l/v \leq t < 5l/v$,

$$I_{sw}^{+} = V_o Y_o (1 + \frac{2(Y^2 + YY_o + 2Y_o^2)}{(Y + 2Y_o)^2}) = V_o Y_o \frac{3Y^2 + 6YY_o + 8Y_o^2}{(Y + 2Y_o)^2} , \qquad (A2.35)$$

$$I_{sw}^{-} = V_o Y_o \frac{2Y + 2Y_o}{Y + 2Y_o} \Gamma_I + V_o Y_o \frac{2Y_o}{Y + 2Y_o} T_I = V_o Y_o \frac{2(Y^2 + YY_o + 2Y_o^2)}{(Y + 2Y_o)^2} , \qquad (A2.36)$$

$$I_{sh}^{+} = V_o Y_o \frac{2Y + 2Y_o}{Y + 2Y_o} T_I + V_o Y_o \frac{2Y_o}{Y + 2Y_o} \Gamma_I = V_o Y_o \frac{2(3YY_o + 2Y_o^2)}{(Y + 2Y_o)^2} , \qquad (A2.37)$$

$$I_{sh}^{-} = V_o Y_o \frac{2(3YY_o + 2Y_o^2)}{(Y + 2Y_o)^2} . \qquad (A2.38)$$

The current flowing through the switch is

$$I_{sw} = I_{sw}^{+} + I_{sw}^{-} = V_o Y_o \frac{5Y^2 + 8YY_o + 12Y_o^2}{(Y + 2Y_o)^2} , \qquad (A2.39)$$

and through the short-circuited end is

$$I_{sh} = I_{sh}^{+} + I_{sh}^{-} = V_o Y_o \frac{12YY_o + 8Y_o^2}{(Y + 2Y_o)^2} , \qquad (A2.40)$$

while the voltage appearing across the load resistance is

$$V_{pre} = (I_{sw}^{+} - I_{sh}^{-}) \frac{T_R}{Y} = V_o Y_o \frac{4Y}{(Y + 2Y_o)^2} . \qquad (A2.41)$$

Notice that $I_{sw}^{+} = V_o Y_o (2Y + 2Y_o)/(Y + 2Y_o)$ and $I_{sh}^{-} = V_o Y_o (2Y_o)/(Y + 2Y_o)$ at the load junction when $t < 5l/v$.

In the period of $5l/v \leq t < 6l/v$,

$$I_{sw}^{+} = V_o Y_o (1 + \frac{2(Y^2 + YY_o + 2Y_o^2)}{(Y + 2Y_o)^2}) = V_o Y_o \frac{3Y^2 + 6YY_o + 8Y_o^2}{(Y + 2Y_o)^2} , \qquad (A2.42)$$

$$\begin{aligned} I_{sw}^{-} &= V_o Y_o \frac{3Y^2 + 6YY_o + 8Y_o^2}{(Y + 2Y_o)^2} \Gamma_I + V_o Y_o \frac{2(3YY_o + 2Y_o^2)}{(Y + 2Y_o)^2} T_I \\ &= V_o Y_o \frac{3Y^3 + 6Y^2 Y_o + 20YY_o^2 + 8Y_o^3}{(Y + 2Y_o)^3} , \end{aligned} \qquad (A2.43)$$

$$\begin{aligned} I_{sh}^{+} &= V_o Y_o \frac{3Y^2 + 6YY_o + 8Y_o^2}{(Y + 2Y_o)^2} T_I + V_o Y_o \frac{2(3YY_o + 2Y_o^2)}{(Y + 2Y_o)^2} \Gamma_I \\ &= V_o Y_o \frac{12Y^2 Y_o + 16YY_o^2 + 16Y_o^3}{(Y + 2Y_o)^3} , \end{aligned} \qquad (A2.44)$$

$$I_{sh}^{-} = V_o Y_o \frac{2(3YY_o + 2Y_o^2)}{(Y + 2Y_o)^2} . \qquad (A2.45)$$

The current flowing through the switch is

$$I_{sw} = I_{sw}^{+} + I_{sw}^{-} = V_o Y_o \frac{5Y^2 + 8YY_o + 12Y_o^2}{(Y + 2Y_o)^2} , \qquad (A2.46)$$

and through the short-circuited end is

$$I_{sh} = I_{sh}^{+} + I_{sh}^{-} = V_o Y_o \frac{12YY_o + 8Y_o^2}{(Y + 2Y_o)^2} , \qquad (A2.47)$$

while the voltage appearing across the load resistance is

$$V_{pre} = (I_{sw}^{+} - I_{sh}^{-})\frac{T_R}{Y} = V_o Y_o \frac{6Y^2 + 8Y_o^2}{(Y + 2Y_o)^3} . \qquad (A2.48)$$

Notice that $I_{sw}^{-} = V_o Y_o (3Y^2 + 6YY_o + 8Y_o^2)/(Y + 2Y_o)^2$ at the switch end and $I_{sh}^{+} = V_o Y_o (6YY_o + 4Y_o^2)/(Y + 2Y_o)^2$ at the short-circuited end when $t < 6l/v$. In the period of $6l/v \leq t < 7l/v$,

$$I_{sw}^{+} = V_o Y_o (1 + \frac{3Y^3 + 6Y^2 Y_o + 20YY_o^2 + 8Y_o^3}{(Y + 2Y_o)^3})$$

$$= V_o Y_o \frac{4Y^3 + 12Y^2 Y_o + 32YY_o^2 + 16Y_o^3}{(Y + 2Y_o)^3} , \qquad (A2.49)$$

$$I_{sw}^{-} = V_o Y_o \frac{3Y^2 + 6YY_o + 8Y_o^2}{(Y + 2Y_o)^2}\Gamma_I + V_o Y_o \frac{2(3YY_o + 2Y_o^2)}{(Y + 2Y_o)^2} T_I$$

$$= V_o Y_o \frac{3Y^3 + 6Y^2 Y_o + 20YY_o^2 + 8Y_o^3}{(Y + 2Y_o)^3} , \qquad (A2.50)$$

$$I_{sh}^{+} = V_o Y_o \frac{3Y^2 + 6YY_o + 8Y_o^2}{(Y + 2Y_o)^2} T_I + V_o Y_o \frac{2(3YY_o + 2Y_o^2)}{(Y + 2Y_o)^2}\Gamma_I$$

$$= V_o Y_o \frac{12Y^2 Y_o + 16YY_o^2 + 16Y_o^3}{(Y + 2Y_o)^3} , \qquad (A2.51)$$

$$I_{sh}^{-} = V_o Y_o \frac{12Y^2 Y_o + 16YY_o^2 + 16Y_o^3}{(Y + 2Y_o)^3} . \qquad (A2.52)$$

The current flowing through the switch is

$$I_{sw} = I_{sw}^{+} + I_{sw}^{-} = V_o Y_o \frac{7Y^3 + 18Y^2 Y_o + 52YY_o^2 + 24Y_o^3}{(Y + 2Y_o)^3} , \qquad (A2.53)$$

and through the short-circuited end is

$$I_{sh} = I_{sh}^{+} + I_{sh}^{-} = V_o Y_o \frac{24Y^2 Y_o + 32YY_o^2 + 32Y_o^3}{(Y + 2Y_o)^3} , \qquad (A2.54)$$

while the voltage appearing across the load resistance is

$$V_{pre} = (I_{sw}^{+} - I_{sh}^{-})\frac{T_R}{Y} = V_o Y_o \frac{6Y^2 + 8Y_o^2}{(Y + 2Y_o)^3} . \qquad (A2.55)$$

Notice that $I_{sw}^{+} = V_o Y_o (3Y^2 + 6YY_o + 8Y_o^2)/(Y + 2Y_o)^2$ and $I_{sh}^{-} = V_o Y_o (6YY_o + 4Y_o^2)/(Y + 2Y_o)^2$ at the load junction when $t < 7l/v$.

In the period of $7l/v \leq t < 8l/v$,

$$I_{sw}^{+} = V_o Y_o (1 + \frac{3Y^3 + 6Y^2 Y_o + 20YY_o^2 + 8Y_o^3}{(Y + 2Y_o)^3})$$

$$= V_o Y_o \frac{4Y^3 + 12Y^2 Y_o + 32YY_o^2 + 16Y_o^3}{(Y + 2Y_o)^3}, \qquad (A2.56)$$

$$I_{sw}^{-} = V_o Y_o \frac{4Y^3 + 12Y^2 Y_o + 32YY_o^2 + 16Y_o^3}{(Y + 2Y_o)^3} \Gamma_I$$

$$+ V_o Y_o \frac{12Y^2 Y_o + 16YY_o^2 + 16Y_o^3}{(Y + 2Y_o)^3} T_I$$

$$= V_o Y_o \frac{4Y^4 + +12Y^3 Y_o + 56Y^2 Y_o^2 + 48YY_o^3 + 32Y_o^4}{(Y + 2Y_o)^4}, \qquad (A2.57)$$

$$I_{sh}^{+} = V_o Y_o \frac{4Y^3 + 12Y^2 Y_o + 32YY_o^2 + 16Y_o^3}{(Y + 2Y_o)^3} T_I$$

$$+ V_o Y_o \frac{12Y^2 Y_o + 16YY_o^2 + 16Y_o^3}{(Y + 2Y_o)^3} \Gamma_I$$

$$= V_o Y_o \frac{20Y^3 Y_o + 40Y^2 Y_o^2 + 80YY_o^3 + 32Y_o^4}{(Y + 2Y_o)^4}, \qquad (A2.58)$$

$$I_{sh}^{-} = V_o Y_o \frac{12Y^2 Y_o + 16YY_o^2 + 16Y_o^3}{(Y + 2Y_o)^3}. \qquad (A2.59)$$

The current flowing through the switch is

$$I_{sw} = I_{sw}^{+} + I_{sw}^{-} = V_o Y_o \frac{7Y^3 + 18Y^2 Y_o + 52YY_o^2 + 24Y_o^3}{(Y + 2Y_o)^3}, \qquad (A2.60)$$

and through the short-circuited end is

$$I_{sh} = I_{sh}^{+} + I_{sh}^{-} = V_o Y_o \frac{24Y^2 Y_o + 32YY_o^2 + 32Y_o^3}{(Y + 2Y_o)^3}, \qquad (A2.61)$$

while the voltage appearing across the load resistance is

$$V_{pre} = (I_{sw}^{+} - I_{sh}^{-}) \frac{T_R}{Y} = V_o Y_o \frac{8Y^3 + 32YY_o^2}{(Y + 2Y_o)^3}. \qquad (A2.62)$$

Notice that $I_{sw}^{-} = V_o Y_o (3Y^3 + 6Y^2 Y_o + 20YY_o^2 + 8Y_o^3)/(Y + 2Y_o)^3$ at the switch end and $I_{sh}^{+} = V_o Y_o (12Y^2 Y_o + 16YY_o^2 + 16Y_o^3)/(Y + 2Y_o)^3$ at the short-circuited end when $t < 8l/v$.

According to this process, the current flowing through the switch, I_{sw}, and the short-circuited end, I_{sh}, and the prepulse, V_{pre}, at the nth round trip time ($t = 2nl/v$) can be determined. By carefully examining the above derivation, the general equations can be expressed as:

$$I_{sw} = nV_oY_o + \frac{V_o}{4}(Y - 2Y_o)\left[1 - \left(\frac{Y - 2Y_o}{Y + 2Y_o}\right)^{n-1}\right]$$

$$= \frac{nV_o}{Z_o} + \frac{V_o}{4}\left(\frac{Z_o - 2R}{RZ_o}\right)\left[1 - \left(\frac{Z_o - 2R}{Z_o + 2R}\right)^{n-1}\right], \qquad (A2.63)$$

$$I_{sh} = (n-1)V_oY_o - \frac{V_o}{4}(Y - 2Y_o)\left[1 - \left(\frac{Y - 2Y_o}{Y + 2Y_o}\right)^{n-1}\right]$$

$$= \frac{(n-1)V_o}{Z_o} - \frac{V_o}{4}\left(\frac{Z_o - 2R}{RZ_o}\right)\left[1 - \left(\frac{Z_o - 2R}{Z_o + 2R}\right)^{n-1}\right], \qquad (A2.64)$$

and

$$V_{pre} = \frac{V_o}{2}\left[1 - \left(\frac{Y - 2Y_o}{Y + Y_o}\right)^{n}\right] = \frac{V_o}{2}\left[1 - \left(\frac{Z_o - 2R}{Z_o + 2R}\right)^{n}\right]. \qquad (A2.65)$$

These final results are also shown in Sec. 5.3. They correspond to Eqns. (5.43), (5.44), and (5.45) respectively.

REFERENCES

[1] G. N. Glasoe and J. V. Lebacqz, "Pulse Generators", Boston Technical Publishers, 1964.

[2] L. L. Alston, ed., "High Voltage Technology, Oxford University Press, Oxford (1968).

[3] J. A. Nation, "High-power electron and ion beam generation", Part. Accel., 10, pp. 1-30, 1979.

[4] S Jayaraman and C. H. Lee, "Observation of two-photon conductivity in GaAs with nanosecond and picosecond light pulse", Appl. Phys. Lett., Vol. 20, pp. 392-395, 1972.

[5] E. A. Chauchard, M. J. Rhee, and Chi H. Lee, "Optically activated semiconductors as repetitive opening switches", Appl. Phys. Lett. 47, (12), pp. 1293-1295, 1985.

[6] Chi H. Lee, ed., "Picosecond Optoelectronic Devices", Academic Press, (1984).

[7] B. H. Kolner and D. M. Bloom, "Electrooptic Sampling in GaAs Integrated Circuits", IEEE J. of Quantum Electronics, Vol. QE-22, No. 1, pp. 79-93, 1986.

[8] A. P. DeFonzo and C. R. Lutz, "Optoelectronic transmission and reception of ultrashort electrical pulses", Appl. Phys. Lett., Vol. 51, pp. 212-214, January 1987.

[9] Chi H. Lee, "Picosecond Optics and Microwave Technology", IEEE Trans. on Microwave Theory Tech., MTT-38, pp. 596-607, May 1990.

[10] Chi H. Lee, "Optical Control of Semiconductor Closing and Opening Switches", IEEE Trans. on Electron Devices, Vol. 37, No. 12, pp. 2426-2438, December 1990.

[11] F. J. Zutavern, G. M. Loubriel, M. W. O'Malley, L. P. Shanwald, W. D. Helgeson, D. L. McLaughlin, and B. B. McKenzie, "Photoconductive

Semiconductor Switch Experiments for Pulsed Power Applications", IEEE Trans. on Electron Devices, Vol. 37, No. 12, pp. 2472-2477, Dec. 1990.

[12] D. H. Auston, "Picosecond optoelectronic switching and gate in silicon", Appl. Phys. Lett. 26, pp. 101-103, 1975.

[13] O. S. F. Zucker, J. R. Long, V. L. Smith, D. J. Page, and P. L. Hower, "Experimental demonstration of high-power fast-rise-time switching in silicon junction semiconductors", Appl. Phys. Lett., Vol. 29, No. 4, pp. 261-263, August 1976.

[14] J. M. Proud, Jr. and S. L. Norman, "High frequency waveform generation using optoelectronic switching in silicon", IEEE Trans. on Microwave Theory Tech., Vol. MTT-26, pp. 137-140, 1978.

[15] C. H. Lee, "Picosecond optoelectronic switching in GaAs", Appl. Phys. Lett., Vol. 30, No. 2, pp. 84-86, Jan. 1977.

[16] C. S. Chang, Ph.D. dissertation, University of Maryland, College Park, 1986.

[17] F. E. Peterkin, T. Ridolfi, L. L. Buresh, B. J. Hankla, D. K. Scott, P. F. Williams, W. C. Nunnally, and B. L. Thomas, "Surface Flashover of Silicon", IEEE Trans. on Electron Devices, Vol. 37, No. 12, pp. 2459-2465, December 1990.

[18] S. H. Nam and T. S. Sudarshan, "New Findings of Pulsed Surface Breakdown Along Silicon in Vacuum", IEEE Trans. on Electron Devices, Vol. 37, No. 12, pp. 2466-2471, December 1990.

[19] G. Mourou, W. H. Knox, and S. Williamson, "High-power picosecond switching in bulk semiconductors", in Picosecond Optoelectronic Devices, C. H. Lee, New York, NY, Academic Press, 1984, Ch. 7.

[20] C. H. Lee and V. K. Mathur, "Picosecond photoconductivity and its applications", IEEE J. Quantum Electron, Vol. QE-17, No. 10, pp. 2098-2112, Oct. 1981.

[21] W. C. Nunnally and R. B. Hammond, "80-MW photoconductor power

switch", Appl. Phys. Lett. 44, (10), pp. 980-982, 1984.

[22] A. Rosen, P. J. Stabile, D. W. Bechtle, W. Janton, A. M. Gombar, J. McShea, A. Rosenberg, P. R. Herczfeld, and A. Bahasadri, "Optically achieved p-i-n diode switch utilizing a two-dimensional laser array at 808 nm as an optical source", IEEE Trans. on Electron Devices, Vol. 36, pp. 367-374, Feb. 1989.

[23] P. T. Ho, C. H. Lee, J. C. Stephenson, and R. R. Cavanagh, "A Diamond Opto-Electronic Switch", Opt. Commun., Vol. 46, Nos. 3, 4, pp. 202-204, July 1983.

[24] P. T. Ho, C. S. Chang, M. J. Rhee, Chi H. Lee, J. C. Stephenson, and R. R. Cavanagh, "Diamond Switches and Blumlein Pulse Generators for Kilovolt Optoelectronics", SPIE Proc. on Picosecond Optoelectronics, edited by Mourou, Vol. 439, pp. 95-100, Aug. 1983.

[25] S. Feng, P. T. Ho, and J. Goldhar, "Photoconductive Switching in Diamond under High Bias Field", IEEE Trans. on Electron Devices, Vol. 37, No. 12, pp. 2511-2516, Dec. 1990.

[26] P. T. Ho, F. Peng, and J. Goldhar, "Photoconductive Switching using Polycrystalline ZnSe", IEEE Trans. on Electron Devices, Vol. 37, No. 12, pp. 2517-2519, Dec. 1990.

[27] P. S. Cho, P. T. Ho, J. Goldhar, and Chi H. Lee, "ZnSe photoconductive switches with transparent electrodes", Digest of Technical Papers, 8th IEEE Pulsed Power Conference (IEEE, New York), paper P7-6, June 17-19, 1991, San Diego, California.

[28] K. H. Schoenbach, M. Kristiansen, and G. Schaefer, "A review of opening switch technology for inductive energy storage", Proc. of IEEE, Vol. 72, pp. 1019-1039, 1984.

[29] R. L. Druce, M. D. Pocha, K. L. Griffin, and W. W. Hofer, "Subnanosecond linear GaAs photoconductive switching", in Proc. 7th IEEE Pulsed Power Conf., pp. 882-886, (Monterey, California, 1989).

[30] M. B. Ketchen, D. Grischkowsky, T. C. Chen, C. C. Chi, I. N. Duling, N. H. Halas, J. M. Halbout, J. A. Kash, and G. P. Li, "Generation of subpicosecond electrical pulses on coplanar transmission lines", Appl. Phys. Lett., Vol. 48, pp. 751-753. 1986.

[31] M. J. Rhee, T. A. Fine, and C. C. Kung, "Basic circuit for inductive-energy pulsed power systems", pp. 4333-4337, J. Appl. Phys., Vol. 67, (9), May, 1990.

[32] E. A. Chauchard, C. C. Kung, M. J. Rhee, C. H. Lee, "Repetitive semiconductor opening switch and application to short pulse generation", Laser and Particle Beams (1989), Vol. 7, Part 3, pp. 615-626.

[33] E. A. Chauchard, C. C. Kung, C. H. Lee, M. J. Rhee, V. Diadiuk, "A New Method to Generate Square Pulses: Optoelectronic Switching in a Current Charged Transmission Line", IEEE Transactions on Plasma Science, Vol. PS-15, No. 1, pp. 70-72, Feb. 1987.

[34] E. A. Chauchard, C. C. Kung, M. J. Rhee, and Chi H. Lee, "Observation of Current Build-Up with a Semiconductor Switch and a Transmission Line", Digest of Technical Papers of the 7th IEEE Pulsed Power Conference (IEEE, New York, 1989), pp. 128-130.

[35] C. C. Kung, E. A. Chauchard, Chi H. Lee, M. J. Rhee, and L. Yan, "Observation of Power Gain in an Inductive Energy Pulsed Power System with an Optically Controlled Semiconductor Opening Switch", Appl. Phys. Lett., Vol. 57, No. 22, pp. 2330-2332, Nov. 1990.

[36] C. C. Kung, E. A. Chauchard, M. J. Rhee, and Chi H. Lee, "Square Pulse Generation with a Photoconductive Semiconductor Opening Switch in the Dual of the Blumlein Line", Digest of Technical Papers of the 8th IEEE Pulsed Power Conference (IEEE, New York, 1991), paper 3-43, June 17-19, 1991, San Diego, California.

[37] C. C. Kung, E. A. Chauchard, M. J. Rhee, L. Yan, and Chi H. Lee, "Peak Power Gain and Pulse Compression in an Inductive Energy Storage System

by a Photoconductive Closing and Opening Switch", Workshop Proceedings of the 2nd Workshop on Optically and Electron-Beam Controlled Semiconductor Switches, August 1990, Norfolk, Va.

[38] C. C. Kung, E. E. Funk, E. A. Chauchard, M. J. Rhee, Chi H. Lee, L. Yan, "Observation of Power Gain in an Inductive Pulsed Power System with an Optically Activated Semiconductor Closing and Opening Switch", Proceedings of the SPIE Conference on Optically Activated Switching, Vol. 1378, pp. 250-258, Nov., 1990.

[39] C. C. Kung, Eve A. Chauchard, M. J. Rhee, Chi H. Lee, and Li Yan, "Voltage Multiplication with an Optically Activated Semiconductor Opening Switch", Conference on Lasers and Electro-Optics, 1990 Technical Digest Series, Vol. 7, pp. 80-82, Optical Society of America, Washington DC, 1990.

[40] C. C. Kung, E. A. Chauchard, M. J. Rhee, and Chi H. Lee, "Generation of square pulses by a dual of the Blumlein line with a photoconductive semiconductor opening switch", Conference on Lasers and Electro-Optics, 1991 Technical Digest Series, Vol. 10, pp. 126-128, Optical Society of America, Washington DC, 1991.

[41] M. D. Pocha and R. L. Druce, "35 kV GaAs Subnanosecond Photoconductive Switches", IEEE Trans. on Electron Devices, Vol. 37, No. 12, pp. 2486-2492, Dec. 1990.

[42] D. C. Stoudt, K. H. Schoenbach, R. P. Brinkmann, V. K. Lakdawala, and R. A. Roush, "The Recovery Behavior of Semi-Insulating GaAs in Electron-Beam-Controlled Switches", IEEE Trans. on Electron Devices, Vol. 37,

[43] W. J. Sargeant, "Energy Storage Capacitors" (Air Force Pulsed Power Lecture Series, Texas Tech University, Lubbock, TX), Lecture No. 10, 1981 (Coord. M. Kristiansen and A. H. Guenther).

[44] M. Kristiansen, "Fundamentals of inductive energy storage", in Proc. Army Research Office Workshop on Repetitive Opening Switches (Tamarron, CO,

1981), DTIC AD-A110770, p. 313.

[45] See e.g., W. H. Hayt, Jr., and J. E. Kemmery, "Engineering Circuit Analysis", 3rd ed. (McGraw-Hill, New York, 1978), p. 158.

[46] E. M. Honig, in "Opening Switches", edited by A. Guenther, M. Kristiansen, and T. Martin (Plenum, New York, 1987), pp. 1-48.

[47] M. J. Rhee and R. F. Schneider, "Compact pulsed accelerator", IEEE Trans. Nucl. Sci. Vol. NS-30, pp. 3192-3194, 1983.

[48] B. A. Larionov and N. A. Mikhaylov, "High speed breaker of repeated action with electrodynamic drive", in Proc. 2nd All-Union Conf. on Engineering Problems of Thermonuclear Reactors (Leningrad, USSR, June 23-25, 1981), Vol. III, pp. 96-102.

[49] D. R. Dettman, R. Dollinger and J. Sarjeant, "Pulsed power characterizations of metal plasma arc switches (MPAS)", in Proc, 4th IEEE pulsed Power Conf. (Albuquerque, NM, June, 1983), pp. 762-763 (IEEE Catalog 83 CH1908-3).

[50] Yu. A. Kotov, N. G. Kolganov and B. M. Koval'chuk, "A fast contact breaker based on electrically exploded wires", translated from Pribory i Tekhnika Eksperimenta, no. 6, p.107, 1974.

[51] D. G. Rickel, I. R. Lindemuth, R. E. Reinovsky, J. H. Brownell, J. H. Goforth, A. E. Greene, H. W. Kruse, H. Oona, J. V. Parker, and P. J. Turchi, "Procyon Experiments Utilizing Foil-Fuse Opening Switches", Digest of Technical Papers, 8th IEEE Pulsed Power Conference (IEEE, New York), paper P1-11, June 17-19, 1991, San Diego, California.

[52] R. D. Ford and I. M. Vitkovitsky, "Explosively actuated 100 KA opening switch for high voltage applications", NRL Memo. Rep. 3561, July 1977.

[53] N. C. Anderson, E. Thornton, G. O'Grade, H. Rellon, "An Explosive High Voltage Closing and Opening Switch", Digest of Technical Papers, 8th IEEE Pulsed Power Conference (IEEE, New York), paper P1-31, June 17-19, 1991, San Diego, California.

[54] M. N. Bystrov, L. V. Dubovoy, Ye. A. Larianov, I. A. Monoszon, I. M. Royfe, A. M. Stolov, Ye, V, Seredenko, V. P. Silin, B. A. Stekol'nikov and L. A. Sairochin, "Thermal non-linear resistances in energy output systems for inductive storage devices", No. 5 in the series: Inductive Energy Storage Devices and Switching Apparatus for Thermonuclear Installation (Report of a joint USSR-USA Seminar, USSR Atomic Energy State Committee, Leningrad, NIIEFA, 1974; translated by W. J. Grimes, P. O. Box 55 Hingham, MA 02043, May 1975).

[55] A. Garscadden, "Arcs vs diffuse discharges", in Proc. Army Research Office Workshop on Diffuse Discharge Opening Switches (Tamarron, CO, 1982), DTIC AD-A115883, p.91.

[56] R. J. Commisso, R. F. Fernsler, V. E. Scherrer, and I. M. Vitkovitsky, "Inductively generated, high voltage pulse using an electron beam controlled opening switch", Appl. Phys. Lett. 47 (10), pp. 1056-1058, November, 1985.

[57] R. Stringfield, P. Sincerny, S. Wong, G. James, T. Peters and C. Gilman, "Continuing studies of plasma erosion switches for power conditioning on multiterrawatt pulsed power accelerators", IEEE Trans. Plasma Sci., Vol. PS-11, p.200, 1983.

[58] Juan M. Elizondo, "Plasma Cathode for High Current Density Plasma Erosion Opening and Closing Switches", Digest of Technical Papers, 8th IEEE Pulsed Power Conference (IEEE, New York), paper 10-6, June 17-19, 1991, San Diego, California.

[59] B. Ecker, J. Creedon, L. Demeter, S. Glidden and G. Proulx, "The reflex switch: A high-current, fast-opening vacuum switch", in Proc. 4th IEEE Pulsed Power Conf. (Albuquerque, NM, June 1983), pp. 354-360 (IEEE Catalog 83CH1908-3).

[60] R. J. Adler, L. L. Torrison, D. L. Johnson, J. M. Wilson, and S. Humphries, Jr., "Pulse Power Switching with Large Vacuum Triodes", Digest of Tech-

nical Papers, 8th IEEE Pulsed Power Conference (IEEE, New York), paper 16-1, June 17-19, 1991, San Diego, California.

[61] G. Mourou and W. Knox, "High Power Switching with Picosecond Precision", Appl. Phys. Lett. 35, pp. 492-495, 1979.

[62] K. H. Schoenbach, V. K. Lakdawala, R. Genuer, and S. T. Ko, "An optically controlled closing and opening semiconductor switch", J. Appl. Phys. Vol. 63, No. 7, pp. 2460-2463, April (1988).

[63] E. A. Chauchard, M. J. Rhee, and Chi H. Lee, "Repetitive opening switches using optically activated semiconductors", 1985 Annual Meeting of the O.S.A., Oct. 14-18, Washington D.C. No. 12, pp. 2478-2485, Dec. 1990.

[64] C. Kittel, "Introduction to Solid State Physics", 6th ed., John Wiley & Sons, Inc., New York, N.Y.

[65] N. W. Ashcroft and N. D. Mermin, "Solid State Physics", New York: Holt, Rinehart, & Winston, 1976.

[66] E. Merzbacher, "Quantum Mechanics", 2nd Ed., John Wiley & Sons, Inc., New York, N.Y.

[67] S. M. Sze, "Physics of Semiconductor Devices", 2nd ed., John Wiley & Sons, Inc., New York, N.Y.

[68] A. Yariv, "Optical Electronics", 3rd Ed., HRW, 1985.

[69] Ghandhi, "Semiconductor Power Devices", John Wiley & Sons, Inc., New York, N.Y., 1977.

[70] Masumi Takeshima, "Effect of Auger recombination on laser operation in $Ga_{1-x}Al_xAs$", J. Appl. Phys., Vol. 58, No. 10, 1985, pp. 3846-3850.

[71] A. S. Grove, "Physics and Technology of Semiconductor Devices", John Wiley & Sons, Inc., New York, N.Y., 1967.

[72] H. Melchior, "Demodulation and Photodetection Techniques", in F. T. Arecchi and E. O. Schulz-Dubois, Eds., Laser Handbook, Vol. 1, North-Holland, Amsterdam, 1972, pp. 725-835.

[73] V. K. Mathur, C. S. Chang, and C. H. Lee, "Measurement of Contact Resis-

tance of an Ohmic Contact Applied to a High Resistivity Photoconductor", Rev. Sci. Instrum., Vol. 2, No. 4, pp. 616-618, 1981.

[74] A. Kim, M. Wade, M. Weiner, R. Youmans, and R. Zeto, "Bulk GaAs Photonic Devices with Two Opposite Gridded Electrodes", Digest of Technical Papers of the 7th IEEE Pulsed Power Conference (IEEE, New York, 1989), pp. 430-432.

[75] L. E. Kingsley and W. R. Donaldson, "Electrooptic Imaging of Surface Electric Fields in High-Power Photoconductive Switches" IEEE Trans. on Electron Devices, Vol. 37, No. 12, pp. 2449-2458, Dec. 1990.

[76] P. S. Cho, M. S. Thesis, University of Maryland, College Park, 1991.

[77] J. Steinbeck, G. Braunstein, M. S. Dresselhaus, T. Venkutesan, and D. C. Jacobson, "A model for pulsed laser melting of graphite", J. Appl. Phys., Vol. 58, p. 4374, 1985.

[78] A. M. Malvezzi, N. Bloembergen, and C. Y. Huang, "Time-Resolved Picosecond Optical Measurements of Laser-Excited Graphite", Phys. Rev. Lett., Vol. 57, pp. 146-149, July 1986.

[79] E. A. Chauchard, Chi H. Lee, and C. Y. Huang, "Graphite Picosecond Optoelectronic Opening Switch", Appl. Phys. Lett., Vol. 50, pp. 812-814, 1987.

[80] E. A. Chauchard, C. C. Kung, Chi H. Lee, C. Y. Huang, "Laser-Induced Conductivity Drop in Graphite", Conference on Lasers and Electro-Optics, 1987 Technical Digest Series, Vol. 14, pp. 288-290, Optical Society of America, Washington DC, 1987.

[81] E. A. Chauchard, C. C. Kung, and Chi H. Lee, "Demonstration of a Graphite Laser Activated Opening Switch", Digest of Technical Papers of the 6th IEEE Pulsed Power Conference (IEEE, New York, 1987), pp. 365-366.

[82] M. K. Wu, J. R. Ashburn, C. J. Torng, P. H. Hor, R. L. Meng, L. Gao, Z. J. Huang, Y. Q. Wang, and C. W. Chu, "Superconductivity at 93 K in

a New Mixed Phase Y-Ba-Cu-O Compound System at Ambient Pressure", Phys. Rev. Lett., Vol. 58, p. 908, 1987.

[83] D. R. Humphreys, T. L. Francavilla, D. U. Gubser, and S. A. Wolf, "Progress toward a Superconducting Opening Switch", Digest of Technical Papers, 6th IEEE Pulsed Power Conference (IEEE, New York), paper 14-3, Arlington, Va., June 29-July 1, 1987.

[84] S. K. Dhali and Mohammed Mohsin, "Thin-Film Superconducting Switch", Digest of Technical Papers, 8th IEEE Pulsed Power Conference (IEEE, New York), paper P1-35, June 17-19, 1991, San Diego, California.

[85] F. J. Zutavern and M. W. O'Malley, "Engineering Limits of Photoconductive Semiconductor Switches in Pulsed Power Applications", IEEE Conf. Record of the 17th Power Modulator Symp., pp. 214-218, 1986.

[86] F. J. Zutavern, B. B. McKenzie, G. M. Loubriel, M. W. O'Malley, R. A. Hamil, and L. P. Shanwald, "Multiple Pulse Photoconductive Semiconductor Switching", IEEE Conf. Record of the 18th Power Modulator Symp., pp. 307-311, 1988.

[87] M. S. Mazzola, K. H. Schoenbach, V. K. Lakdawala, and R. A. Roush, "Infrared Quenching of Conductivity at High Electric Fields in a Bulk, Copper-Compensated, Optically Activated GaAs Switch", IEEE Trans. on Electron Devices, Vol. 37, No. 12, pp. 2499-2505, Dec. 1990.

[88] V. K. Lakdawala, G. R. Barevadia, S Panigrahi, L. Thomas, R. P. Brinkmann, and K. H. Schoenbach, "Deep Level Parameter Studies and their Significance for Optically Controlled Solid State Switches", Digest of Technical Papers, 8th IEEE Pulsed Power Conference (IEEE, New York), paper P3-42, June 17-19, 1991, San Diego, California.

[89] M. E. Van Valkenburg, "Network analysis", 3rd ed., Prentice-Hall, Chapter 6, (1974).

[90] S. Ramo, J. R. Whinnery, T. Van Duzer, "Fields and Waves in communication electronics", John Wiley & Sons, Chapter 1. (1965).

[91] E. A. Chauchard, C. C. Kung, Chi H. Lee, and M. J. Rhee, "Performance of Laser Activated Semiconductor Opening Switches", Conference Record-Abstracts, 1989 IEEE International Conference on Plasma Science, pp. 125-126, Buffalo, New York, May 22-24, 1989.

[92] L. Yan, Ph.D. dissertation, University of Maryland, College Park, 1989.

[93] J. H. Hur, F. Hadizad, S. G. Hummel, J. S. Osinski, P. D. Dapkus, H. R. Fetterman, and M. A. Gundersen, "III-V compound based heterostructure opto-thyristor (HOT) for pulsed power applications", Digest of Technical Papers, 8th IEEE Pulsed Power Conference (IEEE, New York), paper 7-5, June 17-19, 1991, San Diego, California.

[94] M. K. Kennedy, R. P. Brinkmann, K. H. Schoenbach, and V. K. Lakdawala, "Switching Properties of Electron-Beam Controlled GaAs pin-Diodes", Digest of Technical Papers, 8th IEEE Pulsed Power Conference (IEEE, New York), paper 4-2, June 17-19, 1991, San Diego, California.

[95] V. B. Carboni, I. D. Smith, R. M. Pixton, M. D. Abdalla, F. J. Zutavern, G. M. Loubriel, and M. W. O'Malley, "Tests on Photoconductive Semiconductor Switches for Subnanosecond Rise Time, Multimegavolt Pulser Applications", 8th IEEE Pulsed Power Conference (IEEE, New York), paper 4-4, June 17-19, 1991, San Diego, California.

[96] F. J. Zutavern, G. M. Loubriel, M. W. O'Malley, W. D. Helgeson, and D. L. McLaughlin, "High-Gain Photoconductive Semiconductor Switching", 8th IEEE Pulsed Power Conference (IEEE, New York), paper 1-1, June 17-19, 1991, San Diego, California.

[97] R. A. Falk and J. C. Adams, "Optical Probe Techniques for Avalanching Photoconductors", 8th IEEE Pulsed Power Conference (IEEE, New York), paper 1-2, June 17-19, 1991, San Diego, California.

[98] G. M. Loubriel, F. J. Zutavern, W. D. Helgeson, D. L. McLaughlin, and M. W. O'Malley, "Physics and Applications of the Lock-on Effect", 8th IEEE Pulsed Power Conference (IEEE, New York) paper 1-3, June 17-19, 1991,

San Diego, California.

[99] M. S. Mazzola, D. C. Stoudt, R. A. Roush, and S. F. Griffiths, "Evaluation of Deep Level Effects on the Opening Performance of a Laser-Controlled, Copper-Doped GaAs Switch Operating in the Lock-On Mode", 8th IEEE Pulsed Power Conference (IEEE, New York), paper 1-4, June 17-19, 1991, San Diego, California.

[100] D. C. Stoudt, M. S. Mazzola, R. A. Roush, and S. F. Griffiths, "Investigation of a Laser-Controlled, Copper-Doped GaAs Closing and Opening Switch for Pulsed Power Applications", 8th IEEE Pulsed Power Conference (IEEE, New York), paper 1-5, June 17-19, 1991, San Diego, California.

[101] W. Donaldson and L. Kingsley, "Electric-Field Profiles in GaAs Photoconductive Switches", 8th IEEE Pulsed Power Conference (IEEE, New York), paper 1-6, June 17-19, 1991, San Diego, California.

[102] B. Ye and Z. Ma, "Long-pulsewidth pulsed Nd:YAG laser", Appl. Optics, Vol. 27, No. 21, pp. 4371-4373, Nov. 1988.

[103] R. L. Maynard, R. P. Johnson, F. J. Masters, N. K. Moncur, L. D. Siebert, and J. D. Stanely, "Long pulse operation of a Nd:glass laser", in Dig. of CLEO, paper TUJ28, Baltimore, Md., 1989.

CURRICULUM VITAE

Name: Chun Chieh Kung

Permanent address: No.198 Section 1 Ho-Ping East Road, 4F, Taipei City, Taiwan, Republic of China

Degree and date to conferred: Doctor of Philosophy, 1992

Date of birth: November 16, 1958

Place of birth: Taipei City, Taiwan, Republic of China

Secondary education: Cheng-Kung High School, Taipei, Taiwan, June 1977

Collegiate institutions attended:

INSTITUTION	DATES	DEGREE	RECEIVED
National Cheng Kung University Tainan, Taiwan, R.O.C.	9/77-6/81	B.S.	June 1981
University of Maryland College Park, Maryland	1/85-8/86	M.S.	August 1986
University of Maryland College Prak, Maryland	9/86-8/92	Ph.D.	August 1992

Major: Electrophysics in Electrical Engineering

Minors: Microelectronics and Computer in Electrical Engineering

Professional publications:

I. Journal Papers:

1. E. A. Chauchard, C. C. Kung, C. H. Lee, M. J. Rhee, V. Diadiuk, "A New Method to Generate Square Pulses: Optoelectronic Switching in a Current Charged Transmission Line", IEEE Transactions on Plasma Science, Vol. PS-15, No. 1, pp. 70-72, Feb. 1987.
2. E. A. Chauchard, C. C. Kung, M. J. Rhee, C. H. Lee, "Repetitive semiconductor opening switch and application to short pulse generation", Laser and Particle Beams (1989), vol. 7, part 3, pp. 615-626.
3. M. J. Rhee, T. A. Fine, and C. C. Kung, "Basic circuits for inductive-energy pulsed power systems", pp. 4333-4337, J. Appl. Phys. Vol. 67(9), May, 1990.
4. C. C. Kung, E. A. Chauchard, Chi H. Lee, M. J. Rhee, and L. Yan, "Observation of Power Gain in an Inductive Energy Pulsed Power System with an

Optically Controlled Semiconductor Opening Switch", Appl. Phys. Lett. 57 (22), pp. 2330-2332, Nov. 1990.

5. C. C. Kung, E. A. Chauchard, Chi H. Lee, and M. J. Rhee, "Kilovolt Square Pulse Generation by a Dual of the Blumlein Line with a Photoconductive Semiconductor Opening Switch", IEEE Photonics Technology Letters, Vol. 4, No. 6, pp. 621-623, June 1992.

II. Conference Papers:

1. M. J. Rhee, E. A. Chauchard, C. C. Kung, and Chi H. Lee, "Fast Square Pulse Generation by an Optoelectronic Opening Switch and a Current Charged Transmission Line", Conference Record-Abstracts, 1986 IEEE International Conference on Plasma Science, pp. 24, Saskatoon, Sask, Canada, May 19-21, 1986.
2. E. A. Chauchard, C. C. Kung, M. J. Rhee, Chi H. Lee, "Repetitive Optoelectronic Opening Switches for Current Charged Transmission Lines", Conference on Lasers and Electro-Optics, June 9-13, 1986, San Francisco, California, 1986 Technical Digest, pp. 328-329, Optical Society of America, Washington DC, 1986.
3. E. A. Chauchard, C. C. Kung, and Chi H. Lee, C. Y. Huang, "Pulsed Laser Irradiation of Highly Oriented Pyrolytic Graphite", Bulletin of The American Physical Society, New York, N.Y., Vol. 32, No. 3, March 1987, GS7, pp. 608.
4. E. A. Chauchard, C. C. Kung, Chi H. Lee, and M. J. Rhee, C. Y. Huang, "Two New Laser Activated Opening Switches", 1987 International Conference on Lasers, Nov. 15-19, 1987, Xiamen (Amoy), Development & Exchange Center for Science & Technology, Xiamen, P. R. China.
5. E. A. Chauchard, C. C. Kung, Chi H. Lee, C. Y. Huang, "Laser-Induced Conductivity Drop in Graphite", Conference on Lasers and Electro-Optics, 1987 Technical Digest Series, Vol. 14, pp. 288-290, Optical Society of America, Washington DC, 1987.
6. E. A. Chauchard, C. C. Kung, and Chi H. Lee, "Demonstration of a Graphite Laser Activated Opening Switch", Digest of Technical Papers of the 6th IEEE Pulsed Power Conference (IEEE, New York, 1987), pp. 365-366.
7. E. A. Chauchard, C. C. Kung, Chi H. Lee, and M. J. Rhee, "Performance of Laser Activated Semiconductor Opening Switches", Conference Record-Abstracts, 1989 IEEE International Conference on Plasma Science, pp. 125-

126, Buffalo, New York, May 22-24, 1989.

8. E. A. Chauchard, C. C. Kung, M. J. Rhee, and Chi H. Lee, "Observation of Current Build-Up with a Semiconductor Switch and a Transmission Line", Digest of Technical Papers of the 7th IEEE Pulsed Power Conference (IEEE, New York, 1989), pp. 128-130.
9. C. C. Kung and M. J. Rhee, "Circuit Description of Inductive Energy Storage Pulsed Power Systems", Conference Record-Abstracts, 1989 IEEE International Conference on Plasma Science, pp. 125, Buffalo, New York, May 22-24, 1989.
10. C. C. Kung, E. A. Chauchard, Chi H. Lee, M. J. Rhee, and L. Yan, "Experimental Study of Power Gain in an Inductive Energy Pulsed Power System with an Optically Activated Semiconductor Opening Switch", Conference Record-Abstracts, 1990 IEEE International Conference on Plasma Science, May 21-23, 1990.
11. C. C. Kung, Eve A. Chauchard, M. J. Rhee, Chi H. Lee, and Li Yan, "Voltage Multiplication with an Optically Activated Semiconductor Opening Switch", Conference on Lasers and Electro-Optics, 1990 Technical Digest Series, Vol. 7, pp. 80-82, Optical Society of America, Washington DC, 1990.
12. C. C. Kung, E. A. Chauchard, M. J. Rhee, L. Yan, and Chi H. Lee, "Peak Power Gain and Pulse Compression in an Inductive Energy Storage System by a Photoconductive Closing and Opening Switch", Workshop Proceedings of the 2nd Workshop on "Optically and Electron-Beam Controlled Semiconductor Switches", August 1990, Norfolk, Va.
13. C. C. Kung, E. E. Funk, E. A. Chauchard, M. J. Rhee, Chi H. Lee, L. Yan, "Observation of Power Gain in an Inductive Pulsed Power System with an Optically Activated Semiconductor Closing and Opening Switch", Proceedings of the SPIE Conference on Optically Activated Switching, Vol. 1378, pp. 250-258, Nov., 1990.
14. C. C. Kung, E. A. Chauchard, E. E. Funk, Chi H. Lee, M. J. Rhee, and L. Yan, "Generation of Kilovolt Square Pulse by a Current Charged Transmission Line Using an Optically Controlled Semiconductor Opening Switch", Bulletin of the American Physical Society, Division of Plasma Physics, Nov. 12-16, 1990.
15. C. C. Kung, E. A. Chauchard, M. J. Rhee, and Chi H. Lee, "Generation of square pulses by a dual of the Blumlein line with a photoconductive semiconductor opening switch", Conference on Lasers and Electro-Optics,

1991 Technical Digest Series, Vol. 10, pp. 126-128, Optical Society of America, Washington DC, 1991.

16. C. C. Kung, E. A. Chauchard, Chi H. Lee, and M. J. Rhee, "Observation of Square Pulse Generation in a Dual of the Blumlein Line with an Optoelectronic Opening Switch", Conference Record-Abstracts, 1991 IEEE International Conference on Plasma Science, p. 207, June 3-5, 1991.
17. C. C. Kung, E. A. Chauchard, M. J. Rhee, and Chi H. Lee, "Square Pulse Generation with a Photoconductive Semiconductor Opening Switch in the Dual of the Blumlein Line", Digest of Abstracts of the 8th IEEE Pulsed Power Conference (IEEE, New York, 1991), p. 3-43, June 17-19, 1991, San Diego, California. It will also be appeared in the Digest of Technical Papers of the 8th IEEE Pulsed Power Conference.
18. E. E. Funk, P. S. Cho, C. C. Kung, E. A. Chauchard, M. J. Rhee, P.-T. Ho, J. Goldhar, and Chi H. Lee, "Recent advances in research on photoconductive power switching at the University of Maryland", Proceedings of the SPIE Conference on Optically Activated Switching, Paper 1632-27, Jan., 1992.

Professional positions held:

6/85—8/92: Graduate Research Assistant, Solid State Laser Lab., Electrical Engneering Department, University of Maryland, College Park, Maryland.
9/83—12/84: Part-time Teacher, Department of Electronics, Kai-Nan Vocational High School, Taipei City, Taiwan, Republic of China.
8/81—6/83: Military Service, Army Training Camp, Kaoshiung, Taiwan, Republic of China.

Appendix E

Optical Control of Semiconductor Closing and Opening Switches

Chi H. Lee

Reprinted from
IEEE TRANSACTIONS ON ELECTRON DEVICES
Vol. 37, No. 12, December 1990

Optical Control of Semiconductor Closing and Opening Switches

CHI H. LEE, SENIOR MEMBER, IEEE

Invited Paper

Abstract—Recent progress in the research area of high-power photoconductive semiconductor switches is reviewed. Material issues and switch design consideration are discussed. High-power ultra-wide-band microwave generations using these switches and a pulse-forming network are presented. The application of the photoconductive switch both as a closing and opening switch in an inductive energy storage system has been demonstrated. We have observed for the first time an electric pulse compression with a peak power gain of 30. Future prospects in this area of research are also discussed.

I. Introduction

OPTICALLY CONTROLLED photoconductive semiconductor switches (PCSS's)[1] have gained considerable attention recently in the pulsed power, impulse radar, high-power microwave- and millimeter-wave communities because of their unique characteristics: jitter-free response and scalability to handle extremely high power. When these devices are used in conjunction with picosecond laser pulses, electric pulses with rise and fall times of the same time scale have been generated with megawatts of power. Because of their fast opening time, they may also be used both as a closing and opening switch in an inductive energy storage system. We have observed a power gain of a factor of 30. In this paper a review of recent progress in this emerging technology will be presented. A brief historical background and current development of the field will be reviewed in Section II. Material issues and switch design consideration will be discussed in Section III. High-power microwave generations using PCSS and pulse forming network (PFN) are presented in Section IV. Section V deals with the application of PCSS as an opening switch in an inductive energy storage system. Finally, in Section VI, future prospects in this exciting field will be pointed out.

Manuscript received April 6, 1990; revised June 21, 1990. This work was supported by the Air Force Office of Scientific Research.

The author is with the Department of Electrical Engineering, University of Maryland, College Park, MD 20742.

IEEE Log Number 9038831.

[1]There have been a number of different names used for the switches. For example, the name of bulk optically controlled semiconductor switch (BOSS) is used by group at the Old Dominion University. Ft. Monmouth's group refers to them as optically activated switches (OAS). Here we adapt the name used by the Sandia group (PCSS) or simply a photoconductive switch (PS).

II. Historical Background and Current Development

The most attractive characteristic of the photoconductive switches is its instantaneous and jitter-free response when illuminated by an ultrashort optical pulse. It was first reported by Jayaraman and Lee in 1972 [1] that photoconductive response time was indeed in the picosecond time range when illuminated by picosecond optical pulses. Soon after Si [2] and GaAs [3] were used to switch dc voltage using picosecond optical pulses. It was pointed out by Lee [3] that silicon was inadequate as a high repetition-rate switch because of its long carrier lifetime. The thermal runaway problem of Si was reported [4]. GaAs, on the other hand, does not have these drawbacks because of its high dark resistivity and short carrier lifetime. GaAs was used as a high-power switch by Mourou *et al.* [4]. Electric pulse shaping, generating square pulses with variable duration using $CdS_{0.5}Se_{0.5}$ and GaAs with amplitudes in the multi-kilovolts range, was demonstrated by our laboratory [5]. Photoconductive switches caught the interest of the pulsed power community when Nunnally and Hammond demonstrated the performance of a large-size switch holding 150-kV bias voltage and generating 100-kV and 2-kA electric pulses [6]. Many of these early works were reviewed in [7].

In addition to the unique features of jitter-free triggering and scalability mentioned above, PCSS's also have the following advantages: low inductance, fast rise time (closing time), and high repetition rate, fast recovery time (fall-time, opening time), and bulk conducting for high-current operation. These attractive features of the PCSS provide a completely new possibility for pulsed power switch technology. Intense research efforts are currently under way in a number of laboratories. For example, the Sandia group has demonstrated switching in GaAs in excess of 100 kV (67 kV/cm) [8]. Lock-on phenomena have been observed in GaAs and InP but not in Si [9]. It was found that the sample needed to maintain a minimum field (depending on samples) to sustain lock-on. The amount of optical energy requirement to trigger GaAs for lock-on is about three orders of magnitude less than it would require when there was no lock-on (i.e., at low field). Lock-on effect in general is a serious drawback in the opening switch operation. Effort is undertaken to understand and solve the lock-on problem. On the other

0018-9383/90/1200-2426$01.00 © 1990 IEEE

hand, one could use lock-on in the closing switch mode of operation, such as activating the frozen-wave generator [10], because of the reduced laser energy requirement.

Still another possible mechanism in reducing optical pulse energy requirement may be the optically induced avalanche process. This has been studied by Browden and Nunnally [11]. In an effort to find a more efficient closing switch operation, various switch and electrode designs have been tried. 35-kV voltage capacity was demonstrated with a gridded switch electrode [12]. It was found that the maximum switching efficiency depended on the openness ratio on the electrode surface [12]. It is desirable in practical application to use a compact laser source to activate PCSS. An all semiconductor device including two-dimensional (2D) laser diode array and Si P-I-N photoconductive switch has been reported by Rosen *et al.* [13]. P-I-N diode switches have the following distinct advantages: 1) the reverse saturation current is significantly lower than the bulk leakage current reducing greatly the thermal runaway problem. 2) the existence of n^+ and p^+ layers underneath the electrode metal forms an excellent ohmic contact with low contact resistance. 8-kV/cm voltage hold-off capacity has been obtained with megawatt power switched [13].

Electron-beam-controlled bulk semiconductor switch is another way to achieve high power switching capability. A hold-off field of 140 kV/cm has been reported in an e-beam-controlled device [14]. In addition, the e-beam activation of switches provides long on-state time (tens of microseconds) and volume generation of carriers via photo ionization by utilizing cathodoluminescence.

Another important application of PCSS utilizing its fast fall time is to use it as an opening switch in an inductive energy storage system. In such a system, a single switch performs both the closing and opening functions. During the charging cycle, the PCSS acts as a closing switch requiring adjustable duration in switch on-time (usually long on-time) and low on-state resistance. When the stored energy is to be delivered to the load the charging circuit needs to be interrupted with a fast opening and a very large off-resistance. One thus has conflicting requirements on the same piece of switch. One approach to accomplish this is to employ two optical pulses with different wavelengths, one to turn on and the other to turn off the switch with an arbitrary long delay time. In order to achieve this, a copper-compensated silicon-doped GaAs is required so that transition from and into the Cu_B level can be manipulated by using optical pulses with different wavelengths. The Cu_B level is a deep acceptor level located 0.44 eV above the valence band. This work has been reported by the Old Dominion University group [15]. In our laboratory we chose to control the conduction and opening time by specially tailored laser pulses. We have observed an electric pulse compression and peak power gain of a factor of 30. A detailed report on this will be presented in this paper.

In the search for suitable switching materials, a large number of semiconductors have been tested. The most popular is GaAs, both undoped and Cr-doped. For nigh power closing switch operations, the following material properties are important: high voltage hold-off and large mobility. GaAs is better than silicon in these aspects. Other materials investigated included InP, $CdS_{0.5}Se_{0.5}$, ZnSe, and diamond. The wide-bandgap materials have extremely large voltage hold-off capability. For example, breakdown fields larger than 1 MV/cm have been observed. Furthermore, ZnSe and diamond are interesting because both have unusually high mobility. In addition, diamond has good thermal conductivity. The disadvantage in using-large-bandgap material is that short-wavelength optical pulses are required for carrier generation, such as excimer laser or third-harmonic of Nd lasers.

In addition to the use of PCSS's as high-power toggling switches, they can also be used, in conjunction with a pulse-forming transmission line, as ultra-wide-band waveform generators. Megawatt impulses with gigahertz bandwidths have been demonstrated in our laboratory. Sequential waveform generations using a frozen wave generator have also been reported. Impulse excitation of a microwave resonant cavity can generate high-power microwave pulses from a single cycle to hundreds of cycles [16]. A part of this research has been described in a recent review article [17]. Ultra-wide-band high-power microwave pulses can be used as source for impluse radar. Impulse radar has many unique capabilities over conventional narrow-band radar. It can detect low-observable targets and improve the penetration capability in addition to providing high-resolution range measurement.

III. Material Issues and Switch Design Considerations

Photoconductive switches (PS's) have many applications based on their unique characteristics, e.g., extremely high speed, large dynamic range, scalability, and jitter-free response. There are two categories of applications: low-voltage and high-voltage. In the former case, the most important characteristic of the device is its high speed. The switching efficiency is not crucial. One needs a material with carrier lifetime as short as possible even at the expense of sacrificing mobility. In the latter case, the device is required to deliver as much power to the load as possible. The switch transfer efficiency should be near 100%. Speed is not the primary concern. The mobility of the switching material should maintain a reasonable value.

The on-state conductance of the device depends upon the induced plasma density and mobility. For efficient switching functions one requires material with high electron and hole mobilities. The induced plasma density depends upon the carrier generation and transport. We will discuss this issue later. Since photoconductivity responds almost instantaneously to the input optical pulse, PS is ideal for impulse generation. To achieve ultrahigh speed operation it is necessary 1) to use picosecond optical pulses as the optical triggering sources, and 2) to reduce the carrier recombination lifetime. There are several techniques available in reducing the carrier lifetime: deep-

level impurity doping, high-energy proton [18] and neutron [19] bombardment, and low-temperature MBE growth [20]. All aim to increase defect density to speed up carrier recombination at defect sites. Another important issue is voltage stand-off properties of the material. This is a particularly important issue for a high-voltage power switch. In general, we look for large-bandgap materials with high dielectric strength for high-voltage stand-off. These materials generally have high dielectric-breakdown threshold. In addition to the high breakdown field, one also needs to use material with high dark resistivity to reduce leakage current under high biased condition. Under dc or long-pulse bias even a small leakage current can lead to thermal runaway. Table I shows some of the picosecond photoconductors. Note the high dark resistivity of all materials. Among them silicon has the lowest dark resistivity, resulting in serious thermal runaway problem. Diamond has the highest dark resistivity, giving rise to very high dielectric breakdown strength (>1 MV/cm).

The actual design of the switch depends on the specific application. The switch is a chip device which can be scaled in size. For high-frequency and high-speed application the output voltage requirement is low and thus the photoconductive gap length is typically of the order of a few micrometers. For high-power switches, however, the device size is usually in millimeters or even centimeters.

In order to preserve the inherent bandwidth capability of the picosecond photoconductive device, the photoconductor is used as a switch in a charged transmission line pulser arrangement (Fig. 1). In this arrangement, the charging segment of the transmission line is attached to one electrode of the photoconductive switch at one end of the segment and to the charging voltage source at the other. The output end of the switch is connected to the output line which is terminated by a matched load.

The high dark resistivity of the switch makes it nonconductive in the dark state. Assuming that optical pulses illuminate the photoconductor and are being absorbed by the material, electron–hole pairs will be created instantaneously, transforming the photoconductor from an insulating state to a conducting one and thus closing the switch. A fast rise electrical pulse will appear at the load if an ultrashort laser pulse is used for illumination. The actual shape of the electric pulse depends on the duration of the time that the switch remains closed. This time is usually referred to as the photoconductive lifetime which has two contributions: carrier recombination time and sweepout time. In the case where the photoconductive lifetime τ is much greater than the round-trip propagation time of the voltage wave on the charged line section $2L/v$, one expects a square waveform to appear at the load with its rise and fall times equal to the rise time of the laser pulse. Here L is the length of the charged line segment and v is the velocity of the voltage wave propagating on the line. If $\tau \ll 2Lv$, one expects to see a single-sided exponential waveform. Here again the rise time of the pulse is equal to that of the laser pulse but the fall time

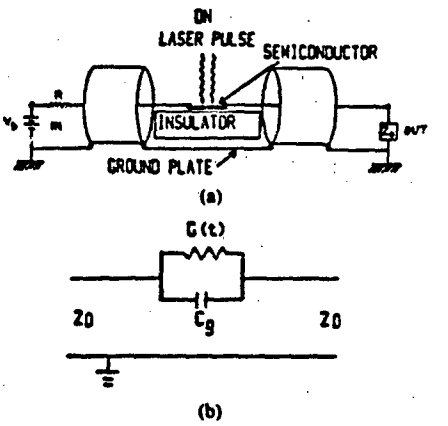

Fig. 1. (a) Schematic of the experimental PS arrangement and (b) its equivalent circuit.

TABLE I
SEMICONDUCTOR MATERIALS INVESTIGATED FOR (KILOVOLT) PHOTOCONDUCTIVE SWITCHING

Semiconductor	Eg (ev)	Carrier Lifetime (ns)	Dark Resistivity (Ω-cm)
Si (intrinsic)	1.16	10^4	5×10^4
Silicon on Sapphire(SoS)		10 ~ 1 ps	
*Cr:GaAs	1.42	< 1	$>10^7$
Fe:InP	1.29	< 1	$>10^7$
*CdS_xSe_{1-x}	1.8 ~ 2.4	> 10	$> 10^7$
GaP	2.24	> 1	$> 10^7$
*(Diamond (IIa))	5.5	< 1	$> 10^{16}$
Fe:In:GaAs		500 ~ 100 ps	
GaAs on SoS		20 ps	

*First developed at the University of Maryland

reflects the photoconductive decay time (assuming that the switch is not saturated). The output voltage V_{out} is given by

$$V_{out} = V_c \frac{Z_0}{2Z_0 + R_s(t)} \tag{1}$$

where V_c is the bias or charging voltage, Z_0 the characteristic impedance of the transmission line, and

$$R_s(t) = l_{gap}^2/\Delta N(t) e u + R_c \tag{2}$$

is the dynamic resistance of the switch under laser illumination. Here l_{gap} is the gap length of the switch, $\Delta N(t)$ is the total number of photo-induced charge carriers which are proportional to the optical energy of the pulse, and R_c is the total contact resistance at the electrodes of the switch. The temporal dependence of $\Delta N(t)$ reflects the dynamics of carrier decay. When the photoconductor is

used as high power switch, one usually requires the switch to transfer energy efficiently to the load and wants $R_s \ll Z_0$. This must be done with high biased voltage across the switch for high power application. The maximum hold-off voltage is

$$V_{max} = l_{gap} E_{Br} \quad (3)$$

where E_{Br} is the intrinsic breakdown field. It is obvious from these expressions that in order to have an efficient high-power switch one requires large l_{gap} and high $\Delta N(t)$, i.e., large optical energy. Switches as large as a few centimeters with 100 kV of hold-off voltage strength have been fabricated in pulse power application. The large optical energy requirement for large power switch can be greatly reduced via a "lock-on" phenomenon [8]. High-power pulsed microwave in the megawatt power range has been generated. Some of these results will be discussed.

The high-speed and jitter-free response of the PS's, in addition to their scalability and large dynamic range, make them ideal for many pulse power applications and for high-power microwave effect simulation. The advantages of a PS-based system over others result from the nature of the switching. The optical triggering of the PS allows for the electrical isolations of the controlled and controlling systems. The whole switch changes states on command as the optical trigger arrives, very fast and with no inherent jitter. The level of conduction can be controlled by design. This allows for very high efficiencies, since turn-on losses are minimized. The simplicity of the switching structure allows for scalability. Thus steps can be taken to design the geometry to enhance desirable properties. For example, thermal energy generated by Joule heating can be removed more efficiently by increasing the width of the PS at a specific gap length without increasing the inherent resistance of the PS. Alternate high voltage (HV) switching techniques suffer from intrinsic limitations in the speed and jitter of their response to a trigger command. For example, HV applications of spark-gaps suffer from nanosecond rise times and several nanoseconds of jitter [21]. Furthermore, their operation suffers from spatially nonuniform and filament-like conduction. This causes the premature malfunction of spark gaps and adversely affects their system use.

In PS, the switching action is provided by the photogeneration of electron-hole pairs which may be direct band to band transition or between the band and the deep levels in the energy gap depending on the laser photon energy. In Fig. 1 we show the schematic of the elemental PS and the equivalent electrical circuit. The gap capacitance C_g is due to the fringing fields associated with the discontinuity in the electrode (i.e., the gap). Modeling of PS has been discussed in [17].

Ideally, the resistance of the PS in the off state (i.e, in the dark and before the optical trigger) should be infinite. Consequently, it is desirable that the dark conductance $G_{dark} = 1/R_{off} = 0$. This requirement is especially important for HV applications. However, in real system G_{dark} is large but finite. This leads to a dark current that loads down the system. More importantly, the dark current will heat the PS, causing a rise in the temperature, which in turn increases the carrier density, causing a further increase in G_{dark}, etc. This process leads to the failure of the PS, a phenomenom called thermal runaway. A lower limit on the time scale of thermal runaway can be obtained by assuming that the generated joule heat is not dissipated. The thermal runaway in silicon PS's commences in about 10 ms when an electric field of 5 kV/cm is applied to them. The presence of surface states between the electrodes and the PS leads to much shorter thermal runaway time scales [2], [3]. For GaAs PS thermal runaway is less of a problem. We have modeled the thermal runaway [23]. In Fig. 2 we show the temporal dependence of the intrinsic resistivity of GaAs PS under various applied electric fields. Note that for a bias of 5 kV/cm, the effect of thermal runaway becomes significant after about 4 s. The much longer time of significant thermal runaway in GaAs, compared with that of Si, is due to its much higher resistivity and larger bandgap, respectively. The resistivities of GaAs and Si, at room temperature, are 10^8 and $3 \times 10^4\ \Omega \cdot$ cm, respectively. Consequently, GaAs is more desirable than Si as the PS material for holding off high voltages.

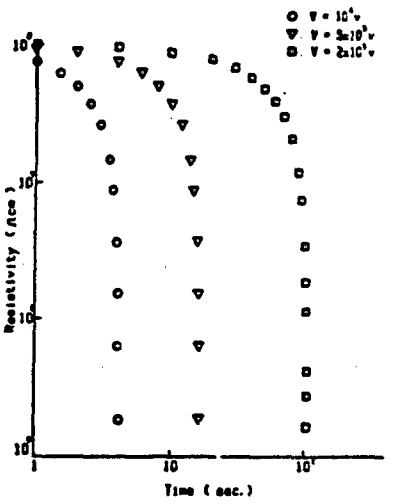

Fig. 2. Resistivity of GaAs PS versus time for several electric fields.

The choice of optical trigger wavelength has important physical consequences. The penetration depth of optical radiation in semiconductors increases monotonically with the wavelength in the visible and near-infrared regime. To avoid unduly high current densities, and thus avoid surface damage, the use of 1.06 μm is desirable instead of 0.532 μm for Si and GaAs switches. The absorption depth of 1.06 μm in GaAs and Si is several millimeters, whereas that of 0.532 μm is less than a few micrometers [24].

IV. High-Power Ultra-Wide-Band Pulsed Microwave Generation

Even with an ideal switch, the simple circuit shown in Fig. 1 generates output pulses with voltage equal to half

of the dc charge voltage. For very high voltage applications it is often advantageous to use circuits, or pulse-forming networks (PFN), which generate higher output voltage for a given dc charge voltage. Marx, Blumlein, and stacked-line generators can be used for this purpose [25]. The Marx and stacked-line generators require a switch per stage for dc bias multiplication. The Blumlein is a generator with output pulse voltage equal to dc bias and it requires a single switch. To keep the fidelity of the PFN operation, nanosecond (or shorter) pulse generators should be designed as distributed circuits. This also affects the requirement for the switching configuration and type. In our laboratory, Chang *et al.* demonstrated a 2-ns Blumlein pulse generator, using a concentric coaxial PFN geometry and a disk-shaped Si PS [26]. In this section three different approaches will be presented for ultrawide-band impulse generation: stacked-line, frozen-wave generator, and impulse excitation of a resonator.

A. Optoelectronic Activated Stacked Line for Megawatt Impulse Generation

In Fig. 3 we show a schematic of our composite device that is capable of generating over 13.5-kV pulses from a dc bias of 9 kV with pulse durations of 5 ns down to 100 ps (laser pulsewidth). Peak output powers of 1–20 MW, depending on load impedance, have been obtained. Two PS's, one GaAs and the other Si, are used in a configuration that retains their intrinsic desirable characteristics and avoids the undesirable characteristics. The first stage is a parallel-plane capacitor that is dc biased to high voltages. The parallel-plane capacitor is also a microstrip transmission line, designed to have a low characteristic impedance $Z_0 \simeq 1\ \Omega$. A GaAs PS is used to hold the dc HV. The PS connects the first stage to the second. The second stage is composed of three transmission lines of higher characteristic impedance $Z_0 \simeq 50\ \Omega$. These transmission lines are connected so as to be electrically parallel at the GaAs PS and in series at the third stage. The third stage is composed of a coplanar strip [27], [28], on a Si PS bulk substrate, designed to have a characteristic impedance equal to the output of the second stage line impedance (150 Ω). The third stage connects to the "outside" world. A single optical pulse is divided into two, the triggering and shaping pulses. The triggering pulse turns the GaAs PS on. This generates a voltage pulse of approximately the same amplitude as the dc charge voltage. This generated pulse is transmitted through the parallel-connected transmission lines. The propagating pulses are added in series at the other end of the second stage, and transmitted to the third stage with a transmission coefficient of $\simeq 1$ (impedance matched transmission). Theoretically, this scheme yields an output voltage pulse that is three times the dc bias voltage, into an impedance-matched load. The length of the output pulse can be controlled by the timing of optical pulse, which is incident on the Si PS and overlaps the coplanar transmission line. The width of the generated HV pulse can be fine tuned because of the precise timing between the triggering and shaping laser pulses (realized by "dialing" the optical path length difference between them).

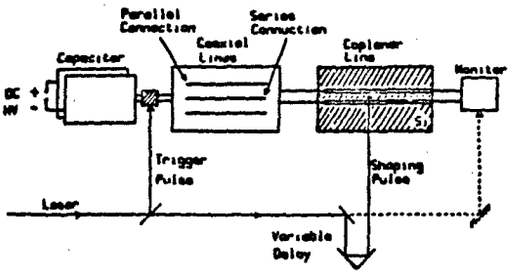

Fig. 3. Schematic of the composite device that generates, multiplies, and shapes pulses of tens of kilovolts in magnitude and megawatts of peak power. See text for details.

It is important to note that the GaAs and Si PS operations are complimentary. The GaAs PS is used to hold the HV dc bias, because of its immunity to thermal runaway, and trigger the pulse-forming operation on command. Whereas the long carrier lifetime of Si allows for the clean shaping of the generated HV pulses. Since the HV pulse will be across the coplanar line for several nanoseconds at most, the Si PS does not have enough time to undergo thermal runaway.

The PS materials were intrinsic GaAs and Si. The GaAs switches were 4.5 × 4.5 × 4.5 mm cubes, and the Si PS was a disk of 5-cm diameter and 1 cm thick. The faces to be illuminated by the 1.06 μm were polished. By using a ceramic-based high dielectric constant microstrip, we have constructed a miniature pulse generator that has produced pulses of over 13.5 kV when dc biased to only 9 kV. The outputs correspond to a voltage multiplication factor of 1.5. The output pulse delivers a peak power of $\cong 1.25$ MW into a 150-Ω load. This experimental result and other design details have recently been reported [29].

In addition to MW level pulsed microwave generation, active pulse shaping has also been demonstrated [29] by using two optical pulses. These two optical pulses, with no delay between them, are directed at the PS, where one illuminates the gap in the "hot" electrode and the other illuminates the gap between the coplanar electrodes. A dipolar HV pulse is obtained at the output, with significantly more power in higher frequency components than that for a monopolar (i.e., flat-top) pulse [16]. The width of the dipolar pulse can be varied by changing the position of the illumination between the coplanar electrodes.

B. Frozen Wave Generator

There are several applications for short pulse signal microwaves, such as extrawide-band resolution radar, time-domain metrology, and plasma diagnostics. A sequence of RF pulses can be generated from a dc source through a series of step recovery diodes with a rise time of 60 ps, although its pulse amplitude is limited. A frozen wave generator [30], a simple and effective device consisting of several segments of transmission lines connected in series by means of switches, is capable of generating a sequential waveform of arbitrary temporal characteristics. We

have designed an experiment using picosecond laser pulses to actuate the frozen-wave generator producing unique broad-band microwave pulses [10]. The work was reviewed recently [17]. The principle of the frozen-wave generator will be given below. The detail experimental results can be found in [17]. Fig. 4 shows a frozen-wave generator with three switches and three segments of transmission lines. The last segment was designed to have length equal to half of that in the previous two segments. The end termination was left open. Here the three segments of transmission lines were charged to V_0, $-V_0$, and V_0, respectively. In the ideal case when all three switches are closed simultaneously, a two and one half cycles square pulses will be generated; the amplitude of the pulse is the same as that in the charged line structure ($V_0/2$), and the pulsewidth is equal to the transit time for the wave to travel across one segment of charging cable of length L.

After the three segments of transmission lines were charged separately to the voltages V_0, $-V_0$, and V_0, each transmission line segment could be considered to have two standing waves stored within it, having amplitude equal to half of the charging voltage. Once the three switches were closed simultaneously and instantaneously with zero resistance, those standing waves (or frozen waves) started to travel in two directions. Therefore, three traveling waves moved toward the output end, which would show up first at the load. And another three traveling waves would follow the previous waves due to total reflection from the open-end termination. Because the length of the third segment was half of the length of the previous two, a two and one half cycles of pulses could be expected, having a pulse width L/v and amplitude $V_0/2$. Using the frozen-wave generator, we have demonstrated the generation of kilovolt sequential waveforms which has only two and one-half cycles with a period of 4.8 ns and peak-to-peak amplitude of 850 V [17].

By varying the length of each transmission line segment, a periodic waveform can also be produced, sometime with coded sequential waveforms. For example, the character 101101 has been generated by the frozen-wave generator [17]. The limit for the amplitude of the pulsed waveform is set by the intrinsic bulk breakdown ($\sim 2 \times 10^5$ V/cm). It, therefore, suggests that in the future experiments, a design utilizing switches with wider gaps will be necessary for the generation of a multikilovolt sequential waveform. This last point suggests that a large-dimension GaAs switch operated under lock-on condition may be a useful closing switch for frozen-wave generator since it has been shown that with lock-on the switch remains close for a long period of time with only low-energy triggering pulse. This is precisely what is needed to operate an efficient frozen-wave generator with a large number of switches.

C. Impulse Excitation for Microwave Generation

Direct dc to RF conversion with an optoelectronically switchable frozen-wave generator has been described in the previous section. It has been shown to be efficient in generating a sequential waveform consisting of a small number of RF cycles. Nevertheless, there are some drawbacks associated with the frozen-wave generator. One of them is that a large number of switches must be simultaneously activated and each switch must operate at close to 100% efficiency in order to form a good pulse sequence. These requirements are rather difficult to meet, because each switch may have somewhat different characteristics owing to the fabrication process. The simultaneous closure of several switches also demands a large amount of laser energy.

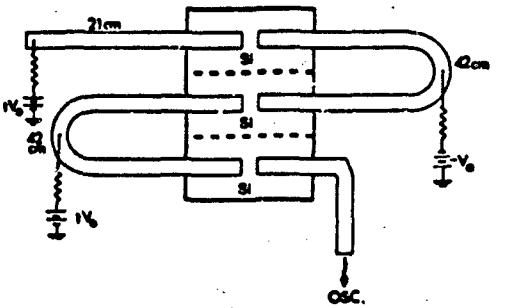

Fig. 4. Schematic of the frozen-wave generator. The dc bias voltages are V_0, $-V_0$, and V_0.

We have investigated a different approach that can generate a large number of RF cycles using only a single photoconductive switch in conjunction with a microwave coaxial resonator. The basic principle is described below (Fig. 5). The electrical impulse generated by an optoelectronic switch is coupled via an antenna to a coaxial structure cavity. This pulse will reflect back and forth inside the resonant cavity which is shorted at one end and opened at the other. At the shorted end of the cavity, the resultant electrical field has to be zero to meet the boundary condition. Thus the reflected electrical field must have the same amplitude but opposite polarity of the incident pulse. At the open end, the total current must be zero. Thus the reflected current pulse has opposite polarity. The pulse bouncing back and forth inside the coaxial cavity forms a series of pulses of alternative polarities. If one uses another antenna inside the cavity to couple these pulses out, the output signal will consist of a damped periodic pulse train. The frequency of this oscillation is equal to the cavity resonant frequency. The damping rate depends on the coupling coefficient of the cavity or the loaded quality factor (Q). The higher the quality factor (Q), the slower the damping rate. For efficient conversion, the number of RF output pulses in the train should be limited, since the total energy of the entire RF output pulse train is less than the energy of the single exciting impulse. Detailed theoretical analysis and experimental results have been discussed in [16]. Only a brief summary of these findings is given here.

A schematic of the experimental arrangement is shown in Fig. 5. Coaxial lines were uses as quarter-wave resonant cavities. A single picosecond laser pulse was used to

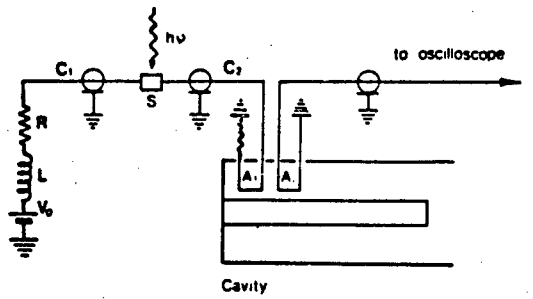

Fig. 5. Schematic of the experimental arrangement for impulse excitation for microwave generation. C_1 is the coaxial charge line. C_2 is the coaxial line, initially uncharged, that connects the photoconductive switch S to the cavity. A_1 and A_2 are input/output coupling elements.

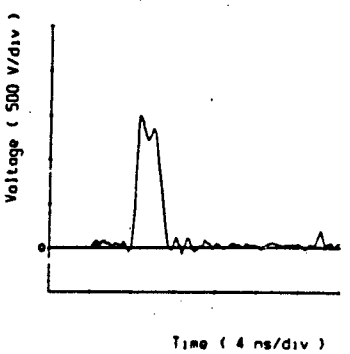

Fig. 6. A typical monopolar electric pulse used to excite the cavity, the pulse is generated by optically triggering the PS.

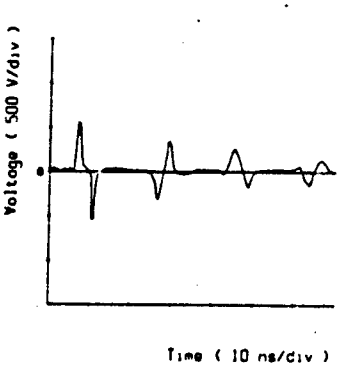

Fig. 7. Successive dipolar microwave pulses generated using the 300-MHz cavity with strongly coupled antennas A_1 and A_2 and 20-ns-long cavity C_2.

trigger the bulk GaAs PS. An electric impulse was generated and coupled into the resonator. The performance of the GaAs PS's were tested, under dc biases of up to 4 kV, with 1.06-μm laser pulses for several thousand consecutive shots without any observable degradation in performance.

In Fig. 6 we show a typical monopolar electric pulse ($\simeq$1.25 kV in magnitude and 2 ns in duration) used to exite the cavities. Two important and useful parameters that control the waveform, and hence the frequency distribution, of the generated microwaves are i) strength of the coupling provided by the input and output loop, and ii) length of the coaxial line connecting the PS to the input loop. In Fig. 7 we show the effect of coupling. The generated waveform corresponds to the strong coupling case. Note that the first dipolar pulse has a peak to peak voltage of $\simeq$1.2 kV, and that the peak power is over 7 kW. The energy conversion efficiency, including the reflected pulses, is over 50%.

V. Photoconductive Semiconductor as Opening Switches

There are two common types of energy storage systems: capacitive and inductive. The ratio of inductive to capacitive energy density is about 25 [31]. The capacitive energy storage system requires large volume and high voltage while the inductive system can be much more compact and operative at relatively low voltage. With the advent of high-T_c superconductors [32], the inductive storage becomes even more attractive since in the ideal case there will be no energy loss during storage and the energy can be stored for a very long time.

The major obstacle to a practical inductive storage system is the opening switches [31] The ideal opening switches for this application should possess the following characteristics:

- fast opening (nanosecond or less)
- fast recovery to achieve high repetition rate
- controllable and long conduction times
- zero resistance during conduction
- high impedance after opening
- large current
- large stand-off voltage
- jitter free.

Common opening switches, such as explosive and plasma erosion switches, can provide high-current and high-voltage operation but lack in fast opening and high repetition rate. Recently we have investigated semiconductor materials for opening switches. It appears that, with a proper laser as the light source, the semiconductor opening switches can fulfill most of the requirements.

In the inductive energy storage system the energy stored in the inductor is transferred to the load by means of an opening switch which breaks the current in the charging circuit. There are two major considerations in an inductive energy storage system: the charging circuit and the opening switch design. The figure of merit (F) as defined by Schoenbach *et al.* [31] for the system is the product of I_0 and dR_{op}/dt, where I_0 is the charging current and dR_{op}/dt is the rate of change of the switch resistance. Among the conventional opening switches which have the best figure of merit are the explosive switch, with $F = 3 \times 10^{13}$ V/s; plasma erosion switch, $F = 10^{14}$ V/s; and diffuse discharge switch, $F = 10^{13}$ V/s [31]. The photoconductive semiconductor switch studied in our laboratory has already achieved $F = 10^{19}$ V/s.

Optical-beam-illuminated semiconductor switches based on the photoconductivity effect can be turned off

rapidly if the optical beam is terminated abruptly. For the conventional opening switches the loss is associated with the slow opening time. Picosecond photoconductor opening switches offer the capability for instant turn-off. A semiconductor (or insulator) with high dark resistivity can be transformed into a quasi-metallic state if the illuminating light intensity is high enough. Some materials, such as GaAs, diamond, and InP have short carrier lifetimes. They can relax back to the semi-insulating (or insulating) state in less than a picosecond (for deliberately damaged materials [19]) to a few nanoseconds (for as grown materials) after the light is abruptly removed. This process can be repeated at a fast rate. When using these materials as repetitive opening switches, a constant current source is used to charge an inductor through the semiconductor switch in its closed state (with light illumination). The light beam is then abruptly terminated, opening the switch. The energy is delivered immediately to the load. It is clear that completely opposite requirements exist between the charging phase (on state) and opening phase (off-state). During the charging phase one wants long carrier lifetime, high carrier mobility (high switch efficiency and low forward voltage drop); while during the opening phase the switch must show high dark resistivity (high opening state impedance), short carrier lifetime for fast opening action, high breakdown field (higher field is induced at opening). One approach to fulfill the conflicting requirements is to control carrier generation and recombination processes by two laser pulses of different wavelengths, one to turn on the photoconductivity and the other, to quench it in a copper-compensated silicon-doped GaAs [15]. This is a very interesting and promising approach since the on-state time can be adjusted to be long enough to match the charging time by simply delaying the arrival time of the quenching pulse. However it usually requires two lasers properly synchronized in time. An alternative is to use only one laser but with its pulse shape and pulse duration properly tailored to fulfill both closing and opening requirements in controlling the semiconductor switch. Laser pulses as long as 3 ms with 40 J of pulse energy at 1.06 μm has been reported [33].

To demonstrate these points we choose to use a current-charged transmission line as the inductive energy storage system [34]. Using a semiconductor switch we have shown 1) subnanosecond opening time with 100% energy transfer efficiency from the storage line to the load, 2) current buildup and multiplication, and 3) peak power gain of a factor of 30.

A. Subnanosecond Opening Time and High-Efficiency Energy Transfer

It has been proposed that by using a current charged transmission line (CCTL) as an inductive storage system, a very fast and efficient energy transfer to the load can be achieved [34]. Fig. 8 shows the schematic of the CCTL. The transferred energy is in the form of a square pulse. The transmission line theory explains the formation of a square pulse as follows. A transmission line of length l and of characteristics impedance $Z_0 = (L/C)^{1/2}$ is initially shorted at both ends and charged with a constant current I_0. The charging current can be considered as the superposition of two traveling waves of constant voltage amplitude $V^+ = -V^- = Z_0 I_0/2$ and accompanying currents $I^+ = I_- = I_0/2$, proceeding in opposite directions, each being constantly reflected from the shorted ends satisfying the boundary conditions, i.e., reflection coefficients $\rho = -1$. The resultant voltage along the line is zero while the current is equal to the charging current I_0. When one end is suddenly opened by the opening switch, which is connected in parallel with a resistive load of matching impedance, the positively traveling wave no longer reflects and proceeds toward the load forming a rectangular pulse. The resultant output has a voltage $V_{out} = Z_0 I_0/2$, a current $I_{out} = I_0/2$, and a pulse duration $\tau_{out} = 2l/c$. All these features have been observed [35]. In fact with a 6-m-long CCTL, a near perfect square pulse of 60 ns has been obtained with Cr:GaAs and InGaAs switches [35].

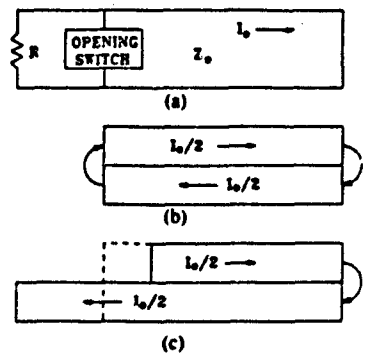

Fig. 8. Current charged transmission line (CCTL) and opening switch. (a) Schematic representations of CCTL and opening switch system to produce a square pulse. (b), (c) Current distribution before and after the opening of the switch.

The energy transfer efficiency from the CCTL to the load can be defined as the ratio

$$Q = \frac{E_{out}}{E_{stored}} \tag{4}$$

where

$$E_{out} = V_{out} \cdot I_{out} \cdot \tau \tag{5}$$

and

$$E_{stored} = \tfrac{1}{2} l L I_0^2 \tag{6}$$

where L is the inductance of the line per unit length. Using the relation $lL = \tau Z_0/2$, the efficiency of the energy transfer can be written as

$$Q = (2V_{out}/Z_0 I_0)^2 \tag{7}$$

and has been measured to be very close to 100% [35].

B. Current Buildup in CCTL

One of the unique features in using CCTL and an ultrafast switch is to observe current buildup. In an ideal in-

ductive energy storage system, the expression of the energy stored (in CCTL of length l) is given by (6). I_0 now represents the final charging current (Fig. 9(a)). After the switch is closed (assuming infinitely fast switch closing and that it remains closed), the current buildup follows the stair-step shown in Fig. 9(b). The current at nth step is $2nV_0/Z_0$. If the switch remains close for a very long time, eventually the current I_0 will approach V_0/R_s, where R_s is the source resistance, or until the circuit fails. The unique feature of the optically controlled opening switch is its abiiity to open at the most appropriate moment delivering the large current to the load before catastrophic failure or when I_0 is at its peak.

We have observed this stair-step type of current buildup process with the circuit shown in Fig. 10. It is similar to the circuit shown in Fig. 9(a) except for a small resistor of 0.1 Ω and an oscilloscope which allow the observation of the time variation of the charging current. The transmission line was 6 m long. A waveform with sharp steps as illustrated in Fig. 9(b) can only be obtained if the switch closing time is much faster than the wave round-trip time in the transmission line. Thus we used short laser pulses (100 ps) generated by a Q-switched mode-locked laser for this experiment. In order to observe several steps, the switch must remain closed for a duration equal to several round trips in the line.

For a 6-m-long CCTL, it is necessary to use a silicon switch in conjunction with a picosecond optical pulse to observe the stair-step current buildup. The charging current waveform obtained with a silicon switch is shown in Fig. 11. For the silicon switch, the carrier recombination time is very long (μs), so that the switch resistance remains small long enough to observe the many steps. Moreover, the picosecond pulse energy (1 mJ) is sufficient to bring the switch to saturation and it remains closed for a longer time than its carrier recombination time. The height of the first step is 88% of that expected for an ideal switch. The decreasing height of the subsequent steps is due to the slow reopening of the switch as the carriers recombine. For the GaAs switch, the carrier recombination time is very short (ns). The transmission line length was reduced to 30 cm to speed up the current build-up. Four steps could be observed before the switch reopened. These results show that voltage multiplication is possible with this circuit if a fast opening action can be realized before the amplitude of the current decreases. It should be pointed out that the fast closing of the switch is not necessary. Large current levels can also be reached with a slow closing switch, the only difference being that the steps would not be well defined.

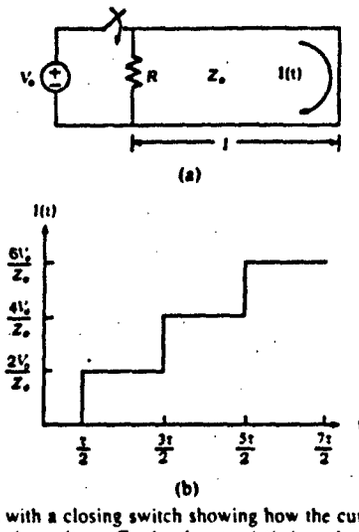

Fig. 9. CCTL with a closing switch showing how the current is built up; V_0 is the charging voltage; Z_0, the characteristic impedance of the CCTL; R the load resistor; and l the length of the CCTL. (b) The ideal current waveform expected at the shorted end of the CCTL during the charging cycle; τ is the round-trip transit time for the wave traveling in the CCTL.

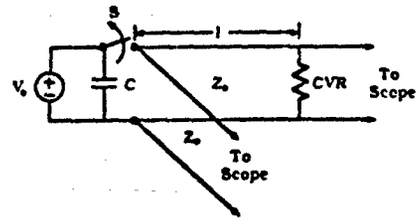

Fig. 10. The experimental circuit employed to observe the current buildup and peak power gain; S, the semiconductor switch; V_0, charge voltage; C, capacitor; l, the length of CCTL; Z_0, characteristic impedance; and CVR, current viewing resistor which is 0.1 Ω.

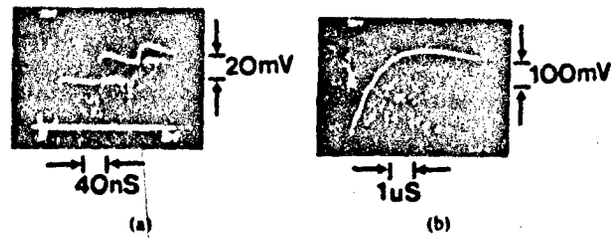

Fig. 11. Charging current waveform showing stair-step current buildup during the closing phase of a silicon switch actuated by a picosecond pulse. (a) Initial current buildup waveform showing in nanosecond time scale. (b) Current waveform after the switch remains closed for a few microseconds. Note that the current starts to drop when the silicon switch starts to open because of carrier recombination.

C. Laser Pulse Shaping

It has been mentioned above that the most important features of the laser pulse shape for a photoconductive opening switch are the slow rise and abrupt termination. When Cr:GaAs is used as the closing and opening switch, as long as the laser energy is sufficient (~ a few millijules), the Cr:GaAs switch will be at saturation with re sistance of less than 0.5 Ω. The abrupt termination of th laser pulse will make the GaAs switch open in a subna nosecond. Laser pulses which possess these features wer generated in our laboratory by an Nd:glass oscillato shown in Fig. 12. The intracavity Pockels cell acts as cavity dumper. By adjusting the relative timing betwee the chopped pumping Ar^+-laser beam and the Pockels cel

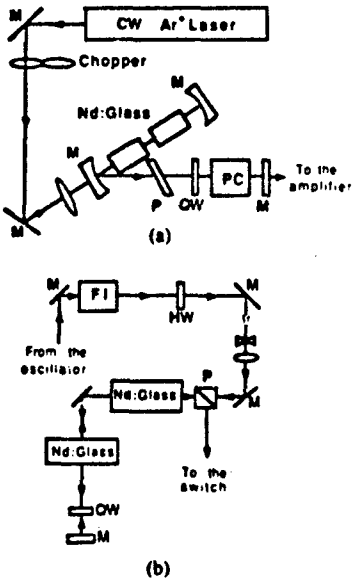

Fig. 12. The laser system. (a) Oscillator generating the specially tailored laser pulse: *M*, mirrors; *P*, polarizing beam splitter; *QW*, quarter wave plate; *PC*, Pockels cell. (b) Two-stage amplifier; *FI*, Farady isolator; *HW*, half-wave plate; *P*, polarizer; *M*, mirrors; *QW*, quater-wave plate.

switching time one can split the laser pulse into two. The portion switched out at the polarizer (P) will have a fast rise time and pulse duration lower than the cavity round-trip time and the other portion leaking out from the end mirror next to the Pockels cell will be a half bell shape with abrupt termination, as shown in Fig. 13. The duration of the slow rise portion can be adjusted. This laser pulse waveform is quite adequate for the present experiment.

D. Power Gains in an Inductive-Energy Pulsed Power System

Power gain in an inductive energy storage pulsed power system (IESPPS) may be defined as the ratio of the output power of the system to the power that the source would produce directly into the same load. Power gains of a factor of 30 has been observed, for the first time, in IESPPS with an optically controlled semiconductor closing and opening switch using the specially tailored 1.054-μm laser pulse shown in Fig. 13. In this section, we report on an experiment that demonstrates this. The IESPPS consists of a current-charged transmission line (CCTL) and an optically activated semicondutor opening switch. The experimental setup is schematically shown in Fig. 10. A transmission line (RG-213) of characteristics impedance $Z_0 = 50\ \Omega$ and length $l = 2.5$ m, with one end shorted (0.1-Ω current viewing resistor, CVR) is connected through a semiconductor switch to a capacitor $C = 0.1\ \mu$F, which is initially charged to V_0. The output waveform was measured at the switch side of CCTL through a 50-Ω transmission line as shown in Fig. 10. In order for the system to be useful as an IESPPS, the period of switch conduction time should be long enough so that the charging current is multiplied in the inductive energy storage

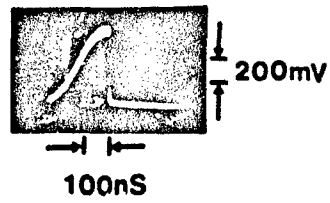

Fig. 13. Laser pulse temporal characteristics showing long duration with slow rise time and abrupt fall time.

circuit, giving rise to power multiplication. The intensity of light increases slowly in time for 200 ns and then falls rapidly to near zero within 10 ns. The switch used in this experiment is a GaAs p-i-n diode [13], for which the carrier recombination time is ~2 ns. The p-i-n diode is 0.5 mm thick, 5×5 mm^2 square wafer of GaAs doped with p-type impurity on one surface and n-type on the other. A ring-shaped gold electrode is evaporated to the p-type surface so that the laser light can penetrate into the switch material, and a flat electrode is evaporated onto the opposite side. The lowest on-resistance for this switch was found to be 0.5 Ω.

The pulse-forming experiment was performed with the CCTL and the GaAs p-i-n diode as shown in Fig. 10. Upon activation of the switch by the laser pulse, the capacitive energy, initially stored in the 0.1-μF capacitor, which is charged to a voltage of 100 V, is transferred to the CCTL. The charging current, which is monitored by a 0.1-Ω current viewing resistor, increases in time up to 16 A as shown in Fig. 14(a). This value indicates current accumulation equivalent to about 4 round trips but is substantially less than 50 A that is predicted by the same circuit with an ideal switch. This indicates that the switch has a higher on-resistance early in time when the laser light intensity is low. As the pulse of laser light ends, the switch opens and releases the inductive energy into the resistive load. The load, in this case, consists of parallel connection of a 50-Ω coaxial cable (connected to a 50-Ω oscilloscope) and the off-resistance of the switch. Therefore, the equivalent load resistance R_L is always less than or equal to 50-Ω. A typical output-pulse waveform with the main pulse amplitude of 360 V, obtained with a charging voltage 100 V, is shown in Fig. 14(c). Higher output voltages are produced with higher charge voltages up to 150 V with output voltage of 480 V. Switch breakdown occurs at charge voltage of 163 V for the 0.5-mm-thick GaAs switch.

It is straightforward to show that the CCTL produces a main pulse and a train of post-pulses into an arbitrary resistive load R_L with amplitudes given by

$$V_{\text{out}}^{n} = R_L Z_0 I_0 (Z_0 - R_L)^n / (Z_0 + R_l)^{n+1} \qquad (8)$$

where n designates the nth post-pulse and $n = 0$ corresponds to the main pulse. In this experiment (see Fig. 10), only an infinitely high switch resistance (matched load, i.e., $R_L = Z_0 = 50\ \Omega$) will produce just one main pulse $V_{\text{out}}^{0} = Z_0 I_0/2$. Otherwise, $R_L < Z_0$ because of finite

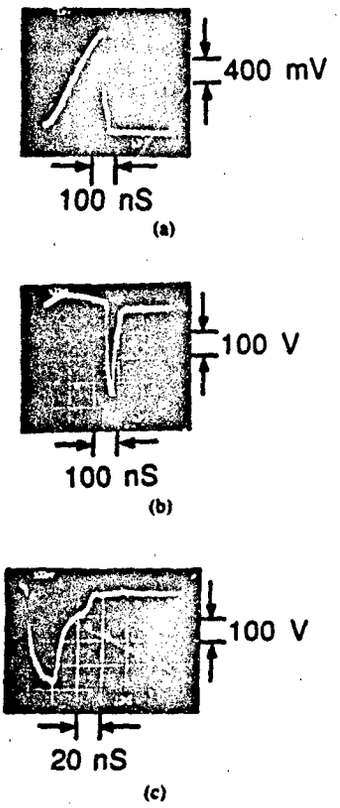

Fig. 14. (a) The charging current waveform monitored by the CVR; the output voltage pulses showing voltage multiplication with different time scale, in (b), 100 ns/major div.; and (c), 20 ns/major div. The data taken with a 0.5-mm-thick p-i-n diode switch. Other parameters are l = 2.5 m, Z_0 = 50 Ω, R = 50 Ω, C = 0.1 μF, and V_0 = 100 V.

switch resistance, and a gradually decreasing, staircase-shaped waveform is produced (see Fig. 15). A typical waveform shown in Fig. 14(c) demonstrates such a decreasing staircase. The ratio of the main pulse to the first post-pulse amplitudes is used to estimate the off-resistance of the switch by using (8), and found to be typically −200 Ω.

In order for a pulsed power system to be useful, the power gain should be greater than unity. In this experiment, the output and the source powers are $P_{out} = (V^0_{out})^2/Z_0$, and $P_s = V_0^2/Z_0$, respectively. We have found that the power gain

$$G = \left(\frac{V_{out}}{V_0}\right)^2 \tag{9}$$

as defined here is a function of charge voltage. The highest power gain occurs at the lowest charge voltage. For charge voltage of 50 V the power gain is 30. It decreases to 13 at 100 V. This suggests that the switch off-resistance becomes lower as the induced electric field (by the output voltage) across the switch increases. This phenomenon may be attributed to an effect similar to the "lock-on" effect [8] observed in the closing switch experiments. However, we observed no such effect when the switch was connected in a closing switch configuration.

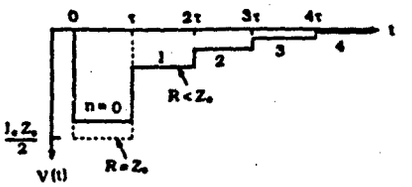

Fig. 15. The output waveform expected from a CCTL. The dotted line corresponds to the matched load situation ($R = Z_0$) and the solid line is for mismatched load ($R < Z_0$).

Thus we have demonstrated for the first time that a current-charged transmission line with a GaAs p-i-n diode switch can produce output pulse with power gains of 30. The system may be scaled up to a higher voltage system by using a thicker switch which will require a higher laser power. The phenomenon of dropping power gain with increased operation voltage needs further investigation.

VI. Conclusion and Future Prospects

Past and recent developments of the optically controlled photoconductive semiconductor switching devices have been reviewed. Progress in this field clearly indicates that multi-megawatt power switches with convenient size optical source, such as semiconductor laser diode array, will be possible in the very near future. To generate extra-wide-band microwave impulse with an all solid state system requires further development in laser system design. One important area in this regard is the development of a compact, laser diode pumped Nd:laser system generating subnanosecond rise time optical pulses as the optical source. The advent in diode laser array technology makes this type of high-power compact system possible. The unique features of the PCSS have been exploited to generate high-power extra-wide-band microwave pulses. Kilo- to megawatt power level microwave pulses have been generated by three different methods: stacked line, frozen-wave generator, and impulse excitation of a resonator. Pulses ranging from one RF cycle to multi-cycle aperiodic coded sequential waveforms have been demonstrated with picosecond rise and fall times.

Power combining of these pulses in space for added power and for beam steering by optically controlled waveform generation should be possible. This will require a large number of switches operated simultaneously. Therefore, it is important to investigate new methods of reducing optical energy, such as optically induced avalanche or "lock-on" effect. Switching jitter may be the price to pay for optical energy reduction. These areas require further investigation.

Development of an opening switch for inductive energy storage circuit has been carried out by using Cr:GaAs in conjunction with a specially tailored optical pulse such that a long charging time and fast opening time are simultaneously satisfied with a single switch and a single optical pulse. It has been observed that an output power gain of 30 is achievable. "Lock-on" occurs only during the opening phase when the field in the switch is between 4 and 8 kV/cm.

The "lock-on" phenomemon should be further studied to gain a complete understanding of its physical mechanism. While "lock-on" is not desirable in the opening phase of an opening switch, it can be used in a frozen-wave generator when many switches are required to close simultaneously. The reduction in optical requirement when "lock-on" occurs is definitely advantageous. In the opening switch operation "lock-on" prevents the recovery of off-state resistance to its high value, resulting in the droping of power gain as the charge voltage increases. This may be a serious problem in opening switch application for materials exhibiting negative differential resistivity (NDR) since the "lock-on" may be related to the Gunn effect. Material without NDR, such as silicon, should be investigated as possible opening switch candidate. To speed up carrier recombination in Si, Au-doped impurity may be a solution.

Acknowledgment

The author would like acknowledge technical contributions from C. S. Chang, E. A. Chauchard, E. Funk, J. Goldhar, C. C. Kung, M. J. Rhee, A. Rosen, and H. A. Sayadian.

References

[1] S. Jayaraman and C. H. Lee, "Observation of two-photon conductivity in GaAs with nanosecond and picosecond light pulse," *Appl. Phys. Lett.*, vol. 20, pp. 392-395, 1972.

[2] D. H. Auston, "Picosecond optoelectronic switching and gating in silicon," *Appl. Phys. Lett.*, vol. 26, pp. 101-103, 1975.

[3] C. H. Lee, "Picosecond optoelectronic switching in GaAs," *Appl. Phys. Lett.*, vol. 30, no. 2, pp. 84-86, Jan. 1977.

[4] G. Mourou, W. H. Knox, and S. Williamson, "High-power picosecond switching in bulk semiconductors," in *Picosecond Optoelectronic Devices*, C. H. Lee, New York, NY: Academic Press, 1984, ch. 7.

[5] C. H. Lee and V. K. Marthur, "Picosecond photoconductivity and its applications," *IEEE J. Quantum Electron*, vol. QE-17, no. 10, pp. 2098-2112, Oct. 1981.

[6] W. C. Nunnally and R. B. Hammond, "Optoelectronic switch for pulsed power," in [7, ch.12].
——"80-MW photoconductor power switch," *Appl. Phys. Lett.*, vol. 44, p. 980, 1984.

[7] C. H. Lee, *Picosecond Optoelectronic Devices*. New York, NY: Academic Press, 1984.

[8] F. J. Zutavern, G. M. Loubriel, B. B. Mckenzie, W. M. O'Malley, R. A. Hamil, L. P. Schanwald, and H. P. Hjalmarson, "Photoconductive semiconductor switch (PCSS) recovery," in *Proc. 7th IEEE Pulsed Power Conf.* (Monterey, CA, 1989), pp. 412-417.

[9] G. M. Loubriel, F. J. Zutavern, H. P. Hjalmavson, and M. W. O'Malley, "Closing photoconductive semiconductor switches," in *Proc. 7th IEEE Pulsed Power Conf.* (Monterey, CA, 1989), pp. 365-367.

[10] C. H. Lee, M. G. Li, C. S. Chang, A. M. Yurek, M. J. Rhee, E. Chauchard, R. P. Fischer, A. Rosen, and H. Davis, "Optoelectronic techniques for microwave and millimeter-wave applications," in *IEEE MIT-S Int. Microwave Symp. Dig.*, pp. 178-181, 1985.

[11] M. K. Browder and W. C. Nunnally, "Investigation of optically induced avalanching in GaAs," in *Proc. 7th IEEE Pulsed Power Conf.* (Monterey, CA, 1989), pp. 433-436.

[12] A. Kim, M. Wade, M. Weiner, R. Youmans, and R. Zeto, "Bulk GaAs photonic devices with two opposite gridded electrodes," in *Proc. 7th IEEE Pulsed Power Conf.* (Monterey, CA, 1989), pp. 430-432.

[13] A. Rosen, P. J. Stabile, D. W. Bechtle, W. Janton, A. M. Gombar, J. McShea, A. Rosenberg, P. R. Herczfeld, and A. Bahasadri, "Optically achieved p-i-n diode switch utilizing a two-dimensional laser array at 808 nm as an optical source," *IEEE Trans. Electron Devices*, vol. 36, pp. 367-374, Feb. 1989.

[14] K. H. Schoenbach, V. K. Lakdawala, D. C. Stoudt, T. F. Smith, and R. P. Brinkmann, "Electron-beam-controlled high-power semiconductor switches," *IEEE Trans. Electron Devices*, vol. 36, pp. 1793-1801, Sept. 1989.

[15] K. H. Schoenbach, V. K. Lakdawala, R. Genuer, and S. T. Ko, "An optically controlled closing and opening semiconductor switch," *J. Appl. Phys.*, vol. 63, p. 2460, 1988.
M. S. Mazzola, K. H. Schoenbach, V. K. Lakdawala, and S. T. Ko, "Nanosecond optical quenching of photoconductivity in a bulk GaAs switch," *Appl. Phys. Lett.*, vol. 55, p. 2102, 1989.

[16] H. A. Sayadian, M. G. Li, and C. H. Lee, "Generation of high-power broad-band microwave pulses by picosecond optoelectronic technique," *IEEE Trans. Microwave Theory Tech.*, vol. 37, pp. 43-50, 1989.

[17] C. H. Lee, "Picosecond optics and microwave technology," *IEEE Trans. Microwave Theory Tech.*, vol. 38, pp. 596-607, May 1990.

[18] M. B. Ketchen, D. Grischkowsky, T. C. Chen, C. C. Chi, I. N. Duling, N. H. Halas, J. M. Halbout, J. A. Kash, and G. P. Li, "Generation of subpicosecond electrical pulses on coplanar transmission lines," *Appl. Phys. Lett.*, vol. 48, pp. 751-753, 1986.

[19] R. L. Druce, M. D. Pocha, K. L. Griffin, and W. W. Hofer, "Sub-nanosecond linear GaAs photoconductive switching," in *Proc. 7th IEEE Pulsed Power Conf.* (Monterey, CA, 1989), pp. 882-886.

[20] F. W. Smith, H. Q. Le, V. Diadiuk, M. A. Hollis, A. R. Calawa, S. Gupta, M. Frankel, D. R. Dykaar, G. A. Mouron, and T. Y. Hsiang, "Picosecond GaAs based photoconductive optoelectronic detectors," *Appl. Phys. Lett.*, vol. 54, pp. 890-895, Mar. 1989.

[21] V. M. Ristic and T. P. Sorensen, "Generation of microwave power with a spark-gap cavity," *IEEE Trans. Microwave Theory Tech.*, vol. MTT-26, p. 369, 1978.
T. P. Sorensen and V. M. Ristic, "Rise-time and time-dependent spark-gap resistance in nitrogen and helium," *J. Appl. Phys.*, vol. 48, p. 114, 1977.

[22] J. C. Koo, G. M. McWright, M. D. Pocha, and R. B. Wilcox, "A low leakage 10000-V silicon photoconductive switch," *J. Appl. Phys.*, vol. 45, p. 1130, 1984.

[23] C. S. Chang, H. A. Sayadian, C. H. Lee, unpublished work.
C. S. Chang, Ph.D. dissertation, University of Maryland, College Park, 1986.

[24] C. H. Lee, "Generation of photoinduced carriers," [7, ch. 5, sec. IIB].
C. H. Lee, P. S. Mak, and A. P. DeFonzo, "Optical control of millimeter wave propagation in dielectric waveguides," *IEEE J. Quantum Electron.*, vol. QE-16, p. 277, 1980.

[25] R. A. Fitch, and V. T. S. Howell, "Novel principle of transient high-voltage generator," *Proc. Inst. Elec. Eng.*, vol. 111, p. 849, 1964.

[26] C. S. Chang, V. K. Mathur, M. J. Rhee, and C. H. Lee, "Ultrafast optoelectronic switching in Blumlein pulse generator," *Appl. Phys. Lett.*, vol. 41, p. 392, 1982.

[27] C. P. Wen, "Coplanar waveguide: A surface strip transmission line suitabel for nonreciprocal gyromagnetic device applications," *IEEE Trans. Microwave Theory and Tech.*, vol. MTT-17, p. 1087, 1969.

[28] K. C. Gupta, R. Garg, and I. J. Bahl, *Microstrip Lines and Slotlines* Dedham, MA: Artech House, 1979.

[29] H. A. Sayadian, S. T. Feng, J. Goldhar, and C. H. Lee, "Generation and shaping of megawatt high voltage pulses by optoelectronic technique," *IEEE Trans. Microwave Theory Tech.*, vol. 38, pp. 622-628, May 1990.

[30] J. M. Proud, Jr., and S. L. Norman, "High frequency waveform generation using optoelectronic switching in silicon," *IEEE Trans. Microwave Theory Tech.*, vol. MTT-26, pp. 137-140, 1978.

[31] K. H. Schoenbach, M. Kristiansen, and G. Schaefer, "A review of opening switch technology for inductive energy storage," *Proc. IEEE*, vol. 72, pp. 1019-1041, 1984.

[32] M. K. Wu, J. R. Ashburn, C. J. Torng, P. H. Hor, R. L. Meng, L. Gao, Z. J. Huang, Y. Q. Yang, and C. W. Chu, "Superconductivity at 93K in a new mixed-phase Y-Ba-Cu-O compound system at ambient pressure," *Phys. Rev. Lett.*, vol. 58, p. 908, 1987.

[33] R. L. Maynard, R. P. Johnson, F. J. Masters, N. K. Moncur, L. D. Siebert, and J. D. Stanely, "Long pulse operation of a Nd:glass laser," in *Dig. CLEO* (Baltimore, MD, 1989), paper TUJ28.

[34] E. A. Chauchard, C. C. Kung, C. H. Lee, M. J. Rhee, and V. Diadiuk, "A new method to generator square pulses: Optoelectronic switching in a current charged transmission line," *IEEE Trans. Plasma Sci.*, vol. PS-15, pp. 70-72, Feb. 1987.

[35] E. A. Chauchard, C. C. Kung, C. H. Lee, and M. J. Rhee, "Repetitive semiconductor opening switch and application to short pulse generation," *Laser and Particle Beams*, vol. 7, pp. 615–626, 1989.

*

Chi H. Lee (M'80–SM'86) received the B.S. degree in electrical engineering from National Taiwan University, Taipei, Taiwan, and the M.S. and Ph.D. degrees in applied physics from Harvard University, Cambridge, MA, in 1959, 1962, and 1968, respectively.

He was with the IBM San Jose Research Laboratory, San Jose, CA, from 1967 to 1968. Since 1968 he has been with the University of Maryland, College Park, where he is now a Professor of Electrical Engineering. His areas of research include picosecond optoelectronics, lasers, optical technique for microwave application, and millimeter-wave devices.

Dr. Lee is a Fellow of the Optical Society of America and a member of the American Physical Society. He also served as the Chairman of the IEEE MTT-3 technical committee for lightwave technology.